Rapid Dynamic Power Rail Switching of OFDM Signal Amplifiers

MATTHEW EVANS

A thesis submitted for the degree of Doctor of Philosophy (Ph.D.) in Electronic Systems Engineering

School of Computer Science and Electronic Engineering

University of Essex

February 2024

Acknowledgements

Firstly, my sincere gratitude goes to Professor Stuart Walker of the University of Essex, without whom this PhD would not have been possible. His unerring patience and willingness to engage in detailed and broad discussions gave me the means to continue. Not to mention his wealth of academic and industry experience to always be able to discuss a prospective solution to overcome any hurdle throughout the process. Professor Anthony Vickers was the person to initially convince me to pursue a PhD having supervised me at undergraduate level. He and Professor Walker supported my application and without them I wouldn't have had the opportunity to embark upon the PhD journey.

I would like to thank my mother and brother for their unwavering and continued support in all aspects of my life; never failing to offer a nugget of wisdom regardless of the situation. My father was an optical engineer for many years and inspired me to pursue a career in an engineering discipline and to this day continues to have a significant influence on my life. I am deeply thankful to the three of you.

This research has been supported and funded by two industry companies, ABER Electronics Ltd and Creo Medical Ltd. Special thanks to Andrew Haynes and Graham Leighton for their support of the research and their helpful suggestions along the way. Both have been great friends and mentors to me since 2015. A further thank you also to Professor Chris Hancock and Craig Gulliford for their continued support of the research from an industry perspective.

I must say thank you to my friends and fellow researchers Syahmi Bin Nordin and Felix Ngobigha, both of whom I met during my undergraduate days, and both have successfully endured the PhD process within the last decade. Early on in my research,

they both provided empathetic insights into the expectations of the process and the struggles and helped to correct my early research direction.

Michael Bridden, Reis Jones, Gary Nieuwenhuis, and Liam King continue to be true friends and regularly gave me the necessary ‘kick’ to ensure I pushed on in the right direction. I can’t thank you all enough for the support and belief.

A special mention must go to Michael Bridden, as a fellow electronic engineer he has always been willing to be the ears to bounce ideas off.

Revenar Narciso, Caroline Senter, Emer O’Donnell, Pawel Pankiewicz, Richard Lister, Anne Quy, and Alastair Wilson, all of ABER Electronics Ltd. have been very protective and supportive of my research throughout the entire process whether it be fending off customers at critical times, offering work-related assistance, or sharing in the late nights working together. A huge thank you to all of you.

Finally, a thank you to John Speak, Tony McNicholl and Phil Vandersteen, all of whom I met within a cue sports environment (pub!) They have all provided support, even if they do regularly beat me at pool and snooker!

Abstract

Global resource usage and allocation is becoming an increasingly critical topic. Efficiency is at the heart of a plethora of current research fields from reducing energy consumption in the manufacturing industry, to increasing energy generation from renewable sources, or reusing waste materials for alternative applications. The telecommunications industry is no different, OFDM as a modulation format is ubiquitous and popular due to its spectral efficiency and robustness to interference but its major drawback is its high peak-to-average power ratio (PAPR) meaning that its efficiency is compromised.

A review of existing methods for improving OFDM signal amplifier efficiency showed a lack of innovative techniques for power supply control for such amplifiers. This thesis proposes two unique solutions to innovate efficiency for a range of applications.

Firstly, a novel power supply control technique to improve the efficiency of OFDM signal amplifiers based on probabilistic analyses. The probability density function of an OFDM signal was analysed and optimum switching thresholds were determined to maximise the efficiency of the power supply. The proposed mechanism considers the theory of Golomb rulers and perfect difference sets, specifically the conversion from linear rulers to modular to achieve a much greater system implementation efficiency. The result is a dynamic fast-switching multi-level power supply which achieves the main benefits of Doherty and Chireix amplifiers but without requiring multiple amplifiers. This class A-G amplifier topology can achieve a 63% efficiency increase compared to amplifiers with single-level voltage supplies.

Secondly, a generalised resource management technique known as Total Resource Utilisation Shuffling Technique (TRUST) to tackle the wider issue of resource utilisation

and management. The focus for TRUST in this work is on batteries but it could be applied to a wide range of resources, not necessarily in the technology sector.

Keywords: Chireix, Class A-G, Doherty, Golomb, OFDM, PAPR, PDF

Table of Contents

List of Figures

List of Tables

Acronyms and Abbreviations

A	Ampere
AC	Alternating Current
ACE	Active Constellation Extension
ACLR	Adjacent Channel Leakage Ratio
ACPR	Adjacent Channel Power Ratio
Ah	Ampere-hour
AI	Artificial Intelligence
BER	Bit Error Rate
BPF	Bandpass Filter
BPSK	Binary Phase Shift Keying
BW	Bandwidth
CCDF	Complementary Cumulative Distribution Function
CDF	Cumulative Distribution Function
CDMA	Code-Division Multiple Access
CFR	Crest Factor Reduction
CGR	Circular Golomb Ruler
COFDM	Coded Orthogonal Frequency Division Multiplexing
CSR	Corporate Social Responsibility
CW	Continuous Wave
dB	Decibel
dBm	Decibels Referenced to 1 Milliwatt
DC	Direct Current
DFT	Discrete Fourier Transform
DPA	Doherty Power Amplifier
DUT	Device Under Test
DVB	Digital Video Broadcasting
EER	Envelope Elimination and Restoration
ET-PA	Envelope Tracking Power Amplifier
FEC	Forward Error Correction
FFT	Fast Fourier Transform
FPGA	Field-Programmable Gate Array

GFDM	Generalised Frequency Division Multiplexing
GHz	Gigahertz
GI	Guard Interval
GPIO	General Purpose Input/Output
HPF	Highpass Filter
ICI	Inter-Carrier Interference
IDFT	Inverse Discrete Fourier Transform
IF	Intermediate Frequency
IFFT	Inverse Fast Fourier Transform
ISI	Inter-Symbol Interference
KDE	Kernel Density Estimation
KHz	Kilohertz
LED	Light Emitting Diode
LF	Linear Flow
LNA	Low Noise Amplifier
LO	Local Oscillator
LPF	Lowpass Filter
LTE	Long Term Evolution
MCU	Microcontroller Unit
MGR	Modular Golomb Ruler, Merry-Go-Round
MHz	Megahertz
MOSFET	Metal Oxide Semiconductor Field Effect Transistor
mW	Milliwatts
NF	Noise Figure
NLM	Non-Linear Matrix
OCP	Over Current Protection
OFDM	Orthogonal Frequency Division Multiplexing
OOB	Out-Of-Band
OTS	Off-The-Shelf
PA	Power Amplifier
PAE	Power Added Efficiency
PAPR	Peak-to-Average Power Ratio
PCB	Printed Circuit Board

PDF	Probability Density Function
PDS	Perfect Difference Set
PSK	Phase Shift Keying
PSU	Power Supply Unit
PTS	Partial Transmit Sequence
QAM	Quadrature Amplitude Modulation
QPSK	Quadrature Phase Shift Keying
RF	Radio Frequency
Rx	Receiver
SLM	Selective Mapping
SMPS	Switch-Mode Power Supply
SNR	Signal-to-Noise Ratio
SOA	Safe Operating Area
TI	Tone Injection
TR	Tone Reservation
TRUST	Total Resource Utilisation Shuffling Technique
TRx	Transceiver
Tx	Transmitter
UPS	Uninterruptable Power Supply
V	Voltage
W	Watt
Wh	Watt-hour

Chapter 1: Introduction

1.1 Motivation

The accelerating use of wireless communication in society has led to a corresponding rise in concerns about the environmental impacts of these technologies. One of the main concerns is the amount of power consumed by wireless communication systems, and the associated carbon emissions. This escalating concern underscores the urgent need for more efficient power-saving techniques.

Despite notable advancements in amplifier technology, the efficiency of OFDM signal amplifiers has plateaued in recent years. This is alarming given the ever-increasing global deployment of telecommunications equipment, especially in the context of the rapidly expanding 5G network infrastructure and its associated contribution to energy consumption [1] [2]. 5G base stations, due to their heightened complexity and power demands, necessitate a closer examination of power efficiency strategies. Generally, 5G stations require more power amplifiers, low noise amplifiers, transceivers, as well as digital circuitry to control it all.

5G networks are designed to offer faster data rates and lower latency compared to previous generations but the deployment of the necessary network infrastructure requires the installation of a vast number of small cells and base stations, resulting in increased energy consumption and resource usage. The move to higher operational frequencies means that propagation distances reduce, there are three solutions to this:

1. Increase the number of base stations with each covering a smaller area, on average.
2. Increase the output power of existing base stations.

3. A combination of both above.

The second option above raises concerns about potential violations of recommended human health limits, as outlined by the International Commission on Non-Ionizing Radiation Protection (ICNIRP) [3] and IEEE [4].

In 2012, the global telecommunications infrastructure accounted for approximately 1% of total global energy consumption, with a year-on-year increasing trend [5]. Some researchers estimate the contribution of ICT to global electricity consumption to reach 21% by 2030 [6] [7] [8]. This pervasive infrastructure growth has raised concerns globally regarding its environmental impact, especially with the advent of 6G and the forthcoming 7G, telecommunications energy efficiency is of paramount interest.

The growing emphasis on environmental consciousness and sustainability has spurred research into efficiency improvements across numerous industries, including those that are heavily reliant on RF power amplifiers, such as outside broadcasting, medical and military applications. These amplifiers are notorious for their substantial power consumption and heat generation. Although the specific requirements for signal power handling, modulation capability and linearity performance vary within these industries, the development of ‘green amplifiers’ has emerged as a common focus amongst many researchers for improving efficiency. There is a compounding effect of increasing the efficiency of these amplifiers whereby heat generation is reduced which leads to reduced active cooling requirements.

There are three major benefits to the increased efficiency presented in this work:

1. **Cost Savings and Reduced Carbon Footprint**

   Enhanced efficiency translates to lower unit power consumption so is an attractive prospect for users in terms of the cost savings and lower carbon

footprint. Heightened environmental awareness and corporate social responsibility (CSR) is also increasing the desire for employers to operate more efficiently and for industries that rely heavily on wireless communications, the RF power amplifier is likely a significant contributing factor to their operating costs and environmental impact.

2. **Extended Battery Life**

   Higher amplifier efficiency can lead to longer battery life and extended operating times, especially in ubiquitous portable devices such as mobile phones and tablets as well as more specialist applications like mobile military equipment. Where long operating times are critical, such as in medical devices like implants, the increased battery life can reap numerous benefits including reliability, safety, and reducing maintenance overheads.

3. **Reduced Heat Generation**

   Generated heat from more efficient amplifiers is lower and therefore the risks of overheating and causing system damage is reduced. Generally running electronic systems at a higher temperature can induce localised stresses and lead to premature component failure. The lower heat can therefore increase the operational lifetime of an electronic system as well as reducing the need for cooling mechanisms. Active cooling can be a significant contributory factor to operational costs in a system. Even passive cooling, such as an appropriately sized aluminium or copper heatsink, generally requires a large amount of physical space and are not the most environmentally friendly materials. In the case of data centres, where space is often at a premium, the reduced amount of real estate occupied by passive cooling could be a huge contributor to operational efficiency.

There are many advantages and disadvantages to the increased usage of telecommunications equipment globally. Benefits include increased global connectivity, potential for increased data throughput and the number of remote locations reducing. Drawbacks, however, include the increased cost of infrastructure manufacture and installation, increased energy consumption and CO2 emissions, and elevated running costs. The oil and gas industries are facing increasing public scrutiny. An initiative developed by the World Bank in collaboration with the United Nations (UN) called the “Zero Routine Flaring by 2030” initiative was proposed in 2015 and, as the name suggests, aims to reduce global flaring from its current level to as close to zero as possible by the year 2030. Endorsed by many [9], this initiative has been recognised as one of the most important initiatives to help combat climate change in a 2020 report by the International Energy Agency (IEA) [10].

1.2 Objectives and Approaches

This research primarily aims to enhance the efficiency of signal amplifiers, particularly OFDM signal amplifiers which are ubiquitous in wireless communication systems. To achieve this goal, the OFDM signal is statistically analysed and an innovative new power supply control system for application in OFDM-based power amplifier systems is proposed.

A secondary objective of the research is to invent a versatile resource management technique which could be applied in a multitude of scenarios and spanning several industries including telecommunications. The proposed method is known as the Total Resource Utilisation Shuffling Technique (TRUST) and has a wide array of potential applications and is presented as a generalised solution.

Using MATLAB, statistical analyses of OFDM waveforms are performed and presented, a probability density function (PDF) is calculated to characterise the incoming RF signal peaks. This PDF informs the system design by guiding the selection of appropriate voltage switching levels, tailored to the desired system complexity. Thresholding the PDF helps to determine the optimal voltage switching levels. The multi-level power supply is dynamically controlled using MOSFETs as switches and a microcontroller unit (MCU) as the brain of the system. It is proven that the difference between optimum switching thresholds and uniformly spaced thresholds quickly diminishes as the number of levels increases. The uniform spacing allows the design of the power supply to benefit from the combinatorial mathematics theories of perfect difference sets and Golomb rulers to space uniform discrete voltage levels in a circular (or modular) arrangement with a low number of regulators, leading to an efficient implementation and operation. The derivation of a new method for constructing modular Golomb rulers is presented and implemented.

A three-stage binary modular/circular Golomb ruler whereby each voltage regulator or DC-DC converter is arranged in a circular formation is considered. This arrangement enables any combination of the three stages to be presented to the powered system thus providing greater flexibility in power management. This technique could be applied to other power management applications where flexibility is a benefit. The initial implementation is a binary composition of 1V, 2V and 4V which enables 7 different output voltage levels (1-7V), plus 0V for switch off condition. This is from the mathematics of combinations and permutations:

$$ {}_3C_1 + {}_3C_2 + {}_3C_3 = 7\ levels \qquad (1\text{-}1) $$

To facilitate these levels, individual switches are controlled by an MCU allowing specific combinations through to the output rails. MOSFETs are used as switches, with their gates driven by optocouplers being controlled by general purpose input-output (GPIO) pins on the MCU.

The input signal power envelope can be tracked with a power detector or envelope detector. This information guides adjustments to the voltage rail based on its location on the PDF, optimising performance.

There are some related areas of existing research including bias modulation, envelope tracking, and class G and class H amplifiers. Class G amplifiers have discrete voltage levels. Class H amplifiers have an analogue supply rail so is continuously variable. Both classes aim to minimise DC power wastage by adjusting the supply just above the requirement to match the instantaneous power requirements. There are some sophisticated techniques coinciding with or following the main 5G rollout, including control mechanisms capable of rapid power-down and power-on of individual network components based on traffic loads, thereby yielding power savings.

The statistical analysis of the OFDM waveform, undertaken to determine the optimum voltage switching threshold levels, is the foundation for the unique technique presented in this work. This is combined with the combinatorics of modular Golomb rulers (MGR), or rather, ‘merry-go-rounds’ (MGR). This delivers a new innovative OFDM amplifier power supply control system for OFDM signal amplifiers. Whilst power supply modulation techniques for RF power amplifiers have been seen before, presented by a multitude of different authors, this research looks at the nuances of the OFDM modulation technique and the statistical analyses of the incoming waveform to achieve an efficient power supply structure and operation, delivering an efficiency enhancement of up to 63%. The proposed solution could be incorporated into new

designs as well as having the potential to be retrofitted into amplifiers in existing systems if applied correctly. Moreover, these methods presented can be adapted for use with other waveform types, with some necessary modifications to the operational approach.

1.3 Thesis Contributions

This work encompasses two primary objectives. The first is to increase OFDM signal amplifier efficiency by introducing a new power supply control mechanism. The second is to propose a resource management technique which can be generalised to have a broad applicability across diverse industries. To the best of the author's knowledge, the following points constitute original contributions.

1. **Probabilistic Envelope Tracking (PET)**

   While envelope tracking (ET) is a well-known method for augmenting power amplifier efficiency, this new approach incorporates rigorous waveform statistical analysis. While the initial exploration in this work focuses on the OFDM modulated waveform, it's important to emphasise that the methodology can be applied to any waveform, provided its probability density function (PDF) is either known or calculable.

2. **A New Method for the Construction of Efficient Modular Golomb Rulers (MGR)**

   Several methods for constructing MGRs have previously been proposed but the new method presented in this work is an efficient alternative using known optimal Golomb rulers as the base structures. This method requires less computation and is easily provable.

3. **Merry-Go-Round, Modular Golomb Ruler (MGR) Power Supply Control System**

   Although Golomb rulers, modular Golomb rulers, and perfect difference sets are well-known, the theory has limited existing uses in electronics and haven't before been applied to power supply control systems. The novel control system presented in this work draws inspiration from the theory and topology of a Golomb ruler in a modular/circular configuration and achieves a modest efficiency enhancement. The MGR system is paired with PET to gain a unique and highly efficient composition.

4. **Total Resource Utilisation Shuffling Technique (TRUST)**

   Referred to as the shuffling technique for brevity, TRUST constitutes a versatile resource management method designed to promote equitable resource utilisation across various industries. The primary focus in this work lies in its application to the electronics industry, particularly concerning batteries and other power sources. The overarching goal is to enhance resource distribution and allocation, a concept that extends well beyond the electronics sector to offer solutions in diverse industries and resource management scenarios.

1.4 Thesis Structure

The following points describe the organisation of the thesis.

Chapter 2 – Literature Review focuses on existing research by other authors, providing context for the concepts underpinning. Different applications of Golomb rulers, as well as alternative efficiency enhancement techniques proposed and developed over the past century are discussed. The foundational combinatorial

mathematics principles used for the power supply constructions are also introduced, providing a mathematical grounding to the work.

Chapter 3 – Probabilistically Envelope Tracking (PET) presents the simulation of a range of different OFDM signals, developed in Matlab, including specific related mathematical and statistical analyses of those signals. The innovative probabilistic envelope tracking (PET) technique is introduced where the optimum switching thresholds are determined which subsequently inform the power supply control system. PET can be applied to a variety of signals, but the OFDM waveform is the focus of this work. PET is the pivotal contribution without which the power supply system would offer only incremental efficiency gains.

Chapter 4 – Implementation of Power Supply Control Techniques introduces the relevant applicability of the concepts of Golomb rulers, perfect difference sets and modular Golomb rulers (MGR) to this research and bridges the gap between theoretical and practical applications. The derivation of a new, efficient method for constructing modular Golomb rulers is explained and implemented. Simulations of circuits are presented which employ the derived efficient configurations designed to maximise the number of uniformly spaced discrete output voltage levels from a minimum number of voltage regulators. The novel power supply control system with uniformly spaced switching thresholds is detailed in this chapter.

Chapter 5 – Experimental Analysis offers a transition from theory to practice by presenting real-world measurements of different amplifiers and discusses the impact of this thesis research on existing technology. The first part of the chapter looks at the power added efficiency measurements (PAE) of 14 different amplifiers varying in RF output power, gain and frequency, establishing a benchmark for efficiency improvement. The second part of the chapter focuses on a 1W s-band amplifier and

conducts several experiments with different waveforms whilst varying the gain device bias current. A CW sine wave is the first input signal to establish correct experiment operation, followed by 3 different modulated OFDM waveforms (QPSK, 16QAM and 64QAM). These tests offer valuable insights into the practical efficiency gains achievable with the techniques in this research.

Chapter 6 – The Shuffling Technique (TRUST) introduces a new unique concept. This new concept is known as the shuffling technique (TRUST) and facilitates equitable distribution of resources. The primary focus of the chapter employs batteries as the resources, but the technique could be applied to other types of resources such as solar panels or data centre servers. TRUST is a versatile generalised resource management technique with far-reaching applications.

Chapter 7 – Conclusions and Future Work is the final chapter and summarises the main findings and contributions of the thesis. It provides a comprehensive review of the body of work, makes suggestions for future work, and discusses other areas where the theory from this research could be applied to enhance efficiency across diverse industries. Additionally, the limitations of the research are acknowledged and areas of further work for potential improvement are identified.

Chapter 2:
Literature Review

2.1 Introduction

In the dynamic domain of RF amplification, the pursuit of greater efficiency and performance has been a constant driving force. Amplifiers form the bedrock of modern communication systems, providing the necessary power to transmit signals over long distances and ensuring the fidelity of the data transmissions. Over the course of the last century, a wide variety of amplifier classes and efficiency enhancement techniques have been developed.

2.2 Amplifier Classes

The landscape of amplifiers is diverse, there are several different classes of RF amplifiers which have been developed over the last few decades. Each with their own strengths and weaknesses and therefore are used in different applications depending on the requirements of the system. Starting with the venerable class A amplifier, known for its high linearity at the expense of efficiency, through to the more recent and specialised classes S and T. The efficacy of different amplifiers can fluctuate significantly, influenced by the intricacies of real-world design and the frequency of application (audio versus RF, for example), as well as variations in components.

2.2.1 Classes A to E

Classes A to E are the most commonly used classes for a variety of audio and RF applications [11] [12] [13] [14].

Table 2-1: Amplifier Classes A to E

Class	Characteristics	Typical Efficiency
A	Biased for continuous conduction. Results in a high level of linearity but also low efficiency. Commonly used in low-power applications. Although the theoretical efficiency can be as much as 50%, in reality it is usually much less [13] [15]	25-40%
B	Biased for conduction for only half the input signal cycle. Results in higher efficiency than A but also a lot of distortion. Commonly used in medium-power applications.	~50%
AB	Combines features of both A and B. Results in better efficiency than class A and less distortion than class B.	50-70%
C	Output device conducts for less than half of the input signal cycle. Results in high efficiency but also very high distortion, highly nonlinear. Commonly used in high-power applications such as TV and radio transmitters.	70-90%
D	Output device is switched rapidly between fully on and fully off states. Results in high efficiency but with the potential for high levels of distortion if poorly designed.	90-95%
E [16]	Switch-mode amplifier that uses a tuned LC circuit to provide a sinusoidal output waveform. Results in very high efficiency but requires careful design and operation. Commonly used in high-frequency applications, such as radio and TV transmitters.	>90%

2.2.2 Classes F to T

Classes F, G, H, I, S, and T are newer and less commonly used but have justified applications and some interesting research surrounding them. Classes G and H are most closely related to the research in this thesis, they are both variations of class AB amplifiers with the key difference being that they have adjustable supply rails which can change based on the input signal level to achieve greater efficiency.

Table 2-2: Amplifier Classes F to T

Class	Characteristics	Typical Efficiency
F [15]	Modification of a class C amplifier with the addition of one or more tuned resonance circuit(s) in the output network. Good overall efficiency which improves more at harmonic frequencies, generally higher efficiency than class C. Difficult to design and requires careful attention to harmonic filtering. Highly sensitive to impedance mismatches.	~90%
G	Modification of a class AB amplifier using multiple power supply rails to improve efficiency. Operates on a lower voltage supply for low-level signals and switches to a higher voltage supply for high-level signals. Improved efficiency without sacrificing output power. Higher efficiency than class AB but lower than class F. Commonly used in audio and RF applications.	~80%
H	Variation of class AB that utilises analogue supply rails to achieve higher efficiency. Tracks the input signal and adjusts the supply voltage in real-time. Like a class AB amplifier with envelope tracking technology. Results in higher efficiency and less heat dissipation than class AB.	~80%

I	Modification of class B amplifier using a bias modulator to dynamically adjust the amplifier bias voltage in real-time based on the input signal. Higher efficiency than class B without sacrificing linearity.	~70%
S	A switch-mode amplifier which uses pulse width modulation (PWM) to achieve greater efficiency by switching the output transistor on and off rapidly with a modulated signal. Achieves high efficiency with low distortion.	~90%
T	Variation of a class D amplifier which uses digital feedback to improve the linearity. Using PWM to drive the output stage and a digital feedback loop to correct errors in the output waveform. Highly efficient and highly linear.	~90%

2.3 Amplifier Efficiency Enhancement Techniques

Along with variations in amplifier classes which can all achieve different levels of efficiency, there are various other techniques that can be employed to also improve the efficiency of RF power amplifiers. Some of these techniques can be paired with different classes to obtain higher efficiencies.

There are many advantages to increasing system efficiency, both obvious and subtle, some are outlined in table 2-3. There are also disadvantages, however, although these tend to be related to the manufacturing of system components.

Table 2-3: Advantages and Disadvantages of Increased System Efficiency

Advantages	**Disadvantages**
Increased efficiency meaning reduced power wastage through heat	Increased base cost of implementation
Reduced system operating costs	Increased system complexity
Gain and output response stability enhancement due to reduced heat	Potentially increased size requirements
Further reduced energy consumption due to decreased requirement for active cooling	
Ability to either maintain RF power and reduce energy consumption, or maintain energy consumption and increase RF power	
Topology can be retrofitted to existing systems	
Increased battery life for mobile devices	
Commercially more attractive	

Some amplifier efficiency enhancement techniques are outlined in table 2-4.

Table 2-4: Overview of RF Power Amplifier Efficiency Enhancement Techniques

Technique	Description and Characteristics
Doherty	Utilises two amplifiers in different bias conditions to deal with different parts of the incoming signal. A carrier amplifier for any input signal and a peaking amplifier to deal with the peaks above the carrier amplifiers' limits. Good efficiency over a very wide range of output power levels.
Chireix (Outphasing)	Like the Doherty technique in that there are two amplifiers which handle differing output powers, but the Chireix technique varies the load impedances of the two amplifiers to change their output powers whilst maintaining a constant overall impedance.
Envelope Tracking (ET)	Minimises wasted power by adjusting the supply voltage of the amplifier in real-time to match the envelope of the input signal. Improves efficiency over a wide range of output power levels.
Envelope Elimination and Restoration (EER)	Processes the amplitude and phase components of the incoming signal separately which allows the use of two separate amplifiers built for individual purposes. One high efficiency amplifier to process the amplitude component. One high linearity amplifier to process the phase component.
Digital Predistortion (DPD)	Involves applying a correction signal to the input signal to compensate for the nonlinearities of the amplifier. Improves efficiency and reduces distortion.
Load-pull	Technique that involves adjusting the impedance of the load seen by the amplifier to maximise power transfer and efficiency. Optimises output power and efficiency of the amplifier over a given frequency range.
Bias Modulation	Adjusts the bias control voltage in response to the input signal. Maintains high linearity by ensuring the amplifier is always operating at its optimum bias voltage.

Multilevel power supplies may be used in many of the above situations to further enhance the efficiency; this is the focus of the research presented here. An example

is the work of Vasić et al. who achieve 49% efficiency enhancement compared to a more conventional regulator solution [17].

2.3.1 Doherty

The Doherty amplifier, first introduced and patented by William H. Doherty of Bell Labs in 1936 [18], has remained a prominent and enduring technique for enhancing the efficiency of power amplifiers. The defining characteristic of a Doherty amplifier is its integration of two separate amplifiers in a single design:

- Carrier amplifier – operating continuously, the carrier amplifier can handle most input signals. Often biased in class A or class AB to provide high linearity.
- Peaking amplifier – when the carrier amplifier approaches compression, the peaking amplifier is turned on. Often biased in class C to prioritise good efficiency albeit at the expense of increased distortion.

The input signal is split into two paths via a quarter wave transformer or hybrid coupler, one path feeds the carrier amplifier and the other goes to the peaking amplifier. Importantly, the phase shift between each of the lines doesn't necessarily have to be 90º even though the original inventor designed it to be [19]. The outputs of the two amplifiers are then combined to have a singular composite output of the amplified signal. A quarter-wave transformer or hybrid coupler is used to combine the outputs of the carrier and peaking amplifiers to get them back in phase with each other.

There has since been incremental research to increase the number of amplifiers beyond two to further distribute the power amplification stages into multiple levels to achieve even greater efficiency.

The main advantage to the Doherty amplifier is its increase in efficiency over existing techniques. While it may not achieve efficiency levels like other, more complicated,

techniques such as envelope tracking, its simplicity and cost effectiveness make it an attractive architecture. There are some disadvantages, however, as kinks can occur in the gain profile as the amplifier switching occurs, the gain and phase vary with output power and there is a higher associated cost in terms of monetary value and PCB real estate when space is at a premium. Very wide bandwidth Doherty amplifiers remain challenging due to the nature of the phase shifting techniques.

Despite its inception in the mid-1930's and a resurgence in interest in the most recent two decades, the Doherty technique experienced a relative lull in research activity between the early 1950's until the mid-1990's, presumably because the research focus wasn't on power consumption and efficiency. One exception was the work of Raab, who proposed a three-amplifier variation of the Doherty technique achieving efficiency improvements of up to 10% compared to the equivalent two-amplifier system which in turn is approximately 20-30% higher than a typical single-amplifier class-B system [20].

William Doherty also patented several other parts of his research, including a new design for a high frequency amplifier in 1943 [21], and an ultra-high frequency amplifier with feedback minimisation in 1947 [22].

One key piece of work on the Doherty technique was performed by Giofrè et al. in which they achieve an ultra-wideband implementation of the technique at 83% fractional bandwidth [23]. The authors do experience a larger gain ripple (1.5dB) compared to other state-of-the-art work but this is across 1.5GHz bandwidth compared to other works at 0.6dB with bandwidth of 700MHz [24], 0.7dB across 800MHz [25] and 1dB across 800MHz [26] so is to be expected.

2.3.2 Chireix Outphasing

Invented by Henry Chireix in 1935, the outphasing technique is a load-modulated scheme whereby the output impedances of the two amplifiers vary based on the input signal, achieved by adjusting the bias conditions of each amplifier to change their impedances in opposite directions to maintain a constant overall system impedance [27]. The dynamic loads seen by each amplifier means that they each vary their output power. This, in turn, increases the operating efficiency of the amplifier as the load is optimised based on the input signal. Load modulation provides high linearity and therefore low distortion; whilst also helping to increase the operational bandwidth of the amplifier. The Chireix amplifier is typically used in applications requiring high linearity and high efficiency.

2.3.3 Envelope Tracking (ET)

Envelope tracking is a widely employed technique to reduce power wastage in RF amplifiers by dynamically adjusting the power supply voltage in response to the input signal amplitude. This approach revolves around the concept of tracking the signal envelope, maintaining the supply voltage slightly higher than the minimum requirement. In contrast to conventional power amplifiers with fixed supply voltages, which often result in power dissipation due to the discrepancy between the supplied and required power, envelope tracking can significantly enhance the efficiency and minimise wasted power. It operates by allowing the amplifier to function at a lower supply voltage when the input signal exhibits lower amplitudes, scaling up the voltage supply only in response to an increase in input signal amplitude.

The process involves splitting the input signal into two paths:

1. A direct amplification path where the input signal passes through to the amplifier.
2. An envelope detection path where the input signal is passed to an envelope detector, which subsequently modulates the amplifiers voltage supply in direct proportion to the input signals amplitude.

Precise phase alignment is required, however, between the two paths by adding an accurate phase delay on the amplifier path. Misalignment can lead to undesirable effects such as signal clipping, distortion, and wasted power which undermines the purpose of the technique.

There have been several iterations and improvements to the ET technique over the decades. Zhu discusses two further types of ET to improve efficiency:

1. Average Envelope Tracking (AET) whereby a long-term average is assessed and acted upon by the system. AET is discussed in greater detail by Staudinger [28] and Sahu [29].
2. Wide Bandwidth Envelope Tracking (WBET) whereby the instantaneous changes are tracked and responded to accordingly [30]. WBET is discussed in further detail by Hannington [31].

Zhu also employs signal detroughing, signal decresting, time alignment, digital predistortion and memory mitigation techniques to further augment the technique [30]. One problem with ET is that it requires a high bandwidth power supply, which becomes more difficult at higher operating frequencies.

The ET technique can be combined with other techniques to further improve the efficiency, Komatsuzaki et al. use digital predistortion (DPD) techniques with ET [32]. However, the Doherty power amplifier presented by Özen et al. which is directly compared with the work of Komatsuzaki et al. has superior performance [33]. Also

utilising DPD techniques, it has a higher modulation bandwidth, higher output power, higher efficiency, and lower adjacent channel leakage ratio (ACLR).

2.3.4 Envelope Elimination and Restoration (EER)

First proposed in 1952 by Kahn, the EER technique was originally designed as an alternative amplification technique which would reduce the need for linear RF amplifiers and increase amplifier efficiency [34]. It is still employed to this day in some applications.

The EER technique involves splitting the amplitude and phase components of an input signal and handling them separately. The phase element is amplified by a high-efficiency class C amplifier as the phase information has a constant envelope and is therefore suitable to a non-linear amplifier such as a class C. The most critical aspect of the EER technique is to accurately synchronise the amplitude and phase information at the output stage to ensure the input signal is faithfully reproduced after amplification.

The original technique from Kahn predates the development of other amplifier classes such as class D and class E which are inherently more efficient, and can have lower distortion, than class C.

The technique has a theoretically higher efficiency gain compared to other techniques such as envelope tracking but it is more complex and requires high quality components so cost might be a consideration.

Some researchers have expanded the breadth of EER and applied it to various amplifiers, including Vasić et al. [17] although they develop a 4-level power supply with a linear regulator to improve the system power supply efficiency. Not without its limitations though, the optimal voltage levels proposed by Vasic et al. seem erroneous

in the context of the 4-level implementation where only one voltage level falls below 0.5 times the maximum (normalised). Considering the signal power distribution, which follows a Rayleigh distribution, a more balanced allocation of voltage levels should be considered to effectively address the fact that most signal powers reside below the 0.5 threshold.

2.3.5 Digital Predistortion (DPD)

Non-linear behaviour in an amplifier can cause distortion so many of the techniques described so far are aimed at combating this behaviour. Digital predistortion (DPD) is another technique which was developed to improve this behaviour. It uses a digital signal processing algorithm to generate a signal which is the inverse of the characteristic amplifier distortion which is then added to the input signal with the aim of eliminating the distortion to significantly improve linearity. This also improves the intermodulation products and therefore the overall quality of the output signal. With modern signal processing techniques, the characterisation of the non-linear behaviour of an amplifier using known test signals is easy to achieve and therefore generating the inverse distorted signal is a relatively simple approach to significantly improve the system performance. It is a continuous process and involves constantly adjusting the predistortion signal in real-time based on the input signal. DPD can also improve the dynamic range of the amplifier, allowing it to operate at higher power levels whilst minimising distortion. It does, however, require a high level of computation and real-time analysis so software and a microcontroller or FPGA is key, inherently generating more complexity and barriers to usage.

2.4 OFDM

Orthogonal Frequency Division Multiplexing (OFDM) is a ubiquitous modulation scheme used all over the world in digital television, Wi-Fi, and LTE (long-term evolution) and was first introduced by Robert Chang of Bell Labs [35]. Its operation involves dividing the data stream into many subcarriers, each of these subcarriers are closely spaced together in the frequency domain. These subcarriers, carefully spaced and orthogonal to each other, mean that OFDM can achieve high spectral efficiency and high data rates whilst increasing robustness to interference. The scheme can also help to mitigate the effects of multipath fading, a common phenomenon in wireless communications which can cause errors [36]. By distributing data streams across an array of subcarriers, OFDM ensures that only small portions of data are at risk of loss. This feature enables the usage of efficient error correction mechanisms and packet retransmission strategies.

Being such a widely used modulation format, there exists a plethora of research with the aim of increasing OFDM system efficiency. A substantial field of research revolves around reducing the notoriously high PAPR. New techniques as well as new approaches to existing techniques are developed periodically.

Each subcarrier in an OFDM system can have modulation applied for data transmission. The most common modulation formats used are BPSK, 4QAM, 16QAM, 64QAM, 256QAM and 1024QAM although other formats are employed on occasion. 4QAM and QPSK are very similar, often used interchangeably. Higher orders of QAM have been tested and may become widely used in future, including 4096QAM up to 16384QAM to further increase data rates but as the order increases, challenges arise such as increased sensitivity to noise, susceptibility to intersymbol interference (ISI), and elevated PAPR.

Peak-to-average power ratio (PAPR) is a measure of the ratio of the maximum instantaneous power of the transmitted signal relative to the average power. PAPR depends on several factors including:

1. **Number of subcarriers**

   The higher the number of subcarriers, the higher the chance of constructive interferences at the peaks and troughs which leads to higher PAPR.

2. **Modulation scheme**

   Higher orders of modulation inherently have a higher PAPR than lower orders.

3. **Channel conditions**

   Environmental noise in the communication channel can constructively add to the level of subcarriers so can contribute to a higher PAPR especially if two or more of these noisy subcarriers combine. Signal reflections can also contribute to higher PAPR.

There are various techniques which have been developed over the last few decades to help to reduce the PAPR and improve the transmission power efficiency. This is still an active area of research.

For most QPSK and 16QAM OFDM transmissions, the peak-to-average power ratio (PAPR) tends to be between 10.3-11.6dB [37] [38] [39] when CCDF = 10^{-3} but theoretically in an OFDM system with 256 QPSK subcarriers, the maximum PAPR is 24dB, although this is extremely rare [40].

A high PAPR can have detrimental effects on the performance of a wireless communication system. The impact of PAPR becomes more significant as it increases, resulting in several problems, including:

1. **Increased Bit Error Rate (BER)**

   High PAPR introduces in-band distortion, leading to a higher (BER). This degradation in signal quality can result in errors in received data.

2. **Intermodulation Distortion (IMD)**

   High PAPR can introduce IMD or exacerbate existing IMD issues. This distortion can lead to out-of-band (OOB) radiation and interference, affecting neighbouring channels and causing further signal degradation.

3. **Nonlinear Distortion**

   Nonlinear distortion, induced by high PAPR, further increases the BER and degrades transmission quality. The nonlinear behaviour of amplifiers under high power peaks can result in signal distortion.

4. **Out-of-Band (OOB) Radiation**

   High PAPR introduces OOB radiation, which can interfere with adjacent channels. Harmonics of the desired signal can encroach into neighbouring channels, making it challenging to filter out this interference.

5. **Spectral Regrowth**

   Spectral regrowth occurs as a consequence of high PAPR, distorting the desired signal and further increasing OOB interference. This overall degradation in signal quality affects system performance.

6. **Increased Power Consumption**

   To handle the spikes in power associated with high PAPR, the system requires amplifiers capable of accommodating such variations. This leads to higher power consumption, reduced energy efficiency, and shorter battery life in wireless devices. Additionally, increased power handling requirements may result in larger component sizes and higher costs, impacting on manufacturing.

In summary, the detrimental effects of high PAPR encompass various aspects of system performance, from increased errors and interference to reduced energy efficiency and increased operational costs. Managing and mitigating high PAPR is essential to maintain the quality and efficiency of wireless communication systems.

2.4.1 PAPR Reduction Techniques

Over the decades, various techniques have been proposed to address the issue of high PAPR in OFDM systems. Some prominent PAPR reduction techniques include:

1. **Companding Transforms**

   Companding combines compression and expansion of the input signal. The high amplitude peaks of the signal are compressed, and the low amplitude parts are expanded. The purpose is to bring the highs down and push the lows up so the PAPR is reduced. However, this approach increases average power and introduces distortion.

2. **Partial Transmit Sequence (PTS)**

   PTS divides the signal into multiple sub-blocks and applies phase sequences to each block, this means the transmitter needs to generate several versions of the signal, each with a different phase sequence. The receiver then recovers the original signal by using an inverse of the transmitter phase sequence and combining the several transmitted signals. PTS has medium complexity but benefits from low distortion.

3. **Linear Block Coding**

   Linear block coding adds extra information to enable error correction at the receiver using a transmitted key, providing some PAPR reduction. This

technique is computationally simple so is easy to implement but offers less error correction capability compared to other techniques like LDPC.

4. **Low Density Parity Check (LDPC)**

   LDPC adds redundant bits to the data stream, primarily for error correction but also resulting in some PAPR reduction. Computationally, it is more complex than linear block coding.

5. **Turbo Coding**

   Turbo coding is a complex technique that employs multiple coding parameters to encode the original data, each of which is then decoded separately at the receiver and combined to provide a reliable recreation of the intended signal. While it provides robust error correction and some PAPR reduction, it demands significant computational resources. More complex than linear block coding and LDPC.

6. **Selective Mapping (SLM)**

   Bauml et al first introduced the idea in 1996 [41]. SLM involves selecting a signal with the lowest PAPR from multiple transmitted signals. Supplementary information is transmitted alongside the chosen transmit signal. This extra information is crucial for the receiver to be able to properly decode the data. It is therefore also critical that the supplement is received without error otherwise integrity of the decoding can be compromised. If the system has good error correction, then this issue is reduced considerably. Consequently, the added complexity and computational requirements mean that this PAPR reduction scheme is potentially less favourable compared to other more computationally efficient alternatives. While it adds complexity due to signal duplication, it does not introduce extra distortion. There have been various versions of this

technique over the years, including time-domain selective mapping (TD-SLM) [42] and sliding selective mapping (SSLM) [43].

7. **Peak Windowing**

   Peak windowing applies a window function to reduce high-power peaks, aiming to minimise distortion.

8. **Tone Injection (TI) and Tone Reservation (TR)**

   Similar techniques, both add a set of low amplitude tones to cancel out the high-power peaks, reducing overall PAPR by spreading the energy out, without significant distortion. But they do reduce the data throughput as some subcarriers are filled with redundant information.

9. **Interleaved OFDM**

   Divides the data stream into multiple sub-streams transmitted on different frequency subcarriers simultaneously. By interleaving the sub-streams, the system can overcome the effects of frequency selective fading and improve the reliability of the transmission. While complex to implement, it enhances performance in frequency selective fading channels.

10. **Active Constellation Extension (ACE)**

    Increases the number of symbols in a constellation diagram, offering a wider range of amplitude and phase combinations for data transmission, potentially increasing data rates or error correction capability.

11. **Clipping and Filtering (CF)**

    Clipping is the simplest way to reduce the PAPR of a signal. Signal components above a predetermined threshold are rejected. This does mean, however, that the signal is not accurately reproduced at the system output and some data will be lost. Clipping can also introduce in-band and out-of-band distortion. Filtering

can mitigate OOB distortion. The in-band distortion is not affected by filtering, so the system BER performance suffers. The in-band distortion can, however, be improved if robust error control parameters are employed [44]. Anoh et al use an iterative clipping method based on the Lagrange multiplier optimisation technique to further reduce the PAPR of an OFDM system, they achieved 0dB after 3 iterations [45]. The out of band distortion and BER performance were marginally improved, but this was not the aim of the research.

The choice of technique depends on factors such as performance requirements, complexity, implementation constraints, and system compatibility. Often, a combination of techniques is employed to achieve greater PAPR reduction, although this may require additional computational resources. Balancing these factors is crucial in selecting the most appropriate PAPR reduction strategy for a given OFDM system.

The 2011 work by Xu et al. presents the PDF of an OFDM signal, proving the Rayleigh distribution shape, which is also derived and used in this work [46]. Their proof uses an AWGN channel which again is used in this work in chapter 3 for the OFDM link.

2.4.2 OFDM Power Amplifiers

Ma et al. present an OFDM digital power amplifier with three different power amplifiers to achieve 8 different possible output power combinations based on analysis of the OFDM probability density function and quantise the signal envelope [47]. They split the input signal using a 3-way Wilkinson splitter and then recombine the output signal using a 3-way Wilkinson combiner, which introduces some loss on top of the switching losses of the transistors. In this thesis, however, an alternative power supply control technique for OFDM power amplifiers is proposed based on the probabilistic analyses

of the OFDM probability density function and combining it with the theory of multi-mark modular Golomb rulers, slicing the OFDM pdf to efficiently determine appropriate voltage switching levels.

Although elegant, the work by Ma et al. has several flaws in that the achieved efficiency of the resultant amplifier does not exceed the efficiencies of the referenced comparisons by Shi et al. [48] and Cao et al. [49]. From a commercial and manufacturing perspective, the configuration is awkward and the physical separation between each port of the power combiner increases the isolation and minimises interference, artificially increasing the achieved efficiency levels. It also operates only at a single frequency which is not useful for data transmission whereas the work by Shi et al. achieves a bandwidth of 1100MHz and the work by Cao et al. achieves a bandwidth of 1200MHz, both straddling some of the L-Band and S-Band designations.

2.5 Rulers and Difference Sets

2.5.1 Types and Definitions

There are several types of mathematical and geometric structure which improve the efficiency of the usual pervasive unit-marked rulers. These structures are intuitive and can be used to measure a large range of distances with a small number of marks at integer separations. These types of rulers contain a set of integers between 1 and X such that each measurable distance can be expressed as the difference between two of the marks. They include sparse rulers, Golomb rulers and difference sets. The key constructions for this work are Golomb rulers and difference sets and their variations. Sparse ruler – can have missing marks. A complete sparse ruler is one which can measure all distances up to its length.

Golomb ruler – a variation of a sparse ruler in which there must be no repeated measurements but there can be missing distances. Each distance that a Golomb ruler can measure must only be measurable in one way. Each distance between two pairs of marks must therefore be unique. A perfect Golomb ruler is one which can measure all distances up to its length [50]. Babcock's original research on Golomb rulers is still key to the understanding of these mathematical constructions [51].

Perfect difference set – must have no repeated measurements and must be able to measure all distances up to its length.

One of the main goals in the study of sparse rulers is to find sets of integers with as few markings as possible that can measure as wide a range of distances as possible. This is a challenging problem, as the number of possible combinations of integers grows exponentially as the number of markings increases.

2.5.2 Perfect Difference Sets (PDS)

A perfect difference set is a finite set of integers such that every non-zero integer in the set can be expressed as the difference between two distinct elements of the set, and the magnitude of each combination of differences is unique [52].

Perfect difference sets have a fundamental connection to the construction of good error-correcting codes in wireless communication systems and are utilised in many fields including cryptography, signal processing, and various narrower fields of physics.

Cyclic difference sets are special type of perfect difference set that can be represented as a subset of the integers modulo n, where n is some positive integer.

2.5.3 Golomb Rulers

Golomb rulers are related to sparse rulers but there are two key differences:

1. Where sparse rulers must cover all distances, Golomb rulers can miss differences.
2. Where sparse rulers can repeat distances between pairs of distinct integers, Golomb rulers cannot; the magnitude of each difference must be unique.

Given the power and incredible potential of Golomb rulers, they appear to be somewhat underutilised in a variety of applications. A few prominent applications of Golomb rulers include:

1. **Frequency-Hopping Spread Spectrum (FHSS)**

   FHSS communication systems use Golomb rulers to increase resistance to interference, improve security and make data transmission more reliable [53]**.**

2. **Information Theory**

   Used to construct efficient error-detecting and error-correcting codes by having unique constructions (the Golomb part) to remove ambiguity and optimise data compression, storage, and encryption [54].

3. **Radio Astronomy and Array Antenna Design**

   They are used to design optimal sequences for pulsar search algorithms. The radio telescopes are placed at Golomb marked intervals and the subtraction of received signals at each site can help determine the location of the source [55] [56].

4. **Spectroscopy**

   Golomb rulers are used to design optimal sequences for measuring frequencies of electromagnetic signals and combining lasers to achieve various output frequencies in the THz range [57].

5. **Crystallography**

   The field of x-ray crystallography utilises the special sequences to arrange the x-ray sensors in non-uniform positions to determine unique structures [58].

6. **Multi-Ratio Current Transformers**

   Golomb ruler structures can be used to efficiently place the tap points on a multi-ratio current transformer [59].

Optimum Golomb rulers were worked on by Robinson and is one which has no shorter equivalent of the same order [60]. There are two proven optimal 5-mark Golomb rulers:

0,1,4,9,11

0,2,7,8,11

Neither of which are perfect.

For this research, optimal linear rulers are not a subject of interest because the overall length is important. For voltages, a wide range with the fewest number of missing values is desirable. A short linear ruler like an optimal one isn't useful. Sparse rulers are also not of interest because repeated measurements are redundant, inefficient, and undesirable.

2.5.4 Modular Golomb Rulers (MGR)

A modular Golomb ruler (MGR), equivalent to a perfect difference set, is a variation of the standard Golomb ruler, one that follows modular arithmetic properties. The modular Golomb ruler may be constructed whereby the first and last marks occupy the

same space, and the ruler wraps around in a circular configuration. Considering the first mark on a linear Golomb ruler is always 0, the first mark on a modular Golomb ruler would be 0 and the integer denoting its length. This means that the order drops by 1. The rest of the construction of modular Golomb rulers is much the same as with the linear version. Indeed, the difference between each set of 2 marks must be unique to be a perfect MGR.

The key difference, however, is that their continuous nature enables a measurement to start at any mark on the ruler and finish at any other mark on the ruler and could be clockwise or anti-clockwise. This allows for a much greater number of distances to be measured.

Their construction enables a wider variety of potential uses and are again often employed in digital communications for producing error correcting codes and in cryptography for creating secure key exchange protocols.

Both of the optimal 5-mark linear Golomb rulers already mentioned are not perfect in their linear form but become perfect when translated into their modular equivalent, with the added benefit of becoming order 4 MGRs instead of order 5 linear Golomb rulers.

In 1938, Singer published a key paper “A Theorem in Finite Projective Geometry and Some Applications to Number Theory” [61] which describes a way of constructing perfect difference sets. The foundational mathematics for the theorem were laid out in 1857 by Kirkman [62]. The finite projective geometries in Singers 1938 paper have been used to construct Golomb rulers. Two alternative methods to achieve the same result were proposed by Bose-Chowla [63] and Rusza [64]. Babcock was perhaps the first to officially study the subject of Golomb rulers before they were formally named after Solomon Golomb, Babcock developed combinatorial designs for applications in

radar and radio astronomy in 1953 [51] which has similar constructions to typical Golomb rulers.

2.6 Conclusion

Close work by other researchers includes that of Ma et al. [47], Cao et al. [49], Vasić et al. [17], and Xu et al. [46] with other key work including Anoh et al. [45], Singer [61], Babcock [51], Bose and Chowla [63], Chang [35], and Doherty [19].

This chapter discusses various topics and areas of existing research which are relevant to this work. Initially, the different amplifier classes (A-E, and F-T) are outline including the achievable efficiencies of each, their uses are also described briefly. Next, the numerous existing amplifier efficiency enhancement techniques (including Doherty, Chireix, ET, EER, DPD) are discussed with specific examples of good implementation described.

The main focus of this work is on efficiency enhancement of OFDM signal amplifiers, so the modulation technique and subcarrier modulation formats are explained and the uses and problems of OFDM are presented. The main drawback with the OFDM modulation scheme is its high PAPR which causes several problems for system designers and communication channels. There are various mitigation techniques which have been developed over the decades and some of these are explained in greater detail in this chapter including companding transforms, PTS, linear block coding, clipping and filtering, and SLM.

Finally, sparse rulers, perfect difference sets, Golomb rulers, and modular Golomb rulers (MGRs) are discussed. The modular, or circular, versions of optimal Golomb rulers have 1 fewer mark than their linear counterparts, making them more efficient and enabling a greater number of distances to be measured. Some constructions of

Golomb ruler might have repeated measurements when translated to their modular equivalent which would mean they are no longer Golomb rulers, but some will still have no repeated distance measurements and will be able to measure every distance up to their length, in which case they are perfect MGRs.

The significance of modular/circular rulers extends beyond efficient mathematical and geometric constructs and their topology serves as the foundation for the power supply control system introduced in chapter 4. The Golomb structure is utilised in that there are a few marks which enable many possible output voltages, but most Golomb constructions are focused on being optimal in that they have a short length with no repeated distances with a secondary goal of maximising the number of measurements between 0-length. The structures in this work have the primary goal of maximising the length (the maximum possible output voltage) whilst ensuring each distance is covered between 0-length (each output voltage between 0-maximum, perfect rulers). Short rulers are therefore not desirable.

The next chapter describes the uses of OFDM, the effects of high PAPR and the different subcarrier modulation schemes in greater detail, using MATLAB to construct an OFDM transmission channel and generate relevant data. The second half of the chapter introduces the new probabilistic envelope tracking (PET) technique for optimising the voltage switching thresholds based on generated OFDM signals and significant calculations using MATLAB. The application of the technique to power supply control systems is briefly described before chapter 4 investigates this.

Chapter 3:
Probabilistic Envelope Tracking (PET)

3.1 Introduction

OFDM is a widely used multi-carrier digital modulation technique which divides the available bandwidth into multiple subcarriers. Each subcarrier is modulated independently by a modulation scheme such as QAM or PSK. The resulting subcarriers are then combined to form the OFDM signal where each subcarrier is orthogonal to its adjacent ones. This method of subcarrier modulation allows for efficient use of the available bandwidth. Some key advantages of the OFDM modulation scheme are:

1. **High Spectral Efficiency**

   The orthogonality of subcarriers means that each subcarrier can be spaced closer together than in some other modulation schemes. Each subcarrier is modulated independently which means that a much higher data rate is possible for the available bandwidth. High data rate applications such as digital television and wireless local area networks (LANs) benefit greatly from OFDM.

2. **Robustness to Multipath Fading**

   This is a common problem in wireless communication systems. Multipath fading occurs when a signal is reflected or scattered off obstacles before reaching the receiver. This can cause destructive interference, signal attenuation and distortion. If one subcarrier is affected by multipath fading, the likelihood of each subsequent subcarrier also being affected reduces exponentially and thus the overall signal quality is not affected significantly.

3. **Flexibility and Versatility**

   OFDM can be easily adapted to different channel conditions and modulation schemes. The number of subcarriers and the modulation scheme can be adjusted to suit the specific requirements of the system. This makes OFDM a versatile modulation technique that can be used in a wide range of applications. In some systems, the OFDM scheme can be dynamically adapted depending on the quality of the transmission link; the system can increase or decrease the modulation order automatically to maximise data rate and minimise errors.

4. **Resistance to Inter-Symbol Interference (ISI)**

   ISI is a form of distortion that occurs when the signal from one symbol interferes with the signal from the next symbol. OFDM is less susceptible to ISI than other modulation techniques because each subcarrier is modulated independently.

These factors combine to make OFDM an attractive modulation format for a wide range of wireless communication applications.

In this chapter, the results of a simulation of a full OFDM system using PSK and QAM subcarrier modulation is presented. The number of subcarriers, N, is chosen depending on the modulation order. The length of the cyclic prefix (CP) is also defined based on the number of subcarriers. The CP is a redundant portion of the OFDM symbol that is added to the beginning of the symbol as part of a guard interval to make the system more robust at the expense of data throughput. The SNR in dB is chosen from a wide array of values so that system performance can be evaluated across a range of link characteristics. The number of trials is also set large enough to generate reliable data.

The final part of the chapter determines the PDF of the amplitude of the signal power and the output voltage level switching threshold values are then sensibly calculated to maximise the system efficiency; this is the probabilistic envelope tracking (PET) technique.

3.1.1 Peak-to-Average Power Ratio (PAPR)

PAPR is a measure of the non-linearity of an OFDM signal and is calculated by taking the ratio of the peak power to the average power of the signal. It is a key parameter in OFDM system design because it can help to indicate efficiency in terms of power consumption and amplifier design. The high PAPR of an OFDM signal can cause several problems:

1. **High-Power Amplifiers**

   High PAPR signals require high-power amplifiers, which are often costly and inefficient.

2. **Distortion**

   High PAPR signals can cause distortion in the amplifier, which leads to signal degradation.

3. **Power Consumption**

   High PAPR signals mean increased power consumption, which can reduce the battery life of mobile devices as well as impacting on green credentials.

For these reasons, PAPR calculations are an important step in OFDM system design. They can be used to determine the efficiency of the system and to identify potential problems that may arise due to high PAPR. Reducing the PAPR is an interesting research topic and there are many ways in which this can be achieved, including clipping, companding, tone reservation/injection, and partial transmit sequence (PTS).

By understanding the PAPR value of the signal and the specific application, a designer can choose the most appropriate PAPR reduction technique for a particular system and can also optimise the transmission system's parameters such as the number of subcarriers, the modulation scheme, and the error correction.

3.1.2 Probability Density Function (PDF)

The PDF of the PAPR of an OFDM signal is a powerful statistical tool for studying the characteristics of the transmitted signal and is useful in the following ways:

1. **PAPR Estimation**

   The PDF can be used to estimate the PAPR of an OFDM signal, which is important for determining the efficiency of the system in terms of power consumption and analysing the quality of the amplifier design.

2. **PAPR Reduction**

   It can be used to evaluate the effectiveness of different PAPR reduction techniques. By comparing the PDF of the original signal with the PDF of the signal after a PAPR reduction technique has been applied, it is possible to determine which technique results in the lowest PAPR in each system.

3. **PAPR-Based Performance Analysis**

   The PDF can be used to study the relationship between the PAPR and other system performance parameters, such as the bit error rate (BER), error vector magnitude (EVM) or signal-to-noise ratio (SNR). This can be used to optimise the system's parameters for different scenarios.

3.1.3 BER and SNR

BER (bit error rate) versus SNR (signal-to-noise ratio) is a commonly used method for analysing the performance of a communication system. The BER is a measure of the number of errors that occur in a transmitted signal, and the SNR is a measure of the ratio of the signal power to the noise power which is effectively the signal quality. By plotting the BER versus SNR, it is easy to understand the system's performance under different conditions.

The BER versus SNR plot is useful in the following ways:

1. **Determining System Performance**

   By studying the system BER and SNR, it is possible to determine the system's performance under different conditions and therefore determine which system parameters might be best suited for a particular set of requirements.

2. **Optimising System Parameters**

   It is easy to see the effects of different system parameters on the system's performance. For example, by varying the modulation scheme or the number of subcarriers, it is possible to determine which parameters result in the lowest BER for a given SNR.

3. **Understanding System Robustness**

   BER decreases as the SNR increases, and the slope of the BER versus SNR curve can be used to determine the system's robustness against noise. A steeper slope, or indeed a curve shifted to the left, indicates that the system is more robust to noise interference.

4. **Determining System Efficiency**

   A system with a low BER and a high SNR is more efficient than a system with a high BER and a low SNR. A high BER results in the requirement of lots of resent data packets which means that the system efficiency is impacted in terms of throughput.

Robustness is a key characteristic to analyse for a system designer, if there are two systems with identical parameters in the same environment with the same SNR performance but one has a lower BER then it indicates that that system might have a better design and be more independent of noise and interference. The better designed system might be able to use lower power amplifiers and therefore save energy during use.

This chapter presents the MATLAB simulation outputs from a variety of experiments with OFDM signals. Focusing on 6 different modulated OFDM signals, namely BPSK, QPSK, 4QAM, 16QAM, 64QAM and 256QAM. The number of symbols per subcarrier increases from 2 to 256. BPSK is a simple modulation method which encodes each subcarrier with 2 symbols to represent data. Similarly, 256QAM encodes each subcarrier with 256 symbols with different amplitude and phase combinations.
4096QAM is employed in some systems but for the purposes of these simulations 256QAM was the highest modulation order which is easily visually represented.

$$QAM\ Order = 2^n \qquad (3\text{-}1)$$

$$where\ n = number\ of\ bits\ per\ symbol$$

Each symbol has a certain number of bits associated with it depending on the modulation order. Higher order modulation formats such as 64QAM compared to BPSK will enable a much higher data rate at the expense of minimum required SNR

to ensure parity of data transmission. With a low SNR during transmission, and with a noisy transmission link, higher order modulation formats become increasingly susceptible to interference and thus are more likely to lead to data errors. Low order modulations are very robust to interference and noise in a system.

Table 3-1: Characteristics of Various Modulation Formats

Modulation Scheme	**Number of Constellation Points**	**Bits per Symbol**	**Susceptibility to Interference**	**Data Rate**
BPSK	2	1	V. Low	V. Low
QPSK	4	2	Low	Low
4QAM	4	2	Low	Low
16QAM	16	4	Medium	Medium
64QAM	64	6	Medium	Medium
256QAM	256	8	High	High
1024QAM	1024	10	High	High
4096QAM	4096	12	V. High	V. High
16384QAM	16384	14	Extreme	Extreme

It is possible, and indeed is often employed in industry, to utilise an adaptive modulation scheme which monitors the quality of the transmission link and can dynamically adapt the modulation scheme to suit the conditions. If a link experiences a surge in noise and interference, then the system can change over to a lower order modulation format to ensure data transmission reliability. This could be due to something uncontrollable such as a dramatic shift in weather conditions or something more affected by humans such as a van parking directly in front of the transmitter or receiver. A 64QAM system which is experiencing a high bit error rate will ultimately reduce its throughput as a high number of packets will need to be sent again; therefore, dropping to 16QAM or 4QAM will reduce the maximum possible data throughput but also significantly reduce the BER (i.e. the requirement for duplicated packets) and thus

the data rate could actually improve somewhat. Sources of noise in a transmission channel can arise from a variety of factors including distance between transmitter and receiver, multipath fading, and direct and indirect competition in the channel causing spectrum congestion.

3.2 MATLAB Simulation

MATLAB was used to generate and simulate a transmission of a modulated OFDM waveform. The signals were constructed by generating pseudo-random data for each subcarrier and then modulating the subcarriers with the chosen modulation format. Then the OFDM signal was converted from the frequency domain to the time domain using an inverse fast Fourier transform (IFFT) and a cyclic prefix was added. The signal was then passed through an additive white Gaussian noise (AWGN) channel with the specified SNR value to mimic a real-world wireless communication link. The cyclic prefix was then removed, and the signal was translated back into the frequency domain by performing a fast Fourier transform (FFT). Finally, the signal was demodulated to extract the received data.

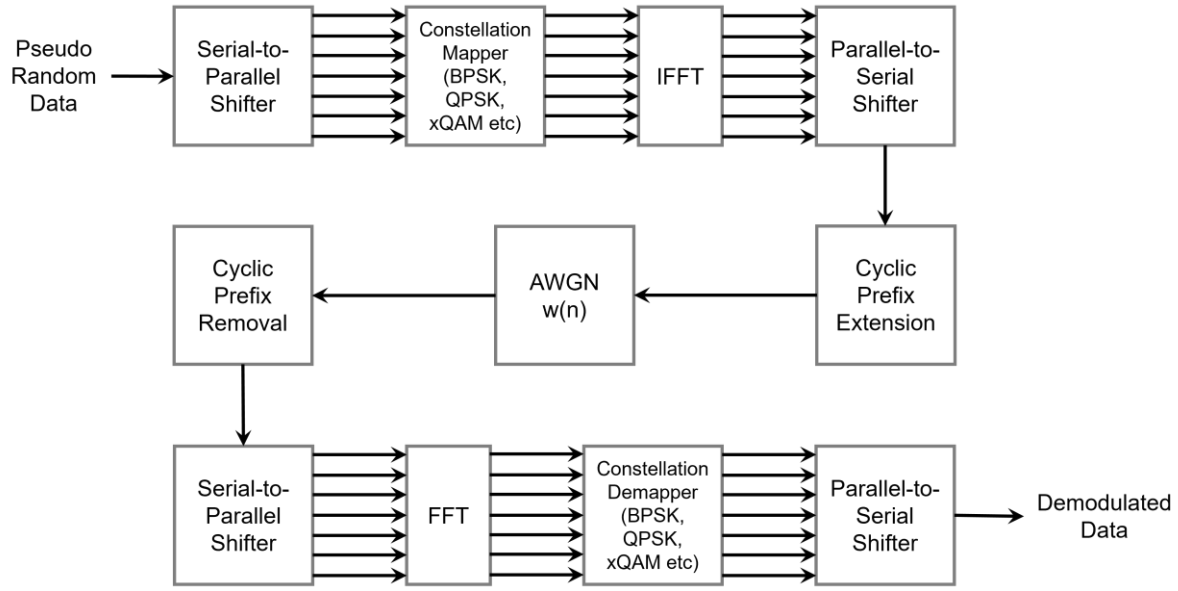

Figure 3-1: MATLAB OFDM Signal Generation and Transmission Flow Diagram

An OFDM signal transmission is simulated in MATLAB and statistically analysed, figure 3-1 depicts a flow diagram of the signal generation and transmission across an AWGN channel.

The PAPR PDF histograms for each of the modulation formats were generated in MATLAB, an extract of the code can be found in appendix A.

The Tx and Rx constellation diagrams, EVM and SNR simulations and diagrams were also generated in MATLAB, an extract of the code can be found in appendix B.

The PDF of the PAPR of a modulated OFDM signal follows a Rayleigh distribution which is shown in the MATLAB simulation results but also independently shown by other researchers, including Anoh et al [45]. The PAPR PDF is essentially the same as the power PDF which is used to determine the switching thresholds.

3.2.1 BPSK

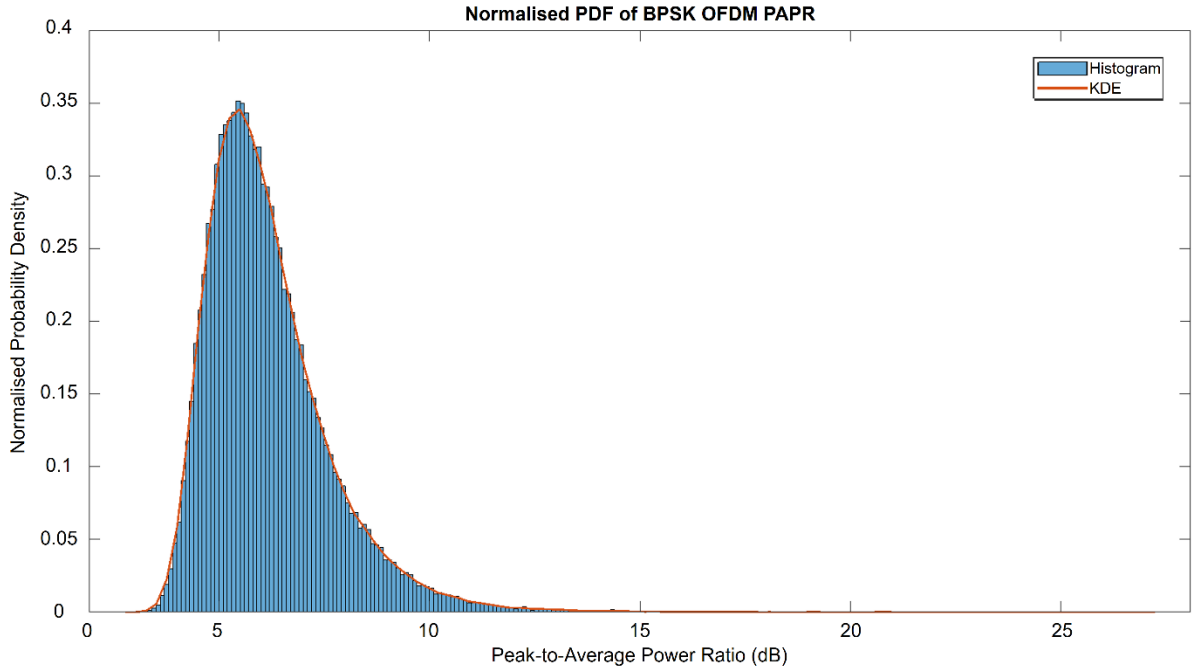

Figure 3-2: BPSK PAPR PDF Histogram

Figure 3-2 shows the PDF histogram of multiple OFDM signals where each of the subcarriers is modulated with BPSK, the shape is a Rayleigh distribution showing that most of the time an OFDM signal has a low PAPR value but infrequently it can be very high. The sample set is 100000 different random OFDM signals.

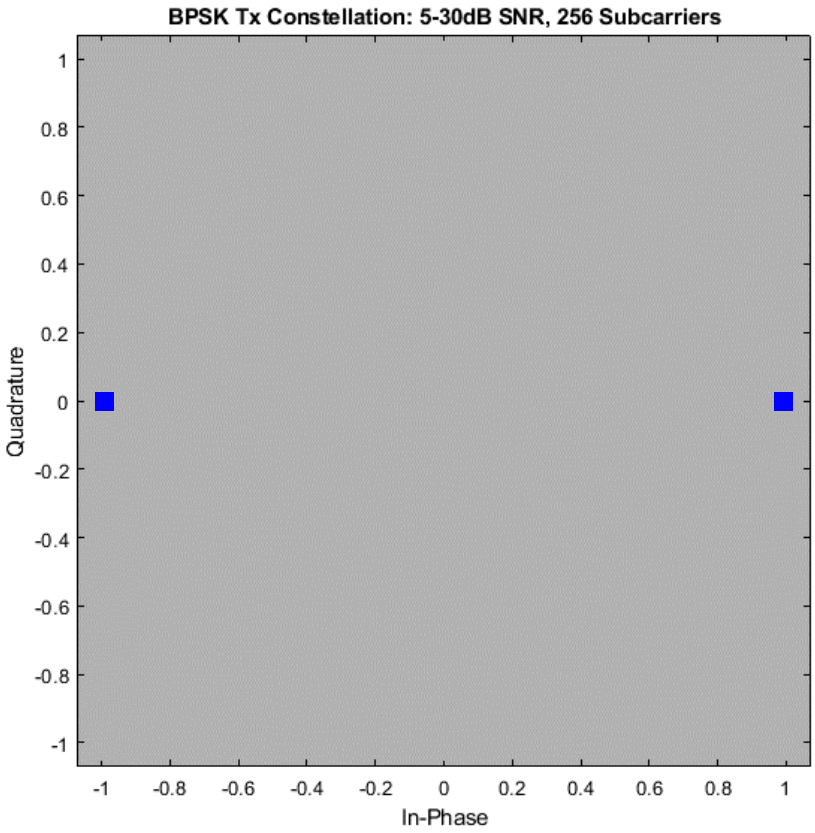

Figure 3-3: BPSK Tx Constellation Diagram

The two blue dots shown at (1,0) and (-1,0) in figure 3-3 are the Tx constellation points. BPSK is a very resilient modulation format although it does also have a low data rate when compared with higher order formats; it only has two distinct amplitude and phase combinations per symbol. It has a low susceptibility to outside interference regardless of low channel quality. 5dB SNR is extremely low for a transceiver system. With 10dB SNR, the constellation already indicates there are no errors whatsoever, a 0 BER. This shows that BPSK can work well in noisy environments and over long distances. The constellation points at 15dB SNR are tightly spaced and highly coherent.

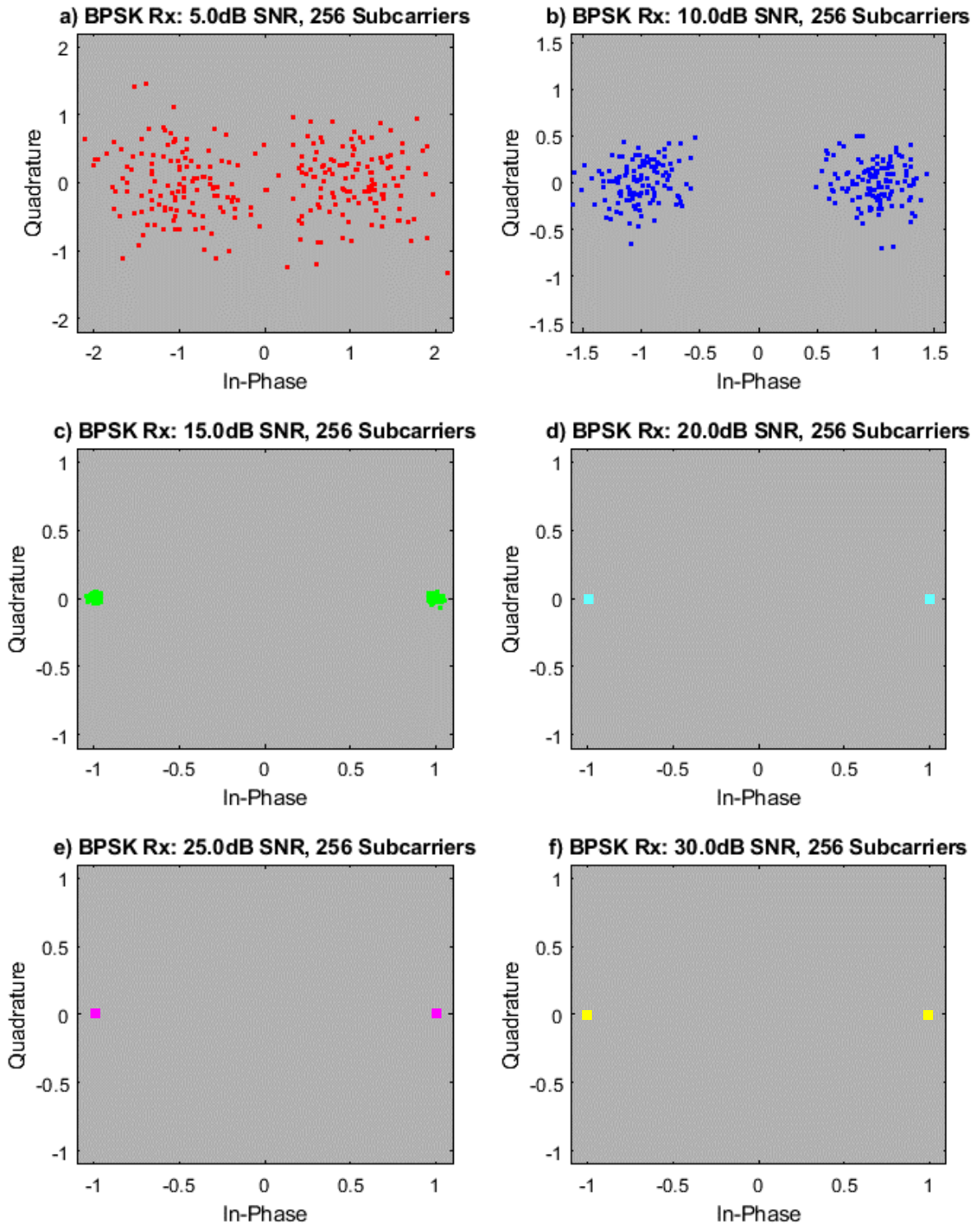

Figure 3-4: BPSK Rx Constellation Diagrams for 5-30dB SNR, 256 Subcarriers

3.2.2 QPSK

QPSK doubles the data rate achievable with BPSK due to having two bits per subcarrier compared to one. There are now four constellation points compared to two, these are the four different amplitude and phase combinations. Much the same as BPSK, QPSK has a high resilience to interference.

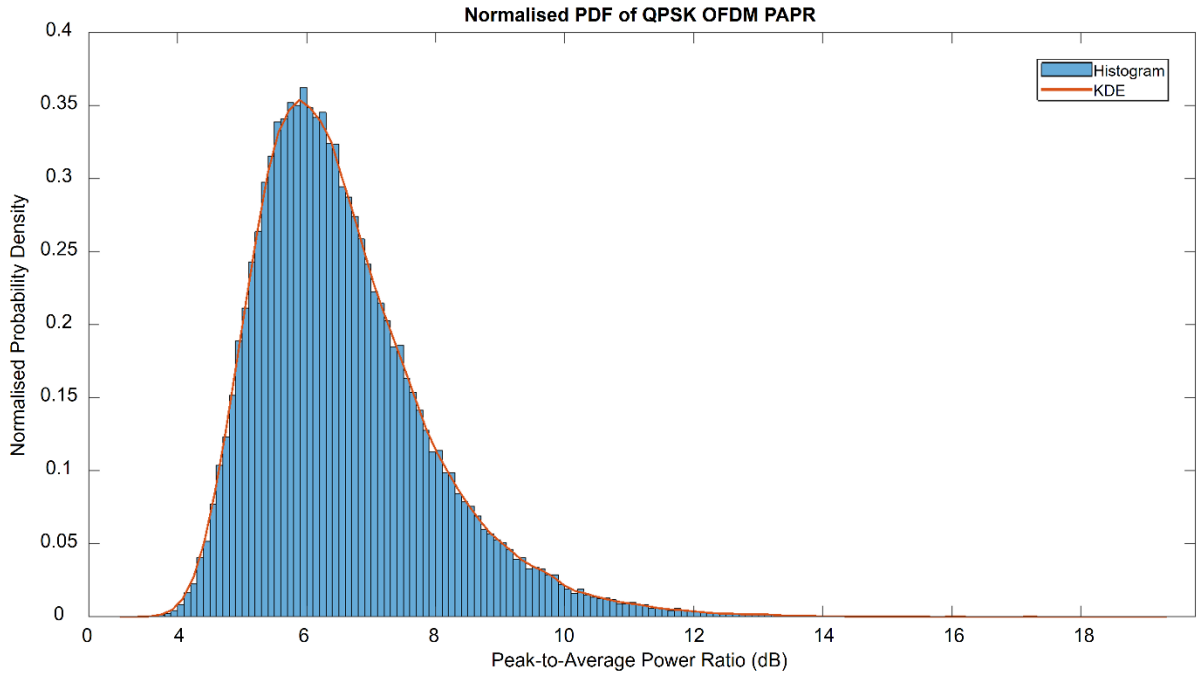

Figure 3-5: QPSK PAPR PDF Histogram

The probability of a PAPR above 10 or 12dB is extremely unlikely. This again shows a Rayleigh distribution.

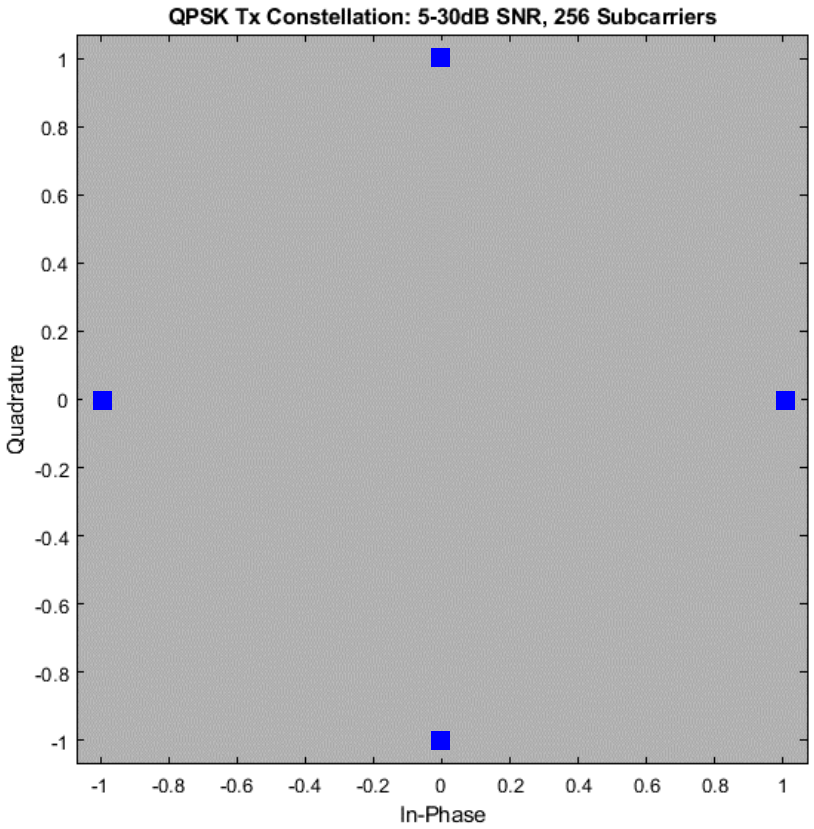

Figure 3-6: QPSK Tx Constellation Diagram

The four constellation points are shown as blue dots at (1,0), (0,1), (-1,0) and (0,-1). With 10dB SNR there are still a few errors experienced but not many. 15dB SNR eliminates errors and shows a good level of coherence between the constellation points.

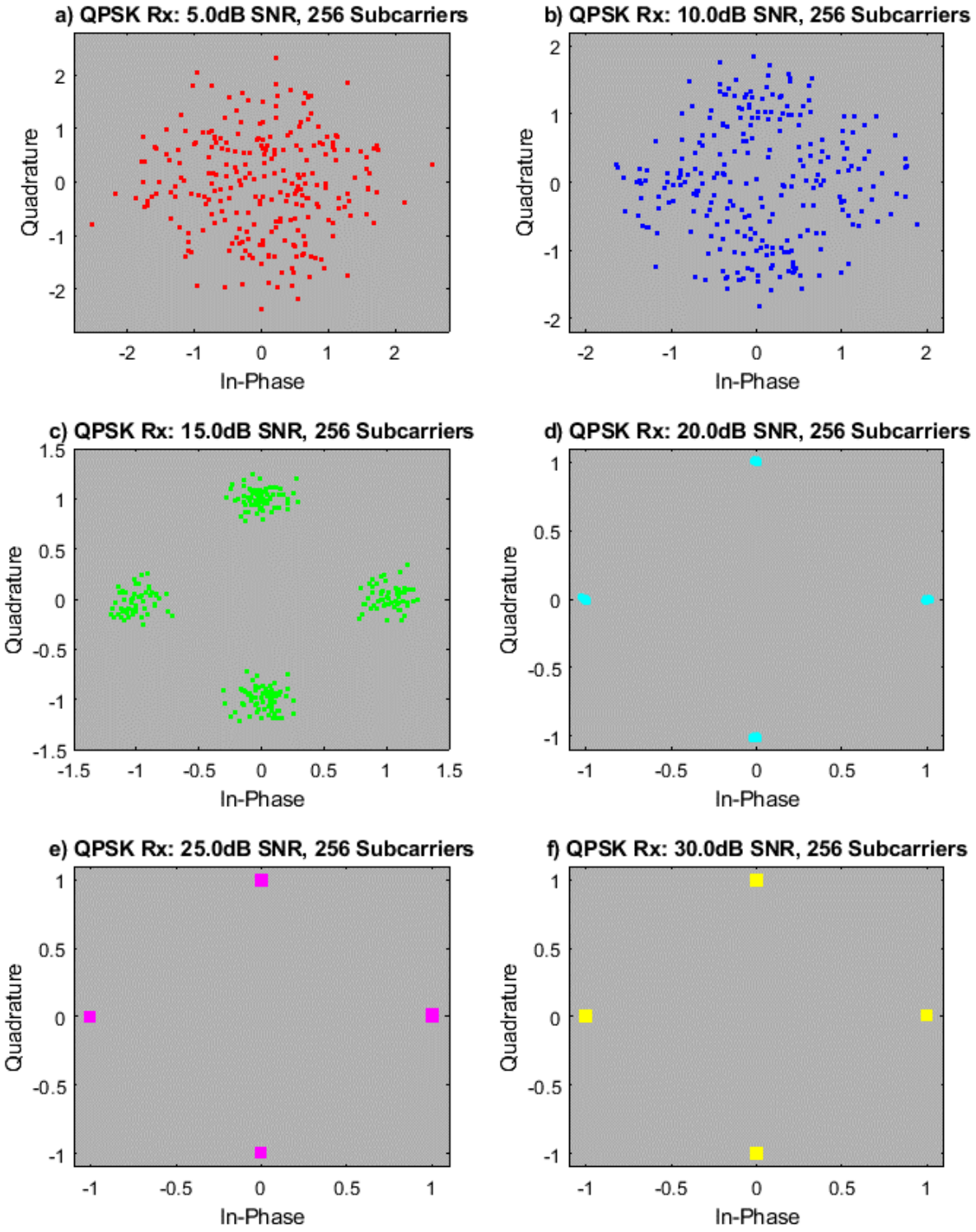

Figure 3-7: QPSK Rx Constellation Diagrams for 5-30dB SNR, 256 Subcarriers

3.2.3 4QAM

4QAM and QPSK are very similar in construction and are of the same order, but the constellation point locations are different, meaning that the amplitude and phase combinations are different.

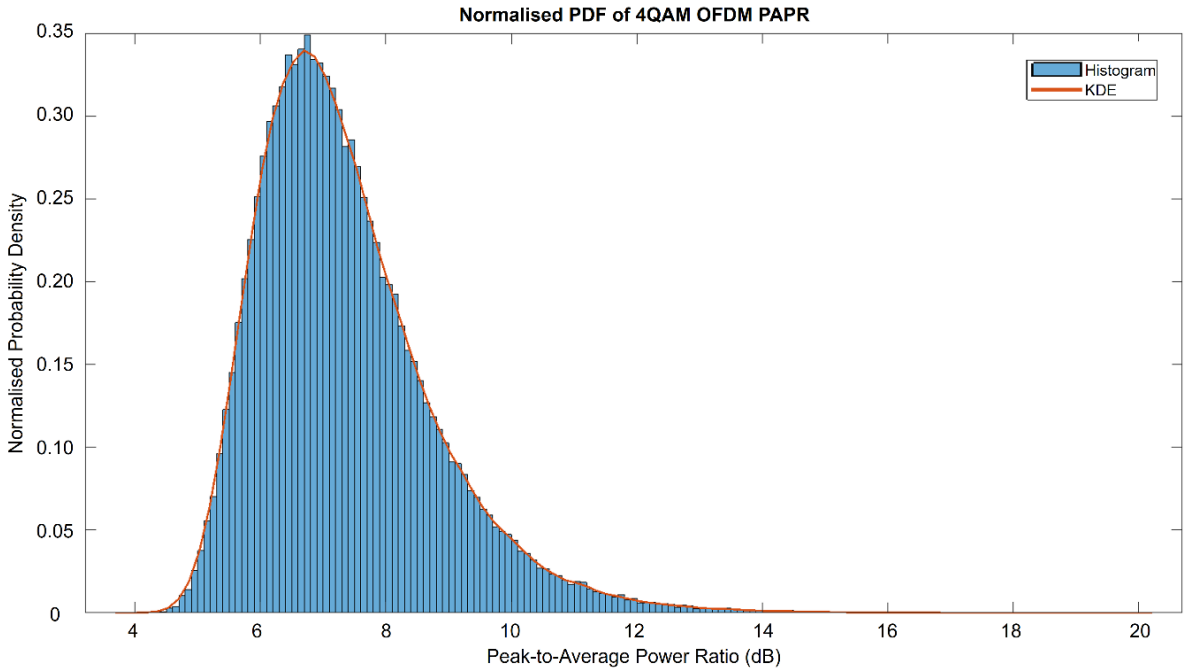

Figure 3-8: 4QAM PAPR PDF Histogram

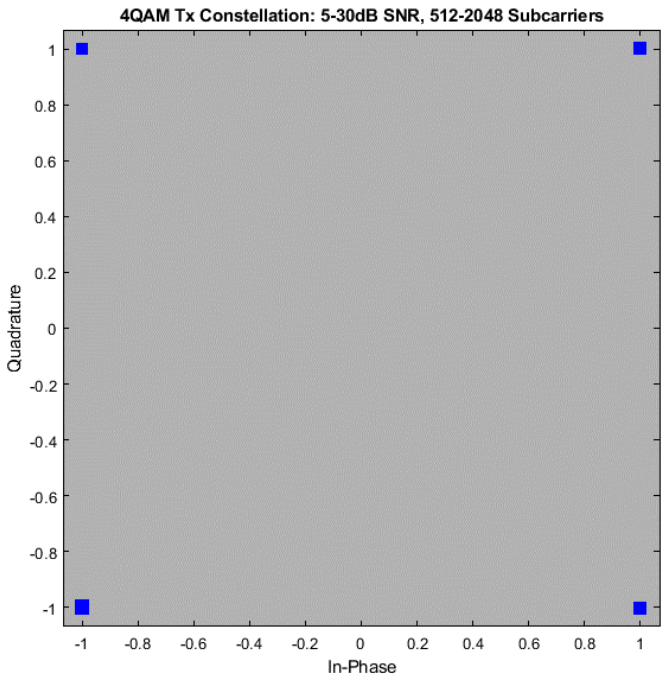

Figure 3-9: 4QAM Tx Constellation Diagram

The four constellation points are shown as blue dots at (1,1), (-1,1), (-1,-1) and (1,-1).

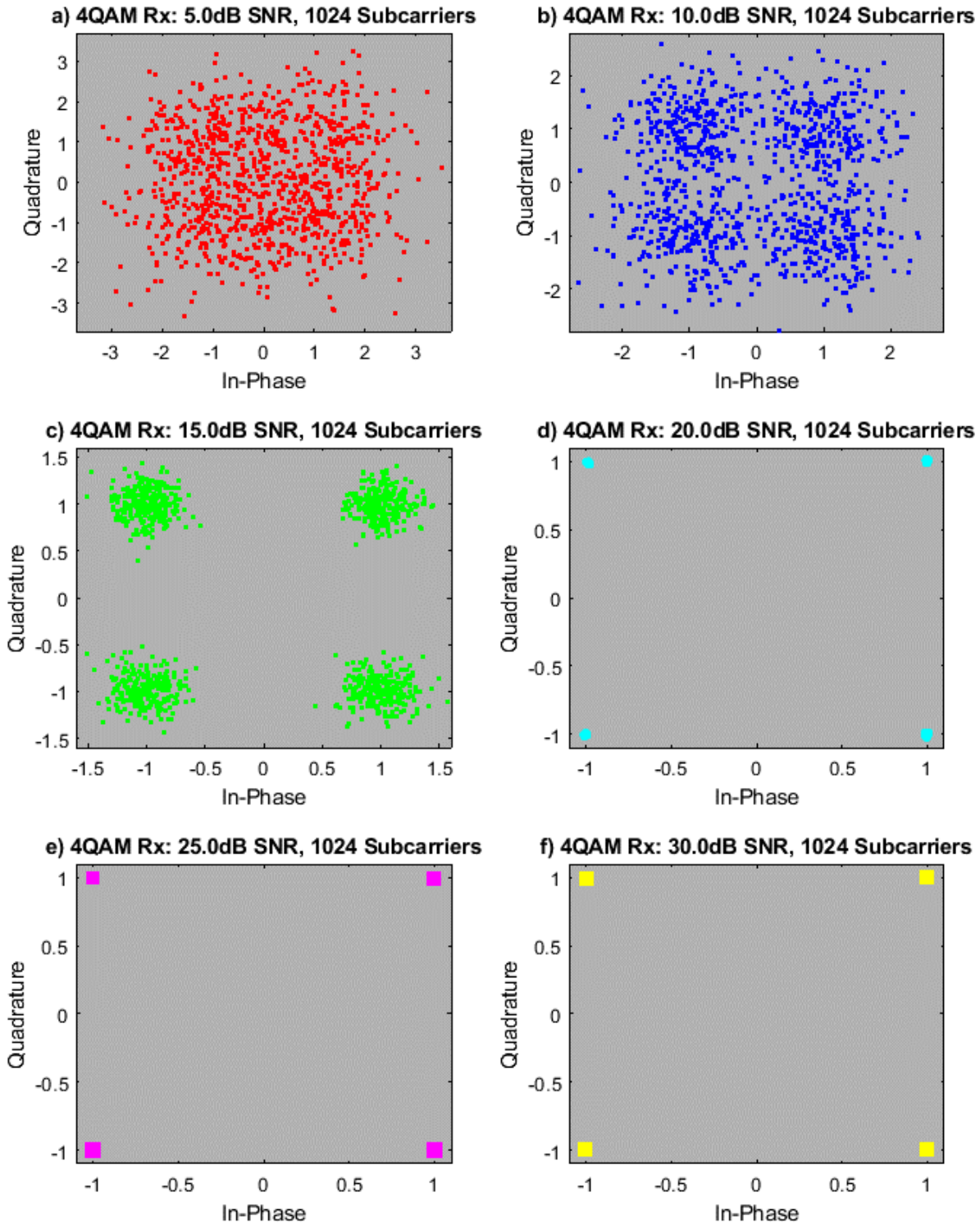

Figure 3-10: 4QAM Rx Constellation Diagrams for 5-30dB SNR, 1024 Subcarriers

3.2.4 16QAM

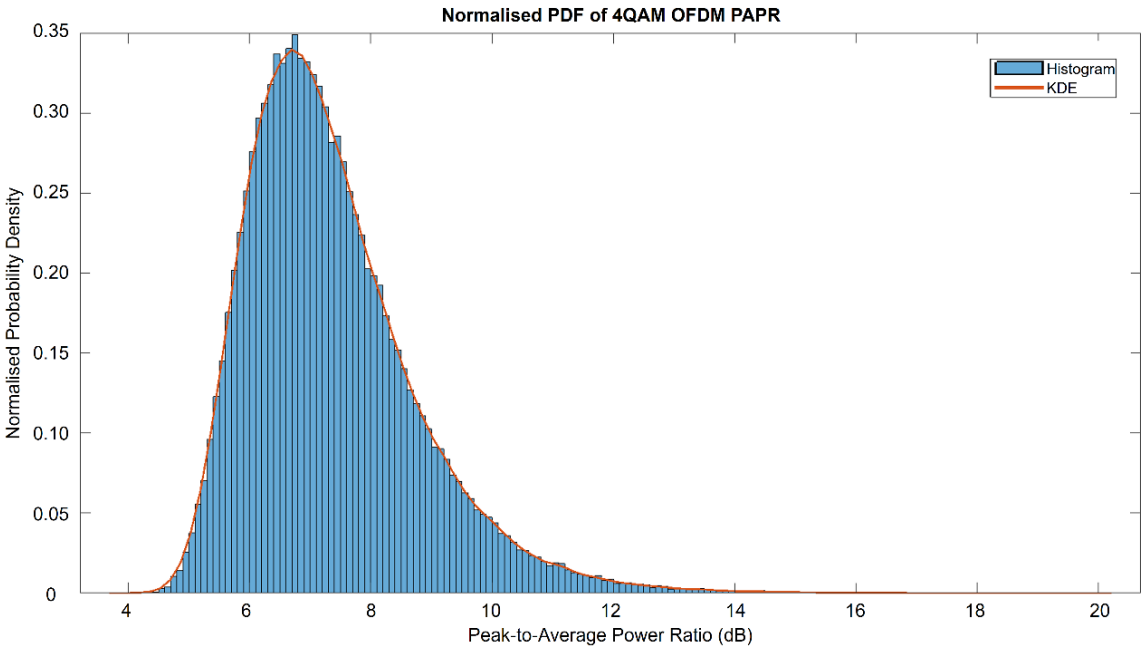

Figure 3-11: 16QAM PAPR PDF Histogram

The probability of higher orders of PAPR increase with 16QAM compared to the lower orders but the probability is still extremely low that a very high PAPR will occur.

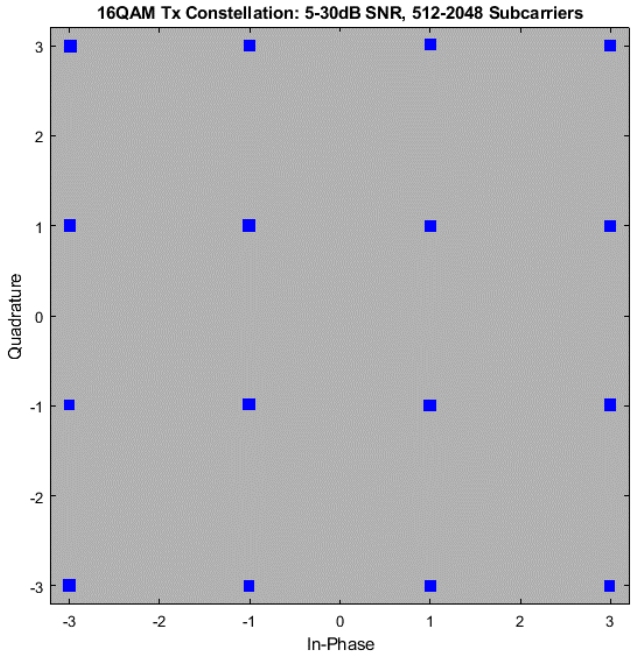

Figure 3-12: 16QAM Tx Constellation Diagram

There are sixteen different amplitude and phase combinations. The sixteen constellation points are shown as blue dots in the locations shown in figure 3-12.

Table 3-2: 16QAM Constellation Points in 4 Quadrants

Quadrant #	Quadrant Definition	Coordinates
Q1	x > 0, y > 0	(1,1), (1,3), (3,1), (3,3)
Q2	x < 0, y > 0	(-1,1), (-1,3), (-3,1), (-3,3)
Q3	x < 0, y < 0	(-1,-1), (-1,-3), (-3,-1), (-3,-3)
Q4	x > 0, y < 0	(1,-1), (1,-3), (3,-1), (3,-3)

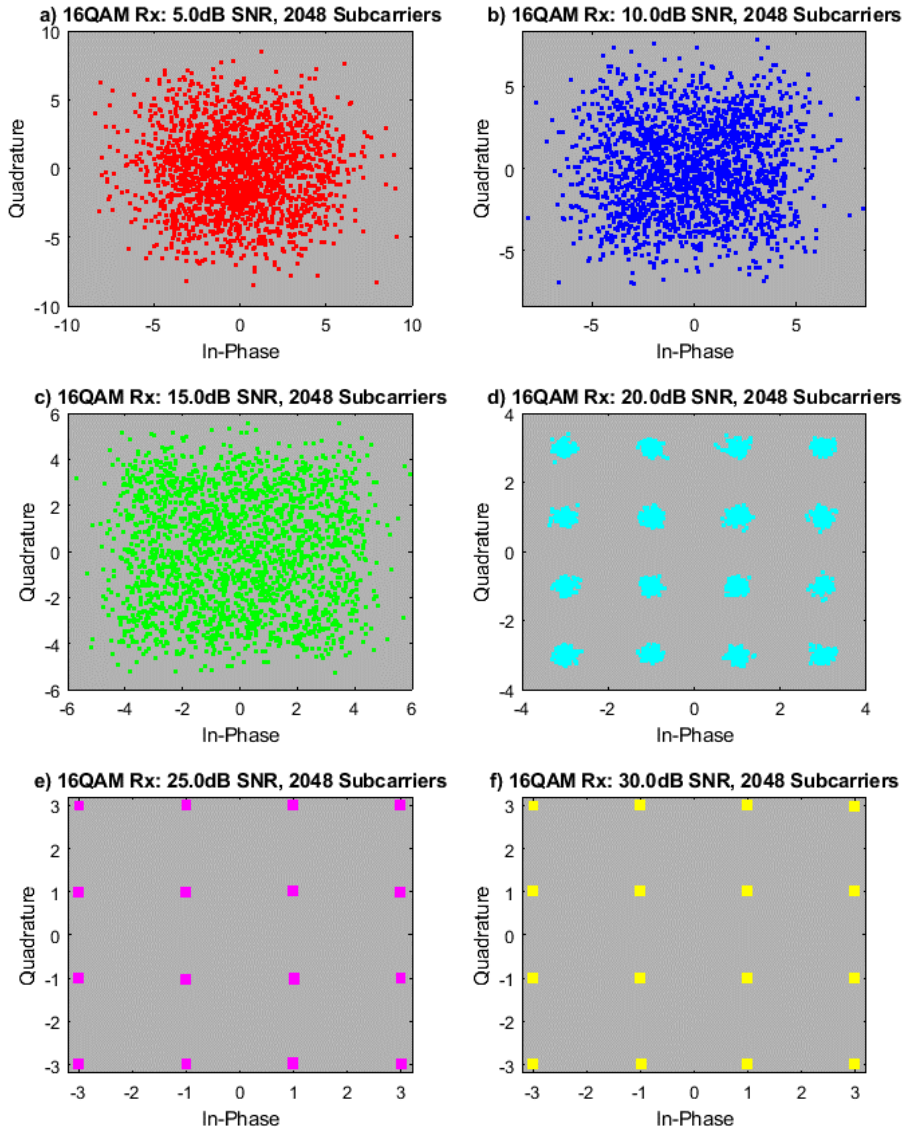

Figure 3-13: 16QAM Rx Constellation Diagrams for 5-30dB SNR, 2048 Subcarriers

For 16QAM, a 15dB SNR is not sufficient to produce a clean output signal with no errors or requirements for duplicated packets. At 20dB SNR, the constellation diagram shows a tight grouping of received points.

3.2.5 64QAM

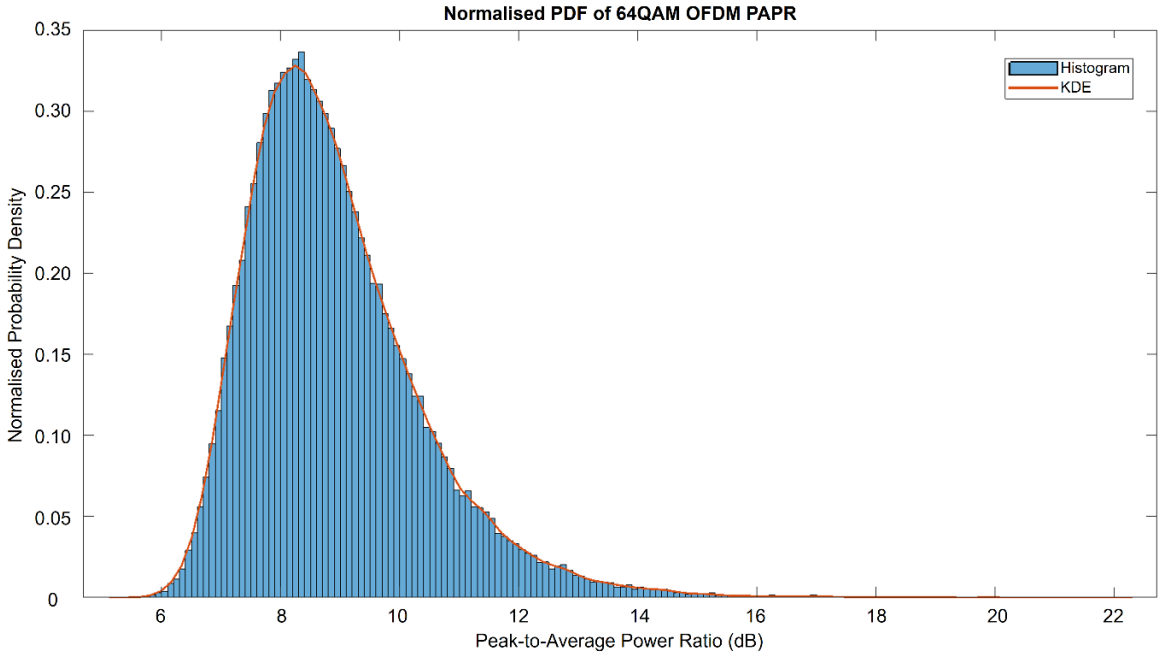

Figure 3-14: 64QAM PAPR PDF Histogram

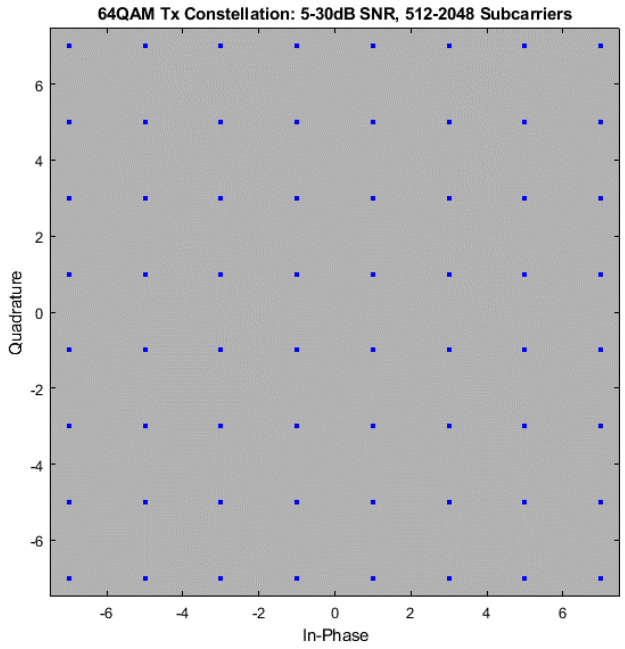

Figure 3-15: 64QAM Tx Constellation Diagram

Figure 3-15 shows a clean 64QAM transmission constellation diagram. There are 64 different amplitude and phase combinations with this modulation order.

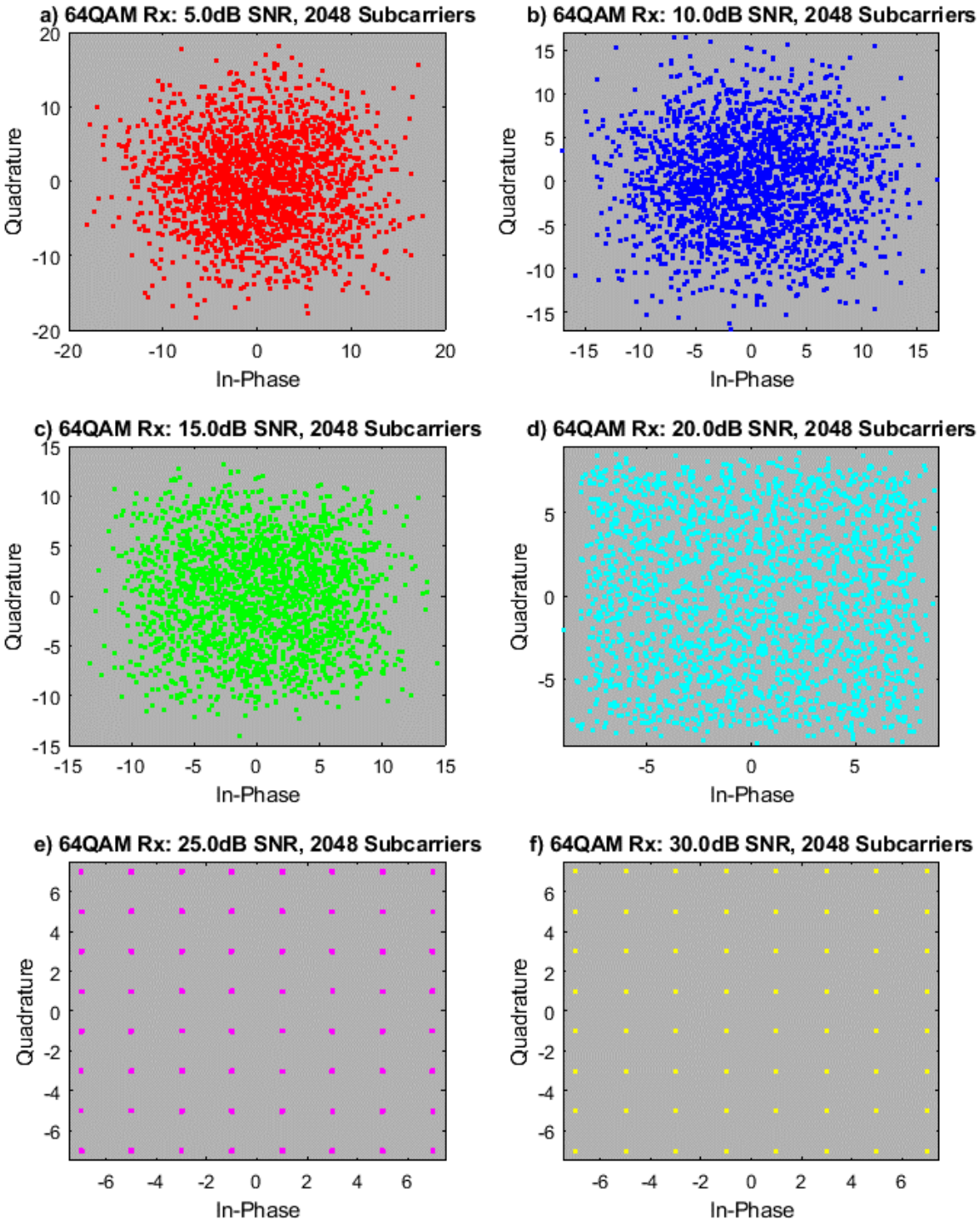

Figure 3-16: 64QAM Rx Constellation Diagrams for 5-30dB SNR, 2048 Subcarriers

For 64QAM, the SNR must approach 25dB before the system can reliably produce no errors. The modulation format is unusable in an environment where the SNR is below 20dB. In those cases, it is advisable to reduce the modulation order down to 16QAM to achieve a satisfactory communication link.

3.2.6 Modulation Order Comparisons

Figure 3-17 to figure 3-21 show the comparisons between the various modulation types and orders: BPSK, 4QAM, 16QAM, 64QAM, 256QAM.

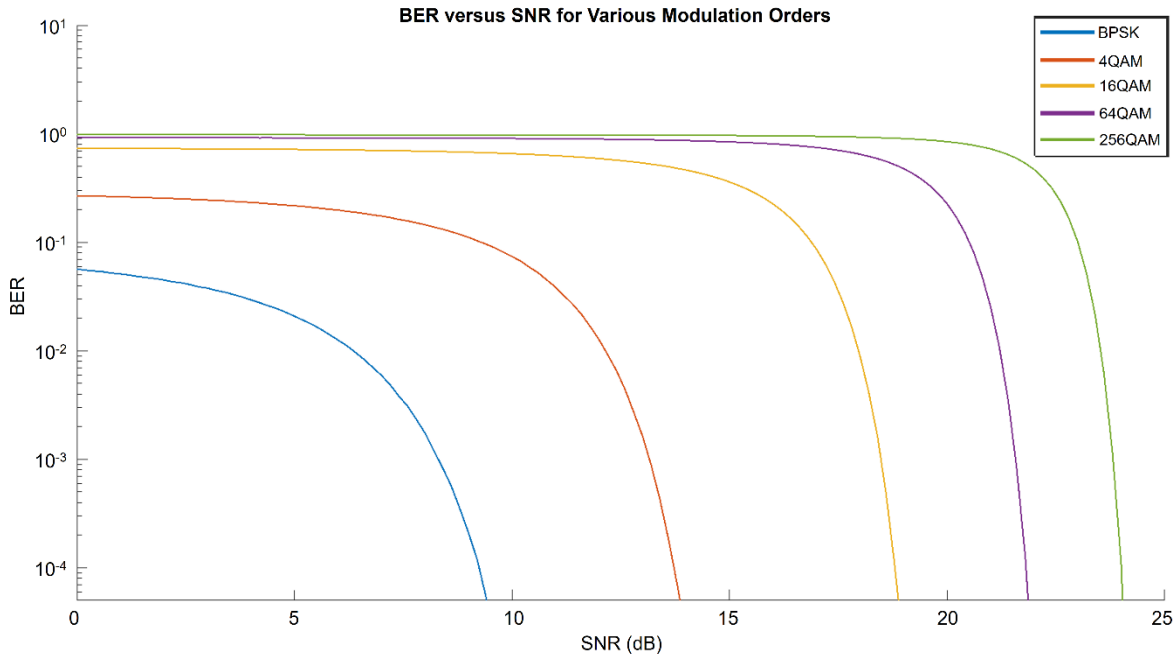

Figure 3-17: BER Versus SNR for Various Modulation Orders

Figure 3-17 shows the BER versus SNR for BPSK, 4QAM, 16QAM, 64QAM and 256QAM. BPSK can still produce good results in an extremely poor channel where the noise floor is significant, for example when the SNR is only 5dB. For higher order modulation formats, the BER is considerable until nearer 20dB SNR. The knee of the curves for 4QAM, 16QAM, 64QAM and 256QAM are approximately 11dB, 17dB, 20dB and 22dB, respectively.

shows the ETSI recommendation to achieve a BER of $2x10^{-4}$ in an AWGN channel [65] for QPSK, 16QAM and 64QAM as these are the most used modulation formats in UK digital video broadcasting (DVB). The recommendation range is dependent on the FEC rate.

Table 3-3: QPSK, 16QAM and 64QAM SNR Requirements for BER = 2x10-4

Modulation Format	Simulated Required SNR (dB) for BER = $2x10^{-4}$ in AWGN	ETSI Recommendation (dB)
QPSK	10.2-13.6	3.5-7.9
16QAM	18.7	9.3-14.4
64QAM	21.8	13.8-20.2

There are wide ranges for the recommendations depending on the type of chosen transmission structure. ETSI also have recommendations for Ricean and Rayleigh channels.

To calculate the error vector magnitude (EVM) the errors in I and Q values must first be determined between the received symbols and the transmitted symbol.

$$I_{err} = I_{Tx} - I_{Rx} \qquad (3\text{-}2)$$

$$Q_{err} = Q_{Tx} - Q_{Rx} \qquad (3\text{-}3)$$

The magnitude of the error is thus found by taking the square root of the sum of the squares of the in-phase and quadrature components:

$$Magnitude_n = \sqrt{{I_{err}}^2 + {Q_{err}}^2} \qquad (3\text{-}4)$$

For multiple symbols as in real-world wireless communication systems, all symbol EVM contributions must be factored into the calculation.

$$Magnitude_{total} = \sqrt{\frac{1}{N}\sum_{n=0}^{N-1} {I[n]_{err}}^2 + {Q[n]_{err}}^2} \qquad (3\text{-}5)$$

$$where\ n = symbol\ index$$

$$and\ N = number\ of\ symbols$$

Therefore, the EVM calculation for the system as a percentage is as follows.

$$EVM(\%) = \frac{Magnitude_{total}}{Normalisation\ Reference}\ x\ 100 \qquad (3\text{-}6)$$

The EVM can be converted from the percentage value to dB:

$$EVM(dB) = 20\log_{10}\left(\frac{EVM(\%)}{100}\right) \quad (3\text{-}7)$$

By subtracting the received signal (vector) from the transmitted signal (vector), the error vector for each of the data points can be obtained. The error vector magnitude (EVM) for each of the modulated signals can then be calculated.

$$Signal\ Error = Tx\ Signal - Rx\ Signal \quad (3\text{-}8)$$

$$EVM(dB) = 20\log_{10}\left(\frac{Signal\ Error}{Tx\ Signal}\right) \quad (3\text{-}9)$$

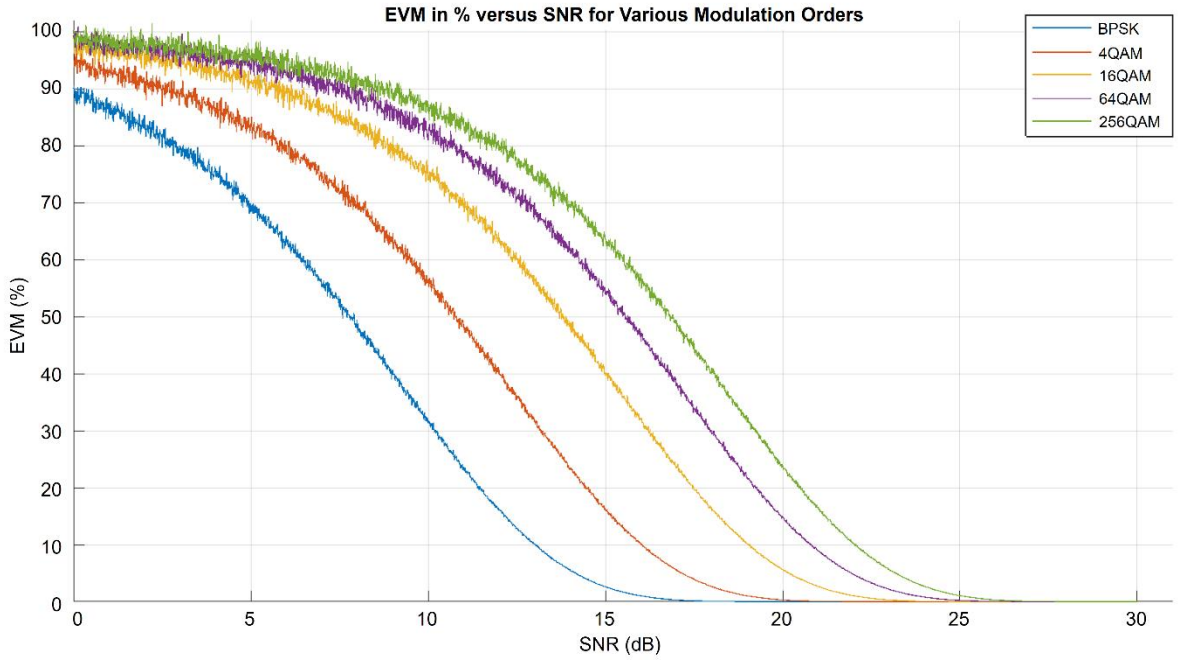

Figure 3-18: EVM in % Versus SNR for Various Modulation Orders

Figure 3-18 shows the EVM in % for the same modulation orders. There is a large spread of values when the SNR is low, this is due to the uncertainty within the system across multiple iterations. As the SNR increases, and EVM decreases, however, the accuracy increases.

ETSI define the requirements for the EVM in their published 5G new radio user equipment conformance specification document as in table 3-4 [66].

Table 3-4: ETSI EVM Conformance Specification

Modulation	EVM (%)
QPSK	17.5
16QAM	12.5
64QAM	8
256QAM	3.5

The acceptable level of EVM for higher orders of modulation are a much stricter requirement, as shown by the 256QAM recommendation of just 3.5% compared to the lower orders. For this AWGN channel simulation, the recommended ETSI EVM values correspond to the SNR values shown in table 3-5. The chosen EVM column is a nominal value which makes it a tighter requirement to ensure a good quality of transmission.

Table 3-5: SNR Values Corresponding to ETSI EVM Recommendations and Chosen Level

Modulation	ETSI EVM (%)	Corresponding Simulated SNR (dB)	Chosen EVM (%)	Corresponding Simulated SNR (dB)
QPSK	17.5	14.8	15	15.2
16QAM	12.5	18.6	10	19.1
64QAM	8	21.2	6	21.7
256QAM	3.5	23.7	2.5	24.1

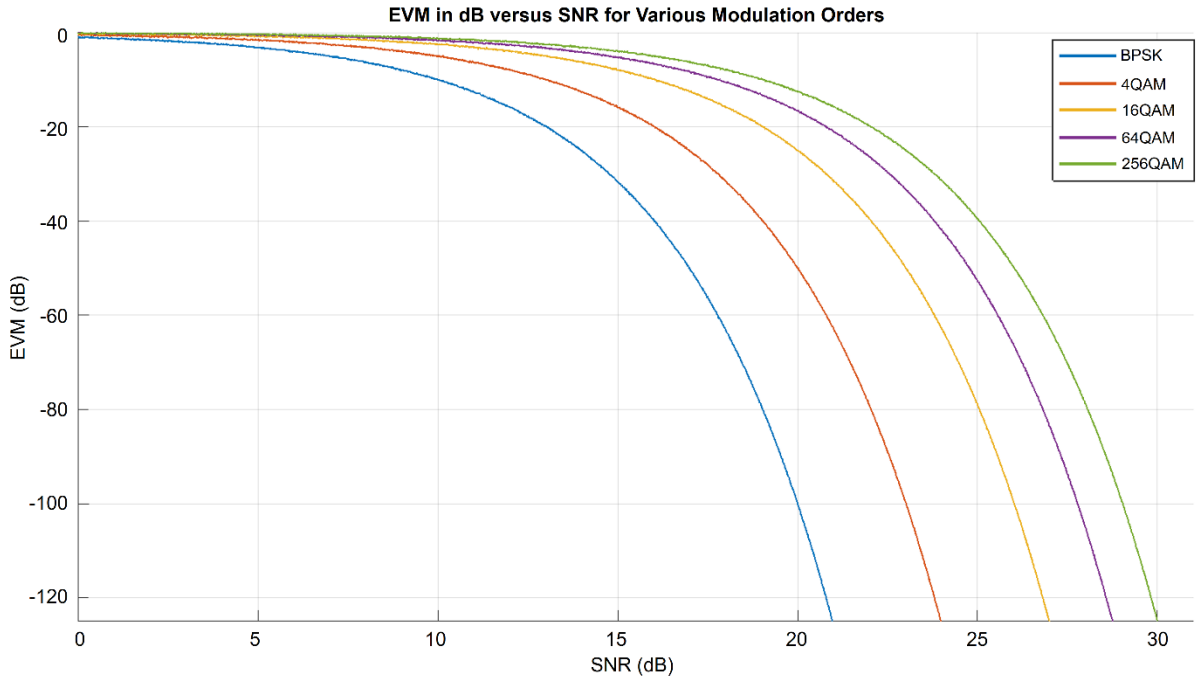

Figure 3-19: EVM in dB Versus SNR for Various Modulation Orders

Figure 3-19 shows the EVM in dB plotted against the SNR between 0-30dB for the various modulation orders.

Table 3-6: SNR Values Corresponding to EVM (dB) Values

Modulation	SNR (dB) 1	EVM (dB) 1	SNR (dB) 2	EVM (dB) 2
QPSK	14.8	-14.8	15.2	-16.4
16QAM	18.6	-18.1	19.1	-20.4
64QAM	21.2	-21.9	21.7	-24.6
256QAM	23.7	-29.3	24.1	-32.1

Table 3-6 shows the corresponding EVM values in dB for the SNR values from table 3-5.

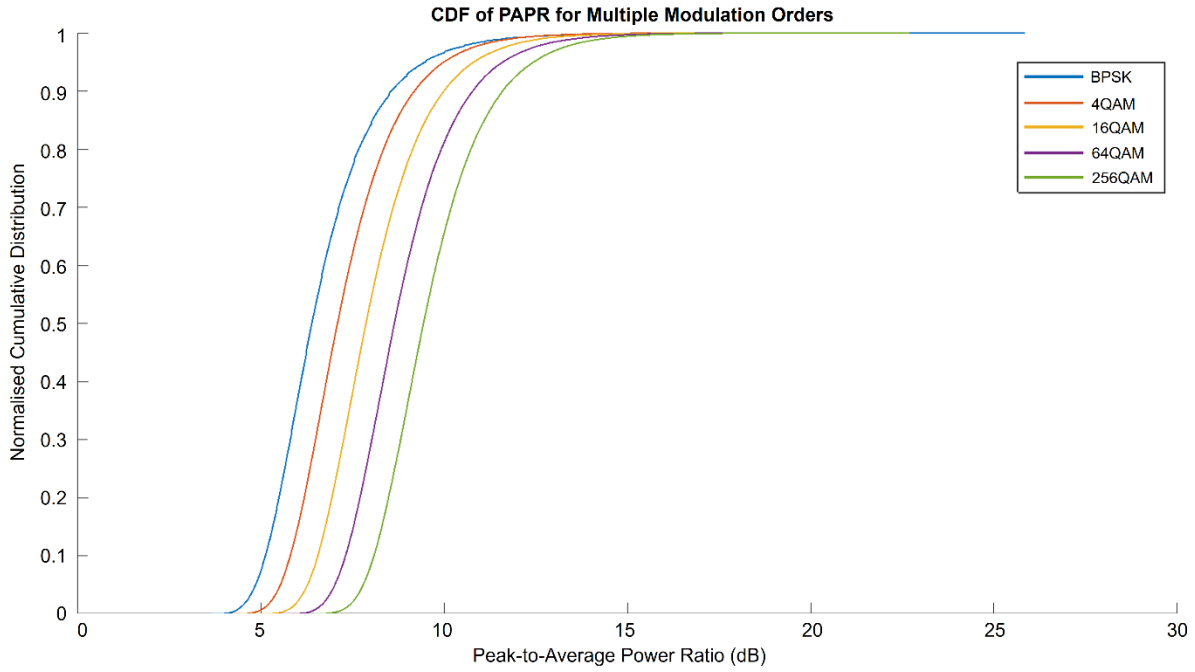

Figure 3-20: CDF of PAPR for Multiple Modulation Orders, Linear Y-Axis

Figure 3-20 shows the normalised cumulative distribution function showing that most of the time the PAPR is at low values as indicated by the steep curves between 5-10dB for all modulation formats. The tail off at high PAPR values resembles an asymptotic relationship up to its maximum PAPR value.

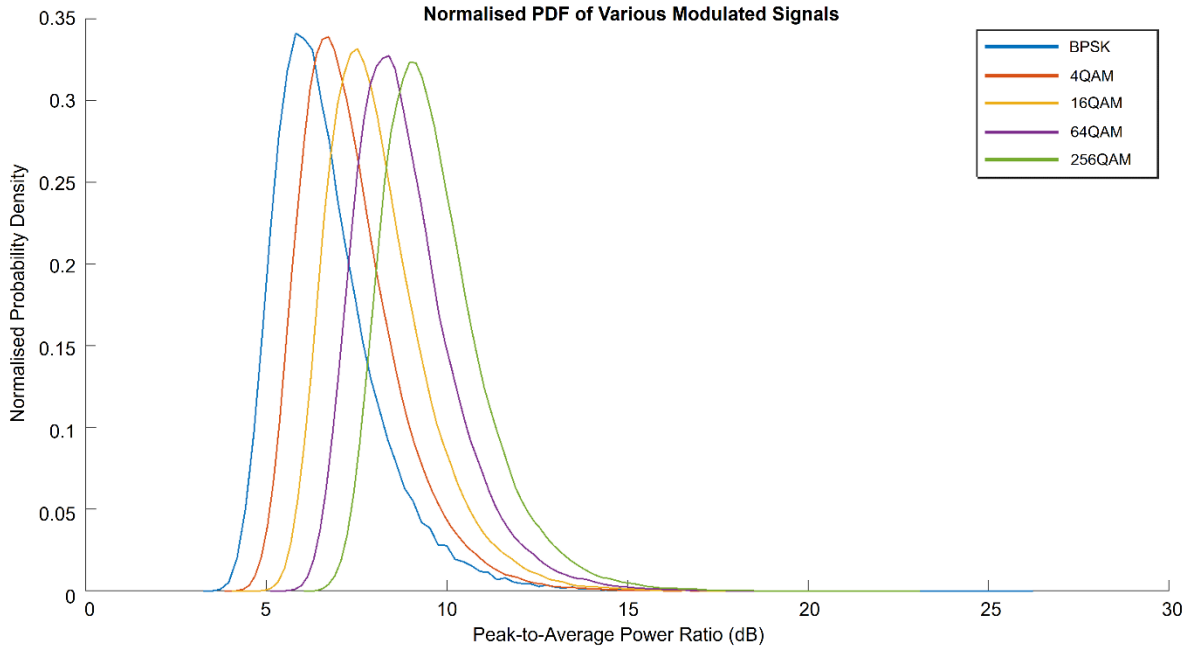

Figure 3-21: Normalised PDF of PAPR of Various Modulated Signals

Figure 3-21 shows the overlaid histogram kernel density estimations for 5 simulated modulated signals. As the modulation order grows, the variance and standard deviation increase, meaning that the spread of each distribution grows, becoming wider and flatter, and therefore having a lower peak probability density value. Figure 3-20 and figure 3-21 show a consistent shift to the right with each higher order modulation format, indicating that the average PAPR increases as the number of symbols increases. One property of the Rayleigh distribution is that the distribution shifts to the right and increases in spread as the number of terms increases, so as the number of subcarriers increases which is the case with higher order QAM signals.

The lowest, average, and highest simulated PAPR values for each modulation format are shown in table 3-7. This is again data from 100000 iterations of the Tx-Rx link (signal generation, modulation, transmission, and demodulation).

Table 3-7: PAPR Information for Various Modulated Signals

Modulation	**BPSK**	**4QAM**	**16QAM**	**64QAM**	**256QAM**
Subcarriers	256	512	1024	2048	4096
Cyclic Prefix	32	64	128	256	512
Min PAPR	3.86	4.65	5.24	6.05	6.74
Average PAPR	6.71	7.36	8.19	8.93	9.79
Max PAPR	19.15	20.65	21.81	22.95	24.19

There is a consistent increase in the minimum, average and maximum PAPR values for each increasing format. The number of subcarriers was predominantly chosen based on data rate as the modulation format increased. The cyclic prefix was chosen as 12.5% of the symbol length number of subcarriers; in LTE the cyclic prefix length is 7% of the OFDM symbol [67] so for a system with 1024 subcarriers, the CP would be 72. 12.5% in this simulation returned a much more robust signal than 7% albeit somewhat reduced data rate due to more subcarriers being assigned redundant data. The major trade-off is to reduce inter-carrier interference (ICI) whilst maximising data

rate. One common design factor for consideration is to choose a cyclic prefix length equal to or longer than the maximum delay spread of the channel to avoid inter-symbol interference (ISI) [68]. Once the maximum delay spread has been determined, other factors such as desired error performance and Doppler spread are considered. Doppler spread estimations were usually performed in the frequency domain but Yucek et al proposed that time domain estimations can reduce processing resources required for computation as well as improving the accuracy of the estimations [69].

3.3 Optimum Switching Thresholds

Using the MATLAB generated OFDM transmissions, the following expression was calculated for the Rayleigh distribution to represent the average modulated OFDM signal power.

$$\int_0^{\infty} 12xe^{-6x^2}\ dx \qquad (3\text{-}10)$$

This is an approximation because with different subcarrier modulation formats, the distribution shifts up in power and spreads out more, so the function changes dependent on the subcarrier construction.

For simplicity, integrating this function from 0 to infinity gives:

$$\int_0^{\infty} 12xe^{-6x^2}\ dx = 1 \qquad (3\text{-}11)$$

As this is a continuous distribution, the probability of the maximum possible power is infinitesimally small, so the distribution is truncated at 1 for ease of calculation. Indeed, infinite power is impossible.

$$\int_0^{1} 12xe^{-6x^2}\ dx = 1 - e^{-6} \cong 0.9975 \qquad (3\text{-}12)$$

At a difference of just 0.25%, the approximation is sufficiently close to pursue the threshold calculations.

The choice of the number of thresholds isn't critical at this stage but the higher the number, the better the power savings could potentially be. In this instance, 3 thresholds are chosen for brevity.

$$
\begin{aligned}
a\int_0^a 12xe^{-6x^2}\ da &= a\left(1-e^{-6a^2}\right)\\
b\int_a^b 12xe^{-6x^2}\ da &= b\left(e^{-6a^2}-e^{-6b^2}\right)\\
c\int_b^c 12xe^{-6x^2}\ da &= c\left(e^{-6b^2}-e^{-6c^2}\right)\\
1\int_c^\infty 12xe^{-6x^2}\ da &= 1\left(e^{-6c^2}\right)
\end{aligned}
\qquad (3\text{-}13)
$$

This leads to the complete expression:

$$a\left(1-e^{-6a^2}\right)+b\left(e^{-6a^2}-e^{-6b^2}\right)+c\left(e^{-6b^2}-e^{-6c^2}\right)+e^{-6c^2} \qquad (3\text{-}14)$$

Computationally, the expressions grow significantly in complexity with each new added threshold, so it is highly inefficient to perform by hand beyond a few. The calculations for 1, 2, 3, and 6 thresholds were also calculated by hand to prove the MATLAB outputs were accurate.

Initial guesses are required as a sensible starting point for the optimisation, this makes it more difficult by hand, but a few iterative guesses generate outputs extremely close to the MATLAB optimisation, giving confidence. An extract of the code for the generation of optimal thresholds in MATLAB is given in appendix D.

Differentiating the expression with respect to a, b, and c obtains the equations for the switching thresholds. This is where the optimisation occurs and is far easier in MATLAB.

Equation 1: wrt a

$$\frac{d}{da}\left[a\left(1-e^{-6a^2}\right)+b\left(e^{-6a^2}-e^{-6b^2}\right)+c\left(e^{-6b^2}-e^{-6c^2}\right)+e^{-6c^2}\right] = e^{-6a^2}\left(e^{6a^2}+12a(a-b)-1\right) \quad (3\text{-}15)$$

Equation 2: wrt b

$$\frac{d}{db}\left[a\left(1-e^{-6a^2}\right)+b\left(e^{-6a^2}-e^{-6b^2}\right)+c\left(e^{-6b^2}-e^{-6c^2}\right)+e^{-6c^2}\right] = e^{-6\left(a^2+b^2\right)}\left(e^{6b^2}+e^{6a^2}(12b(b-c)-1)\right) \quad (3\text{-}16)$$

Equation 3: wrt c

$$\frac{d}{dc}\left[a\left(1-e^{-6a^2}\right)+b\left(e^{-6a^2}-e^{-6b^2}\right)+c\left(e^{-6b^2}-e^{-6c^2}\right)+e^{-6c^2}\right] = e^{-6\left(b^2+c^2\right)}\left(e^{6c^2}+e^{6b^2}(12c^2-12c-1)\right) \quad (3\text{-}17)$$

As a set of simultaneous equations, they can be solved to determine the optimum thresholds. Again, this is far simpler in MATLAB and after optimisation, the optimum switching thresholds are displayed.

$$a = 0.27134$$
$$b = 0.44189 \quad (3\text{-}18)$$
$$c = 0.64458$$

The expression scales well and can grow to any number of thresholds up to infinity, dependent on computational time and as already mentioned, an infinite number is not possible in practical applications.

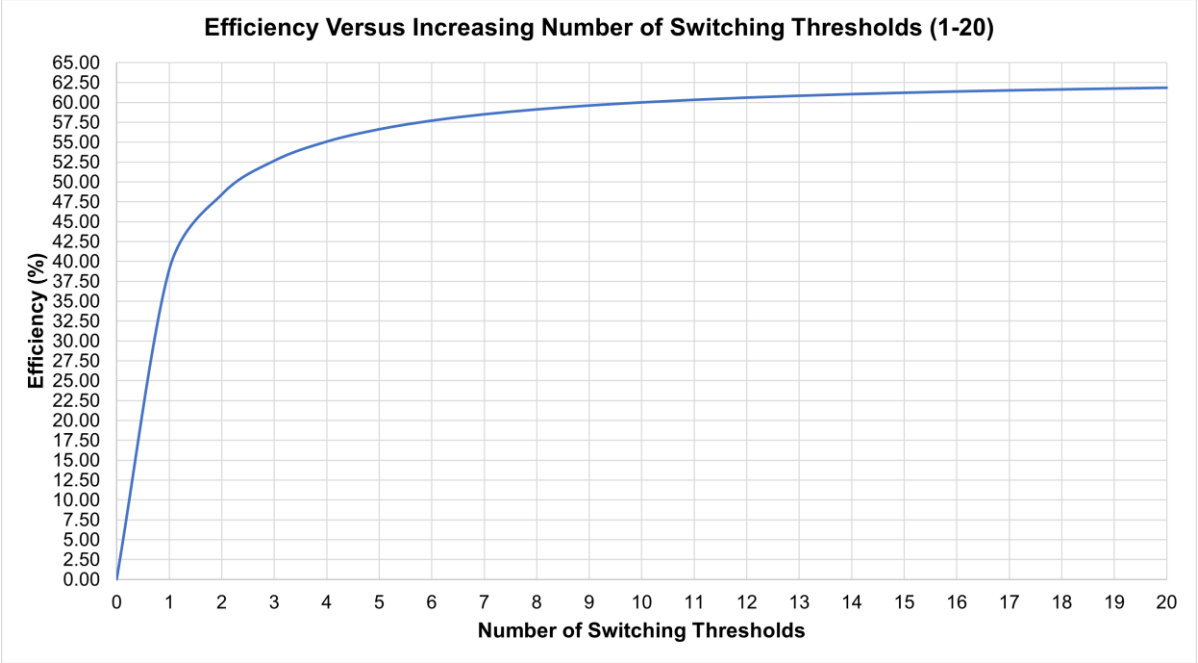

Figure 3-22: Efficiency Achievable with 1-20 Optimum Switching Thresholds

Expectedly, introducing the first switching threshold has the biggest impact on the system in terms of efficiency improvement. An amplifier running with a constant power supply is highly inefficient, but by introducing just 1 optimum switching threshold to lower the power supply voltage whenever the high level is not required achieves up to 38.95% efficiency. Increasing the number of switching threshold levels to 20 can further increase the efficiency up to 61.87%.

The calculation for these efficiency figures comes from the number of thresholds affecting the complete expression such as in equation (3-14) for 3 thresholds. The complete expression for a single threshold is shown in equation (3-19) and the efficiency figure is simply 1 minus the expression.

$$a\left(1 - e^{-6a^2}\right) + e^{-6a^2} + e^{-6} \qquad (3\text{-}19)$$

Table 3-8 shows that there is less than a 5% efficiency enhancement between 6 thresholds to 20 thresholds, which means the added circuit cost and complexity would need consideration. This becomes ever more important with more switching thresholds.

Table 3-8: Achievable Efficiency for 1-20 Optimum Switching Thresholds

Number of Switching Thresholds	**Theoretical Achievable Efficiency (%)**
1	38.95
2	48.43
3	52.68
4	55.09
5	56.65
6	57.73
7	58.53
8	59.15
9	59.63
10	60.03
11	60.35
12	60.63
13	60.86
14	61.07
15	61.24
16	61.40
17	61.54
18	61.66
19	61.77
20	61.87

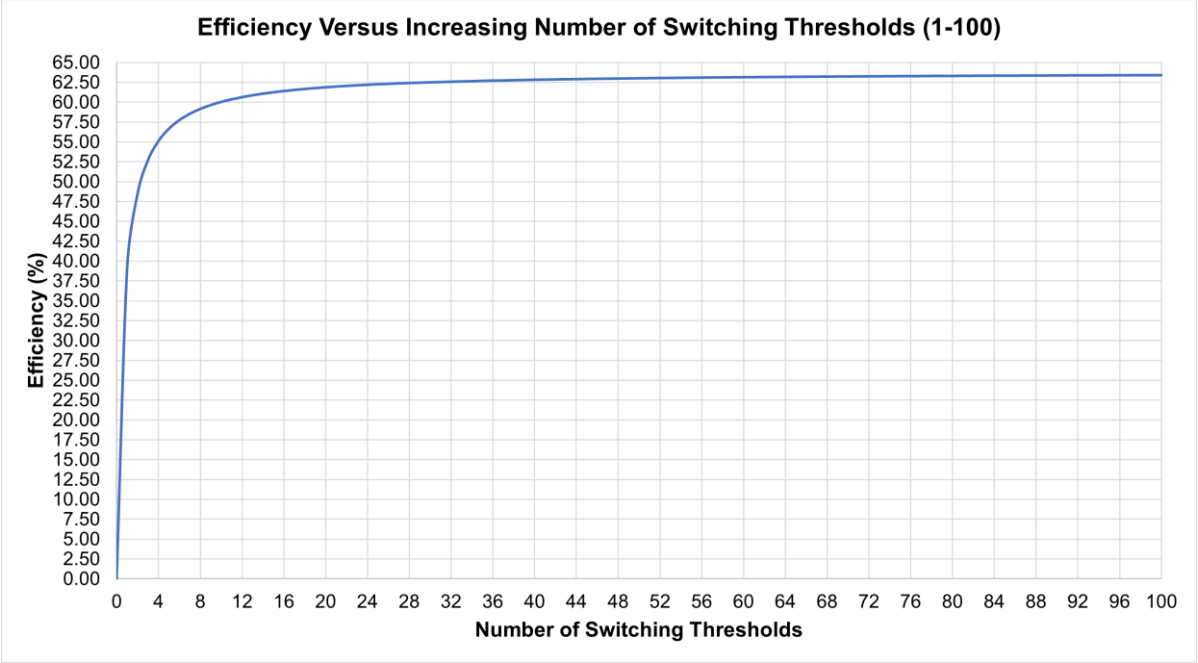

Figure 3-23: Efficiency Achievable with 1-100 Optimum Switching Thresholds

Figure 3-23 shows up to 100 thresholds, it is clearly asymptotic indicating a law of diminishing returns. The efficiency achievable with 31 thresholds is 62.53% but for 100 thresholds it is 63.4%; this increase in the number of thresholds would result in far more complex circuitry and only achieve approximately 0.87% efficiency improvement so is likely not sufficiently valuable to pursue.

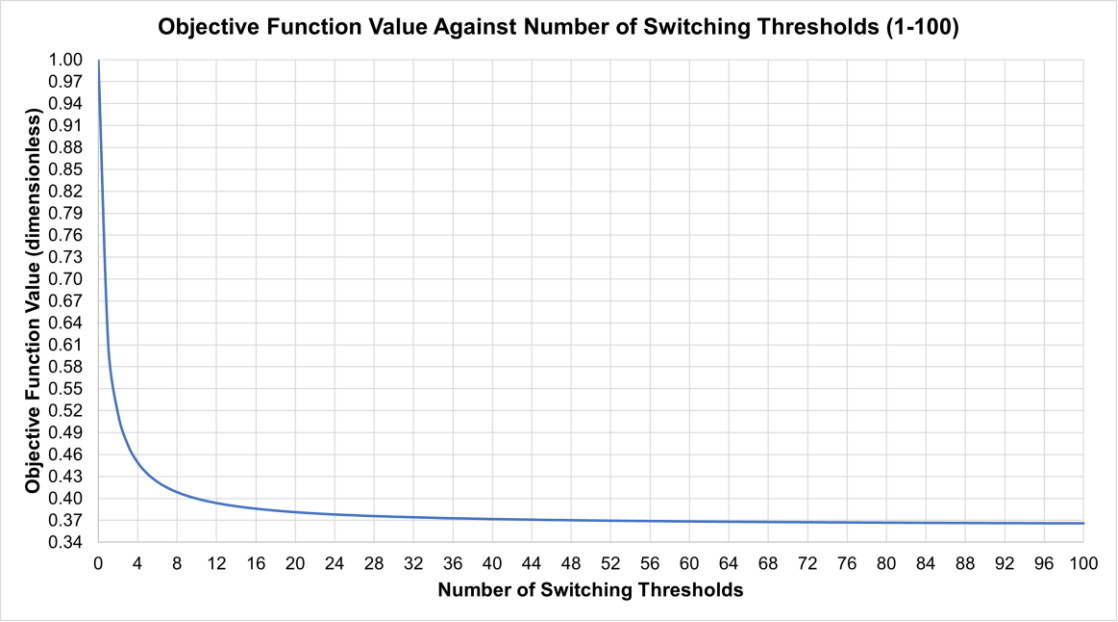

Figure 3-24: Objective Function Value Asymptotic Trend 0-100 Thresholds

It can be seen from figure 3-24, the curve is asymptotic towards ~0.36. There exists a theoretical limit of efficiency as the number of switching thresholds approaches infinity. As the number of thresholds grows, the space between each threshold approaches 0 which means that the thresholds eventually cross at all values of x in the continuous data set, therefore the distribution can be multiplied by x which leads to an evaluation of the PDF average:

$$\int_0^\infty 12x^2 e^{-6x^2}\ dx$$

$$\frac{\sqrt{\pi}}{2\sqrt{6}} \qquad (3\text{-}20)$$

$$\approx 0.3618$$

$$\left(1 - \frac{\sqrt{\pi}}{2\sqrt{6}}\right) \times 100 \approx 63.82\% \qquad (3\text{-}21)$$

The theoretical limit of efficiency is 63.82%, as shown in equation (3-21). As the number of switching thresholds increases, it tends towards this limit, as shown in the figures.

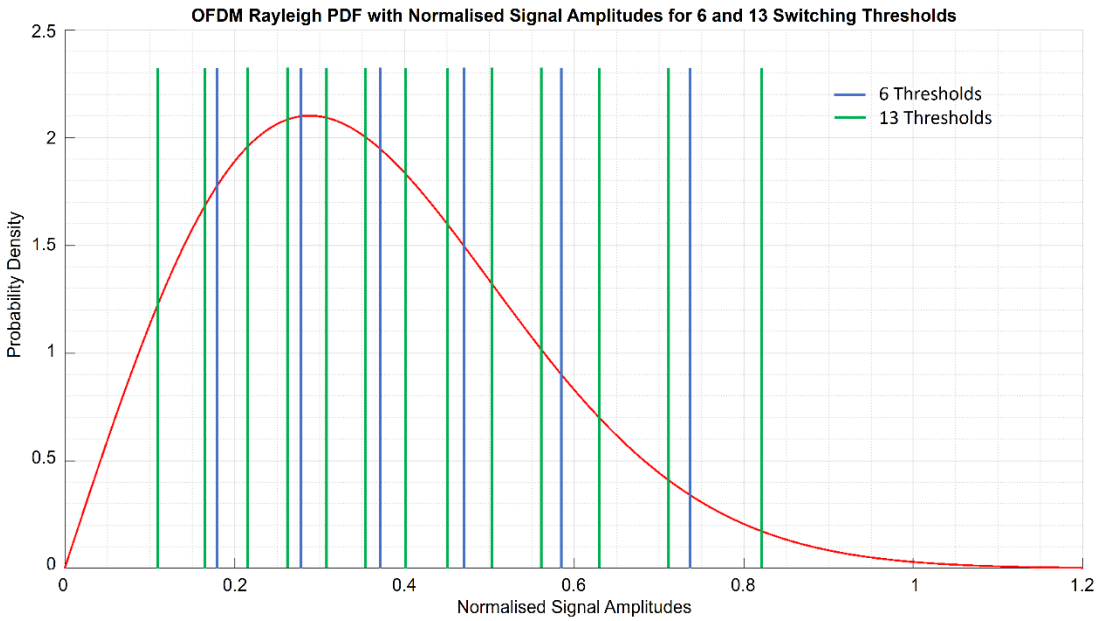

Figure 3-25: OFDM Signal Amplitudes PDF with 6 and 13 Optimised Switching Thresholds

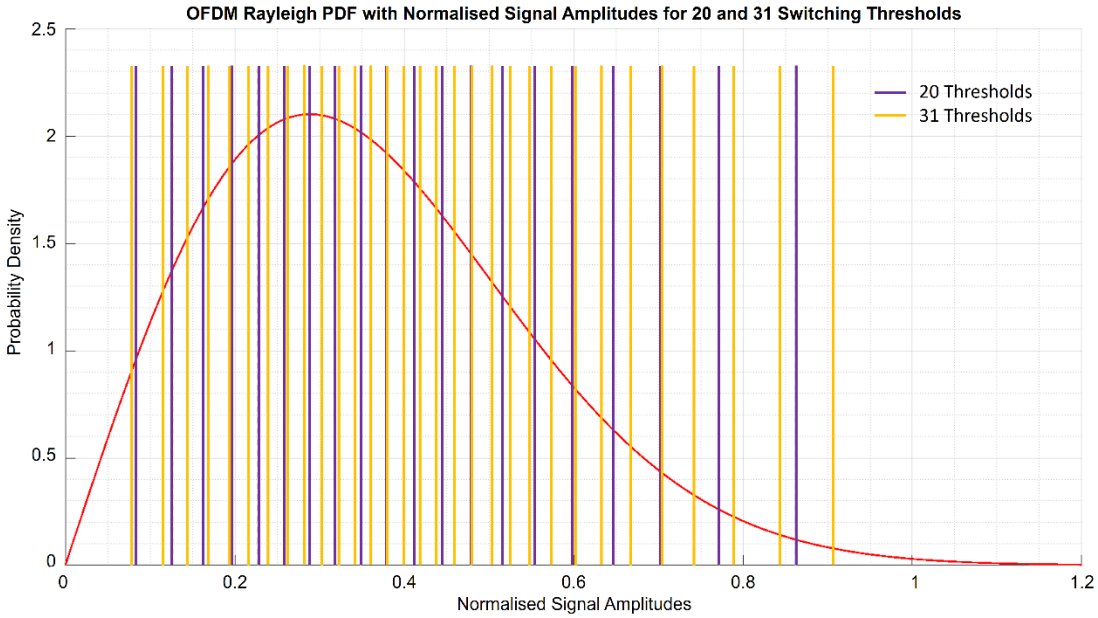

Figure 3-26: OFDM Signal Amplitudes PDF with 20 and 31 Optimised Switching Thresholds

By increasing the number of switching threshold levels, the system efficiency increases towards the 63.82% limit in steps as shown in table 3-8.

3.4 Uniform Switching Thresholds

In each of the optimum threshold examples, figure 3-25 and figure 3-26, the main bulk of the probability density function appears to have thresholds which are roughly uniform in spacing, this would suggest that a power supply with uniform output voltage steps would provide an efficiency enhancement very close to the theoretical maximum efficiency in each case. This would be advantageous as the uniform spacing would facilitate a much simpler hardware and software implementation. An extract of the code for the generation of uniform thresholds in MATLAB is given in Appendix E.

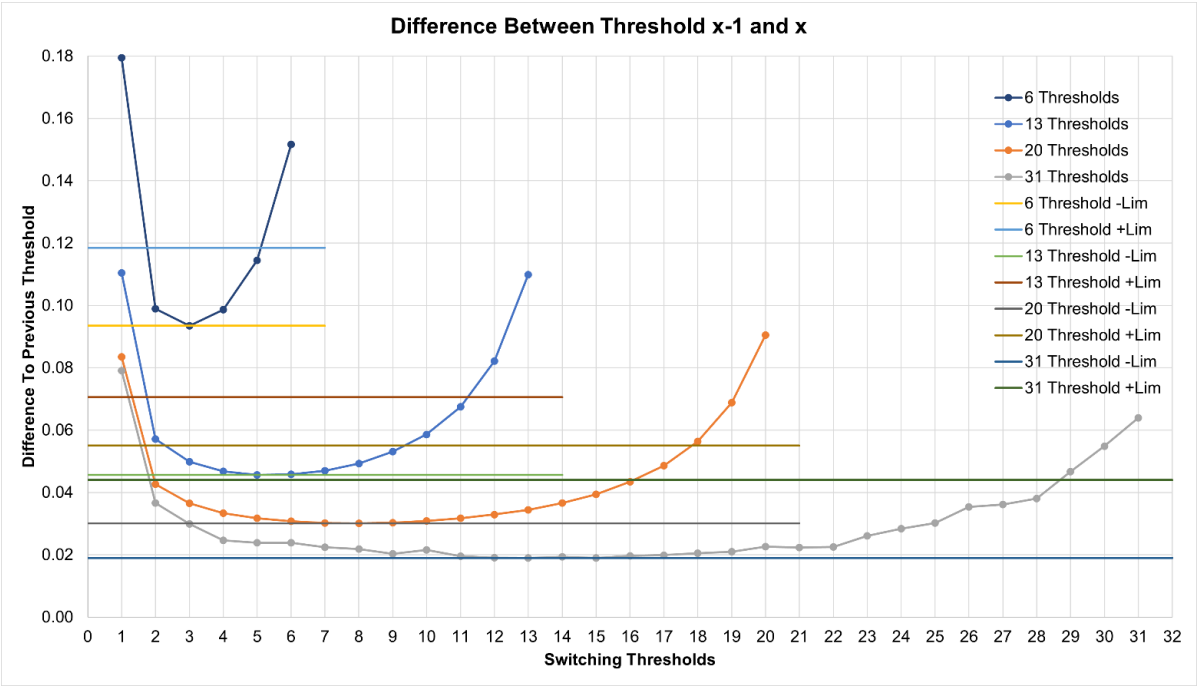

Figure 3-27: Difference Between Threshold x-1 and x for 6, 13, 20 and 31 Thresholds

Figure 3-27 shows the differences between each pair of consecutive optimum threshold values for the 6, 13, 20, and 31 switching threshold configurations. In each case, the first and last thresholds are significant outliers but to be expected as the spread clearly increases towards the edges of the distribution. A limit of 0.025 (1/40) from the minimum value of each threshold set was chosen as the bounds for being able to assume uniform spacing, in each set it is just the first threshold and the final 1-3 thresholds which do not fall within the chosen bounds. This shows that most of the thresholds within each set for the distribution exhibit uniform spacing (within 0.025). Assuming uniform spacing, the implementation is far simpler and the trade-off between achievable efficiency compared to the optimum equivalent is sufficient. Table 3-9 shows a comparison between the efficiency of the uniform and optimum equivalents.

Table 3-9: Efficiency Comparison Between Optimum and Uniform Spacing

Number of Thresholds	Efficiency with Optimum Thresholds	Efficiency with Uniform Threshold Spacing	Efficiency Difference
1	38.95%	37.03%	-1.92%
2	48.43%	46.66%	-1.77%
3	52.68%	51.33%	-1.35%
6	57.73%	56.84%	-0.89%
13	60.86%	60.34%	-0.52%
20	61.87%	61.58%	-0.29%
31	62.53%	62.34%	-0.19%
100	63.40%	63.35%	-0.05%

The difference in efficiency between a system employing the optimum switching threshold locations and one using uniform spacing between each threshold decreases as the number of thresholds increases. Table 3-9 proves that uniform spacing in the supply voltage from the power supply can achieve close to the maximum theoretical efficiency for each set of switching thresholds. The differences start at 1.92% for just 1 threshold but reduce to 0.19% for 31 thresholds and even further to 0.05% for 100 thresholds. Therefore, the uniform spacing PET method should be used.

A further enhancement to the technique is to consider the lowest threshold in the 100-threshold case could be utilised for an idle situation. This would be the lowest power at which everything is still turned on and ready to be used but minimal power is wasted when no output is desired. Combine that low level with the remaining uniformly spaced thresholds in the 6-threshold case to total 7 thresholds for a highly efficient system during operation (56.84%) and during idle scenarios.

Applying this 7-threshold configuration results in an efficiency of 56.85% during operation, an increase of just 0.01% over the 6-threshold version but the benefit of this

configuration is to save significant power during times when the system is idling. Therefore, the real usage benefits are difficult to quantify as it depends on how the system is employed by the user.

3.5 Conclusion

The goal for the work in this chapter was to determine the optimal switching levels for the output voltage rail of the PSU based on the statistical characteristics of a modulated OFDM signal. Ultra-fast switching is possible with available components. For OFDM, the PAPR can be relatively high, this depends on the modulation format that is employed; higher modulation orders lead to greater PAPR.

There is a clear trade-off between circuitry cost, complexity and efficiency gains as the trend is that of diminishing returns as the number of thresholds increases. The largest jumps in efficiency enhancement come when introducing the first few thresholds.

For 31 switching thresholds of uniform spacing, the achieved efficiency is 62.34% compared to the 62.53% achievable with the optimum thresholds, just a 0.19% difference for a much simpler implementation. With less than a 1% difference in efficiency for 6 thresholds between optimum and uniform threshold spacing, uniform spacing should be chosen in most cases due to much simpler hardware and software implementation. 6 thresholds are likely sufficient in most cases. Realistically, a system with more than 31 thresholds is likely unnecessary and excessive.

Alternatives to this implementation include the PWM-based approaches but these require complex circuitry and large power supply bandwidths which increase as the amplifier operation frequencies increase.

There are three different approaches which could be taken:

1. **Equal Power Distribution**

   The PDF could be sliced into equal areas of power. This is a generic simple approach but can result in errors and does not achieve a high efficiency.

2. **Optimum Thresholds**

   Optimum threshold spacing based on the probability of each power level. This is the probabilistic analysis and the raw form of PET and can achieve the highest theoretical efficiency but can have a high implementation complexity.

3. **Uniform Thresholds**

   Sensible, uniform threshold spacing informed by PET, with the addition of an extra level for the system idling scenario. This is the best version as the efficiency is close to the theoretical maximum with optimum thresholds, it scales well and benefits from a low implementation complexity; especially with the approaches outlined in chapter 4.

A final improvement to the PET technique was the consideration of the idling scenario in which amplifiers often remain switched on with no input signal, therefore wasting significant DC power unnecessarily. In these situations, the amplifier supply rail could be switched to the lowest calculated switching threshold so that the amplifier idles at a much lower power but can quickly be ready when an input signal is detected. The recommended configuration is therefore to utilise a small number of uniform thresholds, 6, with an extra level for the idle scenario, totalling 7 thresholds. This benefits from a low implementation complexity combined with a high efficiency enhancement.

Whilst this envelope tracking technique adds a delay into the system whereby the envelope of the incoming signal is determined and used to inform the amplifier power

supply, the consequences of the delay are no greater than existing ET systems. The delays include the incoming signal sniffing, the determination of the closest location on the PDF to properly serve the incoming signal envelope, and the power supply switching propagation for the output amplifier. If the delays in the system are too great or are misaligned, then the effects are likely to be to either clip the signal or waste power. If accurately aligned, however, the benefits are considerable. An intentional delay line is configured to achieve proper alignment, other delays may be minimised with better and higher frequency components.

Concluding, the PET technique could be generalised and applied to any signal based on its statistics if the signal probability density function is known or calculable.

In the next chapter, the implementation efficiency is explored using Golomb ruler theory, and some different system configurations are presented as viable case studies, including one simulated for 6 thresholds, and the theory for 31 thresholds. The chapter also discusses an improvement to a well-established construction method for modular Golomb rulers (MGRs), creating a new and simpler method.

Chapter 4: Implementation of Power Control Unit Techniques

4.1 Introduction

In this chapter, two different topology proposals are presented and explored as valid approaches, called linear flow (LF) and non-linear matrix (NLM), both of which have their own advantages. The LF topology is investigated further because it has more viable use cases. Circuit simulations are presented with respect to the LF topology, analysis of the circuit simulations is given.

A new method of generating modular Golomb rulers (MGRs) from optimal Golomb rulers is also introduced, known as the merry-go-round (MGR) technique. The aim is to achieve the maximum number of levels for the minimum number of regulators in the system to augment efficiency. This is the crux of the Golomb ruler research. MATLAB is used to prove that the new MGR technique works. The generated ruler compositions are used in conjunction with the PET technique from the previous chapter to present unique constructions to enable a higher power efficiency for OFDM signal amplifiers. The version of the PET technique taken forward into this chapter is the one for uniform thresholds as it lends itself well to the MGR formations.

4.2 Linear Flow (LF) Topology

The first topology presented is the LF topology whereby each resource only has a total of two connections to/from it which are its adjacent resources.

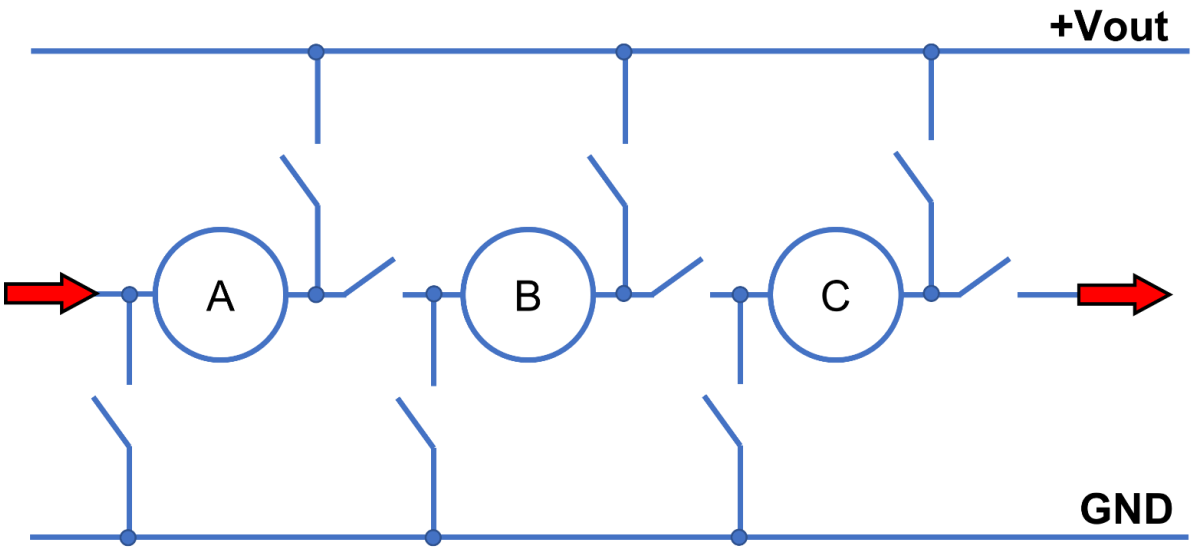

Figure 4-1: 3-Resource Generalised Linear Flow (LF) Topology

The simplest circular system to employ would be the 3-resource system illustrated in figure 4-1, whereby all resources are adjacent to each other so 100% of possible output configurations are covered. The arrows indicate that the system is circular and wraps-around from right to left; resource ‘C’ is adjacent to resource ‘A’ as well as ‘B’. Any circular linear flow system is perfect when there are only 3 resources.

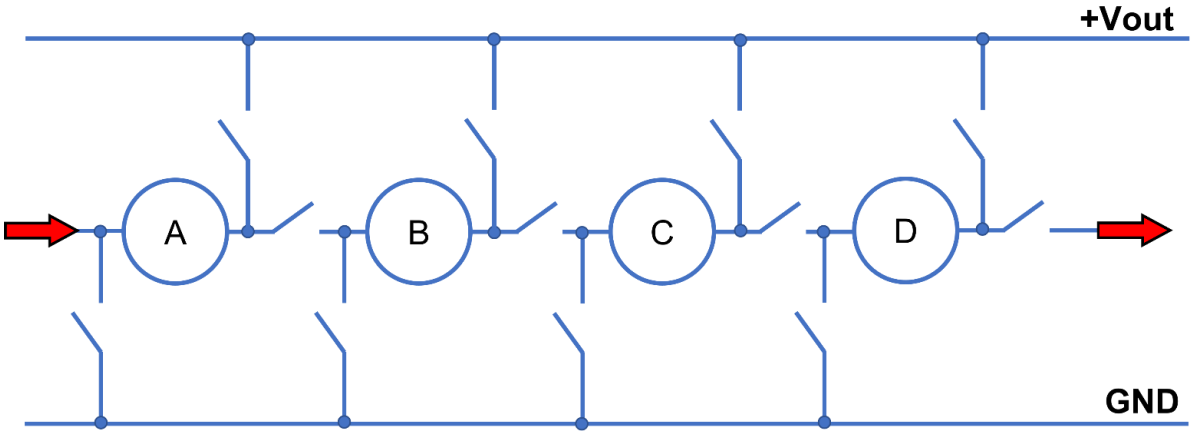

Figure 4-2: 4-Resource Generalised Linear Flow (LF) Topology

With 4 resources, however, there is no direct link between resources A and C, and likewise between resources B and D. Therefore, there are 2 outputs which are impossible to achieve in the current arrangement, but which could be achievable in an alternative configuration.

$$Missing\ Output\ 1 = A + C \qquad (4\text{-}1)$$

$$Missing\ Output\ 2 = B + D \qquad (4\text{-}2)$$

Any LF system with 4 or more resources will have missing possible outputs and therefore is non-perfect.

4.2.1 3-Regulator Binary Sequence LF

In this context, the binary sequence is a geometric sequence containing the following subsequent terms 1, 2, 4, 8, 16; also known as the powers of 2. Mathematically derived from the well-known geometric sequence formula, shown in equation (4-3).

$$a_n = a_1 r^{(n-1)}$$
$$Where\ a_1 = first\ term,$$
$$r = common\ ratio,$$
$$n = placement\ of\ term \qquad (4\text{-}3)$$

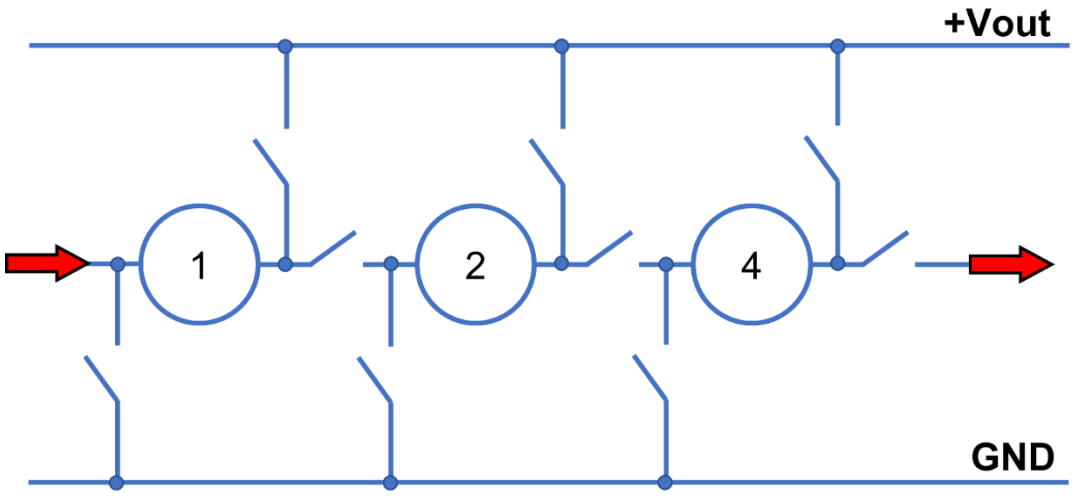

Figure 4-3: 3-Regulator Binary Sequence Linear Flow (LF) Topology

Figure 4-3 shows a simplified schematic of a 3-regulator binary sequence configuration circuit, the characteristics of which can be found in table 4-1 below. The required MOSFETs are denoted by a simple switch symbol. The right-hand side of the 4V regulator is connected to the left-hand side of the 1V regulator. This is essential to enable all possible outputs.

Table 4-1: Statistical Summary of the 3-Regulator Binary Sequence LF Topology System

Number of Voltage Regulators	3
Number of MOSFETs Required	9
Number of Different Possible Output Voltages	7 (8 including 0V)
Possible Output Voltages (V)	0, 1, 2, 3, 4, 5, 6, 7
Number of Different Impossible Output Voltages	0
Impossible Output Voltages (V)	None
Maximum Possible Output Voltage (Vmax)	1 + 2 + 4 = 7

This system is perfect because every voltage from 0 to Vmax can be output by the system, in this case Vmax is 7V.

4.2.2 4-Regulator Binary Sequence LF

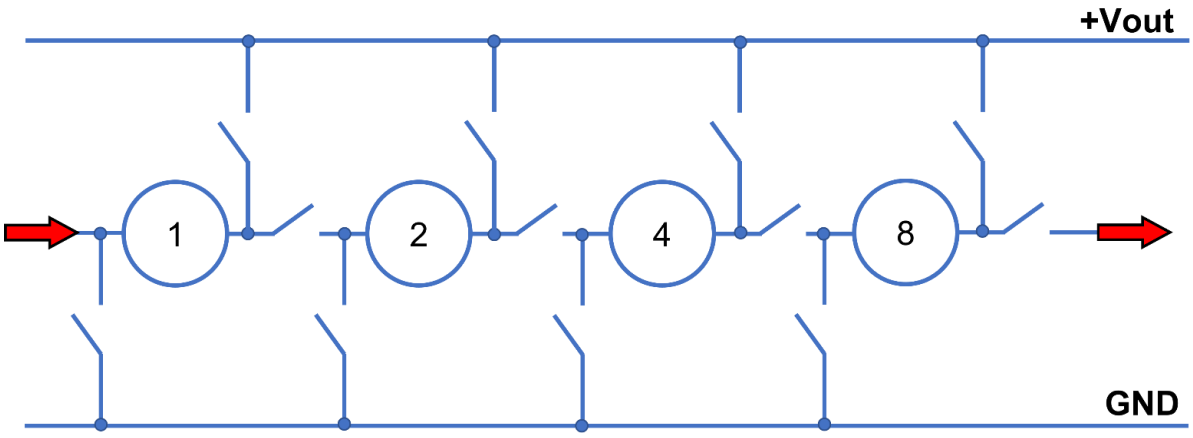

Figure 4-4: 4-Regulator Binary Sequence Linear Flow (LF) Topology

Figure 4-4 shows a simplified schematic of a 4-regulator binary sequence configuration circuit, the characteristics of which can be found in table 4-2 below.

Table 4-2: Statistical Summary of the 4-Regulator Binary Sequence LF Topology System

Number of Voltage Regulators	4
Number of MOSFETs Required	12
Number of Different Possible Output Voltages	13 (14 including 0V)
Possible Output Voltages (V)	0, 1, 2, 3, 4, 6, 7, 8, 9, 11, 12, 13, 14, 15
Number of Different Impossible Output Voltages	2
Impossible Output Voltages (V)	5, 10
Maximum Possible Output Voltage (Vmax)	1 + 2 + 4 + 8 = 15

This is a non-perfect system as there are missing output voltages. There is no direct connection between regulators 1 and 4, or between regulators 2 and 8; hence the missing 1 + 4 = 5V and 2 + 8 = 10V.

4.2.3 Design Considerations

With any design process, careful consideration should be given to each aspect of the design with justified decisions as to which components are employed for the implementation.

MOSFETs were chosen as electronic switches for the DC paths. They can have fast switching times, low on-resistance (RDSon) and have high power capability depending on the device choice. The critical point is to not exceed the safe operating area (SOA) of any MOSFET.

A microcontroller unit (MCU) was chosen as the system brain. Shortcomings include the GPIO pins only being able to source low amounts of current and they tend not to have a wide GPIO pin voltage range so driving the gates of the MOSFETs directly can be difficult.

Optocouplers on the MOSFET gates as isolated gate drivers. A choice based on their ability to completely isolate the DC between input and output. This vastly reduces

electrical noise getting back to the microcontroller; harmful feedback could otherwise occur and damage the GPIO pins.

The system described in this work was originally conceived to be used for OFDM communication infrastructure which is often used in RF ‘hot’ environments that can wreak havoc on analogue and digital circuitry. Optocouplers operate independently of RF interference so switching errors are significantly reduced even in electrically noisy RF environments.

The input side of an optocoupler is mostly always the same – an LED. The output side, however, can be one of a few different types, two of which could be appropriate for this system – the phototransistor type or the photodiode type:

The phototransistor type generally has higher current gain than the photodiode type so might be a better choice depending on the MOSFET requirements, but at the disadvantage of usually being slower.

The photodiode type can have fast operation times and is generally quicker than the phototransistor type. A consideration could be dual package optocouplers with the output photodiodes connected in series which would enable a higher output voltage to drive the MOSFET gates harder if needed, depending on the choice of MOSFET and its gate threshold voltage requirements. Most optocoupler photodiodes don’t provide much current (often less than a few tens of mA) which means that the MOSFET turn on time might be limited if the MOSFET gate-drain and gate-source capacitances are large. There are some optocouplers designed for IGBT gate drive with a high output current in the region of 200mA to hit the devices hard and reduce their turn on time. These circuit design considerations are summarised in table 4-3.

Table 4-3: Summary of Design Considerations

Design Aspect	Advantages	Disadvantages
MOSFETs to be used as electronic switches	Fast switching times	Relatively high cost, especially at higher powers
	High power capability	Can have complex gate drive requirements
	Low on-resistance (RDSon)	Can be sensitive to temperature variations
Microcontroller (MCU) to control the switching of individual MOSFETs	Flexible and capable – can be used in a wide range of applications	Have limited memory and processing power and ability to parallel tasks
	Often cheaper than some alternatives such as an FPGA	Not suitable for applications requiring high processing power or speeds
	Simpler requirements for implementation compared to FPGAs, including programming	GPIO pins only capable of driving low-current loads
	Often designed for low-power applications so can be energy-efficient	Typically have limited GPIO pins but can be expanded with external shift registers or GPIO expander chips
Optocouplers included in the MOSFET gate control circuitry	RF-independent so won't be affected by RF environment	Increases circuit complexity
	Electrically isolated to prevent noise reaching microcontroller, protecting the GPIO pins	Increases physical circuit size
	Enables a small switching signal to control a larger DC rail	Increases implementation cost

4.2.4 Implementation

Electrically, the different MOSFETs control which regulators are isolated, and which are connected to output the required voltage.

Figure 4-5 shows the electrical path for the ‘A’ regulator output. This structure would be the same for the ‘B’ regulator output as well as the ‘C’. The blue crosses indicate the circular structure. The red crosses show the MOSFET gates which would be controlled by a microcontroller or FPGA, with gate driver circuit. The thick red lines show the path to both the negative and positive rails. The green circles around the M2 and M3 MOSFETs indicate they are conducting, when all other MOSFETs are switched off.

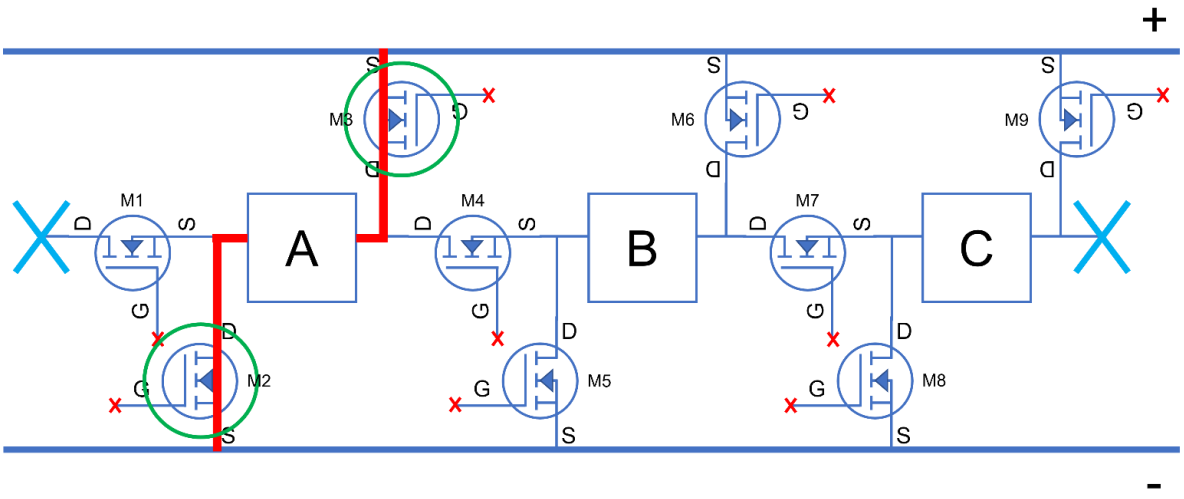

Figure 4-5: 'A' Output Electrical Path

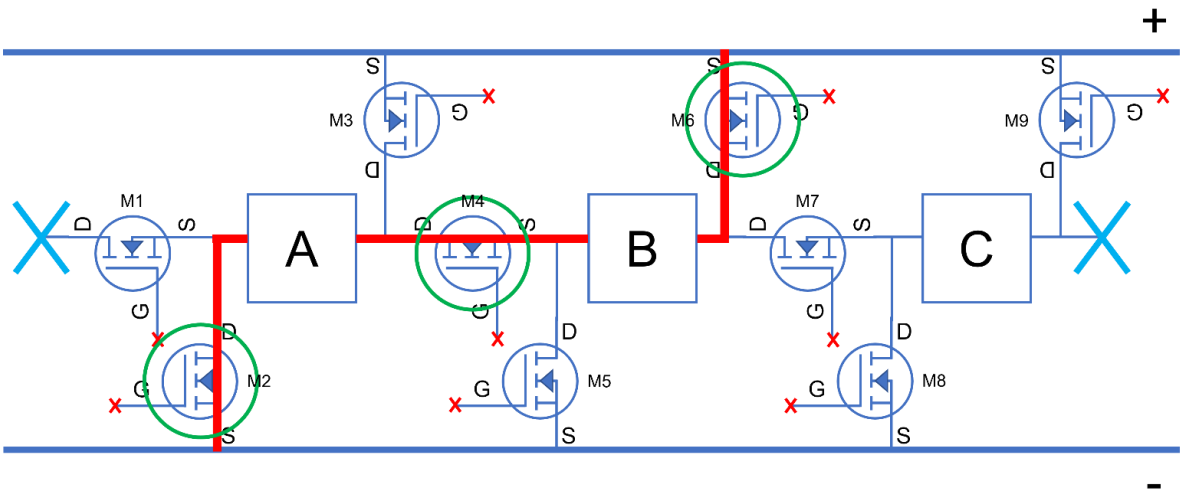

Figure 4-6: 'A+B' Output Electrical Path

Figure 4-6 shows the ‘A+B’ output path. MOSFETs M2, M4 and M6 are conducting to enable the path. ‘B+C’ and ‘C+A’ would have very similar arrangements just with different MOSFETs turned on and off. These structures are described in table 4-4.

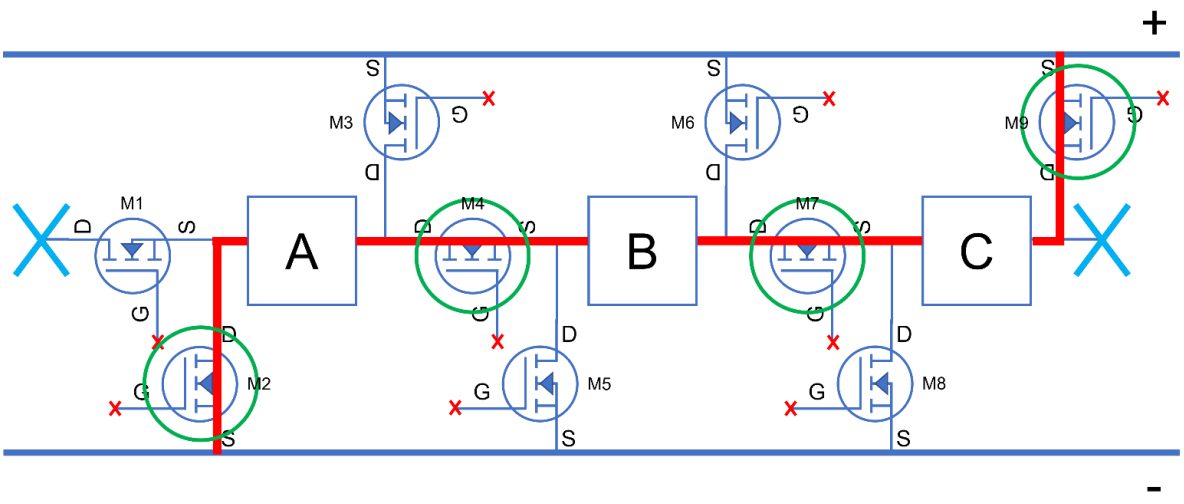

Figure 4-7: 'A+B+C' Output Electrical Path

Figure 4-7 depicts the most complex configuration, whereby all 3 regulators are connected in series. MOSFET M1 is not conducting, this is critical to ensure a continuous loop is not created which would damage the circuit. It is also therefore important to consider this during transition periods when switching to a different output configuration. At no point can MOSFETs M1, M4 and M7 all be conducting at the same time; at least one of these must be always turned off.

Table 4-4: MOSFETs Conduction Status for Each Output Configuration

Output	**'On' MOSFETs**	**'Off' MOSFETs**
A	M2, M3	M1, M4, M5, M6, M7, M8, M9
B	M5, M6	M1, M2, M3, M4, M7, M8, M9
C	M8, M9	M1, M2, M3, M4, M5, M6, M7
A+B	M2, M4, M6	M1, M3, M5, M7, M8, M9
B+C	M5, M7, M9	M1, M2, M3, M4, M6, M8
C+A	M8, M1, M3	M2, M4, M5, M6, M7, M9
A+B+C	M2, M4, M7, M9	M1, M3, M5, M6, M8
B+C+A	M5, M7, M1, M3	M2, M4, M6, M8, M9
C+A+B	M8, M1, M4, M6	M2, M3, M5, M7, M9

A+B+C, B+C+A, and C+A+B are all equivalent in terms of total output but there may be nuances with output magnitude of each configuration.

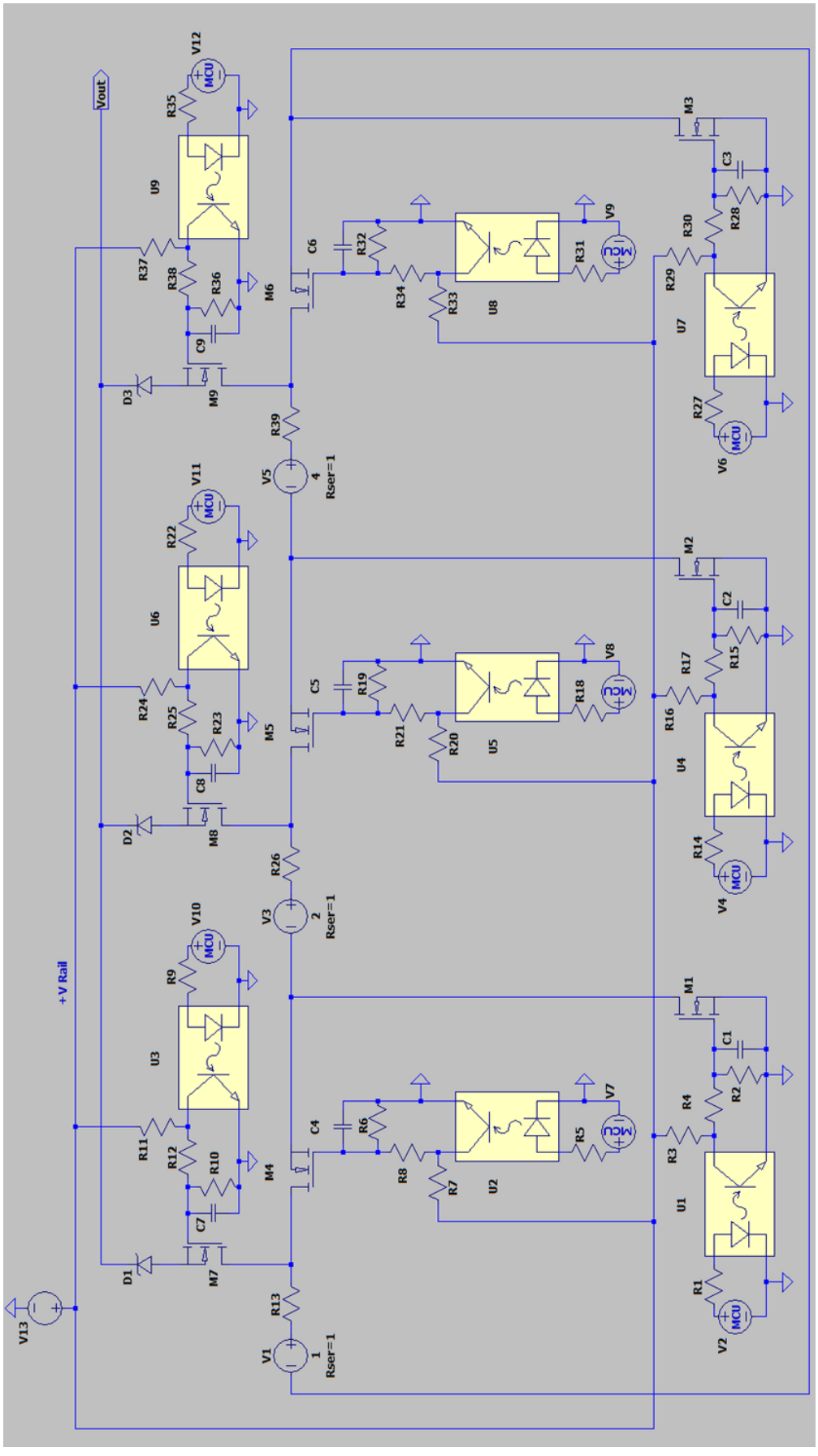

Figure 4-8: LTSpice Circuit Simulation for 3-Regulator Binary Sequence Topology

Figure 4-8 shows the initial 3-regulator binary sequence topology system, following the 1,2,4 format. This requires 9 MOSFETs, with 9 optocouplers to control the gates of the MOSFETs.

			Desired Voltage Out (V) @ Vout4											
			0 (V1/V3)	0 (V3/V5)	0 (V5/V1)	1	2	3	4	5	6	7 (M9 Out)	7 (M8 Out)	7 (M7 Out)
Voltage Control - Functions	*V1*	Fixed voltage source	*1*	*1*	*1*	*1*	*1*	*1*	*1*	*1*	*1*	*1*	*1*	*1*
	V2	MCU logic for U1 opto, controls M1	0	0	0	0	0	3.3	0	0	0	3.3	3.3	0
	V3	Fixed voltage source	*2*	*2*	*2*	*2*	*2*	*2*	*2*	*2*	*2*	*2*	*2*	*2*
	V4	MCU logic for U4 opto, controls M2	0	0	0	0	0	0	0	0	3.3	3.3	0	3.3
	V5	Fixed voltage source	*4*	*4*	*4*	*4*	*4*	*4*	*4*	*4*	*4*	*4*	*4*	*4*
	V6	MCU logic for U7 opto, controls M3	0	0	0	0	0	0	0	3.3	0	0	3.3	3.3
	V7	MCU logic for U2 opto, controls M4	3.3	0	0	3.3	3.3	0	3.3	3.3	3.3	0	0	3.3
	V8	MCU logic for U5 opto, controls M5	0	3.3	0	3.3	3.3	3.3	3.3	3.3	0	0	3.3	0
	V9	MCU logic for U8 opto, controls M6	0	0	3.3	3.3	3.3	3.3	3.3	0	3.3	3.3	0	0
	V10	MCU logic for U3 opto, controls M7	3.3	3.3	3.3	0	3.3	3.3	3.3	0	3.3	3.3	3.3	0
	V11	MCU logic for U6 opto, controls M8	3.3	3.3	3.3	3.3	0	0	3.3	3.3	3.3	3.3	0	3.3
	V12	MCU logic for U9 opto, controls M9	3.3	3.3	3.3	3.3	3.3	3.3	0	3.3	0	0	3.3	3.3
MOSFETs ON/OFF		M1	ON	ON	ON	ON	ON	OFF	ON	ON	ON	OFF	OFF	ON
		M2	ON	ON	ON	ON	ON	ON	ON	ON	OFF	OFF	ON	OFF
		M3	ON	ON	ON	ON	ON	ON	ON	OFF	ON	ON	OFF	OFF
		M4	OFF	ON	ON	OFF	OFF	ON	OFF	OFF	OFF	ON	ON	OFF
		M5	ON	OFF	ON	OFF	OFF	OFF	OFF	OFF	ON	ON	OFF	ON
		M6	ON	ON	OFF	OFF	OFF	OFF	OFF	ON	OFF	OFF	ON	ON
		M7	OFF	OFF	OFF	ON	OFF	OFF	OFF	ON	OFF	OFF	OFF	ON
		M8	OFF	OFF	OFF	OFF	ON	ON	OFF	OFF	OFF	OFF	ON	OFF
		M9	OFF	OFF	OFF	OFF	OFF	OFF	ON	OFF	ON	ON	OFF	OFF
Desired Voltage Out (V) @ Vout4			0	0	0	1	2	3	4	5	6	7	7	7
Actual Voltage Out (V) @ Vout4			0.0119487	0.0120841	0.0123409	1.0058657	1.9833977	2.9833748	3.9715538	4.9715576	5.9711933	6.8426647	6.9715514	6.9712095
Difference Between Desired and Actual Output Voltage (V)			0.0119487	0.0120841	0.0123409	0.0058657	0.0166023	0.0166252	0.0284462	0.0284424	0.0288067	0.1573353	0.0284486	0.0287905
Difference Between Desired and Actual Output Voltage (%)			N/A	N/A	N/A	0.5831494	0.8370636	0.5572615	0.7162486	0.5721024	0.4824279	2.2993279	0.4080670	0.4129915

Figure 4-9: 3-Regulator Binary Circuit Test Results. Larger Version in Appendix F

The on (green) and off (red) states of each MOSFET are given in figure 4-9 for each possible output voltage 0-7V.

4.3 Non-Linear Matrix (NLM) Topology

The second topology is the NLM whereby each resource is connected to each other resource in the system via a matrix configuration. This can have advantages in some scenarios but generally leads to a much higher complexity and lower efficiency.

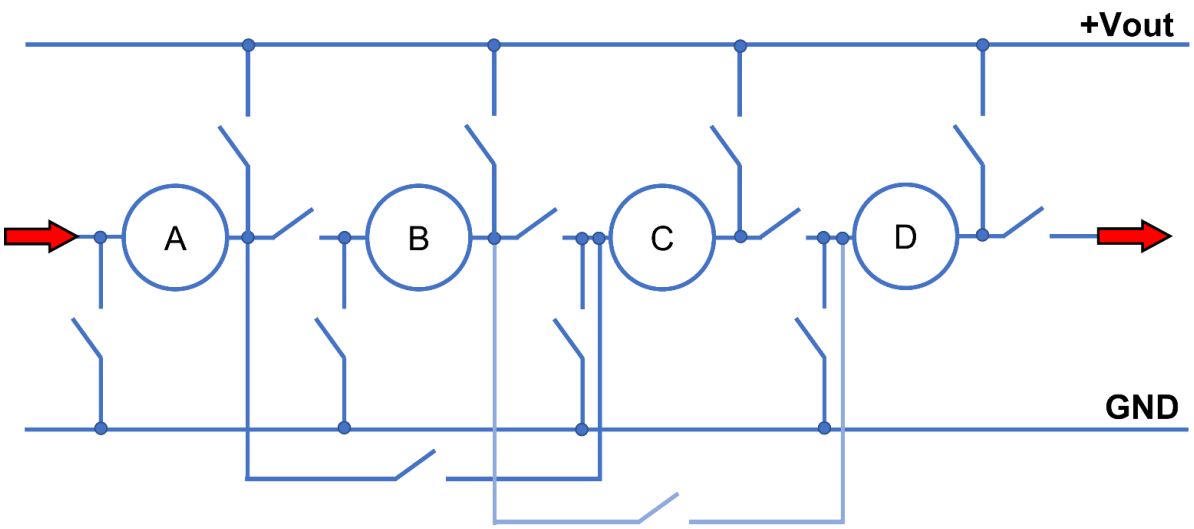

Figure 4-10: 4-Resource Generalised Non-Linear Matrix (NLM) Topology

This system allows for all possible outputs to be realised so it is a perfect system. There are, however, disadvantages such as the increased system complexity which in some cases might outweigh the benefits. The connections between the resources, or regulators, are MOSFETs driven by optocouplers and a microcontroller acting as the brain of the system. In this case, the added complexity of the circuit would increase manufacturing costs as well as consume more real estate on a physical PCB.

When adding one extra voltage source (regulator) to increase the number of possible output voltage levels, the increased complexity in terms of additional MOSFETS and optocouplers required to be able to output any voltage level between 0V and the maximum possible can be defined in the following way:

$$For\ n > 3,$$

$$x = \frac{1}{2}(n^2) + \frac{3}{2}(n) \qquad (4\text{-}4)$$

$$x = \frac{n^2 + 3n}{2} \qquad (4\text{-}5)$$

Alternatively, equation (4-4) or (4-5) can also be written in sigma notation form, as in equation (4-6).

$$For\ n > 3,$$

$$x = 3n + \sum_{m=2}^{n} (n - m) - 1 \qquad (4\text{-}6)$$

$$Where\ n\ =\ number\ of\ voltage\ regulators$$

Each MOSFET has an optocoupler to drive the gate so the number of MOSFETs and the number of optocouplers in each system is the same.

If the number of MOSFETs required (x) for a particular number of voltage regulators (for example, 6) is known, then to calculate the number required (y) for one more voltage regulator (a = 7) it is simply:

$$y = x + a + 1 \qquad (4\text{-}7)$$

Table 4-5 shows the number of required MOSFETs for up to 20 voltage regulators.

Table 4-5: Number of MOSFETs Required per Number of Voltage Regulators

Number of Voltage Regulators (n)	**Number of MOSFETs Required (x)**	**Increase from n-1 to n**
1	0-2 (depending on desired topology requirements and circuit operation)	N/A
2	6	4-6
3	9	3
4	14	5
5	20	6
6	27	7
7	35	8
8	44	9
9	54	10
10	65	11
11	77	12
12	90	13

13	104	14
14	119	15
15	135	16
16	152	17
17	170	18
18	189	19
19	209	20
20	230	21

For n < 3 the number of MOSFETs doesn't follow the same pattern as for n > 3.

The quadratic from equation (4-4) can be rearranged to make n the subject as in equation (4-8).

$$x = \frac{1}{2}(n^2) + \frac{3}{2}(n)$$

$$n = -\frac{3}{2} \pm \sqrt{2x + \frac{9}{4}} \qquad (4\text{-}8)$$

Equation (4-8) can be used to calculate useful statistics such as when the number of MOSFET/optocoupler pairings required for a system exceeds 100 for the first time.

$$n = -\frac{3}{2} \pm \sqrt{2(100) + \frac{9}{4}}$$

$$n = -\frac{3}{2} \pm 14.22146265 \qquad (4\text{-}9)$$

$$n = 12.72146265 \; and \; n = -15.72146265$$

Equation (4-9) shows the minimum size of the system which would result in the requirement of 100 or more MOSFETs. There cannot be a system which has a negative number of regulators, so the -15.72 result is ignored. A system with 12.72 regulators clearly cannot exist, so it is rounded up to the nearest whole number which in this case is 13.

If the number of regulators was 13:

$$x = \frac{1}{2}(13^2) + \frac{3}{2}(13)$$

$$x = \frac{169}{2} + \frac{39}{2} \qquad (4\text{-}10)$$

$$x = 104$$

If the number of regulators was 12:

$$x = \frac{1}{2}(12^2) + \frac{3}{2}(12)$$

$$x = 72 + 18 \qquad (4\text{-}11)$$

$$x = 90$$

Therefore, the first system which requires 100 or more pairs of MOSFETs and optocouplers is a system which contains 13 regulators.

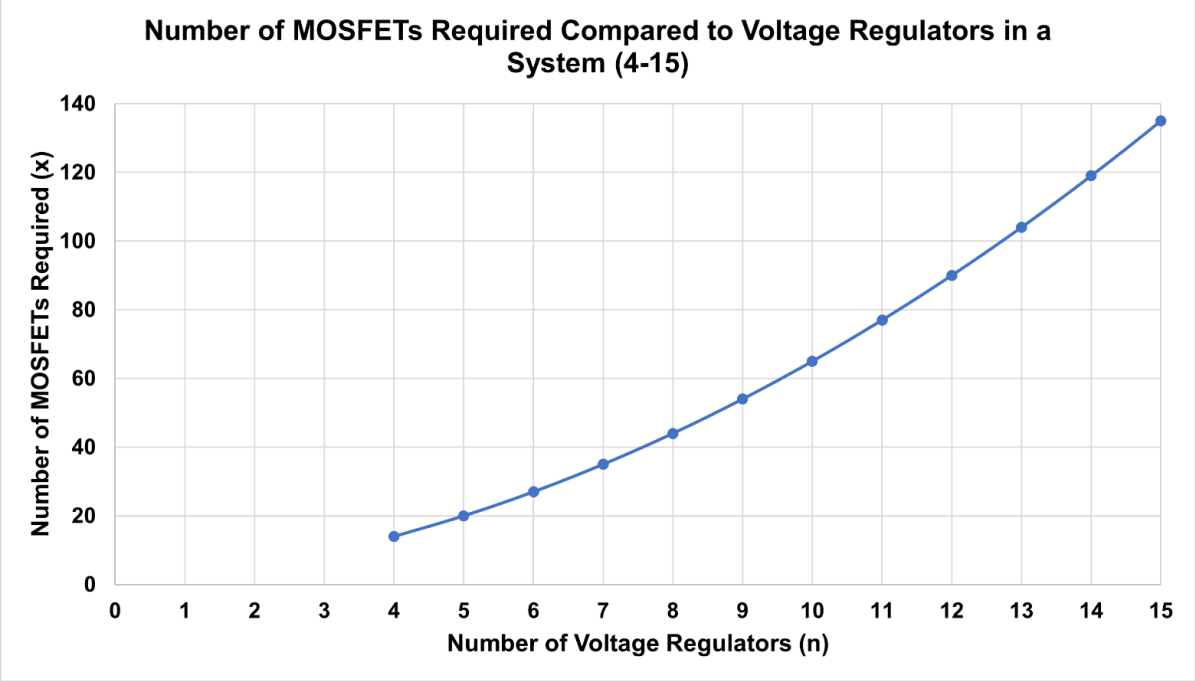

Figure 4-11: Number of MOSFETs Required Compared to Regulators (4-15)

Figure 4-11 shows the increasing relationship between the required number of MOSFET-optocoupler pairings compared to the number of regulators in a system. The shortest Golomb ruler of order 10 was found in 1972 to be of length 55 [70] which means that a system with 10 regulators could offer a minimum of 55V range.

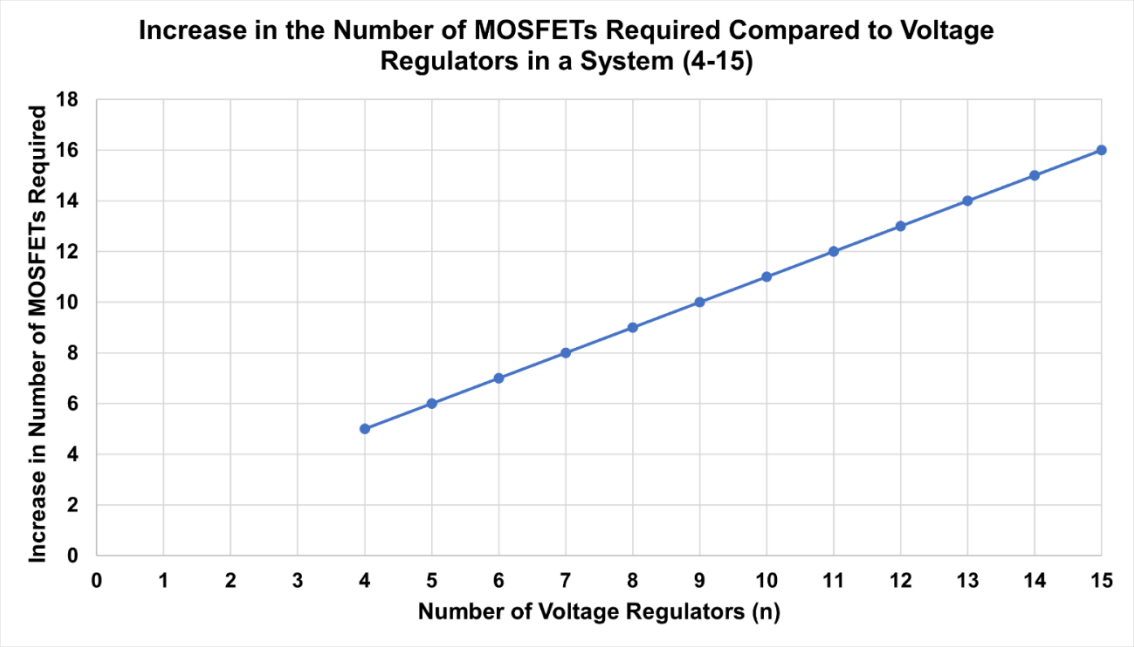

Figure 4-12: Increase in # of MOSFETs Required Compared to Regulators (4-15)

Figure 4-12 shows the linear relationship between the number of voltage regulators in a system and the increase in the number of MOSFETs required compared to the previous term, it is a very simple equation.

$$for\ n \geq 4$$
$$y = x + 1 \qquad (4\text{-}12)$$

With fewer than 4 regulators, there is no need for additional circuitry as all regulators are adjacent to one another, therefore, the relationship is not true for $n < 4$.

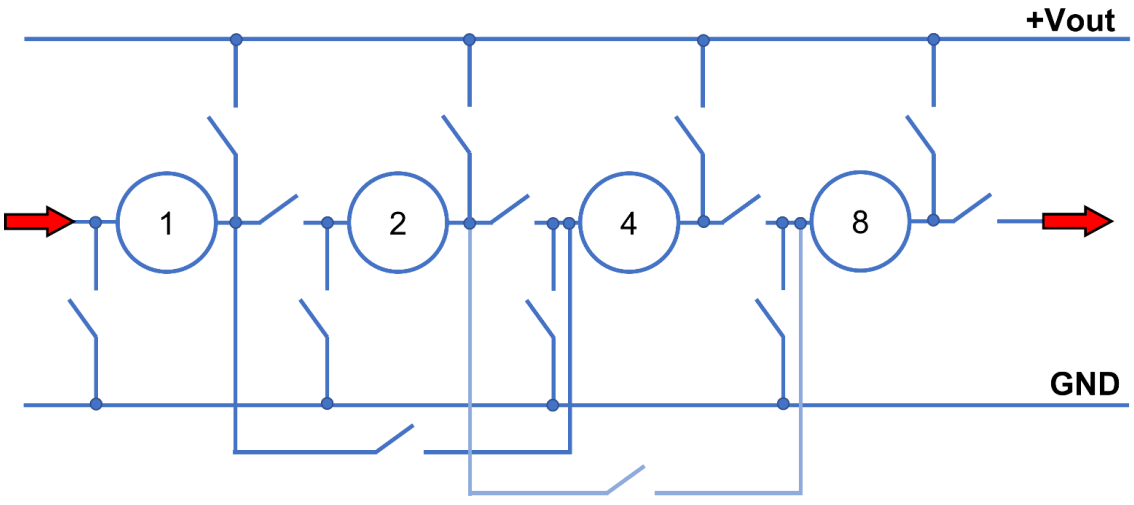

Figure 4-13: 4-Regulator Binary Sequence Non-Linear Matrix (NLM) Topology

Figure 4-13 shows a simplified schematic of a 4-regulator NLM binary sequence configuration circuit, the characteristics of which can be found in table 4-6 below.

Table 4-6: Statistical Summary of 4-Regulator Binary Sequence Topology System

Number of Voltage Regulators	4
Number of MOSFETs Required	14
Number of Different Possible Output Voltages	15 (16 including 0V)
Possible Output Voltages (V)	0, 1, 2, 3, 4, 5, 6, 7, 8, 9, 10, 11, 12, 13, 14, 15
Maximum Possible Output Voltage (V)	1 + 2 + 4 + 8 = 15

For 5 regulators in an NLM construction, the statistics are shown in table 4-7.

Table 4-7: Statistical Summary of 5-Regulator Binary Sequence Topology System

Number of Voltage Regulators	5
Number of MOSFETs Required	20
Number of Different Possible Output Voltages	31 (32 including 0V)
Possible Output Voltages (V)	0, 1, 2, 3, 4, 5, 6, 7, 8, 9, 10, 11, 12, 13, 14, 15, 16, 17, 18, 19, 20, 21, 22, 23, 24, 25, 26, 27, 28, 29, 30, 31
Maximum Possible Output Voltage (V)	1 + 2 + 4 + 8 + 16 = 31

4.4 Linear Flow (LF) Versus Non-Linear Matrix (NLM)

In either topology, there is a very important condition to maintain; at least one of the MOSFETs between the regulators always needs to be ‘off’ otherwise the circuit will be damaged. There needs to be a break between at least 2 of the regulators to prevent a loop being created. This also needs to be taken into consideration when designing the control circuitry and software to turn the MOSFETs on and off; sequencing is critical to be able to avoid the loop scenario. The ‘break’ MOSFET *must* be switched off *before*

any of the other MOSFETs are switched on. Synonymous with the well-known ‘fire break’ technique used for minimising the spread of wildfires.

Table 4-8 shows the characteristics of several topologies organised in the linear flow topology.

Table 4-8: Linear Flow (LF) Topology Statistics

# of Regulators	3	3	4	4
Ruler	0, 1, 4, 6	0, 2, 6, 7	0, 1, 4, 6, 13	0, 2, 6, 7, 15
Sequence	1, 3, 2	2, 4, 1	1, 3, 2, 7	2, 4, 1, 8
Length	6	7	13	15
Possible Outputs	1, 2, 3, 3, 4, 5, 6	1, 2, 3, 4, 5, 6, 7	1, 2, 3, 4, 5, 6, 7, 8, 9, 10, 11, 12, 13	1, 2, 4, 5, 6, 7, 8, 9, 10, 11, 13, 14, 15
# of Possible Outputs	7	7	13	13
Missing Outputs	N/A	N/A	N/A	3, 12
# of Missing Outputs	0	0	0	2
Repeated Outputs	3	N/A	N/A	N/A
# of Repeated Outputs	1	0	0	0
# of MOSFET + Optocoupler Pairs	9	9	12	12

Table 4-9 outlines some statistics for different ruler configurations for the NLM topology.

Table 4-9: Non-Linear Matrix Topology Statistics

# of Regulators	4	4	5
Ruler	0, 1, 4, 6, 13	0, 2, 6, 7, 15	0, 1, 3, 7, 15, 31
Sequence	1, 3, 2, 7	2, 4, 1, 8	1, 2, 4, 8, 16
Length	13	15	31
Possible Outputs	1, 2, 3, 3, 4, 5, 6, 7, 8, 9, 10, 10, 11, 12, 13	1, 2, 3, 4, 5, 6, 7, 8, 9, 10, 11, 12, 13, 14, 15	1, 2, 3, 4, 5, 6, 7, 8, 9, 10, 11, 12, 13, 14, 15, 16, 17, 18, 19, 20, 21, 22, 23, 24, 25, 26, 27, 28, 29, 30, 31
# of Possible Outputs	15	15	31
Missing Outputs	N/A	N/A	N/A
# of Missing Outputs	0	0	0
Repeated Outputs	3, 10	N/A	N/A
# of Repeated Outputs	2	0	0
# of MOSFET + Optocoupler Pairs	14	14	20

The NLM structures would allow for many more output combinations when the system has 4 or more regulators. There are drawbacks, however, with the main consequence being the radical increase in complexity as a non-linear topology requires far more MOSFETs, optocouplers and passive components. The relationship between increasing number of regulators in the system and the subsequent number of MOSFETs and optocouplers required is exponential.

Table 4-10: LF and NLM Advantages and Disadvantages

Topology	Advantages	Disadvantages
LF	Simple implementation, even at higher orders	Poor ruler construction results in low number of outputs, especially at higher system orders
	Low implementation cost	Efficient ruler construction requires time and computation
	Economical with an efficient ruler construction	
NLM	Achieves 100% output coverage if mathematical construction allows	High implementation cost
	Number of achievable outputs grows in line with system order	High circuit complexity, drastically increasing at higher system orders
		Exponential increase in required number of MOSFETs and optocouplers as system order grows
		Size and cost of control circuitry (larger microcontroller or FPGA) increases at higher orders
		Redundant at low system orders if an efficient ruler can be constructed

There are more advantages to the LF topology compared to NLM, and there are far more disadvantages than advantages to NLM. The non-linear matrix configuration only becomes relevant with 4 or more regulators. A system with 3 regulators or fewer is equivalent to already being a matrix as each of the regulators is already adjacent to each of the others. With an NLM system that has 4 or more regulators, they can be said to be ‘unordered’ as it wouldn’t matter what order they are arranged in; each one still has a direct connection to every other one. Therefore, the well-known binomial

coefficient theory can be used to determine the number of possible outputs from the system. This is standard well-known theory of combinations.

Binomial Coefficient:

$$ {}_nC_k = \binom{n}{k} = \frac{n!}{k!\,(n-k)!} \qquad (4\text{-}13) $$

Summation of binomial coefficients

$$ \sum_{i=0}^{k} \binom{n}{i} \qquad (4\text{-}14) $$

Where n = number of regulators

k = index number for the binomial coefficient

There should be 8 outcomes from combining 3 regulators and 16 outcomes from 4 regulators, but the $3C0$ and $4C0$ terms can be ignored as they both correspond to 0V output, this leaves 7 possible outcomes for 3 regulators and 15 relevant possibilities for 4 regulators.

Table 4-11: Binomial Theorem for n = 1 to 10

n	k = 1	k = 2	k = 3	k = 4	k = 5	k = 6	k = 7	k = 8	k = 9	k = 10	Total
1	1										1
2	2	1									3
3	3	3	1								7
4	4	6	4	1							15
5	5	10	10	5	1						31
6	6	15	20	15	6	1					63
7	7	21	35	35	21	7	1				127
8	8	28	56	70	56	28	8	1			255
9	9	36	84	126	126	84	36	9	1		511
10	10	45	120	210	252	210	120	45	10	1	1023

For all ‘n’, there is only one way to choose nothing (0V output). Therefore, if the k=0 term is also included, the total column becomes the following:

Table 4-12: Including k=0 (choose nothing)

n	Total Excluding k=0	Total Including k=0
0	0	1
1	1	2
2	3	4
3	7	8
4	15	16
5	31	32
6	63	64
7	127	128
8	255	256
9	511	512
10	1023	1024

Table 4-13: Matrix vs Linear Topology Possible Unique Outputs

Number of Regulators (n)	NLM Possibilities	LF Topology Possibilities	Difference Between LF and NLM Topologies	% Achievable with LF
1	1	1	0	100
2	3	3	0	100
3	7	7	0	100
4	15	13	2	86.67
5	31	21	10	67.74
6	63	31	32	49.21
7	127	43	84	33.86
8	255	57	198	22.35
9	511	73	438	14.29
10	1023	91	932	8.90

Table 4-13 shows that for low numbers of regulators, the possible number of unique outputs is not affected much by the topology. A linear/consecutive system with 4 regulators can output 87% (13/15) of the possible outputs that a matrix system could present. This gap widens as the order grows, however, as shown in figure 4-14 by the orange and blue curves.

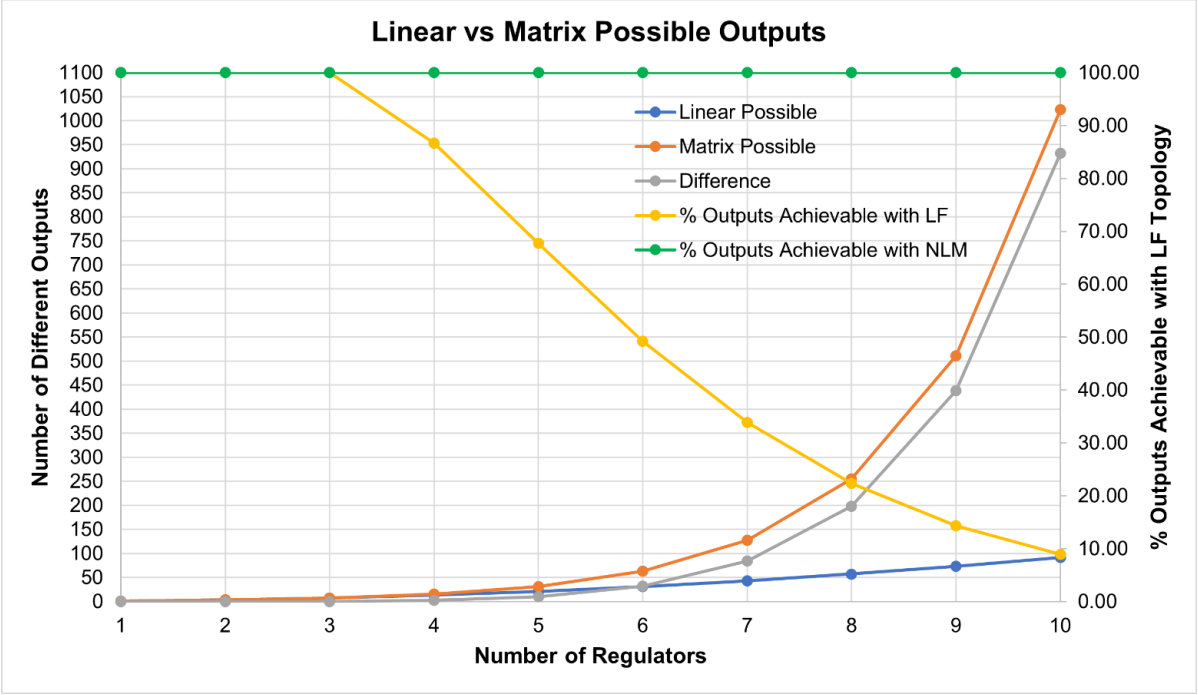

Figure 4-14: Linear vs Matrix Possible Outputs

LF systems with 1, 2, and 3 regulators are perfect systems and can output 100% of the possible values. Systems with 4 or 5 regulators can output more values than they are unable to. Systems with 6 or more regulators have a larger number of impossible outputs compared to possible outputs. The difference between possible and impossible outputs increases exponentially as shown in figure 4-15.

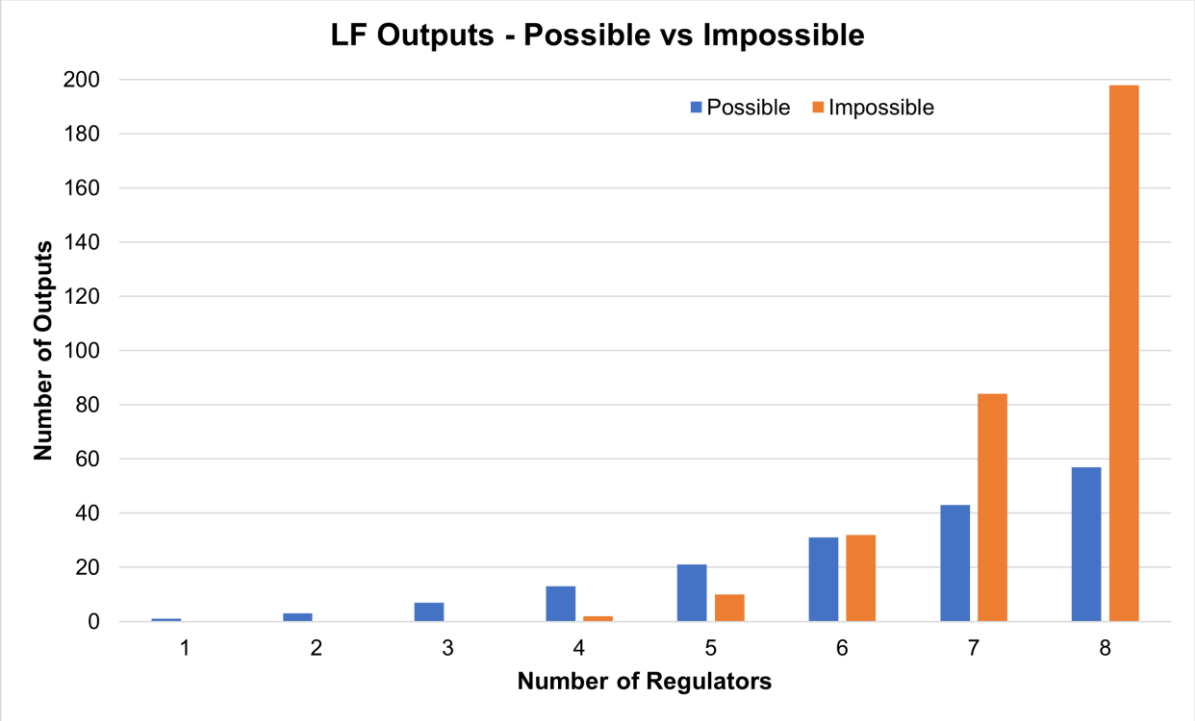

Figure 4-15: LF Outputs - Possible vs Impossible

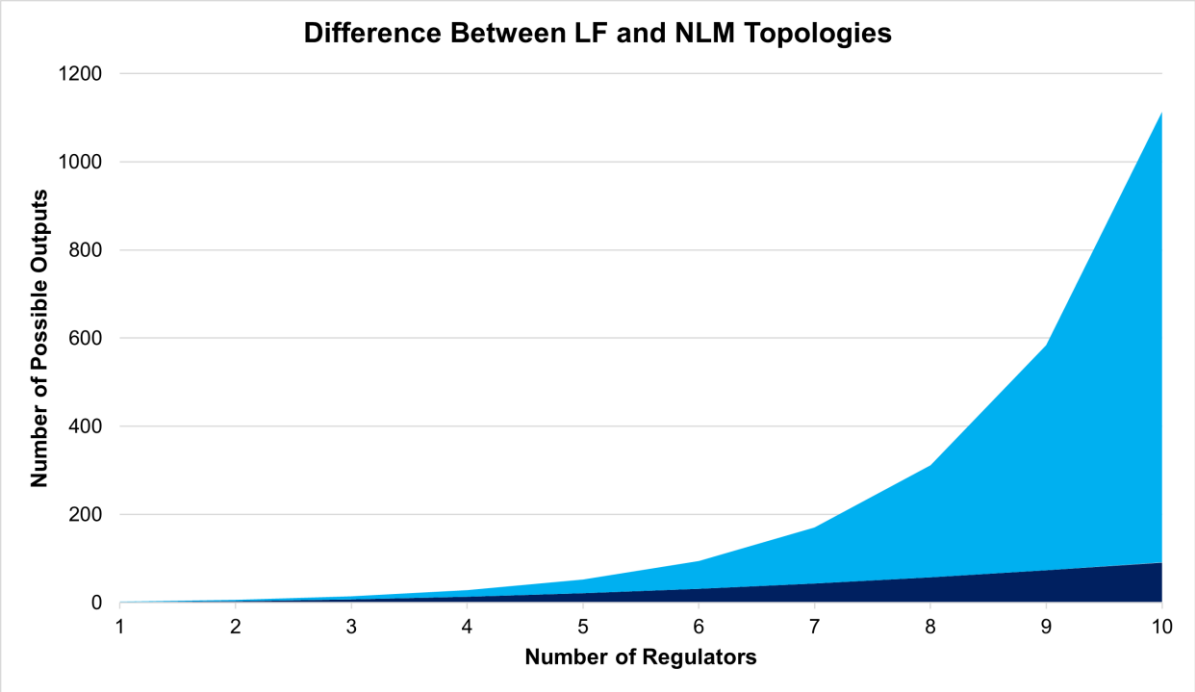

Figure 4-16: Difference Between LF and NLM Topologies

The main difference between the LF and NLM topologies is the number of possible outputs. Figure 4-16 shows that there is an exponential increase in the difference between possible outputs for a LF system and possible outputs for a NLM system.

Alternative ruler compositions should be explored. If a good mathematical ruler is constructed and chosen as the basis for the system, then it is much better to choose the LF topology as it can minimise circuit complexity and implementation cost and therefore have a high efficiency.

4.5 Golomb Ruler Topologies

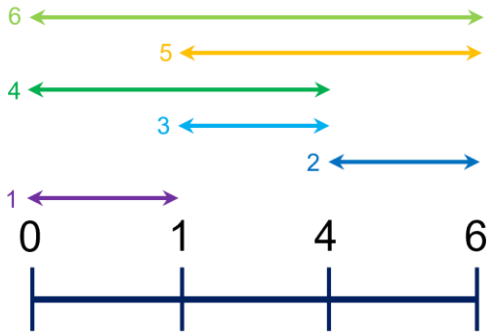

Figure 4-17: 0146 Order 4 Linear Golomb Ruler, Perfect

When considering a Golomb ruler, the length (L) is the final mark along the ruler so for the example (0, 1, 4, 6) the length is 6; this is the greatest magnitude of distance that can be measured. The 0, 1, 4, 6 system is 'perfect' because all numbers between 0 to L can be covered by considering the difference between 2 different marks (a_i and a_j) along the ruler.

Table 4-14: 0146 Order 4 Linear Golomb Ruler Output Calculations

a_i	a_j	$a_i - a_j$	Output
1	0	1-0	1
6	4	6-4	2
4	1	4-1	3
4	0	4-0	4
6	1	6-1	5
6	0	6-0	6

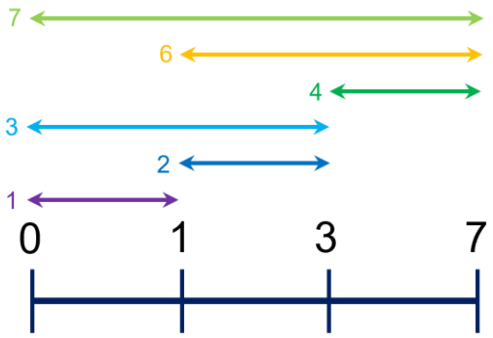

Figure 4-18: 0137 Order 4 Linear Golomb Ruler, Non-Perfect

The ruler shown in figure 4-18 is longer than that in figure 4-17 as it can measure a greater overall distance (7 compared to 6) but is non-perfect because it has a missing distance of 5 (as shown in table 4-15).

Table 4-15: 0137 Order 4 Linear Golomb Ruler Output Calculations

a_i	a_j	$a_i - a_j$	Output
1	0	1-0	1
3	1	3-1	2
3	0	3-0	3
7	3	7-3	4
7	1	7-1	6
7	0	7-0	7

Figure 4-19 shows a second example which is also a Golomb ruler but again non-perfect as it cannot measure 3.

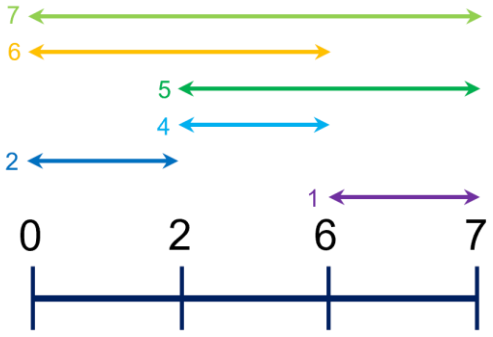

Figure 4-19: 0267 Order 4 Linear Golomb Ruler, Non-Perfect

Table 4-16: 0267 Order 4 Linear Golomb Ruler Output Calculations

a_i	a_j	$a_i - a_j$	Output
7	6	7-6	1
2	0	2-0	2
6	2	6-2	4
7	2	7-2	5
6	0	6-0	6
7	0	7-0	7

As can be seen from table 4-14, table 4-15, and table 4-16, there are only 6 possible measurements to be made with linear ruler of order 4.

Table 4-17: Number of Possible Measurements for Different Linear Ruler Orders

Number of Marks (Ruler Order)	**Number of Measurable Distances**	**Increase in Number of Measurable Distances from Ruler X to Ruler Y**
3	3	N/A
4	6	3
5	10	4
6	15	5
7	21	6
8	28	7
9	36	8
10	45	9

$$\#\, measurable = (n-1) + (n-2) + \cdots + (n-n) \qquad (4\text{-}15)$$

$$where\ n\ is\ the\ number\ of\ marks$$

This is a pattern that occurs in Pascal's triangle on the diagonals starting on row 3.

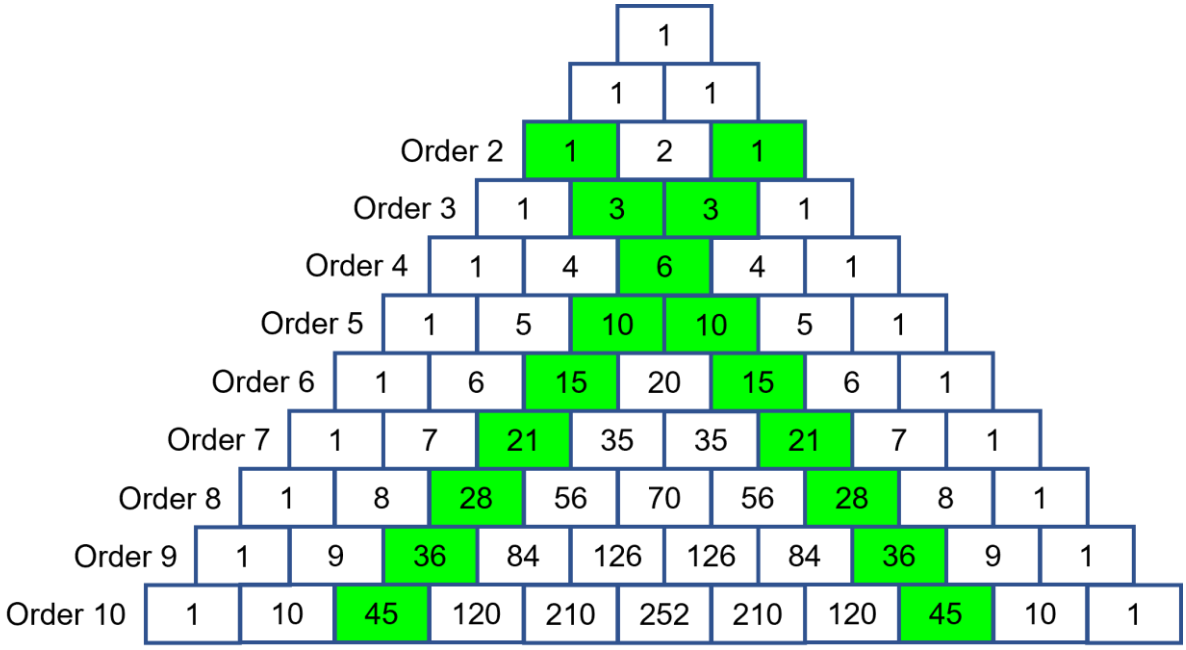

Figure 4-20: First 11 Rows of Pascal's Triangle with Sequence Highlighted

The highlighted sequence describes the number of possible measurements with a linear ruler of increasing order, the ruler orders are shown beside each relevant row.

4.6 New Method for Constructing Modular Golomb Rulers (MGRs)

The circular construction of MGRs makes them far more beneficial in many applications than their linear counterparts. The main benefit being the wrap-around characteristic whereby the first mark (must be 0) and the final mark (the length) occupy the same space which enables a greater number of possible distance measurements. There is an additional benefit that the ruler order reduces by 1. Thus, by adding an extra mark, the length can be greatly increased but the order remains the same as the linear equivalent.

If a linear Golomb ruler is converted into its modular or circular equivalent, then it will become perfect in that all distances between 0 and its length will become measurable, but it may not necessarily remain a Golomb ruler, as there is a possibility that some measurable distances may be repeated.

The maximum number of measurements that can be made within a single rotation of the circular ruler is given by equation (4-16):

$$\#\ Distance\ Measurements = n^2 - n + 1 \qquad (4\text{-}16)$$
$$where\ n\ is\ the\ number\ of\ marks$$

Table 4-18: Maximum Possible Number of Distance Measurements

Ruler Order (n)	$n2-n+1$
2	3
3	7
4	13
5	21
6	31
7	43
8	57
9	73
10	91
11	111
12	133
13	157
14	183
15	211

The key is to design a ruler structure which has the properties of one of the rows from table 4-18. If it is possible to choose a construction which has a length equal to that of the number of measurements for a particular order and the ruler has no repeated measurements, then its efficiency will be maximised, and the ruler will be perfect. Any Golomb ruler with missing measurements will increase in efficiency when translating to a circular arrangement.

The length of an MGR is the only unavoidable repeated measurement in that the measurement can be taken from any mark with a full 360º rotation back to the same mark, this is obvious and therefore is excluded from consideration when evaluating repeated measurements.

Considering the linear Golomb ruler examples 0, 1, 3, 7 (figure 4-18) and 0, 2, 6, 7 (figure 4-19), both have 1 missing distance when in linear form but both become perfect when converted to their modular form, as shown in figure 4-21.

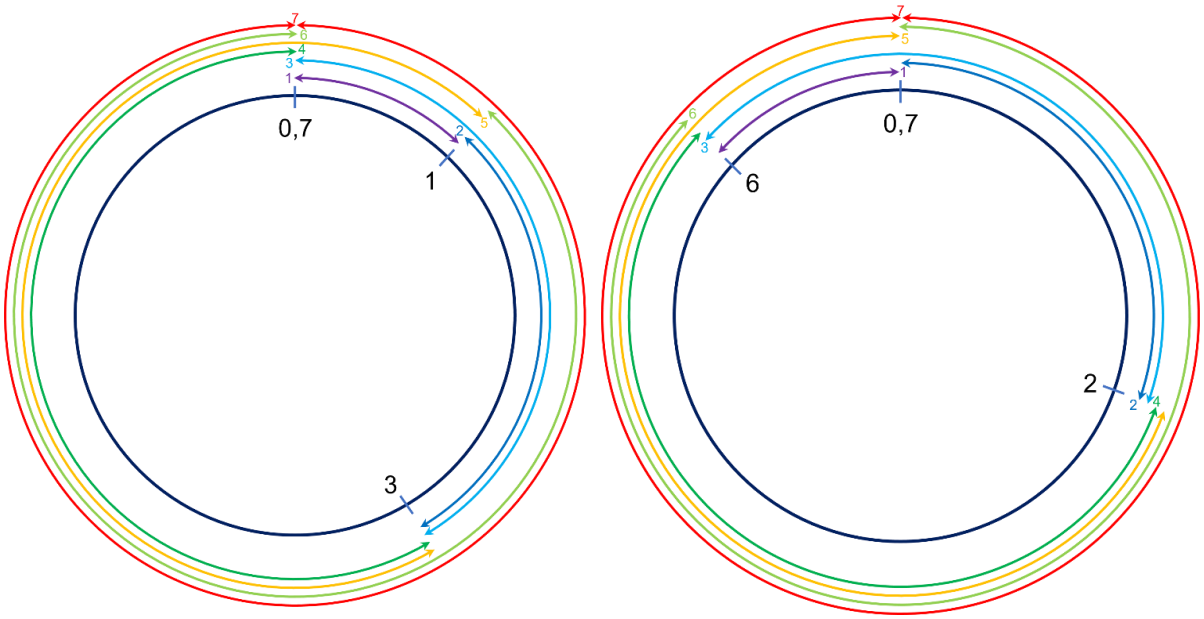

Figure 4-21: Two Order 4 Linear Golomb Rulers Translated into MGR's

As the starting point for any measurement using these MGRs could be at any mark on the circumference of the circle, and any measurement can go through the '0' mark, it means that there are no longer any missing measurable distances and both rulers are now perfect and of a lower order than their linear equivalents. As order 4 rulers, both structures are maximally efficient as there are no missing measurable distances.

The three main construction methods for modular Golomb rulers are the Singer theorem, the Bose-Chowla theorem and the Rusza theorem. As the Singer theorem is the oldest, this was the starting point of an evaluation of a new method to produce MGRs. This new method is simpler and has the following 3 steps:

1. Start with any known optimal Golomb ruler and identify its first unmeasurable distance.
2. Add that unmeasurable distance to the magnitude of the final mark to create a new final mark which becomes its new length.
3. Translate the new ruler into its modular equivalent.

$$Ruler\ Y = Ruler\ X + (L_x + Unmeasurable_1)$$
$$where\ L_x\ is\ the\ length\ of\ ruler\ X \qquad (4\text{-}17)$$

When adding the lowest missing distance from ruler X as the next distance to make ruler Y (going from figure 4-24 to figure 4-26) the number of measurable distances increases by the number of marks on ruler X.

$$m_y = m_x + o_x$$
$$where\ m_x = number\ of\ measurable\ distances\ for\ ruler\ x \qquad (4\text{-}18)$$
$$o_x = order\ of\ ruler\ x, or\ number\ of\ marks\ on\ ruler\ x$$

$$m_{xy} = o_x$$
$$where\ m_{xy} = increase\ in\ \#\ of\ distances\ from\ ruler\ x\ to\ ruler\ y \qquad (4\text{-}19)$$

The 0, 1, 4, 6 ruler is an order 4 perfect and optimal Golomb ruler. Being perfect means that the lowest unmeasurable distance is 7 as it is 1 greater than the ruler length. If one more mark is added to the ruler at a distance of 7 away from the final mark, the ruler shown in figure 4-22 can be obtained:

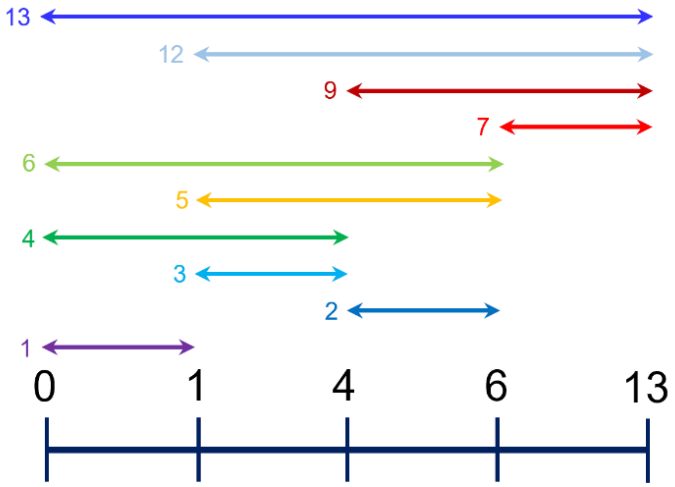

Figure 4-22: Order 5 Linear Golomb Ruler, Non-Perfect

Figure 4-22 satisfies the first two steps of the new construction method and shows a 5-mark linear Golomb ruler. The statistics for this ruler are shown in table 4-19.

Table 4-19: Order 5 Linear Ruler Measurable Distances Summary

Distance	**Count**	**Measurable? (Yes/No)**	**% Measurable/ Unmeasurable**
1, 2, 3, 4, 5, 6, 7, 9, 12, 13	10	Yes	77
8, 10, 11	3	No	23

This ruler is not perfect as there are three distances which cannot be measured, only achieving a 77% measurable distance completion.

For step 3 of the method, it is translated to its modular equivalent so becomes the order 4 perfect MGR in figure 4-23.

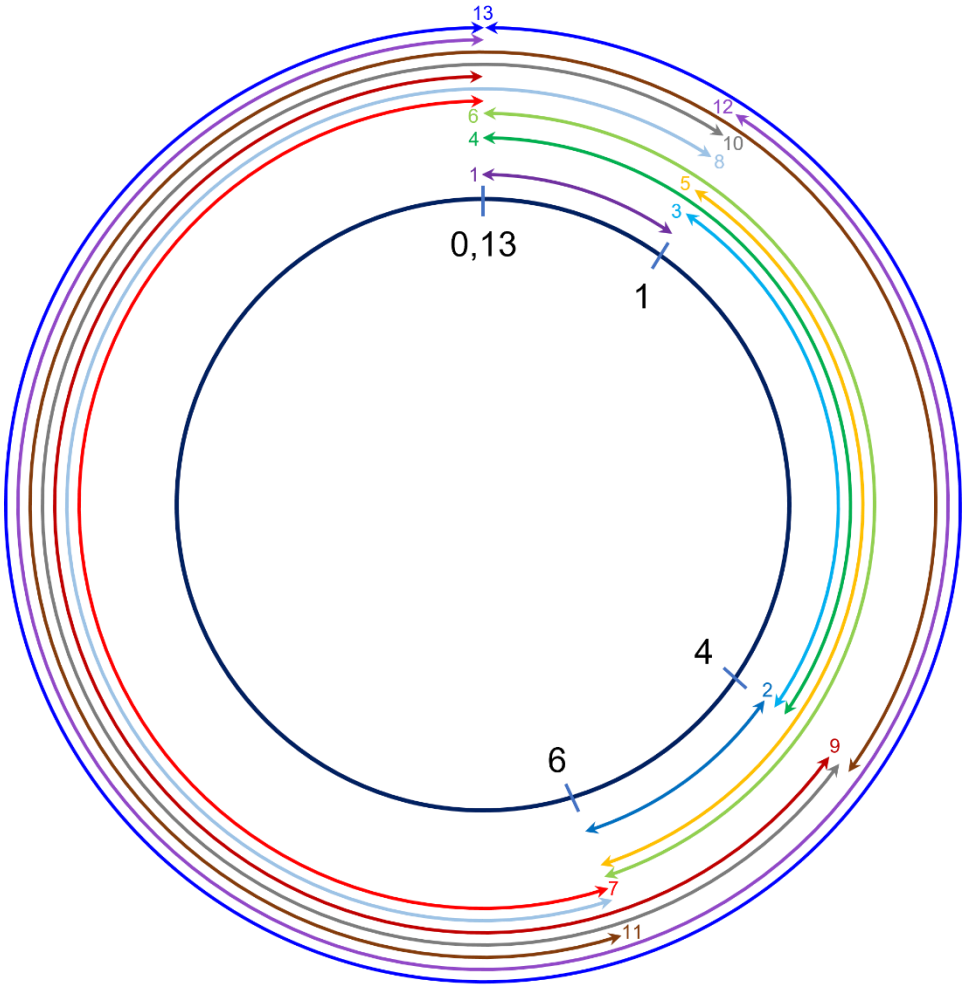

Figure 4-23: Order 4 Perfect MGR with Length of 13

The overall length is still the same as the figure 4-22 linear version at 13 but there are no unmeasurable distances between 0 and its length.

Table 4-20: Order 4 MGR Measurable Distances Summary

Distance	**Count**	**Measurable? (Yes/No)**	**% Measurable/ Unmeasurable**
1, 2, 3, 4, 5, 6, 7, 8, 9, 10, 11, 12, 13	13	Yes	100
N/A	0	No	0

Table 4-20 shows that the MGR version of the 5-mark linear ruler is a perfect Golomb equivalent. With a 4-mark circular ruler, the number of possible distance

measurements is 13 (from table 4-18), therefore when the length of the ruler is 13 and there are 13 unique distance measurements, it follows that it is perfect.

An alternative optimal Golomb ruler construction with order 6, shown in figure 4-24, has just two missing measurable distances so has a higher level of completion compared to the order 5 ruler.

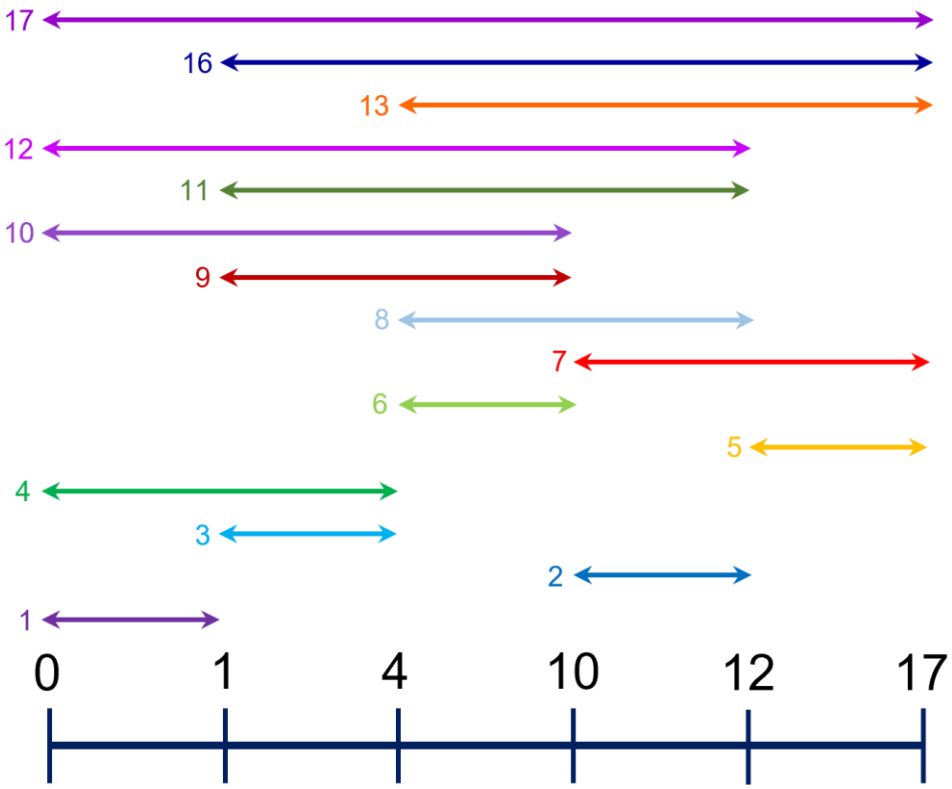

Figure 4-24: Order 6 Linear Golomb Ruler, Non-Perfect

Table 4-21: Order 6 Linear Ruler Measurable Distances Summary

Distance	Count	Measurable? (Yes/No)	% Measurable/ Unmeasurable
1, 2, 3, 4, 5, 6, 7, 8, 9, 10, 11, 12, 13, 16, 17	15	Yes	88
14, 15	2	No	12

The order 6 non-perfect Golomb ruler in figure 4-24 becomes the order 5 perfect modular ruler in figure 4-25 when translated into a circular topology.

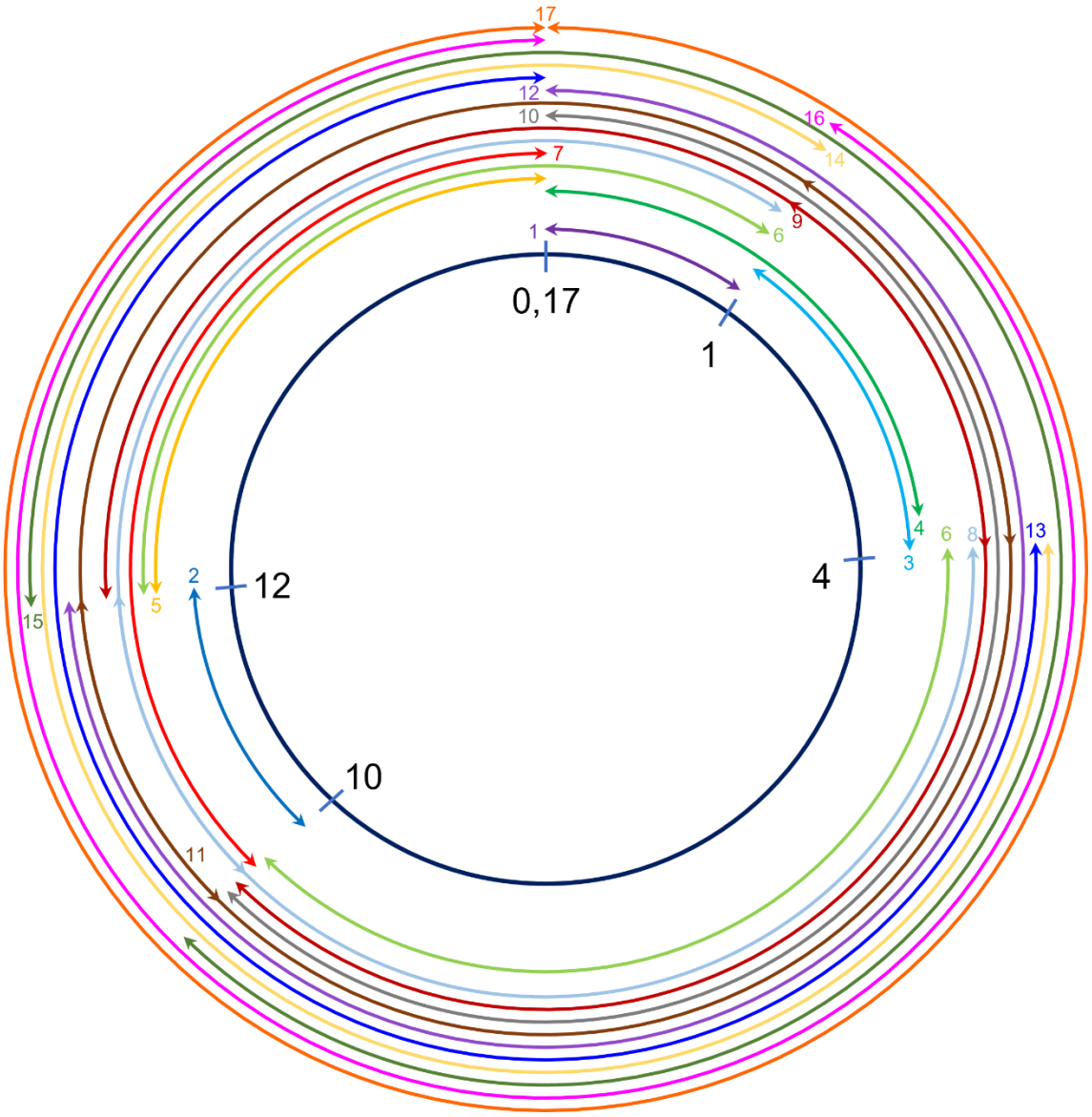

Figure 4-25: Order 5 Modular Ruler with Length of 17

Table 4-22: Order 5 MGR Measurable Distances Summary

Distance	Count	Measurable? (Yes/No)	% Measurable/ Unmeasurable
1, 2, 3, 4, 5, 6, 7, 8, 9 10, 11, 12, 13, 14, 15, 16, 17	17	Yes	100
N/A	0	No	0

Table 4-22 shows that there are no missing distances between 0 to the length of the ruler meaning that the ruler is perfect. There is a problem, however, there are 21

possible measurable distances with a 5-mark circular ruler, so it follows that there will be 4 repeated distances when the length of the ruler is 17. The repeated distance measurements in this instance are 6, 8, 9, and 11. This is therefore no longer a Golomb ruler.

However, by following the proposed MGR method, a perfect MGR can be obtained. The lowest unmeasurable distance is 14 so if this is added to the length (17+14=31) as the next mark, the 7-mark linear ruler in figure 4-26 is obtained:

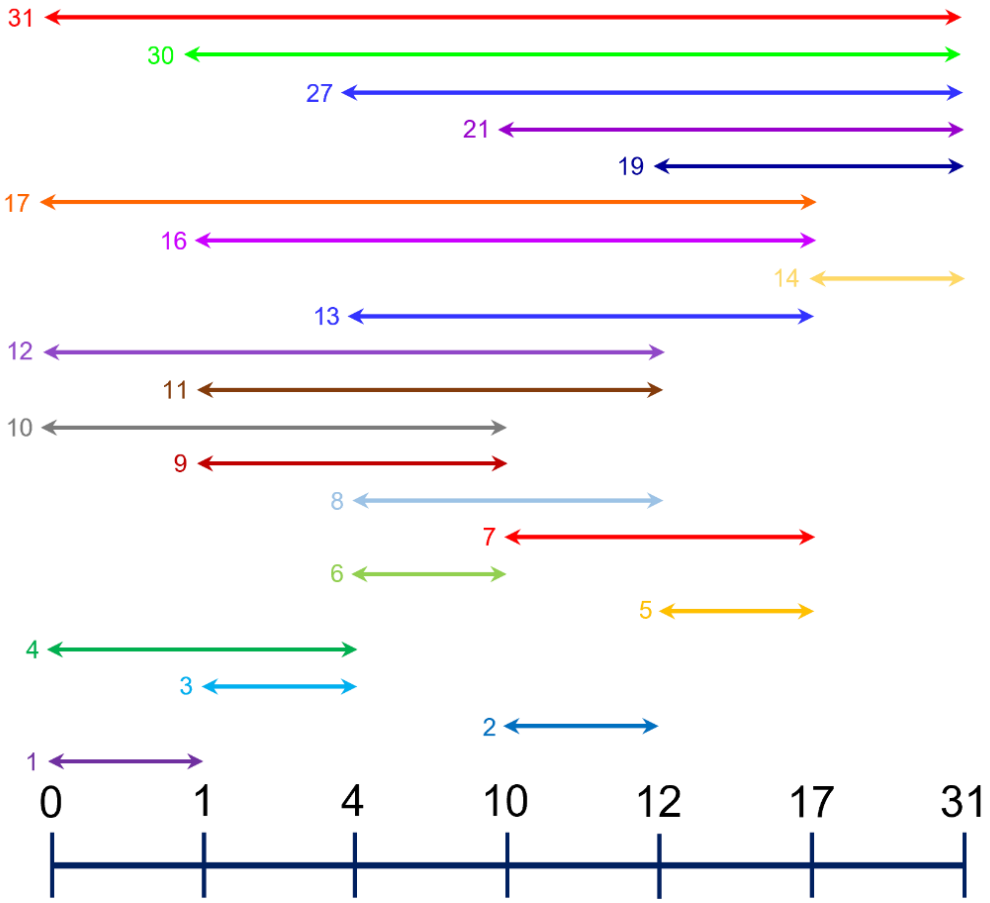

Figure 4-26: Order 7 Linear Golomb Ruler, Non-Perfect

Table 4-23: Order 7 Linear Ruler Measurable Distances Summary

Distance	Count	Measurable? (Yes/No)	% Measurable/ Unmeasurable
1, 2, 3, 4, 5, 6, 7, 8, 9, 10, 11, 12, 13, 14, 16, 17, 19, 21, 27, 30, 31	21	Yes	68
15, 18, 20, 22, 23, 24, 25, 26, 28, 29	10	No	32

Table 4-23 shows that the 7-mark linear Golomb ruler has a large range of measurable values but is missing a high percentage of the values between 0 to its length. This ruler is still a Golomb ruler as no differences between any pair of marks is repeated, but it achieves a lower completion rate of 68% compared to the 6-mark version in figure 4-24. This adds an extra 6 measurable distances, with a greater magnitude, but it also adds 8 more unmeasurable distances which reduces the efficacy of the ruler. Following step 3 of the MGR method means translating the 7-mark linear ruler into a 6-mark modular equivalent as shown in figure 4-27.

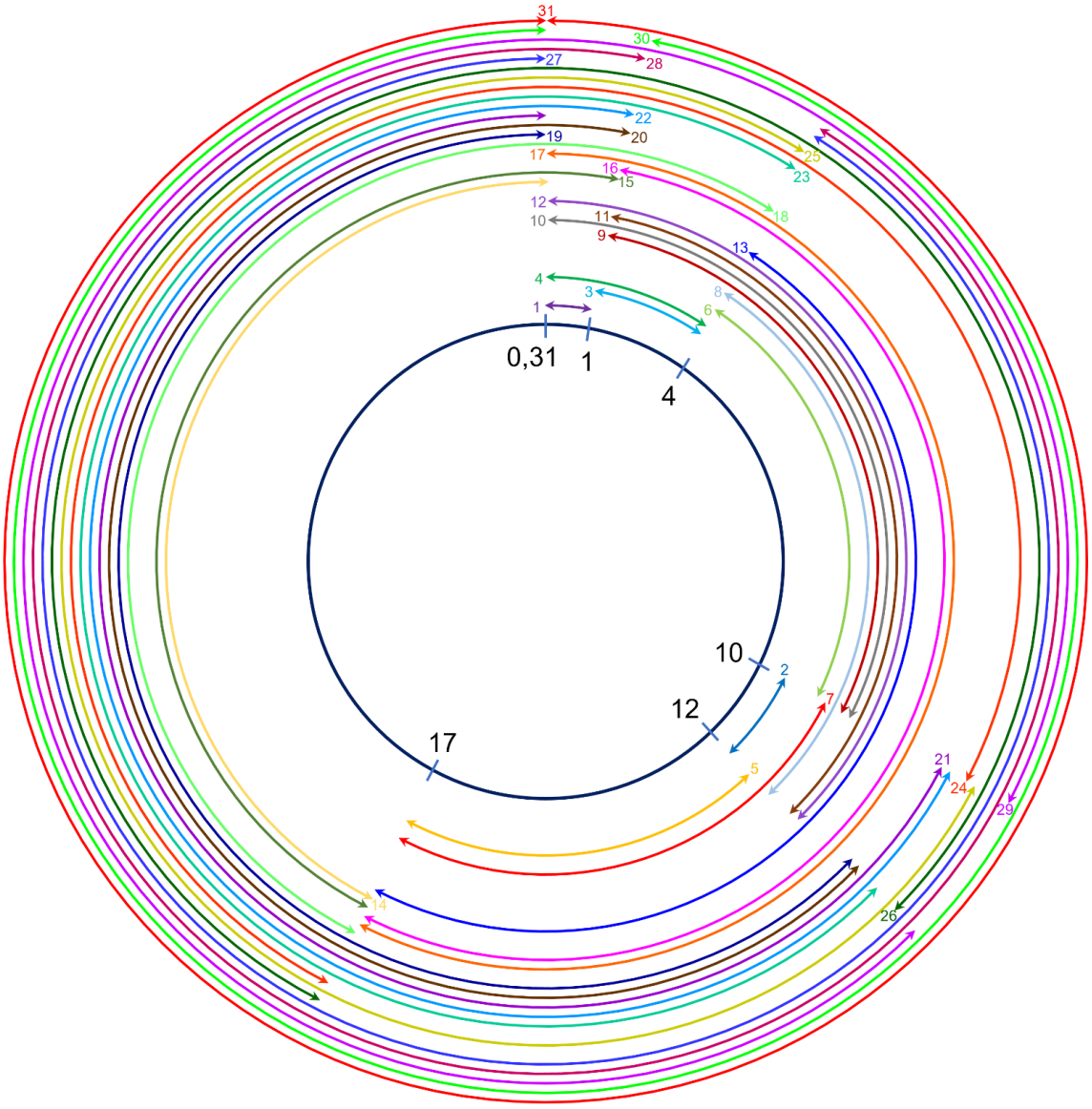

Figure 4-27: Order 6 MGR with Length of 31

Table 4-24: Order 6 MGR Measurable Distances Summary

Distance	Count	Measurable? (Yes/No)	% Measurable/ Unmeasurable
1, 2, 3, 4, 5, 6, 7, 8, 9, 10, 11, 12, 13, 14, 15, 16, 17, 18, 19, 20, 21, 22, 23, 24, 25, 26, 27, 28, 29, 30, 31	31	Yes	100
N/A	0	No	0

There are a possible 31 unique distance measurements with a 6-mark circular ruler (from table 4-18). This ruler has a length of 31 with no repeated measurements so it is a perfect MGR and is a maximally efficient structure.

Table 4-25: Linear Ruler and Circular/Modular Equivalent Comparison

Type	Order	Structure	% Measurable	% Unmeasurable
Linear	5	0,1,4,6,13	77	23
Modular	4	1,4,6,13/0	100	0
Linear	6	0,1,4,10,12,17	88	12
Modular	5	1,4,10,12,17/0	100	0
Linear	7	0,1,4,10,12,17,31	68	32
Modular	6	1,4,10,12,17,31/0	100	0

Table 4-25 compares the linear structures with their equivalent modular constructions. The advantage of the modular structure is clear to see in the statistics. Linear ruler equivalents are of 1 higher order and the three structures described here only have between 68-88% completion.

The main advantage of the circular/modular structure is that the missing measurable distances from the linear version are eliminated and can be measured. This is achieved by the ability to begin at any mark on the circle and rotate clockwise (or indeed anti-clockwise) to measure a distance, with the unique property of continuing 'through' the 0 mark which is at the same point on the circle as the largest mark (a rulers' *length*). In theory, this structure can also be used to measure all distances which are multiples of the length of the MGR as unlimited full 360-degree rotations can be made, as well as all distances between 0 to X where X is the length multiplied by the number of full 360-degree rotations.

Being circular in nature, the distance between any two of the marks is given by the length of the arc between those two marks whereas a linear ruler is a simple straight-line distance between the two. Arc length is given by the well-known formula:

$$L = \frac{2\pi r\theta}{360} \qquad (4\text{-}20)$$

Where *L* is the arc length, *r* is the circle radius, *θ* is the arc central angle in degrees.

MATLAB code was written to analyse and construct different rulers when presented with a linear ruler of any order and composition of marks. The code calculates each possible measurable distance from the linear ruler and presents them in a matrix format, then displays them in ascending order. The code then translates the ruler into its modular equivalent form and evaluates all additional achievable distances due to the new construction and it outputs them in a matrix format followed by ascending order. Finally, the code calculates the missing distances and therefore whether the presented linear ruler is an MGR. If there are any repeated distances or missing distances, then these are also displayed. Appendix G shows an extract of the code. Below is the output when presented with the linear ruler marks from figure 4-26:

0, 1, 4, 10, 12, 17, 31

The number of differences between pairs of marks in this linear ruler is 21, shown in table 4-26.

Table 4-26: iy – ix Mark Differences in Linear Ruler

	iy-i0	iy-i1	iy-i2	iy-i3	iy-i4	iy-i5	iy-i6
i6	31	30	27	21	19	14	0
i5	17	16	13	7	5	0	0
i4	12	11	8	2	0	0	0
i3	10	9	6	0	0	0	0
i2	4	3	0	0	0	0	0
i1	1	0	0	0	0	0	0
i0	0	0	0	0	0	0	0

Linear measurable distances in ascending order:

1, 2, 3, 4, 5, 6, 7, 8, 9, 10, 11, 12, 13, 14, 16, 17, 19, 21, 27, 30, 31

When translated to a circular ruler, the marks are therefore:

1, 4, 10, 12, 17, 31

The number of additional differences for the circular configuration is 10. The total number of measurable distances for the circular configuration is therefore 31. The additional 10 distance measurements are shown in table 4-27.

Table 4-27: iy – ix Mark Differences in Circular Ruler

	i6+iy-i5	i6+iy-i4	i6+iy-i3	i6+iy-i2
i6+i1-iy	15	20	22	28
i6+i2-iy	18	23	25	0
i6+i3-iy	24	29	0	0
i6+i4-iy	26	0	0	0

Circular differences in ascending order:

15, 18, 20, 22, 23, 24, 25, 26, 28, 29

There are no repeated differences with this circular ruler.

There are no missing differences with this circular ruler.

This is a maximally efficient ruler construction.

4.7 Merry-Go-Round (MGR) Power Systems

Optimal Golomb rulers are those which have no shorter alternative with the same number of marks. Following construction of the MGRs from optimal Golomb rulers, a power supply control system can be developed.

Like the binary regulator system, the Golomb structures can be used to construct power systems involving regulators or batteries. The modular type of ruler is far more appealing in these situations. The number of regulators/batteries in a system is its order. The highest possible output voltage is equivalent to the ruler length. These modular constructions are designated the merry-go-round (MGR) technique, synonymous with the modular Golomb rulers (MGRs).

To construct voltage regulator system topologies, only the distances between adjacent pairs of marks are noteworthy. For a system with 3 regulators, 7V would be the maximally efficient output.

The order 4 linear optimal perfect Golomb ruler (0,1,4,6) is shown again in figure 4-28 but this time with the differences between adjacent marks displayed (1,3,2).

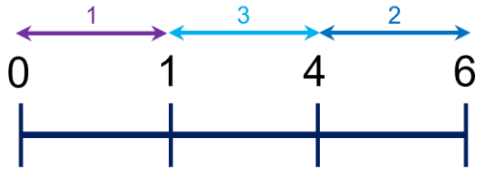

Figure 4-28: Order 4 Optimal Golomb Ruler Showing Distances Between Marks

This would translate to a voltage regulator system of 1V, 3V, 2V which could output the following voltages – 1,2,3,3,4,5,6. There are two different ways to output 3V; either directly from the 3V regulator or by combining the 1V and the 2V regulators. This means that there is a wasted output possibility (proving again that 7V would be optimal) so an alternative structure should be investigated. The linear Golomb rulers 0,1,3,7 and 0,2,6,7 both have a maximum output possibility of 7V but unfortunately

both have a missing measurable distance (5 and 3, respectively). As modular constructions, however, they are perfect so can both output all voltages from 1-7V.

For a system with 4 regulators, the maximally efficient output would be 13V.

When considering the ruler from figure 4-22, the following ruler is acquired:

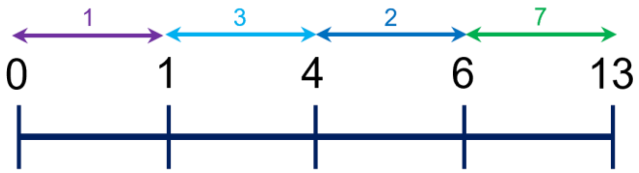

Figure 4-29: Order 5 Linear Golomb Ruler Showing Distances Between Marks

The 0,1,4,6 ruler (order 3 voltage regulator system) is inefficient but the 0,1,4,6,13 (order 4 system) is efficient.

As the constructions still follow the rules of Golomb rulers, the 1V steps can be multiplied by a constant to achieve a lower or higher set of voltages and achieve outputs correspondingly.

4.7.1 Simulation

From figure 4-23 and figure 4-29 the following circuit can be constructed which depicts the 0, 1, 4, 6, 13 Golomb ruler in terms of the differences between marks, resulting in a 1V, 3V, 2V, 7V regulator system. This is perfect as it allows for all voltages up to the maximum 13V to be output by the circuit, with no repeated outputs. This system has been extensively tested in simulation.

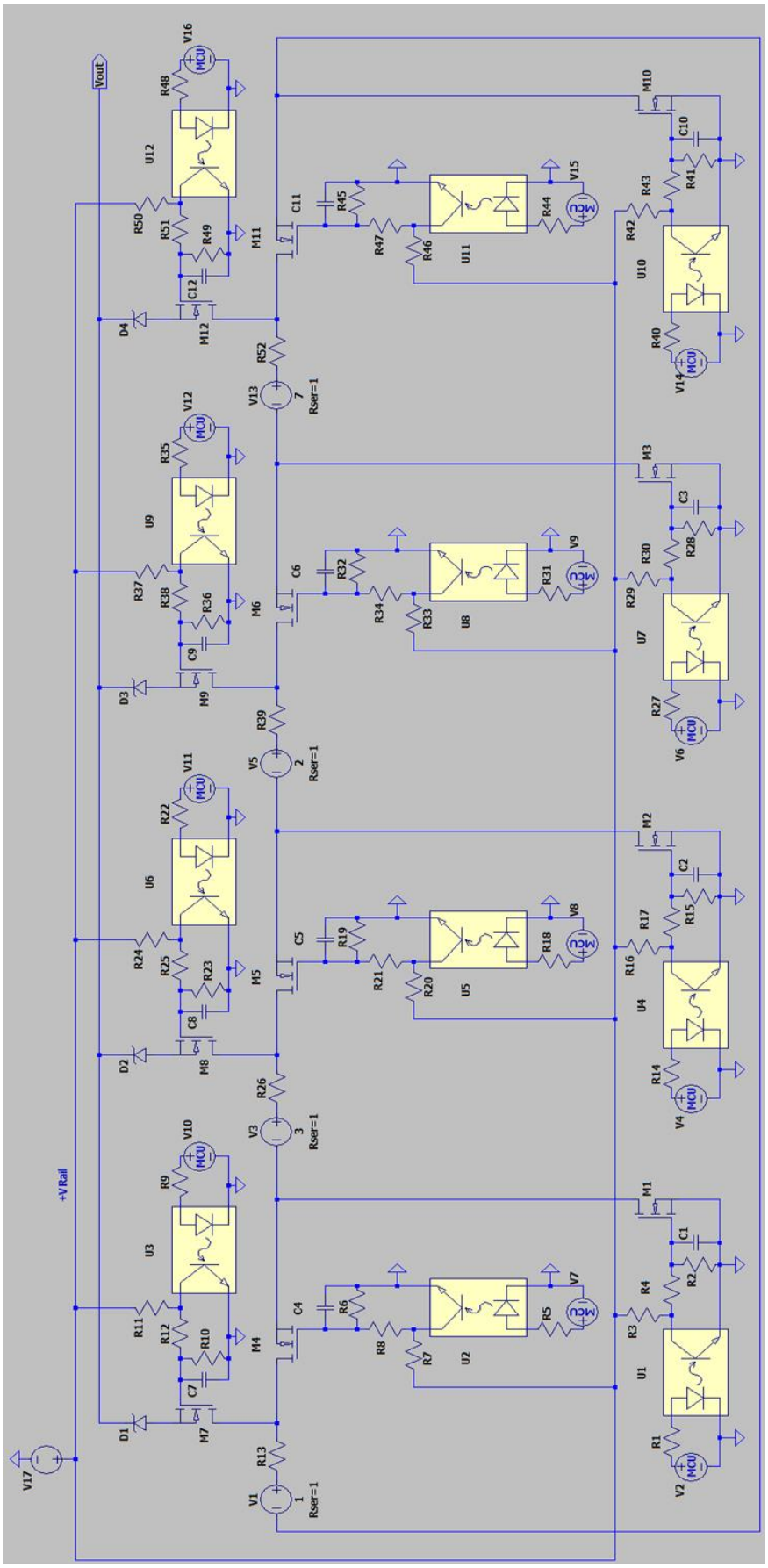

Figure 4-30: 4-Regulator Perfect MGR Topology

By combining each of these 4 regulators in various ways, 1-13V can be output in 1V increments. The required circuit configurations for each of the output voltages are described in table 4-28.

Table 4-28: Output Voltage Configurations for Order 4 MGR System, 1, 3, 2, 7

Output Voltage (V)	**Configuration Description**
1	Turn all MOSFETs off except those connecting the 1V regulator to the output rail
2	Turn all MOSFETs off except those connecting the 2V regulator to the output rail
3	Turn all MOSFETs off except those connecting the 3V regulator to the output rail
4	Isolate the 3V regulator from GND reference. Run the 1V regulator into the 3V regulator and turn on MOSFETs connecting the 4V to the output rail
5	Isolate the 2V regulator from GND reference. Run the 3V regulator into the 2V regulator and turn on MOSFETs connecting the 5V to the output rail
6	Isolate the 3V and the 2V regulators from GND reference. Run the 1V regulator into the 3V regulator and into the 2V regulator. Turn on MOSFETs connecting the 6V to the output rail
7	Turn all MOSFETs off except those connecting the 7V regulator to the output rail
8	Isolate the 1V regulator from GND reference. Run the 7V regulator into the 1V regulator and turn on MOSFETs connecting the 8V to the output rail
9	Isolate the 7V regulator from GND reference. Run the 2V regulator into the 7V regulator and turn on MOSFETs connecting the 9V to the output rail
10	Isolate the 7V and the 1V regulators from GND reference. Run the 2V regulator into the 7V regulator and into the 1V regulator. Turn on MOSFETs connecting the 10V to the output rail

11	Isolate the 1V and the 3V regulators from GND reference. Run the 7V regulator into the 1V regulator and into the 3V regulator. Turn on MOSFETs connecting the 11V to the output rail
12	Isolate the 2V and the 7V regulators from GND reference. Run the 3V regulator into the 2V regulator and into the 7V regulator. Turn on MOSFETs connecting the 12V to the output rail
13	Isolate the 3V, 2V and 7V regulators from GND reference. Run the 1V regulator into the 3V regulator, into the 2V regulator and into the 7V regulator. Turn on MOSFETs connecting the 13V to the output rail. This is a special condition as all regulators are in use so there are 4 different ways to output the 13V depending on which MOSFET is used as the ‘circuit break’

These different configurations vary greatly in complexity; some are trivial such as the single regulator outputs (1V, 3V, 2V, 7V), but others are more complex as adjacent connections are required. In one case, the 13V output, there are four different circuit arrangements which can achieve 13V output.

			Desired Voltage Out (V) @ Vout															
			1	2	3	4	5	6	7	8	9	10	11	12	13 (M12 Out)	13 (M9 Out)	13 (M8 Out)	13 (M7 Out)
Voltage Control - Functions	V1	Fixed voltage source	1.0	1.0	1.0	1.0	1.0	1.0	1.0	1.0	1.0	1.0	1.0	1.0	1.0	1.0	1.0	1.0
	V2	MCU logic for U1 opto, controls M1	0.0	0.0	0.0	3.3	0.0	3.3	0.0	0.0	0.0	0.0	3.3	0.0	3.3	3.3	3.3	0.0
	V3	Fixed voltage source	3.0	3.0	3.0	3.0	3.0	3.0	3.0	3.0	3.0	3.0	3.0	3.0	3.0	3.0	3.0	3.0
	V4	MCU logic for U4 opto, controls M2	0.0	0.0	0.0	0.0	3.3	3.3	0.0	0.0	0.0	0.0	0.0	3.3	3.3	3.3	0.0	3.3
	V5	Fixed voltage source	2.0	2.0	2.0	2.0	2.0	2.0	2.0	2.0	2.0	2.0	2.0	2.0	2.0	2.0	2.0	2.0
	V6	MCU logic for U7 opto, controls M3	0.0	0.0	0.0	0.0	0.0	0.0	0.0	0.0	3.3	3.3	0.0	3.3	3.3	0.0	3.3	3.3
	V7	MCU logic for U2 opto, controls M4	3.3	3.3	3.3	0.0	3.3	0.0	3.3	3.3	3.3	3.3	0.0	3.3	0.0	0.0	0.0	3.3
	V8	MCU logic for U5 opto, controls M5	3.3	3.3	3.3	3.3	0.0	0.0	3.3	3.3	3.3	3.3	3.3	0.0	0.0	0.0	3.3	0.0
	V9	MCU logic for U8 opto, controls M6	3.3	3.3	3.3	3.3	3.3	3.3	3.3	3.3	0.0	0.0	3.3	0.0	0.0	3.3	0.0	0.0
	V10	MCU logic for U3 opto, controls M7	0.0	3.3	3.3	3.3	3.3	3.3	3.3	0.0	3.3	0.0	3.3	3.3	3.3	3.3	3.3	0.0
	V11	MCU logic for U6 opto, controls M8	3.3	3.3	0.0	0.0	3.3	3.3	3.3	3.3	3.3	3.3	0.0	3.3	3.3	3.3	0.0	3.3
	V12	MCU logic for U9 opto, controls M9	3.3	0.0	3.3	3.3	0.0	0.0	3.3	3.3	3.3	3.3	3.3	3.3	3.3	0.0	3.3	3.3
	V13	Fixed voltage source	7.0	7.0	7.0	7.0	7.0	7.0	7.0	7.0	7.0	7.0	7.0	7.0	7.0	7.0	7.0	7.0
	V14	MCU logic for U10 opto, controls M10	0.0	0.0	0.0	0.0	0.0	0.0	0.0	3.3	0.0	3.3	3.3	0.0	0.0	3.3	3.3	3.3
	V15	MCU logic for U11 opto, controls M11	3.3	3.3	3.3	3.3	3.3	3.3	3.3	0.0	3.3	0.0	0.0	3.3	3.3	0.0	0.0	0.0
	V16	MCU logic for U12 opto, controls M12	3.3	3.3	3.3	3.3	3.3	3.3	0.0	3.3	0.0	3.3	3.3	0.0	0.0	3.3	3.3	3.3
MOSFETs ON/OFF		M1	ON	ON	ON	OFF	ON	OFF	ON	ON	ON	ON	OFF	ON	OFF	OFF	OFF	ON
		M2	ON	ON	ON	ON	OFF	OFF	ON	ON	ON	ON	ON	OFF	OFF	OFF	ON	OFF
		M3	ON	ON	ON	ON	ON	ON	ON	ON	OFF	OFF	ON	OFF	OFF	ON	OFF	OFF
		M4	OFF	OFF	OFF	ON	OFF	ON	OFF	OFF	OFF	OFF	ON	OFF	ON	ON	ON	OFF
		M5	OFF	OFF	OFF	OFF	ON	ON	OFF	OFF	OFF	OFF	OFF	ON	ON	ON	OFF	ON
		M6	OFF	OFF	OFF	OFF	OFF	OFF	OFF	OFF	ON	ON	OFF	ON	ON	OFF	ON	ON
		M7	ON	OFF	OFF	OFF	OFF	OFF	OFF	ON	OFF	ON	OFF	OFF	OFF	OFF	OFF	ON
		M8	OFF	OFF	ON	ON	OFF	OFF	OFF	OFF	OFF	OFF	ON	OFF	OFF	OFF	ON	OFF
		M9	OFF	ON	OFF	OFF	ON	ON	OFF	OFF	OFF	OFF	OFF	OFF	OFF	ON	OFF	OFF
		M10	ON	ON	ON	ON	ON	ON	ON	OFF	ON	OFF	OFF	ON	ON	OFF	OFF	OFF
		M11	OFF	OFF	OFF	OFF	OFF	OFF	OFF	ON	OFF	ON	ON	OFF	OFF	ON	ON	ON
		M12	OFF	OFF	OFF	OFF	OFF	OFF	ON	OFF	ON	OFF	OFF	ON	ON	OFF	OFF	OFF
Desired Voltage Out (V) @ Vout			1	2	3	4	5	6	7	8	9	10	11	12	13	13	13	13
Actual Voltage Out (V) @ Vout			1.0382956	1.9894640	2.9738798	3.9737866	4.9736195	5.9735608	6.9639835	7.9640141	8.9639177	9.9639702	10.9639700	11.9638530	12.9638160	12.964002	12.963948	12.963938
Difference Between Desired and Actual Output Voltage (V)			0.0382956	0.0105360	0.0261202	0.0262134	0.0263805	0.0264392	0.0360165	0.0359859	0.0360823	0.0360298	0.0360300	0.0361470	0.0361840	0.0359980	0.0360520	0.0360620
Difference Between Desired and Actual Output Voltage (%)			3.6883138	0.5295899	0.8783206	0.6596580	0.5304085	0.4426037	0.5171824	0.4518563	0.4025282	0.3616008	0.3286218	0.3021351	0.2791153	0.2776766	0.2780943	0.2781716

Figure 4-31: 4-Regulator MGR Circuit Test Results. Larger Version in Appendix H

Table 4-29: Simulated Outputs for Order 4 Golomb Regulator System 1, 3, 2, 7

Desired Voltage Out (V) @ Vout	Actual Voltage Out (V) @ Vout	Difference Between Desired and Actual Output Voltage (V)	Difference Between Desired and Actual Output Voltage (%)
1	1.0382956	0.0382956	3.6883138
2	1.9894640	0.0105360	0.5295899
3	2.9738798	0.0261202	0.8783206
4	3.9737866	0.0262134	0.6596580
5	4.9736195	0.0263805	0.5304085
6	5.9735608	0.0264392	0.4426037
7	6.9639835	0.0360165	0.5171824
8	7.9640141	0.0359859	0.4518563
9	8.9639177	0.0360823	0.4025282
10	9.9639702	0.0360298	0.3616008
11	10.9639700	0.0360300	0.3286218
12	11.9638530	0.0361470	0.3021351

The circuit break (non-conducting MOSFET) to prevent a loop from forming and damaging the circuit is before the first regulator in each of the listed series below.

Table 4-30: Four Different Circuit Arrangements to Achieve 13V Output

Arrangement	Output Voltage (V)	Voltage Difference (V)	Difference (%)
1 → 3 → 2 → 7 → Output	12.963816	0.036184V	0.2791153
3 → 2 → 7 → 1 → Output	12.963938	0.036062V	0.2781716
2 → 7 → 1 → 3 → Output	12.963948	0.036052V	0.2780943
7 → 1 → 3 → 2 → Output	12.964002	0.035998V	0.2776766

The most efficient arrangement is the fourth configuration in table 4-30 as it offers the closest output voltage to 13V. The circuit break is between the 2V and 7V regulators, the ground reference is for the 7V regulator with the other regulators floating, and the path to the output rail is after the 2V regulator.

There are slight differences between each of these ‘equivalent’ outputs because of the differences in the conduction of each MOSFET based on the drain-source voltage. With a real circuit, there will also be slight differences in the MOSFET gate threshold as well as differences in each gate-source voltage and therefore the switching times of each MOSFET will differ somewhat. Real components have tolerances which will also affect the circuit performance.

This circuit configuration is scalable and can be applied to any maximally efficient modular Golomb ruler. The 0,1,4,10,12,17,31 ruler construction would allow 31 different voltage levels up to the maximum 31V.

For each MOSFET, the gate is controlled with an optocoupler which is enabled or disabled by the microcontroller unit (MCU). Each optocoupler has an LED between a GPIO pin on the MCU (with a current limiting resistor) at the anode and the system ground at the cathode. When the MCU GPIO pin is set to output 3V3, the optocoupler LED conducts current and emits, and the photodiode also starts to conduct current and switch on; this forces the gate of the MOSFET low. Otherwise, the MOSFET gate is held high by the positive voltage rail.

4.8 PET and Application to OFDM

An example of an arbitrary OFDM time domain signal envelope is show in figure 4-32, it fluctuates rapidly and has peaks of considerable magnitude compared to the average signal level hence the problem of high PAPR which adversely affects the power consumption of the system and the required power supply design which needs to be able to handle the peaks. Were the peaks to be of lower magnitude, the power supply construction could be simpler, less expensive and waste less power.

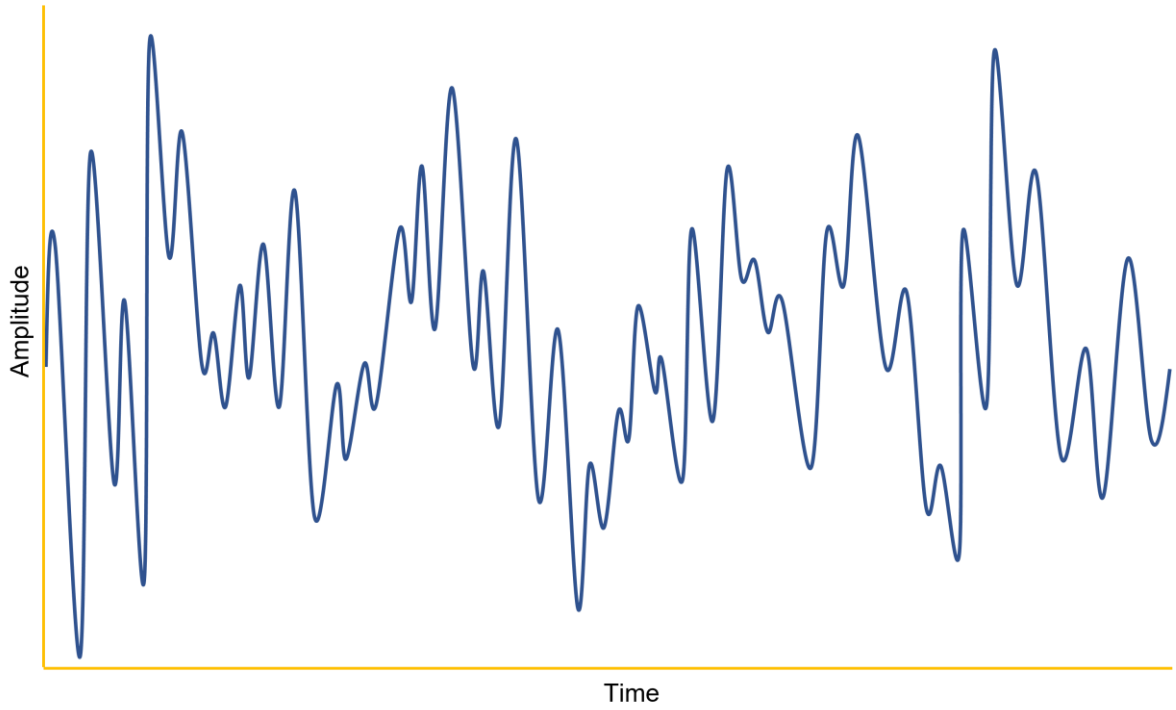

Figure 4-32: OFDM Signal Envelope in Time Domain

One approach to determining power supply switching thresholds would be to use an estimative technique. For a standard OFDM waveform, peaks occur in the time domain at regular intervals the inverse of the subcarrier spacing. An example is shown in equation (4-21).

$$Subcarrier\ spacing = 10kHz$$

$$Time\ Domain\ Waveform\ Peaks = \frac{1}{10x10^{-3}} \qquad (4\text{-}21)$$

$$= 100\mu s$$

If the subcarrier spacing is known, then the power supply could be ramped up or down in advance of the expected peaks. This would be a high-risk and coarse approach, however, and could lead to some problems:

- If the estimation isn't accurate then the signal will be chopped and distorted, and data loss will occur.
- To increase the robustness of the approach and to maintain signal fidelity, a margin of error could be introduced which would reduce the possible efficiency.

When considering the time domain signal for OFDM, the voltage tracking levels must be sensible to allow for the possible efficiency improvements; incorrect level choices will result in poor performance. The supply circuitry efficiency must be high otherwise it introduces noise and distortion to the ET amplifier output. Using linear regulators is considered due to their cleanliness but they are not as efficient as switch-mode power supplies (SMPS). The problem with SMPS is that they are inherently electrically noisy due to the switching components and generally have a higher output ripple which requires extra smoothing components.

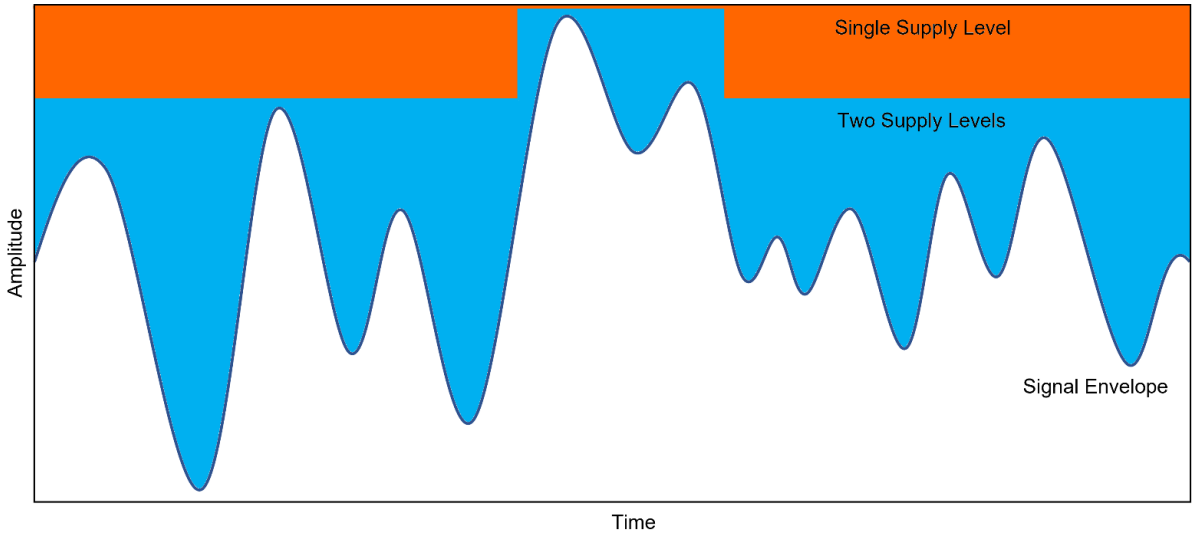

Figure 4-33: Wasted Power with Two Supply Levels, Option 1

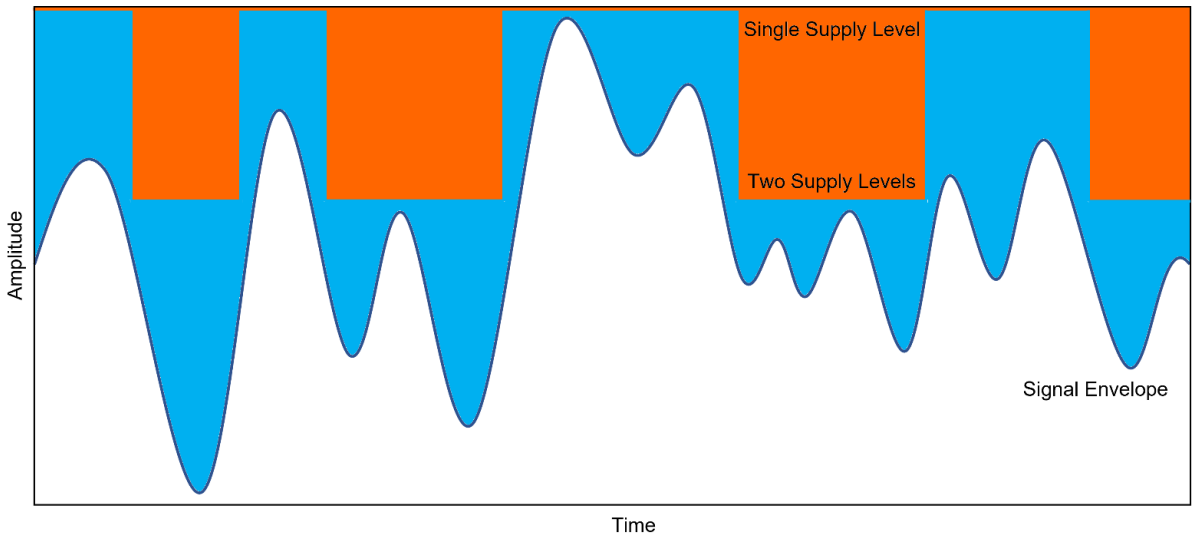

Figure 4-34: Wasted Power with Two Supply Levels, Option 2

Figure 4-33 and figure 4-34 both show a smaller segment of the signal shown in figure 4-32. Each one shows two different power supplies, one is a supply that has two different voltage levels and can switch between them as required. This supply would waste the power depicted by the light blue shaded area. The other supply is a single fixed voltage supply which would waste the power shown by the blue and orange shaded areas combined. Both are valid options but have different chosen levels for the two-level supply. For the depicted signal, option 2 would marginally be the better choice as the supply spends more time at the lower level. Both options are crude, however, which is where the PET technique presents its benefits.

A system with 6 levels would look like figure 4-35, which shows 4 of the available 6 voltage levels, with 2 spare levels which can be allocated depending on the shape of the remaining signal. One level will likely need to be at the base of the lowest point, and the other set to the highest peak shown.

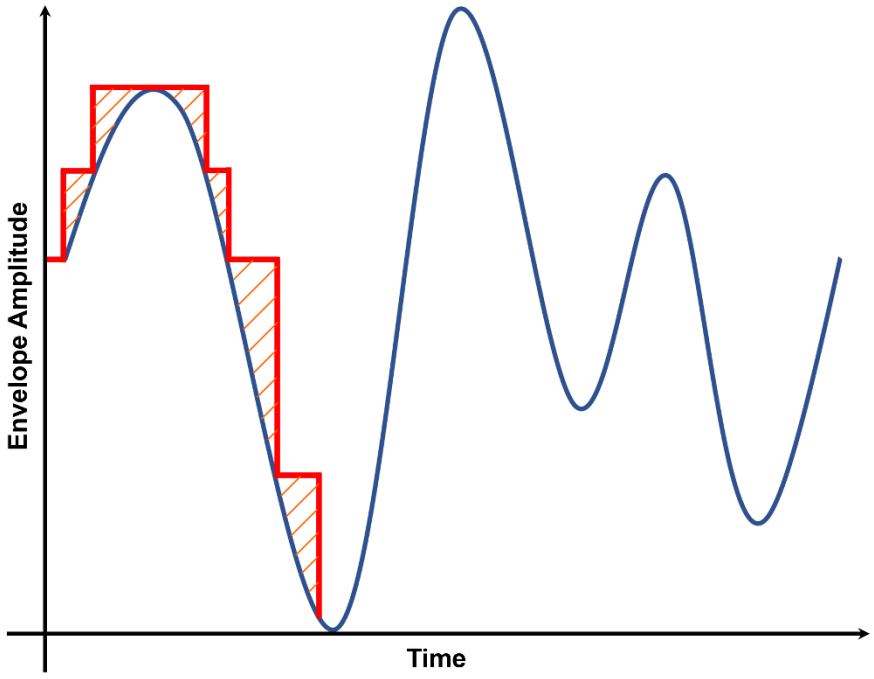

Figure 4-35: 6 Levels, 4 Shown, 2 Spare for Remaining Signal

The higher the number of levels that the supply can output, the closer the supply can get to the envelope signal and therefore the amount of wasted power is minimised. A system with 31 levels would look more like that in figure 4-36, which shows 27 of the available 31 levels, leaving 4 levels spare for the remaining signal.

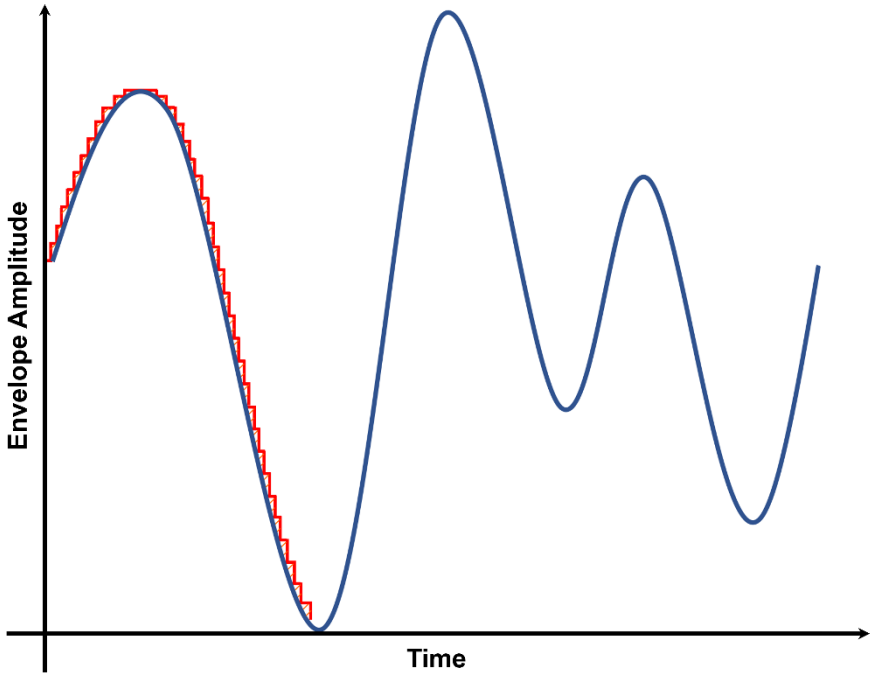

Figure 4-36: 31 Levels, 27 Shown, 4 Spare for Remaining Signal

The choices of where to place the thresholds determines the system efficiency. Therefore, the PET technique introduced in chapter 3 could be employed. If the probability density function of the signal is known, an advanced form of envelope tracking can be used to monitor the power envelope of the incoming signal and then follow the technique steps:

1. Use the power envelope to inform whereabouts on the normalised PDF the signal is.
2. Calculate the required voltage to handle the incoming signal power.

3. Determine which of the available signal voltages would be best used for that signal power, the closest voltage above the calculated. If the closest were below the required, then there would likely be signal clipping and distortion.
4. Switch the power supply accordingly to output the determined voltage.

With a higher number of available voltages (switching thresholds on the PDF), the waveform could be tracked more closely and therefore waste less power. This is a more efficient form of envelope tracking and doesn't rely on high bandwidth power supplies. It was also proven in chapter 3 that there is very little difference between the optimum switching thresholds and uniformly spaced ones. This means that a perfect MGR would be a very efficient construction technique for such power supplies. The 0,1,4,6 Golomb ruler shown in figure 4-17 would enable 6 uniformly spaced voltage levels using three regulators (1V, 3V, 2V). Whereas the 31-level MGR derived in figure 4-27 (0,1,4,10,12,17,31) is a far more efficient design. 31 uniformly spaced voltage levels achieved from 6 regulators. The 6 regulators would be 1V, 3V, 6V, 2V, 5V, 14V. When the system is idling, the power supply could utilise a very low operating voltage based on the lowest level for the 100-threshold calculation. This would enable faster turn-on and wake up times. It has been reported that of the energy consumed by the equipment at a base station, approximately 19% is consumed by the transceiver in idle mode [71], this could be drastically reduced with the addition of an idle mode threshold voltage.

4.8.1 Switching Considerations

MOSFET switching can introduce some noise but there are techniques to combat this.

Modern MOSFETs can switch very quickly with some in the order of tens of picoseconds. Faster switching times means that heat dissipation during the transition periods is minimised, therefore improving efficiency. There are several knock-on effects of the switching process, addressed in table 4-31.

Table 4-31: Techniques to Reduce System and MOSFET Switching Noise

Technique	Consideration and Difficulties
Filtering	Large values of capacitance (in the order of μF or tens of μF) on the output can help to reduce switching noise
Dead time	Having some dead time between switching off one MOSFET and switching the next on can help to reduce noise but at the cost of system efficiency as some signal fidelity may be lost
Component choices	Choosing the correct components can make a huge difference to the operation of any circuit. In this case for example, capacitors must have low ESR and inductance to help with noise and minimise wasted power. High tolerance components, albeit usually expensive, give the designer confidence in circuit operation
RF decoupling capacitors	Filtering out RF frequencies to reduce noise in the DC circuitry is a common practice in the RF world. This does not, however, help with MOSFET switching noise.
Linear regulators instead of switching regulators	Linear regulators don't suffer from the switching problems of switching regulators and switch-mode power supplies (SMPS). The big drawback, however, is their lack of efficiency compared to switchers, wasting lots of energy in the form of heat

4.9 Conclusion

This chapter presents two different topologies for power supply layout known as linear flow (LF) and non-linear matrix (NLM). The LF topology is useful and efficient if a suitable Golomb ruler structure can be designed. NLM topology achieves 100% mathematically possible output coverage but also suffers from exponential growth in circuit complexity and the required number of MOSFETs and optocouplers as the number of regulators grows. Therefore, there are serious cost implications as well as practical implementation issues. For those reasons, the best topology is LF, but only in circumstances where a suitable Golomb structure can be developed and implemented.

A new method for deriving modular Golomb rulers from linear optimal Golomb rulers is presented, this method is known as the merry-go-round (MGR) technique. This method is simple and is used to inform the power supply constructions towards the end of this chapter.

The MGR technique works by taking an optimal Golomb ruler, determining its lowest unmeasurable distance and adding that to its length to achieve a new final mark and increase its order by 1. If the ruler is then translated to its modular form, it will be a perfect MGR. MATLAB code was generated to prove that the technique works.

The order 4 optimal Golomb ruler (0, 1, 4, 6) was chosen initially. The lowest unmeasurable distance for this ruler is 7, this was taken as the next distance between marks, so the structure was expanded to the order 5 linear ruler (0, 1, 4, 6, 13).

MOSFETs, used as electronic switches, were operated by the brain of the system which was a microcontroller unit (MCU) to enable and disable current paths to the +/- output voltage rails. Optocouplers were chosen as part of the MOSFET gate driver circuitry for their electrical isolation properties.

PWM-based control systems for power supplies for signal amplifiers do exist but they require a large power supply bandwidth which is often impractical, especially for amplifiers operating at RF frequencies.

Finally, the uniformly spaced version of the PET technique from chapter 3 was applied in this chapter to the OFDM signal to determine the best switching thresholds for a designated number of levels to achieve the greatest efficiency enhancement. The 31-level implementation can achieve 62.53% efficiency increase over a single level version. In the case of the 3-regulator, 6-level version (1V, 3V, 2V), one additional level can be easily added to handle idling power which further improves the system efficiency. There are also compound benefits by correctly adjusting the power supply when required, the amplifier reduces heat dissipation through unnecessary power wastage, which can in turn increase the lifetime of the product.

The next chapter investigates the power added efficiency (PAE) of real OFDM amplifiers, with some real-world testing of an available amplifier product on the market. With a performance benchmark it is easier to understand the scope and potential for future product development. The bias current for the amplifier was manipulated under various conditions to determine the possible benefits of the PET technique being retrospectively applied to the power supply of an RF OFDM amplifier.

Chapter 5:
Experimental Analysis

5.1 Introduction

Transmitter/receiver (Tx/Rx) systems are complex and therefore evaluation of their performance is essential to understanding context. A typical Tx/Rx system comprises of multiple parts including antennas, amplifiers, filters, and mixers, that work together to transmit and receive wireless signals. Each of these components is critical to the performance of the overall system. When using a new system, it is common to evaluate it as a whole and then delve into the individual aspects of the network if specific performance parameters are not met. Accurate measurement of performance parameters requires careful consideration of potential sources of signal degradation, such as cabled connections, antenna quality and suitability, interference, and environmental factors.

This chapter explores the performance of several amplifiers manufactured by ABER Electronics Ltd. an RF electronics specialist company whose amplifiers, antennas, filters, downconverters and upconverters are commonly used in the outside broadcast industry.

Calibrated benchtop equipment was also necessary to facilitate the testing process. Table 5-1 describes a list of the test equipment utilised during the testing process.

Table 5-1: Laboratory Test Equipment

Type and Model Name/Number	**Description and Use Case**
2-2.5GHz COFDM transmitter	OTS transmitter used in the outside broadcast industry. Generate the COFDM transmission signal for the DUT.
Digital signal generator HP ESG-D4000A (Calibrated)	Provide CW signal for initial testing, 250kHz-4.0GHz, up to +13dBm. Generate an LO signal to mix with the COFDM signal to downconvert the frequency of the transmitted signal
Spectrum analyser HP 8562A (Calibrated)	View the shape and rough amplitude of the signal of interest. 1kHz-22GHz
RF power meter Agilent E4418B (Calibrated)	Paired together to read and display absolute power of the Rx signal
RF power sensor HP 8481A (Calibrated)	
Variable digital bench power supply Agilent 66312A (Calibrated)	Source of DC power for the DUT, with current monitoring and over current protection (OCP). Up to 20V, 2A output
Digital multimeter Fluke 15B+ (Calibrated)	Monitors parameters such as voltage and resistance in areas of circuitry during testing
Flir i5 Thermal Imaging Camera	Monitor temperatures of DUT and components. 0.1^{o}C accuracy, +250^{o}C maximum

For all testing, the bench equipment Tx and Rx chains were calibrated to ensure accurate output results. All peripheral equipment should be calibrated out of the chain as the DUT is the focus of the experimentation. There are many sources of performance degradation in a Tx/Rx system, so it is important to minimise it where possible.

All tests were performed using cabled connections instead of Tx and Rx antennas between devices. Cabled connections ensure repeatable and are easily calibrated point-to-point, they also negate the effects of multipath loss. Shielded RF cables were used so that outside interference was minimised. If using antennas instead, they would need to be calibrated so that their specific gain and radiation pattern were known. In the field, antennas are generally used for convenience especially over long distances, it is not always feasible to have a cabled connection, for example at a race circuit in the outside broadcast industry.

There are some easily measured sources of loss in a system, including RF cables, external filters, and external mixers. These sources are also easily calibrated out of the system. More difficult sources of loss come when the system is installed and used in a real-world environment with uncontrolled characteristics such as terrain or competing transmissions from nearby sources.

When a power amplifier is designed, a system hierarchy is first considered which includes a gain distribution diagram. The purpose of this is to indicate what each stage of the system is contributing to the final output signal level. For example, the amplifier chain will have gain whereas cabling, attenuators, and components such as filters and mixers will have loss; any physical separation between Tx and Rx via antennas will also have significant attenuation. The use case for the amplifier is also considered carefully as different environments and Tx/Rx setups can have wildly different performance characteristics.

5.2 Power-Added Efficiency (PAE) Measurements

PAE is a good measure of the efficiency of an RF amplifier. It is more useful for system evaluators and designers compared to drain efficiency which doesn't account for the amplifier gain.

Figure 5-1 to figure 5-4 show various PAE (%) measurements for 14 different amplifiers across different operating frequency bands, with different output powers between 100mW to 10W and a variety of amplifier gains between 10-45dB. These amplifiers were all tested with an OFDM input waveform at varying input powers depending on the amplifier requirements.

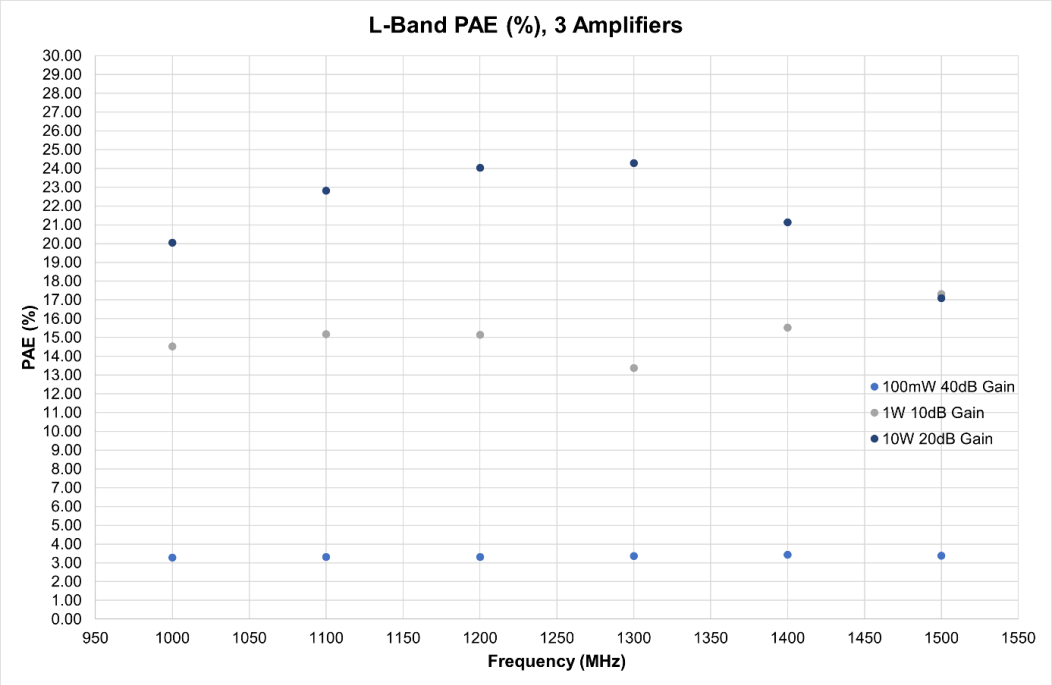

Figure 5-1: L-Band PAE (%) for 3 Different Amplifiers

Figure 5-1 shows 3 amplifiers operating in l-band (generally considered to be 1-2GHz). It shows that the higher gain unit (40dB) exhibits much lower PAE. The 40dB gain amplifier has an output power of +20dBm so the input power is approximately -20dBm.

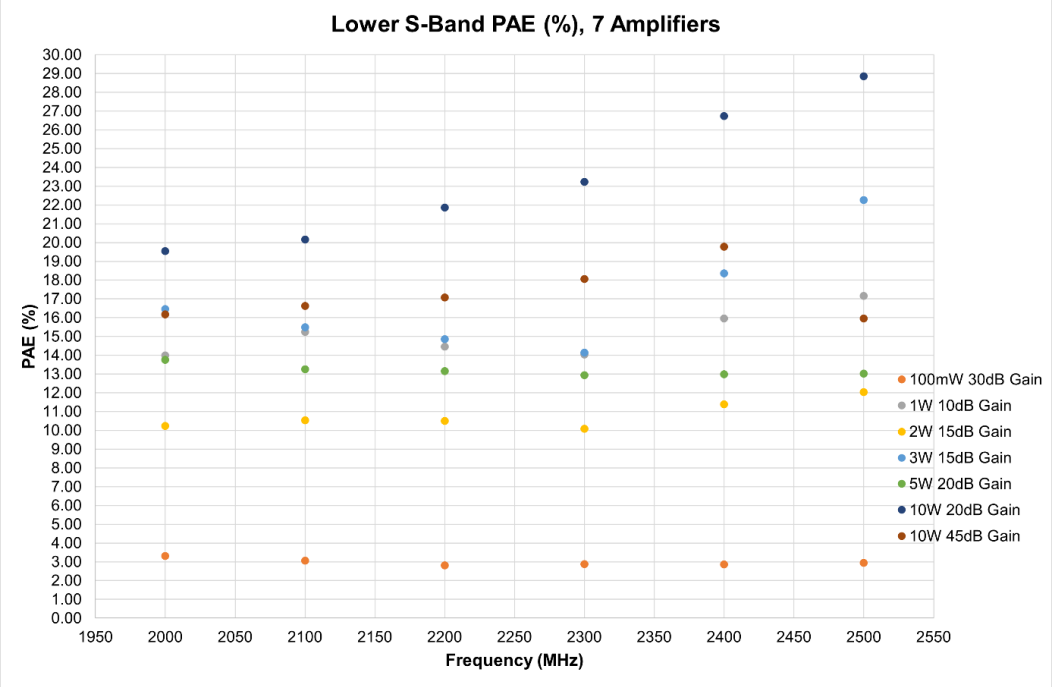

Figure 5-2: Lower S-Band PAE (%) for 7 Different Amplifiers

S-band (generally considered to be 2-4GHz) shows that the high gain (30dB), lower output power (100mW) amplifier has a low PAE compared to the higher output power (10W), lower gain (20dB) amplifier. This band is common in outside broadcast and is one of the main operating bands for wi-fi so 7 amplifiers were tested in this band.

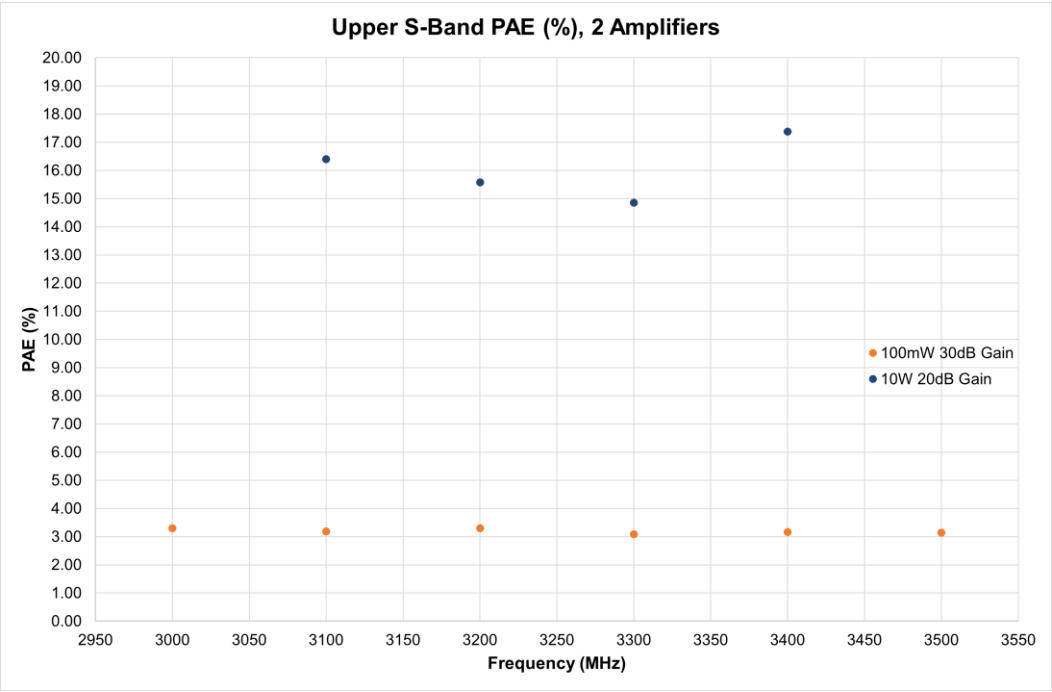

Figure 5-3: Upper S-Band PAE (%) for 2 Different Amplifiers

Again, the higher gain, lower output power amplifier has a low PAE, 30dB gain with +20dBm output, meaning that the input power is approximately -10dBm. This amplifier has a consistent PAE across the operating band. The higher output power (10W), lower gain (20dB) amplifier in comparison has a much higher PAE but fluctuates by nearly 3% depending on the operating frequency across the band. A total of 9 different amplifiers have been tested at s-band.

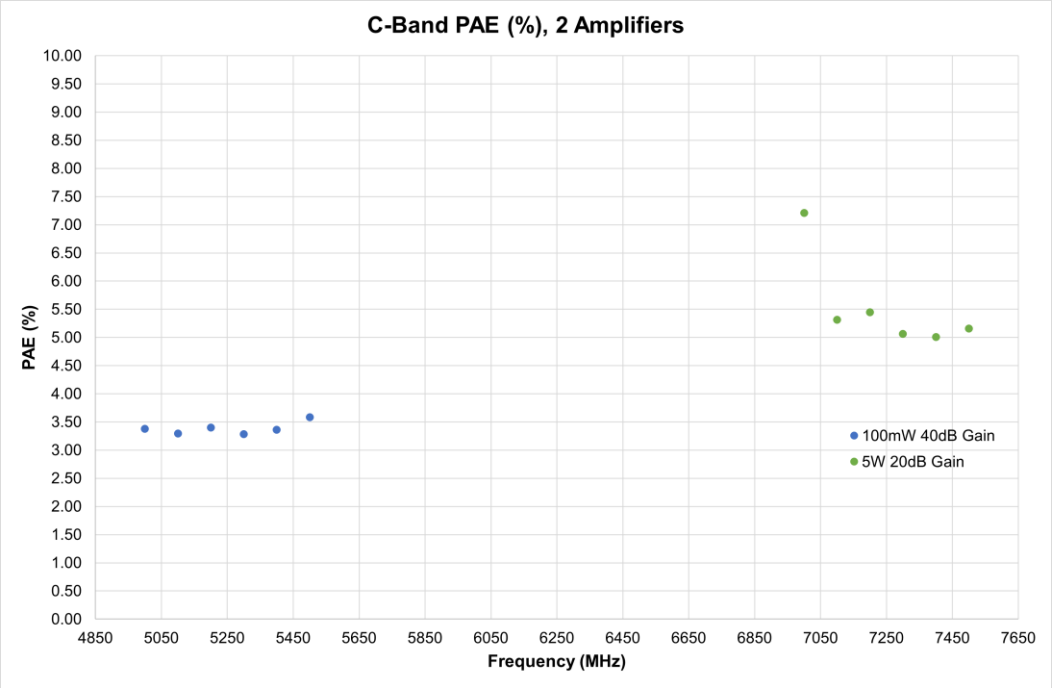

Figure 5-4: C-Band PAE (%) for 2 Different Amplifiers

2 amplifiers were tested at c-band, generally considered to be the 4-8GHz operating frequency band. Like the 40dB gain unit at l-band, the c-band equivalent also demonstrates a poor PAE. The 5W, 20dB gain amplifier across 7-7.5GHz also has a low PAE but this is because higher frequency units generally have lower PAE than their lower frequency equivalents, this is due to a variety of factors including efficiency of devices at the higher frequencies plus a shortage of device options at c-band. Commercially, l-band and s-band are more utilised, so research and development is

generally inclined towards these frequency bands. 5G has added c-band to its available usage frequencies so development on devices in this band is growing.

The biggest benefits could be seen with the high gain units as these tend to have lower PAE, especially at lower RF output powers. These measurements prove the requirement for more efficient techniques like those proposed in this thesis.

5.3 CW Sine Wave Amplifier Analysis

Figure 5-5 shows the construction of the CW testing whereby the amplifier was subjected to a CW signal in the range 2-2.5GHz up to an output power of +13dBm (~20mW) from a benchtop signal generator. The amplifier was fed by a stable bench power supply.

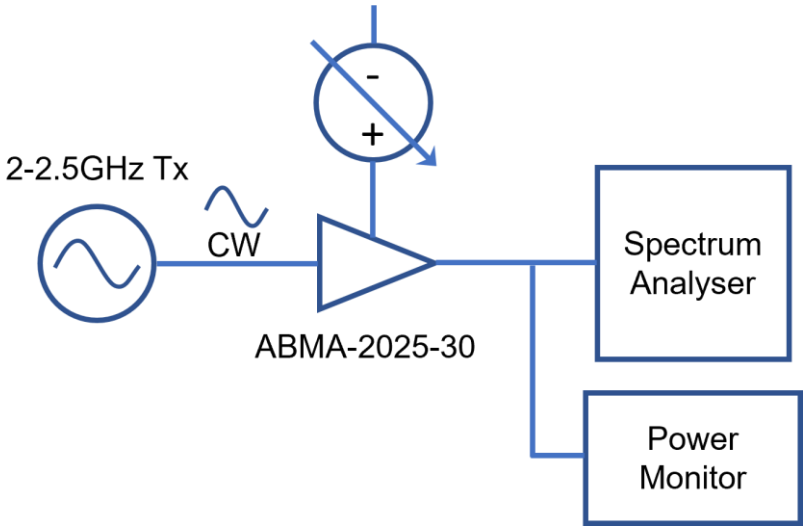

Figure 5-5: Amplified CW Signal

The amplifier under test was optimised for the 2.0-2.5GHz band but does operate beyond these frequencies so the signal generator was used on a sweep from 2.0-2.7GHz to see the amplifier roll-off but the transmitter used for the modulated waveform tests only operates up to 2.5GHz.

The output of the amplifier was passed to a spectrum analyser and calibrated power monitor. The spectrum analyser is used to check that the waveform is as expected and

to observe any signal degradations and interference in or out-of-band (OOB). The calibrated power monitor is used to accurately measure the RF output power.

The amplifier bias current was easily controlled via a potentiometer. A wide range of bias conditions were tested. The reason for testing the amplifier with a CW signal before a modulated OFDM signal is due to the simpler setup and fewer parameters, analysis is easier to ensure that the amplifier operation is sensible before progressing with modulated tests.

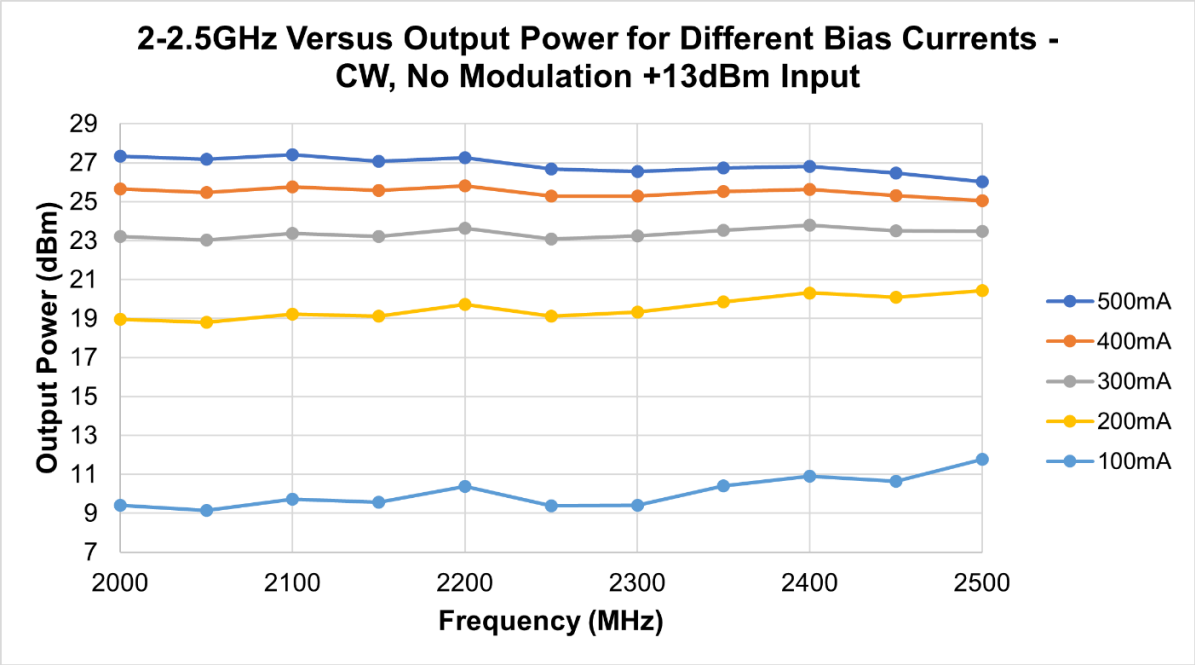

Figure 5-6: 2-2.5GHz Amplifier with +13dBm CW Signal at Various Bias Currents

Figure 5-6 shows the test results from the CW analysis across the band 2-2.5GHz with the 1W PA as the DUT. The amplifier was tested at five different bias currents to see the change in the output power across the band.

5.4 OFDM Amplifier Analysis

5.4.1 Introduction

When designing a data transmission system, the choice of transmission parameters such as FEC and guard interval (GI), is a critical factor in the performance of the link.

In the tests described in this chapter, an FEC of 2/3 was chosen. This means that every third bit of the transmitted data is a parity check for the corresponding two bits of useable data. This choice of FEC enables a high data transmission rate, but only a low throughput of usable information (~67%). 2/3 was chosen for robustness.

If a higher FEC was used, such as 9/10, only 10% of the transmitted data would be used for error correction, and thus 90% for usable information. There is, however, a big trade-off in system performance, as a lower error correction would mean that useful data transmission can be much higher, but it also runs the risk of errors occurring.

The guard interval (GI) is another important transmission parameter that affects system performance. In these tests, a GI of 1/32 was used, which allows for a high data rate but also has the possibility of a high error rate due to inter-symbol interference (ISI). 1/32 was chosen for this system due to the environment being more easily controlled compared to a real-world outside broadcast location so the probability of high ISI is significantly reduced. The FEC and GI parameters were not changed between tests.

Balancing the choice of FEC and GI is crucial to achieving high data throughput whilst maintaining immunity to errors. In a noisy channel, a higher FEC and GI might be more appropriate, albeit at the expense of data throughput. The selection of transmission parameters should be done based on the specific needs of each system, considering factors such as the quality of the transmission environment, required data throughput and desired error correction level. In a system with error handling, a high bit error rate (BER) will mean that lost data is re-transmitted, thereby limiting throughput. In a system without error handling, however, data will be permanently lost.

OFDM or COFDM is transmitted and the receive side processes these OFDM signals.

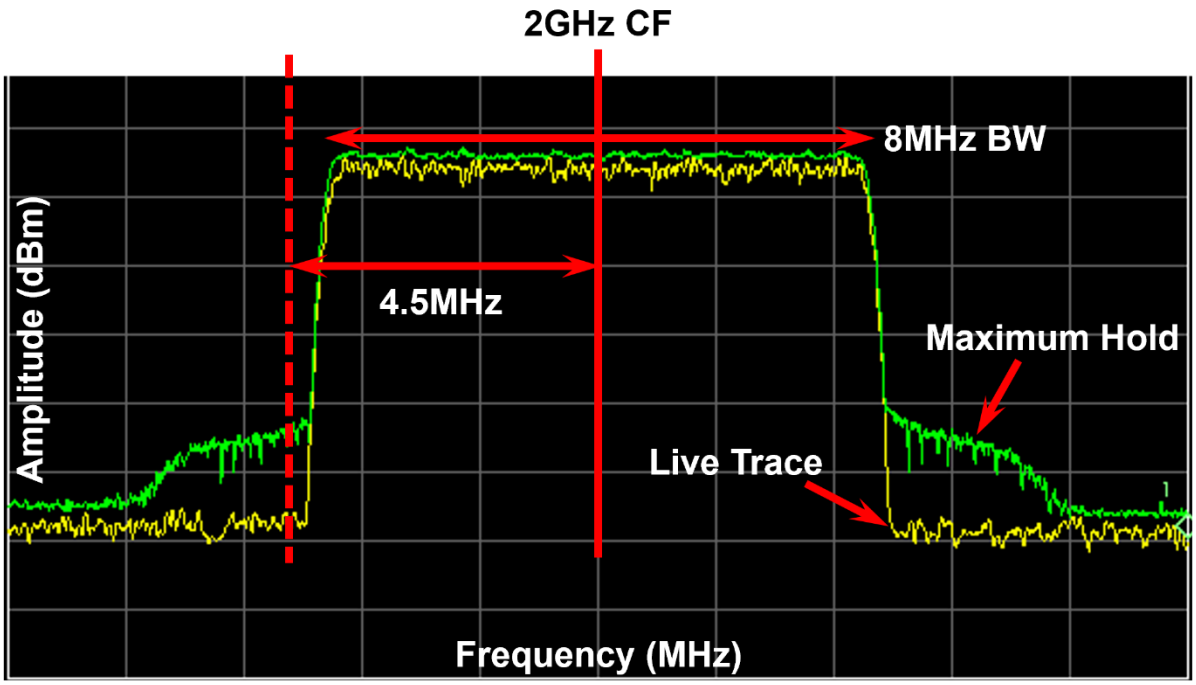

Figure 5-7: 2GHz OFDM Trace on Spectrum Analyser

Figure 5-7 shows a 2GHz OFDM trace captured on a spectrum analyser during tests on the 1W PA. The green trace is the maximum hold of the received signal, meaning that across the spectrum the maximum value at each data point is saved. The yellow trace is the live capture. The transmitted signal in each instance is an 8MHz wide modulated OFDM signal. The SNR measurement is taken arbitrarily 4.5MHz from the centre frequency of the waveform. A more accurate method is to monitor the adjacent channel power.

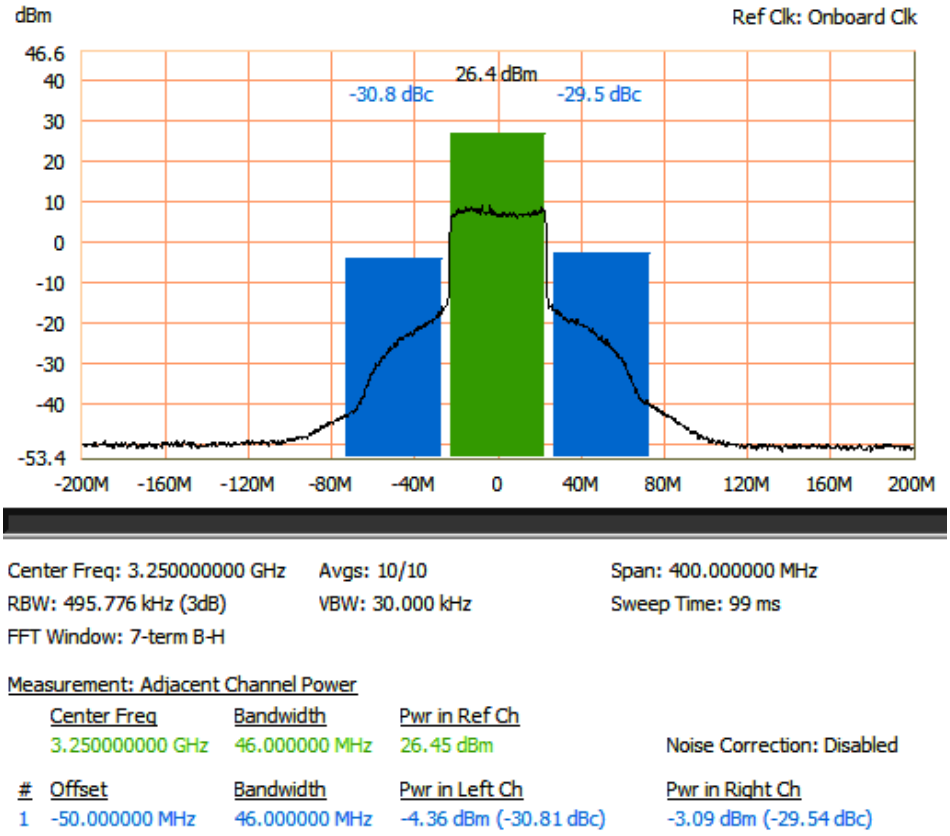

Figure 5-8: 3.25GHz 0.5W Amplifier Showing Adjacent Channel Power [72]

Figure 5-8 shows a spectrum analyser output of an amplifier at 3.25GHz centre frequency with -19dBm input power, +26.4dBm output power, with approximately -30dBc in the adjacent channel. This is taken from project testing at ABER Electronics Ltd.

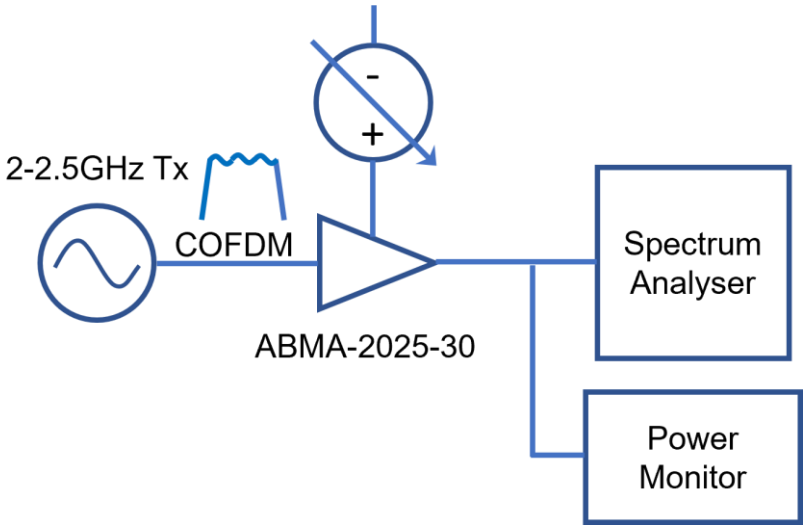

Figure 5-9: Amplified Modulated COFDM Signal

Figure 5-9 depicts the OFDM testing scheme. A commercially available COFDM transmitter was used as the signal source supplying the amplifier input. The amplifier was powered by a variable bench power supply. The transmitter can output a modulated waveform of powers up to +16.5dBm (~45mW) with a variety of available modulation parameters. The amplified signal on the output is passed to the spectrum analyser and the RF power monitor. Three commonly used modulation formats were used during testing: QPSK, 16QAM and 64QAM. These are the three available formats in the DVB-T broadcast scheme. In the laboratory conditions within which the experiments in this chapter were undertaken, environmental noise wasn't much of a factor, so the possibility of errors was controlled. This is further compounded by the fact that all connections were cabled instead of wireless.

A 1W power amplifier was the subject of the tests with the three different modulation formats at five different bias currents. The different bias currents emulate a 5-level power supply as the voltage was not able to be varied due to a SMPS and linear regulators internal to the amplifier.

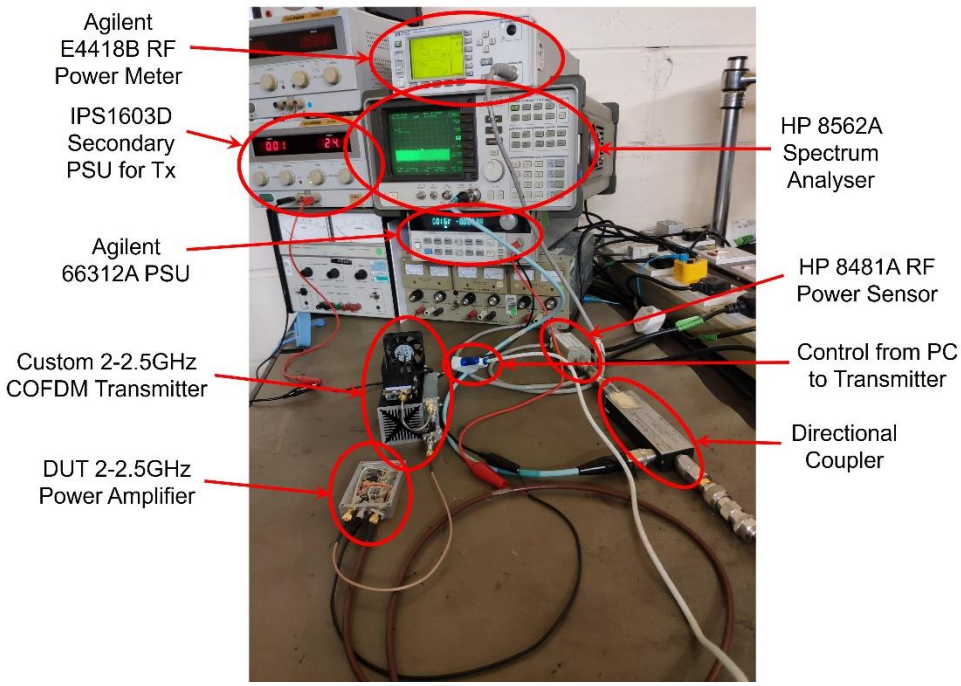

Figure 5-10: Experimental Setup - Equipment

Figure 5-10 shows the experimental setup, including all the relevant test equipment annotated, as well as the DUT. This represents the physical implementation of the block diagram in figure 5-9.

5.4.2 QPSK

QPSK is highly robust to ISI; albeit with a low data rate when compared to higher modulation orders. The settings on the transmitter were set to 2-2.5GHz frequency band, 2/3 FEC and 1/32 guard interval and the modulation scheme was set to QPSK.

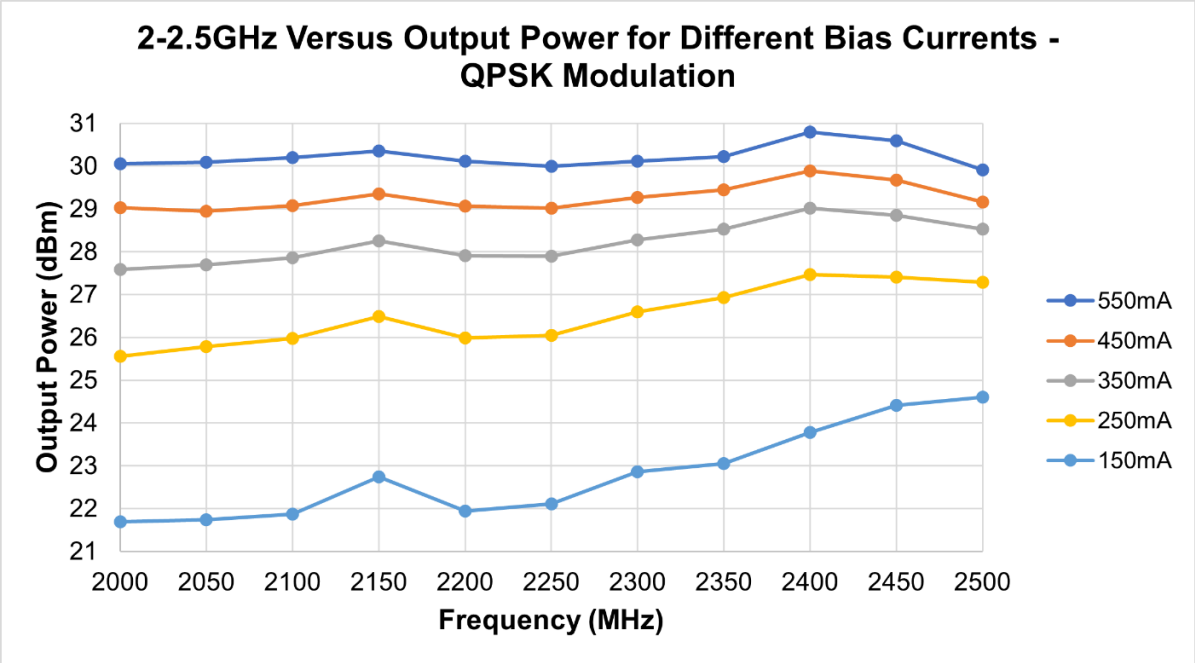

Figure 5-11: 2-2.5GHz Amplifier with +16.5dBm QPSK Signal at Various Bias Currents

Figure 5-11 shows the output power of the 1W amplifier across the 2-2.5GHz band with the input signal modulated with QPSK, tested at five different bias currents to see the variation in output power across the band. The gain is approximately 5.5-8.5dB when the amplifier is biased for 150mA, compared to 13.5-14.5dB at 550mA. The difference between each bias current level gets smaller as it increases, indicating that the amplifier is entering compression.

5.4.3 16QAM

16QAM has a higher possible data rate than QPSK but also has a higher risk of errors due to the constellation points being spaced closer together.

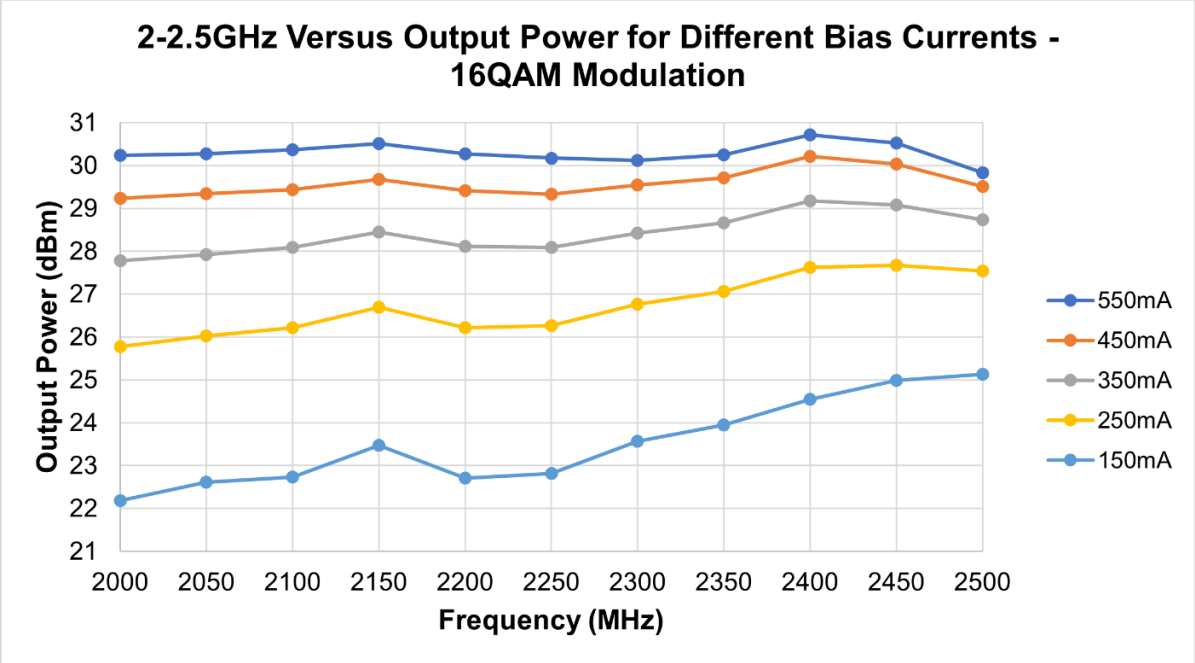

Figure 5-12: 2-2.5GHz Amplifier with +16.5dBm 16QAM Signal at Various Bias Currents

For 16QAM modulation, the amplifier was tested across 2-2.5GHz at five different bias currents. Compared to QPSK, the output power on average is higher, and compression occurs at a slightly lower bias current as depicted by the 550mA and 450mA curves being closer together, particularly from 2.3-2.5GHz.

5.4.4 64QAM

64QAM further increases the possibility of errors but also further increases the possible data rate compared to 16QAM and QPSK. Due to the spacing of the constellation points for 64QAM, an electrically clean transmission environment is desirable to minimise risk of transmission interference and errors.

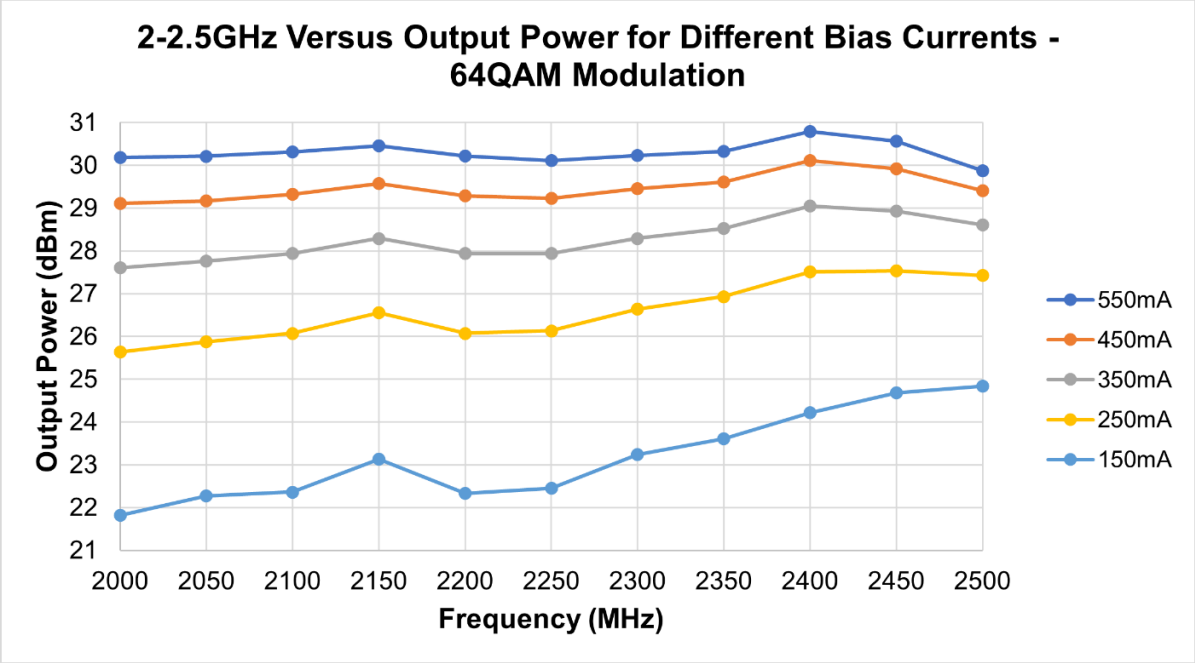

Figure 5-13: 2-2.5GHz Amplifier with +16.5dBm 64QAM Signal at Various Bias Currents

The output powers and general shape of each curve is very similar to the 16QAM case with the amplifier again entering compression earlier than with QPSK modulation.

5.5 Downconversion Analysis

In addition to the fact that higher frequency signals don't propagate as far as lower frequency signals of the same power, they are also more difficult to process which means that it requires more expensive equipment. It is therefore sometimes more useful to downconvert a signal to be able to analyse it more easily at the receiver. Downconversion is a very common technique in many RF systems, particularly in the outside broadcast industry. In many wireless communication systems, the transmit and receive parts of the system share a common antenna so by downconverting the receive path it makes it easier to filter out the transmitted signal using a basic low pass filter thereby reducing interference. In some instances, the radio environment is congested so moving to higher frequency transmissions reduces interference from

competition. Then at the receiver, downconversion is required to return to the desired processing band.

Filtering, amplifying, and demodulating an intermediate frequency is often easier hence why downconversion is common. Low pass filters (LPF), high pass filters (HPF) and band pass filters (BPF) are designed and employed to reject undesirable signal frequencies from the transmission chain. In the following examples of tests performed on the real-world amplifier, the downconversion was performed from the 2-2.5GHz band down to the intermediate frequency band of 400-900MHz.

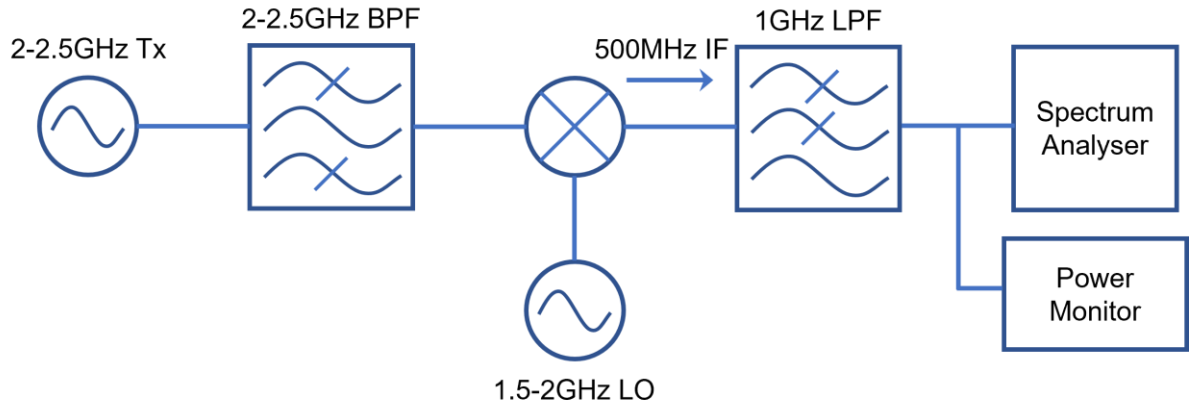

Figure 5-14: Downconverted and Filtered Tx

The Tx signal is passed through a 2-2.5GHz BPF to ensure cleanliness of the RF chain. The downconverting process involves mixing the Tx signal with a local oscillator signal (LO) of a lower or higher frequency by a difference of the desired output frequency. The output is the intermediate frequency (IF). The result of the mix is two different output frequencies as below:

$$RF + LO = IF1$$
$$RF - LO = IF2 \qquad (5\text{-}1)$$

Filtering is then used to remove the undesirable mix output. When the LO signal is of a higher frequency than the RF signal, it is known as a high-side LO and vice-versa for a low-side LO. In the case shown in figure 5-14 a low-side LO is used at a frequency

500MHz below the incoming Tx signal. For example, when the Tx input is 2.1GHz, the LO is set to 1.6GHz resulting in the following IF mix outputs:

$$IF1 = 2.1 + 1.6 = 3.7GHz$$
$$IF2 = 2.1 - 1.6 = 0.5GHz \quad (5\text{-}2)$$

The undesirable 3.7GHz output is then filtered out using an LPF tuned to a 1GHz cut-off frequency which will also strongly reject any leakage from the 1.6GHz LO as well as the 2.1GHz input. Assuming no filter re-entry around 3.7GHz, it will be rejected down at the absolute rejection level which in this case is approximately -60dB.

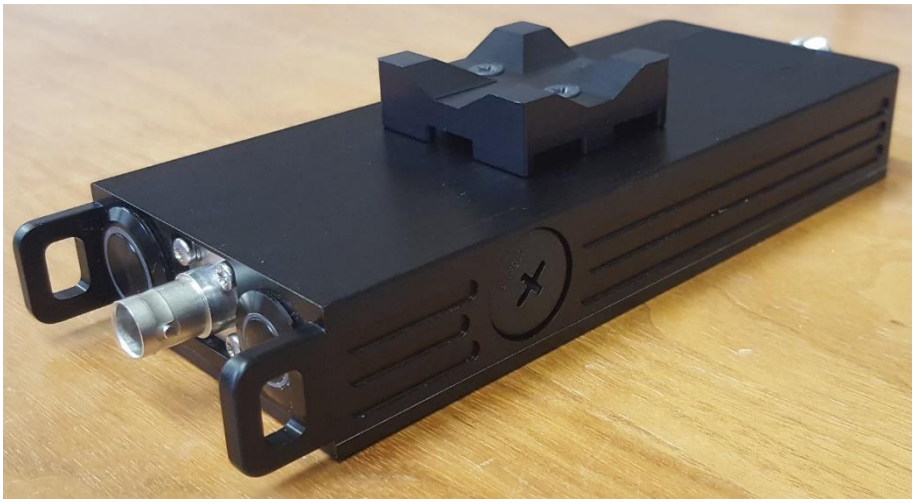

Figure 5-15: ABER S-Band Downconverter [73]

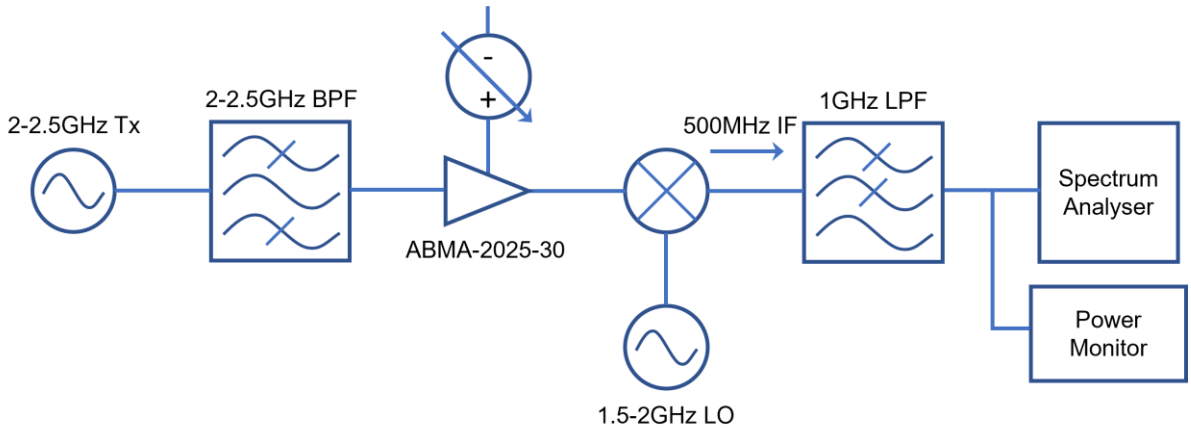

Figure 5-16: Amplified, Downconverted, Filtered Tx

Figure 5-16 includes the amplifier stage in the downconversion tests. The signal is monitored by visual inspection on the spectrum analyser and the RF power monitor.

5.6 Conclusion

This chapter describes tests performed on real-world amplifiers designed and manufactured by ABER Electronics Ltd. Initially a succession of PAE measurements were taken for a range of amplifiers of different output powers, gains, and frequency bands. The amplifiers ranged from 100mW-10W RF output power, 10-45dB gain and across 1.0-7.5GHz. The PAE measurements range from 3-29% which proves the need for an efficient power supply control technique such as that presented in chapter 4.

Following the PAE measurements, a 1W s-band PA optimised for 2.0-2.5GHz was chosen as the DUT for a further series of tests including CW sine wave analysis, OFDM modulated waveforms with three different subcarrier modulation formats and orders, and downconversion analysis.

The amplifier used as the DUT contained existing crude internal power regulation via a SMPS and linear regulators, meaning that the voltage could not be varied so the bias current for the amplifier device was tackled. The aim of these tests was to see the effects of a wide range of amplifier bias currents, to push the amplifier in and out of compression. It is concluded that the performance of the amplifier drastically changed based on the amplifier bias current under different modulation conditions.

The aim of the testing described in this chapter was to study the impact of varying the bias current on the performance of real-world amplifiers. The use of different modulation parameters for the OFDM amplifier resulted in varying levels of performance. This underscores the importance of carefully selecting the modulation parameters to optimise the performance of the Tx/Rx system for the intended application. All tests were performed in a controlled laboratory environment using repeatable cabled connections, whereas in a real-world application it is more likely

that Tx and Rx antennas would be employed, and the transmission channel would experience fluctuations in quality.

These tests highlight the need for the power supply control technique and the gap in existing research surrounding real-world applications. This work also shows that the existing research often takes time to filter through to commercialised products. This research can provide the necessary stimulus to develop appropriate, efficient amplifiers for use in real-world applications.

The next chapter introduces the shuffling technique (TRUST), where a generalised resource management technique is proposed to improve the efficiency of a variety of systems. This is applicable to the usage of amplifiers, batteries, and other resources.

Chapter 6:
The Shuffling Technique (TRUST)

6.1 Introduction

Systems which consist of multiple nodes often face the problem of unequal utilisation of each node, herein referred to as resources. This can lead to a quicker failure of individual resources as they are excessively stressed or overloaded. To address this issue, a method is presented to ensure that each resource is equally utilised, thereby prolonging the lifespan of each individual resource and thus, the whole system.

In this chapter, a system consisting of multiple batteries (the resources) is presented with a novel technique to equally load each resource. The focus is on how to equally share the load between each battery to ensure that they are all utilised the same amount and avoid any one battery from being overstressed.

6.2 Total Resource Utilisation Shuffling Technique (TRUST)

The aim of the technique is to be able to optimise component and system lifespan regardless of what the resources are and the size of the system. The efficiency comes from the equal resource utilisation of every resource. The term ‘shuffling’ comes from the well-known reordering of a deck of cards [74] [75]. This is a common problem in a similar branch of mathematics of number theory as the Golomb ruler theory presented in previous chapters. The usage of the term shuffling in this case is because when the technique is employed, each resource in the system is cycled round in a ring (shuffled) until each one has been used equally; they are combined in different ways. This technique is to be known as the Total Resource Utilisation Shuffling Technique (dubbed TRUST).

There are a few identities that the technique is defined by. The maximum number of shuffle steps is equal to one less than the number of resources, regardless of system composition, and the number of unique stages in the shuffling sequence is equal to the number of resources. To arrive back at the original arrangement, the number of shuffle steps must equal the number of resources. This leads to equations (6-1) and (6-2).

$$Shuffle\ Steps = Number\ of\ Resources - 1 \qquad (6\text{-}1)$$

$$Unique\ Stages = Number\ of\ Resources \qquad (6\text{-}2)$$

If a system has 4 resources, then the number of shuffle steps is 3 as shown in figure 6-1.

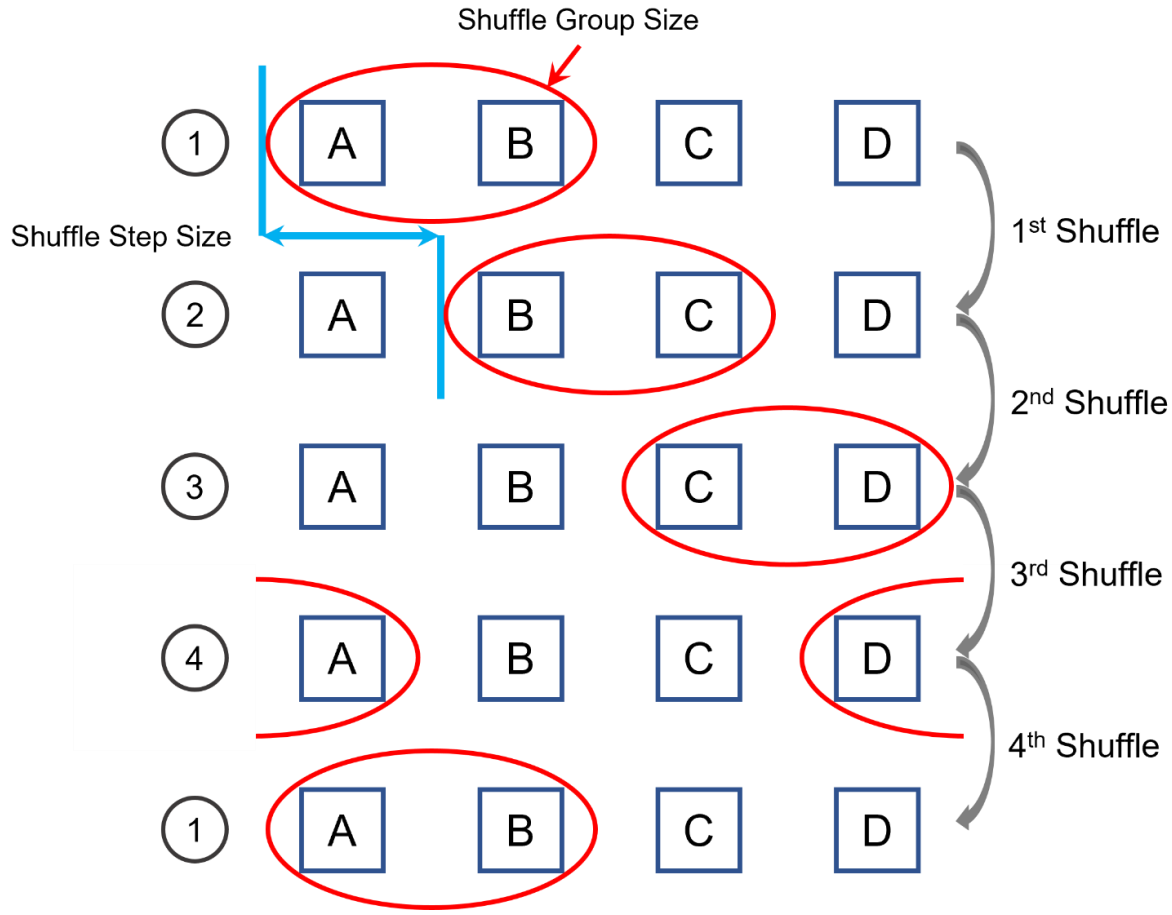

Figure 6-1: Shuffling Technique for 4 Resources, Group Size 2, Step Size 1

Figure 6-1 shows 4 resources and the shuffling stages. The right-hand side indicates each shuffle. The number of unique system configurations via shuffling is 4. After 4 shuffles, the original arrangement is presented again. The circled numbers on the left-hand side depict this. The red circles indicate the shuffle group size, in this case 2. The blue arrow and lines show that the shuffle step size is 1 in this example.

The shuffling technique works best with the linear or consecutive system as described in chapter 4. Although it's possible, the matrix topology does not lend itself to the shuffling technique very well. The complexity is exponential with no further benefit.

To illustrate the shuffling technique, the example of a symmetrical system consisting of 12 batteries (resources) each with a 1V output and capacity of 500mAh is used. The output voltage capability of the system is from 0-12V in 1V steps, while each battery is utilised equally. The configuration of the system changes for different output voltage demands, which are described in detail in table 6-1. Each configuration also varies in complexity. The corresponding shuffling techniques for various output voltage demands are depicted in figure 6-6 and figure 6-8.

Table 6-1: Configurations for all Scenarios in a Twelve 1V Battery System

Output (V)	**Configuration**
0	All 12 batteries turned off, no output demand
1	All 12 batteries in parallel. This allows for maximum system current capability as it is equally shared between all batteries. Shown in figure 6-2
2	Split the 12 batteries into 6 groups of 2 batteries in series and configure those 6 groups in parallel. Each pair must be consecutive. Shown in figure 6-3
3	Split the 12 batteries into 4 groups of 3 batteries in series and configure those 4 groups in parallel. Shown in figure 6-4

4	Split the 12 batteries into 3 groups of 4 batteries in series and configure those 3 groups in parallel. Shown in figure 6-5
5	Connect 5 consecutive batteries in series, then connect the next 5 consecutive batteries in series, then connect the two groups of 5 batteries in parallel to have a shuffle group of 10. Then shuffle those contiguous 10 around the ring to equally load all 12 batteries whilst maintaining the constant 5V output. Shown in figure 6-6
6	Split the 12 batteries into 2 groups of 6 batteries in series and configure those 2 groups in parallel. Shown in figure 6-7
7	7 batteries connected in series and then shuffle those connected 7 around in a ring to keep a constant 7V output but load each of the 12 batteries equally on average. Shown in figure 6-8
8	Same shuffling technique as described in the 7V scenario. 4 batteries not in use at any one time therefore two thirds are in use at any one time. Shown in figure 6-8
9	Same shuffling technique as described in the 7V and 8V scenarios. 3 batteries not in use at any one time. Shown in figure 6-8
10	Same shuffling technique as described in the 7V, 8V and 9V scenarios. 2 batteries not in use at any one time. Shown in figure 6-8
11	Same shuffling technique as described in the 7V, 8V, 9V and 10V scenarios. 1 battery not in use at any one time. Shown in figure 6-8
12	All 12 batteries in series. This only allows for the minimum current to be drawn by the system as determined by the current capability of a single battery. Shown in figure 6-9

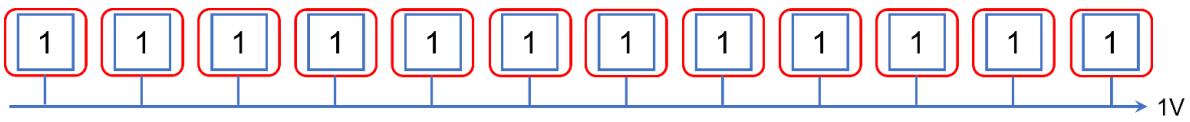

Figure 6-2: 1V Output from Twelve 1V Batteries

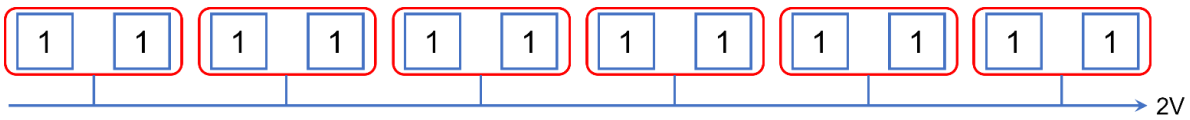

Figure 6-3: 2V Output from Twelve 1V Batteries

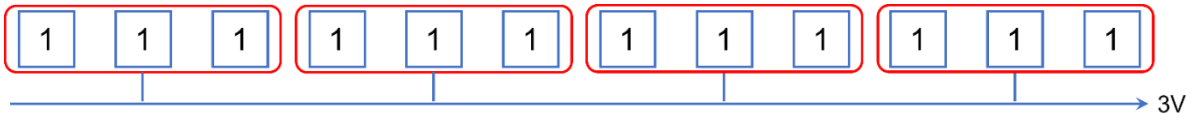

Figure 6-4: 3V Output from Twelve 1V Batteries

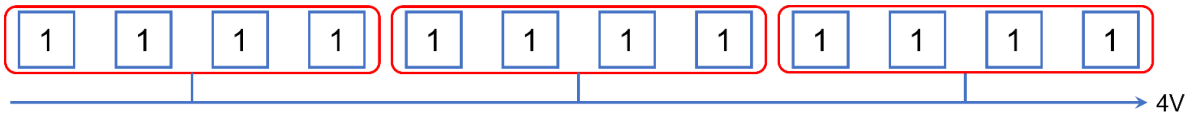

Figure 6-5: 4V Output from Twelve 1V Batteries

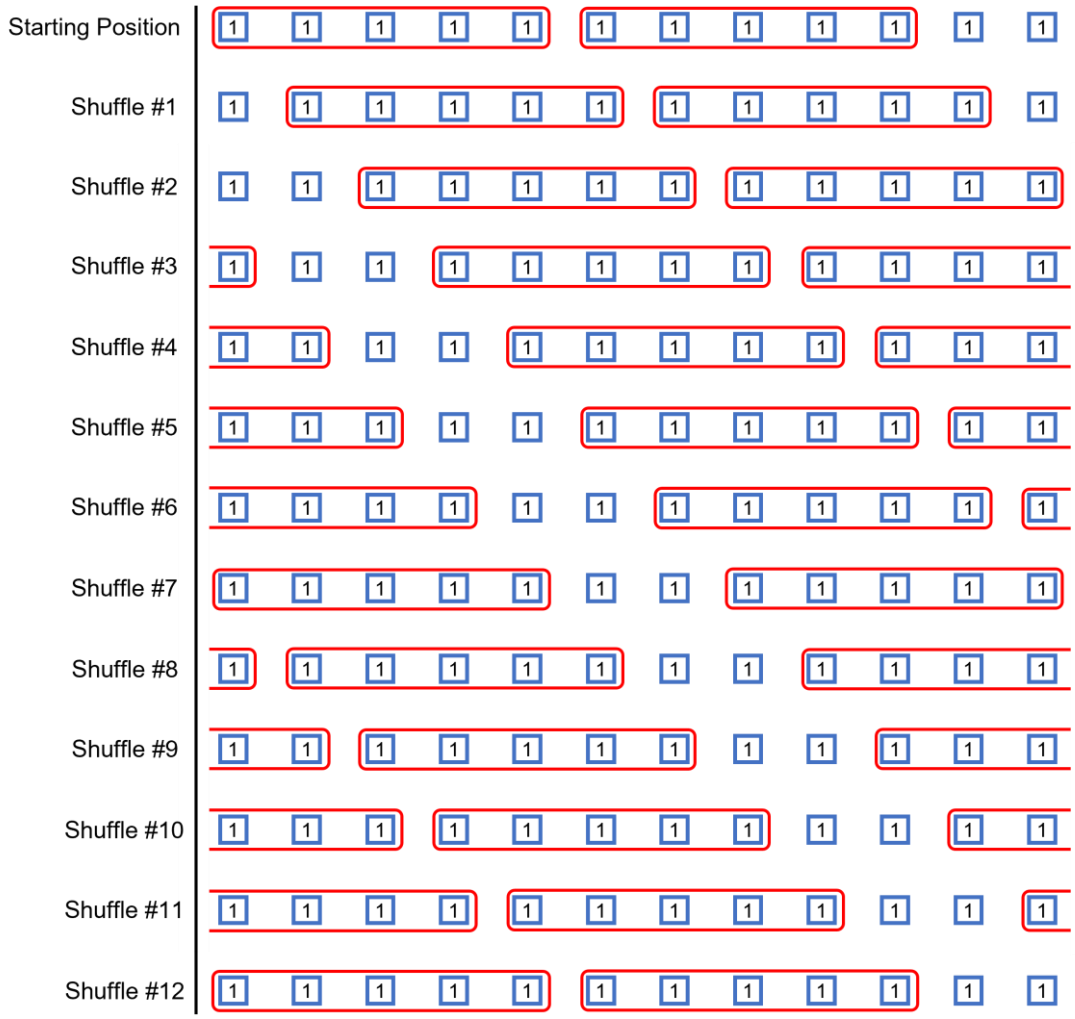

Figure 6-6: Shuffling Technique Depicted for 5V Output from Twelve 1V Batteries

Figure 6-6 depicts the required shuffling steps for the system which has twelve 1V batteries to achieve a 5V output. The simplest implementation would be to have 5 batteries in series and shuffle those around the ring to load all equally. This is inefficient, however, as there would be 7 batteries at any one time which are unused.

Instead, two groups of 5 series batteries should be shuffled together which would double the output power capability and leave just 2 batteries unused at each stage. The two groups of 5 batteries must be contiguous, resulting in a single group of 10 otherwise it violates the shuffling technique. To complete an equal load rotation, 11 shuffle steps are required, on the 12th shuffle step, the configuration has returned to the starting position. Although even this configuration is still inefficient as the step size is just 1. Larger step sizes are explored later.

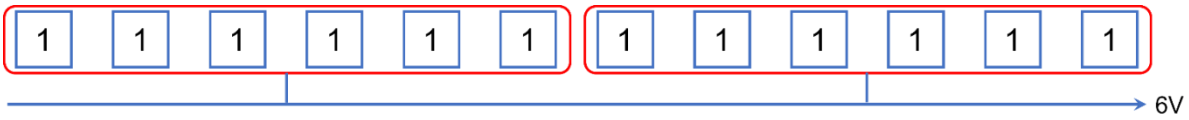

Figure 6-7: 6V Output from Twelve 1V Batteries

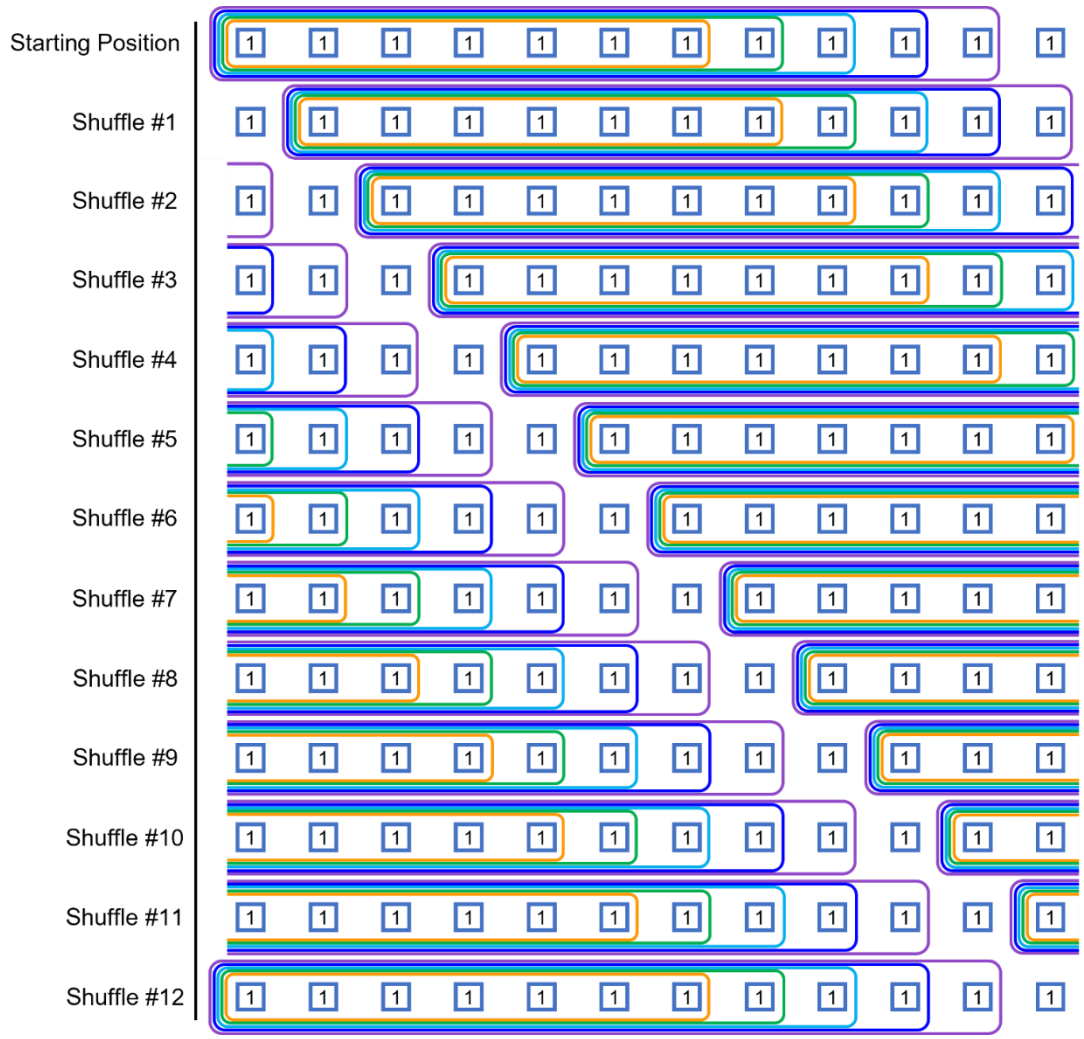

Figure 6-8: Shuffling Technique Steps for 7-11V Outputs from Twelve 1V Batteries

Figure 6-8 shows the shuffling technique for 7V, 8V, 9V, 10V, 11V outputs with each step shown to achieve a complete shuffle. As with the shuffle for 5V in figure 6-6, all batteries are equally loaded after 11 shuffles in each case because the shuffle step size is 1. Table 6-2 identifies which colour indicates which output voltage set.

Table 6-2: Colour Key for 7-11V Shuffle Diagram

Output Voltage	Colour
7V	Orange
8V	Green
9V	Light Blue
10V	Dark Blue
11V	Purple

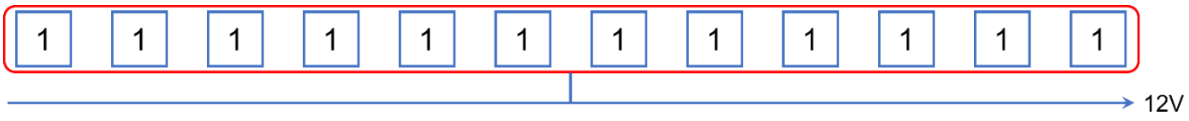

Figure 6-9: 12V Output from Twelve 1V Batteries

The examples shown above would result in an output voltage ability of 0-12V in 1V steps whilst always utilising the 12 batteries equally. The output current capability varies depending on the output voltage. Each 1V 500mAh battery means each battery has a power capacity of 0.5Wh (depending on discharge current, different battery technologies have different discharge characteristics, not necessarily linear); therefore 12 batteries have a power capacity of 6Wh if all used together in the same system in combinations of series and parallel, if using the shuffling technique (7V output for example) then there will be batteries unused at each shuffle stage which will lower the output power capability from the maximum 6Wh but this is no different to existing power systems.

The simplest scenarios are when the output voltage is set to either 0V, 1V or maximum (in this case, 12V) where the batteries are either disconnected, all connected in

parallel, or all connected in series respectively. If the output voltage is a factor of the maximum voltage (12V), such as 2V, 3V, 4V, 6V, then no shuffling is required to evenly distribute the load among the batteries. When the output voltage is a non-factor, however, such as 5V or 9V, the shuffling technique must be employed.

Table 6-3: Different Categories of Desired Output

Output Voltage Type	**Output Voltage (V)**	**Configuration**
Nothing	0	None, N/A
Minimum	1	All in parallel
Maximum	12	All in series
Factor of Maximum	2, 3, 4, 6	Combination of series and parallel
Non-Factor of Maximum	5, 7, 8, 9, 10, 11	Shuffle required

The proposed technique is demonstrated where each battery is 1V, but the technique can be applied to other systems with different voltages if required. A system where each battery is 2V, for example, would also benefit from the technique although only voltages with even values could be output. 1V was chosen as any whole number value of voltage from 1 to the number of batteries in the system could be constructed.

The technique could also be applied to systems where each voltage source has a different magnitude, but it would be extremely wasteful, and the control circuitry would require significant complexity to still achieve accurate outputs. Commissioning substantial complexity in systems where each resource is weighted unequally would need to have obvious advantages to be beneficial.

The sequential version of the technique is when the shuffling step size (S) is equal to the shuffling group size (G), defined by equation (6-3).

$$S \equiv G \qquad (6\text{-}3)$$

Table 6-4 shows a summary of the shuffling statistics for a system with 6 resources and varying shuffle group sizes, with a step size equal to the group size.

Table 6-4: Shuffle Statistics for 6 Resources

Shuffle Group Size	# of Shuffles for Equal Load Distribution	# of Shuffles to Return to Origin	# of Unique Stages
1	5	6	6
2	2	3	3
3	1	2	2
4	2	3	3
5	5	6	6
6	0	0	1

For a system with 6 resources, it is most efficient to shuffle in groups of 3 where the equal resource utilisation happens in 1 shuffle step.

Table 6-5: Shuffle Statistics for 7 Resources

Shuffle Group Size	# of Shuffles to Return to Origin	# of Unique Stages
1	7	7
2	7	7
3	7	7
4	7	7
5	7	7
6	7	7
7	0	1

For a system with 7 resources, it is no more efficient to shuffle in steps larger than 1.

Table 6-6: Statistical Summary of Different Numbers of Resources

# of Resources	Optimum Shuffle Group Size	# of Shuffles
1	N/A	N/A
2	1	2
3	1,2	3
4	2	2
5	1,2,3,4	5
6	3	2
7	1,2,3,4,5,6	7
8	4	2
9	3	4
10	5	2

Table 6-6 summarises the statistics for shuffle group sizes for a range of system sizes, showing a variety of system shuffling properties. Clearly, when there is only one resource, there is no possible way to shuffle it. When there are 2 resources, there is only one way in which they can be shuffled and that is when the shuffle group size is equal to 1. With a group size of 2 it would eliminate the need for shuffling.

This is again highly inefficient and very restrictive; in some cases, a larger step size would reduce the number of required shuffles. Furthermore, in most systems the resource group size is often predetermined (for example, a specified output voltage from a bank of ten 1V batteries), therefore the shuffling technique targets only the shuffle step size. When the step size is not equal to the group size, it is the non-sequential shuffling technique.

Non-sequential shuffling is defined by equation (6-4), when the shuffling step size (S) is not equal to the shuffling group size (G).

$$S \neq G \qquad (6\text{-}4)$$

This version has the potential to be much more efficient than the sequential type, but only in some circumstances. It is not necessarily more efficient for every possible configuration of a single system; it is likely that some outputs will be less efficient so a combination of both versions might be more beneficial.

For a system with 6 batteries, each 1V, if 4V output is desired (the group size), there are a range of options for the shuffle step size. It is important to choose the most efficient option to minimise redundant shuffle stages and therefore computational power.

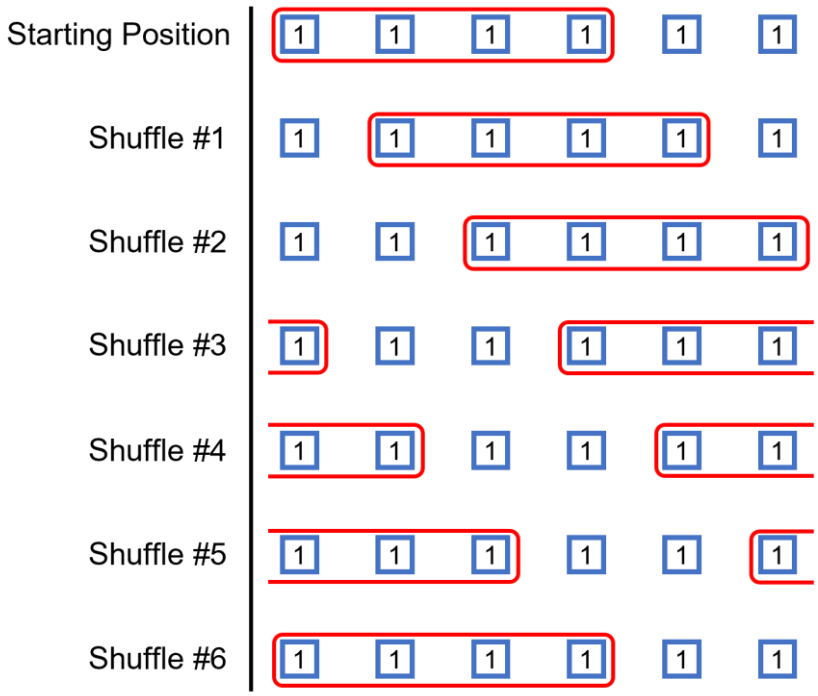

Figure 6-10: 6 Batteries, 4V Output, Shuffle Step Size = 1

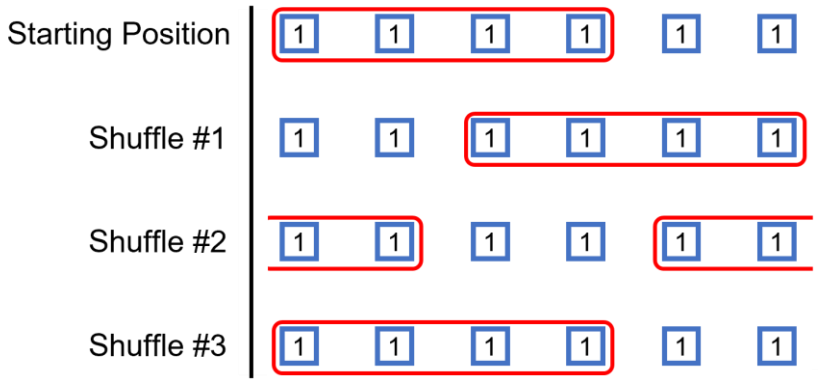

Figure 6-11: 6 Batteries, 4V Output, Shuffle Step Size = 2

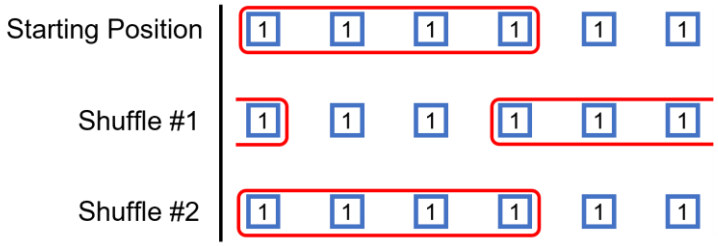

Figure 6-12: 6 Batteries, 4V Output, Shuffle Step Size = 3

A step size of 3 with a group size of 4 does not equally use all 6 resources during a complete shuffle. A complete shuffle is achieved in 1 shuffle stage and figure 6-12 shows that the resources in positions 1 and 4 are used twice whereas the resources in positions 2, 3, 5, and 6 are only used once each. This would put undue strain on the 1st and 4th resources and likely cause them to fail sooner than the others.

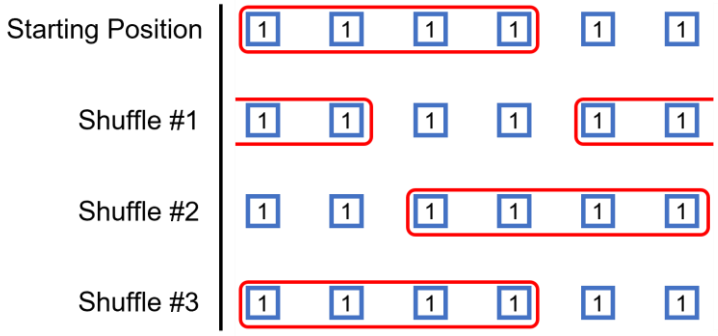

Figure 6-13: 6 Batteries, 4V Output, Shuffle Step Size = 4

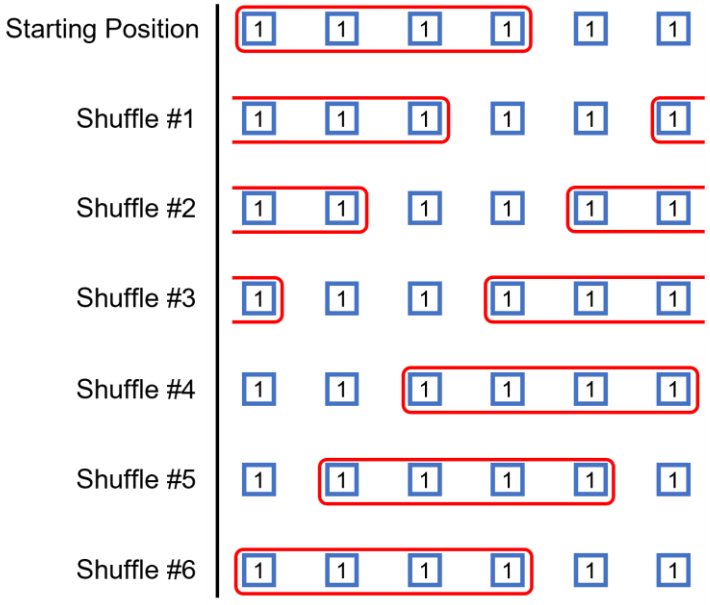

Figure 6-14: 6 Batteries, 4V Output, Shuffle Step Size = 5

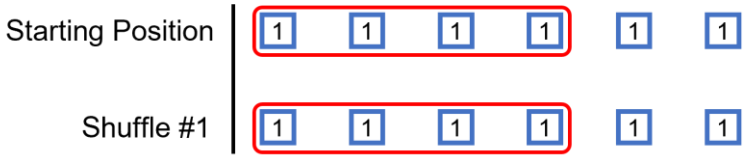

Figure 6-15: 6 Batteries, 4V Output, Shuffle Step Size = 6

The resources in positions 5 and 6 are not used at all when the step size is 6 with a group size of 4; only resources 1-4 are employed so this is highly inefficient.

Table 6-7: 6 Resources, Group Size of 4, Various Shuffle Step Sizes

Shuffle Step Size	**Equal Resource Utilisation?**	**# of Shuffles for Equal Load Distribution**	**# of Unique Stages**
1	Yes	5	6
2	Yes	2	3
3	No	N/A	2
4	Yes	2	3
5	Yes	5	6
6	No	N/A	1

In any system, a step size of 1 results in the easiest and most predictable shuffling, the number of shuffle stages to achieve equal loading is simply 1 less than the number of resources in the system. All other step sizes result in varying levels of efficiency and predictability, with some step sizes meaning that the shuffling technique fails so they are to be avoided.

The shuffling technique is governed by several rules:

1. The number of resources (R) in the system must be a positive integer and must be greater than 1.

$$1 < R \qquad (6\text{-}5)$$

2. The shuffling group size (G) must be a positive integer and must be less than the number of resources (R).

$$0 < G < R \qquad (6\text{-}6)$$

3. The shuffling step size (S) must also be a positive integer and must be less than the number of resources (R).

$$0 < S < R \qquad (6\text{-}7)$$

4. Each individual resource is whole and cannot be divided into multiple parts.

There are a few other interesting features of the group sizes and number of shuffles (N) noted from the rules and statistics above. When there is only 1 resource, a shuffle is impossible, this is defined by equations (6-5) and (6-6) as the only possible group size is 1. If the shuffle group size is equal to the number of resources, it means that no shuffling is required, the number of shuffles is 0 and therefore the number of unique stages is 1, this is defined by equation (6-6) and is shown in equation (6-8). In the case where the resources are all batteries, it means that they are already all arranged in series or parallel or a combination of both.

$$If\ G = R$$
$$N = 0 \qquad (6\text{-}8)$$

When the shuffle group size is 1, the number of shuffles required to return to the original configuration is equal to the number of resources and therefore to equally load all resources is one less than the number of resources.

$$If\ G = 1$$
$$N = R - 1 \qquad (6\text{-}9)$$

When the shuffle group size is 1 less than the number of resources, the number of required shuffles is also equal to the number of resources.

$$If\ G = R - 1$$
$$N = R \qquad (6\text{-}10)$$

All even numbers of resources have an optimum group size of half the number of resources such that the number of shuffles is equal to 2.

$$If\ R = 2k$$
$$Where\ k \geq 1 \qquad (6\text{-}11)$$
$$Optimum\ G = \frac{R}{2} \equiv k$$

For all even numbers, the number of shuffle steps is equal to the number of resources divided by the group size. Using equation (6-11), (6-12) shows that this is equal to 2 shuffle steps.

$$N = \frac{R}{G}$$
$$N = \frac{R}{\frac{R}{2}} \equiv 2 \qquad (6\text{-}12)$$

When the shuffle step size is equal to the shuffle group size, the following is true.

Table 6-8: Resource Utilisation for 6 Resources for Each Shuffle Group Size

Resource Index	**Shuffle Group Size**					
	1	**2**	**3**	**4**	**5**	**6**
1	1	1	1	2	5	1
2	1	1	1	2	5	1
3	1	1	1	2	5	1
4	1	1	1	2	5	1
5	1	1	1	2	5	1
6	1	1	1	2	5	1

Table 6-9: Resource Utilisation for 8 Resources for Each Shuffle Group Size

Resource Index	Shuffle Group Size							
	1	**2**	**3**	**4**	**5**	**6**	**7**	**8**
1	1	1	3	1	5	3	7	1
2	1	1	3	1	5	3	7	1
3	1	1	3	1	5	3	7	1
4	1	1	3	1	5	3	7	1
5	1	1	3	1	5	3	7	1
6	1	1	3	1	5	3	7	1
7	1	1	3	1	5	3	7	1
8	1	1	3	1	5	3	7	1

Table 6-8 and table 6-9 show the equal resource utilisation for 6 resources and 8 resources, respectively. Each column represents how many times each individual resource is employed during a full shuffle cycle (the equal utilisation), also representing the number of shuffles required to achieve equal loading. For all group sizes of 1, the number of times each resource is used is 1, likewise with all group sizes equal to the number of resources. Both tables show that each resource is employed the same amount throughout the complete shuffle cycle no matter what the shuffle group size.

Odd numbers of resources are more difficult than even numbers to optimise. The most complicated cases are those where the number of resources is an odd prime number. For example, when the number of resources is 7, all possible shuffle groups (1 to 6) results in the number of shuffles being the same as the number of resources, this is illustrated in table 6-5 and table 6-6. For odd prime numbers (P) of resources, the number of shuffles is equal to the number of resources (i.e. the magnitude of the prime number) assuming the group size is not equal to the number of resources.

$$If\ R = P$$
$$And\ G \neq R \qquad (6\text{-}13)$$
$$then\ N = R = P$$

Table 6-10: Optimum Shuffle Group Size Statistics for Different Types of System

# of Resources (R)	Optimum Shuffle Group Size (G)	# of Shuffles (N)
1	N/A	N/A
Even Numbers	$G = \frac{R}{2}$	2
Odd Composite Numbers	Largest factor of R	Corresponding factor pair
Odd Prime Numbers	$0 < G < R$ (i.e. any)	R

In the case where the system resources are batteries, the group size is decided by the desired output voltage so there may not always be an option to choose, therefore the shuffle step size is the only parameter which can be optimised.

6.3 Shuffling Efficiency

The goal of the research is to develop an efficient algorithm that is scalable to any number of resources and any output voltage demand, up to the maximum possible voltage where all batteries are connected in series. Factor voltages are trivial to handle but non-factor voltages are where the shuffling technique becomes necessary. The aim is to determine the optimum shuffle step size to minimise the number of shuffles for each output voltage case.

Voltage sources such as batteries is just one type of system which would benefit from shuffling resources, but the group size is dictated by the desired output voltage. In

other types of system, it may be more beneficial to shuffle in varying sized groups depending on the output required. If the equal load sharing could be achieved in fewer shuffle steps if the step size is greater than 1, then it is a more efficient approach.

MATLAB code was developed to simulate the shuffling technique for a wide range of system sizes and determining which step size(s) were optimal for each group size. The code first determines if the unique combination of the number of resources and group size on each iteration needs to employ TRUST. If the technique isn't required, the program records the simple series and parallel combinations and then moves to the next system composition. If the shuffling technique is required, the evaluation of each step size occurs and the step size(s) which result in the minimum number of shuffles is recorded as well as what the number of shuffles is. An extract of the code can be found in appendix I. Simulations were run for 1-120 batteries, plus again just for 720 batteries because it is an interesting factorial number. An extract of the data set (1-15 batteries) can be found in appendix J. The full data set can be made available upon request.

6.4 Factorials and Primes

There are some interesting situations and configurations which need to be handled uniquely. The first interesting set of numbers is the factorials. TRUST has been applied to the first 6 factorials. The 7^{th} factorial (5040) is too large to simulate, it is also a huge number of resources which is unlikely to ever exist in a situation where the technique is required in this format.

Table 6-11: Shuffling Requirements for First 6 Factorial Numbers of Batteries

Factorial	Number of Batteries	Number of Times Shuffling Required	Number of Times Shuffling Unnecessary	% Required
1	1	0	1	0
2	2	0	2	0
3	6	2	4	33.33
4	24	16	8	66.67
5	120	104	16	86.67
6	720	690	30	95.83

The fourth column in table 6-11, the number of times the technique is unnecessary is equal to the number of factors of the number of batteries in the system. 6 has 4 factors, 24 has 8 factors and so on.

Table 6-12 shows the output voltages for each of the first 4 factorial numbers of batteries which requires the shuffling technique to equally utilise each battery. As seen in table 6-11, factorial 1 and 2 do not require the shuffling technique. Factorial 3 only requires the shuffling technique to be employed a third of the time, whereas factorial 4 requires the technique two thirds of the time.

Curiously, for factorials 3 and 4 (the first two factorials which require the shuffling technique) the minimum number of shuffles whenever the technique is employed equals a prime number, as seen in the right-hand column of table 6-12. This is not true for factorials above 4, however. As 24 has 8 factors, the shuffling technique is only required for 16 output voltages as there are 8 voltages which can be constructed using simple series and parallel combinations.

Table 6-12: Shuffling Requirements for Factorials 3 and 4 Numbers of Batteries

Number of Batteries	Output Voltage (V)	Shuffle Required?	Best Step Size	Minimum Number of Shuffles
6	4	Y	2, 4	2
6	5	Y	1, 5	5
24	5	Y	4, 20	5
24	7	Y	3, 9, 15, 21	7
24	9	Y	6, 18	3
24	10	Y	4, 20	5
24	11	Y	2, 10, 14, 22	11
24	13	Y	1, 5, 7, 11, 13, 17, 19, 23	23
24	14	Y	2, 10, 14, 22	11
24	15	Y	3, 9, 15, 21	7
24	16	Y	8, 16	2
24	17	Y	1, 5, 7, 11, 13, 17, 19, 23	23
24	18	Y	6, 18	3
24	19	Y	1, 5, 7, 11, 13, 17, 19, 23	23
24	20	Y	4, 20	5
24	21	Y	3, 9, 15, 21	7
24	22	Y	2, 10, 14, 22	11
24	23	Y	1, 5, 7, 11, 13, 17, 19, 23	23

The other interesting set of numbers is the prime numbers, particularly odd prime numbers. These have the fewest factors and therefore will be awkward to divide into combinations of series and parallel groups so will often require TRUST.

Table 6-13: First 25 Prime Numbers of Batteries

Number of Batteries	Number of Times TRUST Required	Number of Times TRUST Unnecessary	% Required
2	0	2	0
3	1	2	33.33
5	3	2	60.00
7	5	2	71.43
11	9	2	81.82
13	11	2	84.62
17	15	2	88.24
19	17	2	89.47
23	21	2	91.30
29	27	2	93.10
31	29	2	93.55
37	35	2	94.59
41	39	2	95.12
43	41	2	95.35
47	45	2	95.74
53	51	2	96.23
59	57	2	96.61
61	59	2	96.72
67	65	2	97.01
71	69	2	97.18
73	71	2	97.26
79	77	2	97.47
83	81	2	97.59
89	87	2	97.75
97	95	2	97.94

Table 6-13 contains all prime numbers below 100 and shows the % of possible output voltages which requires TRUST. Figure 6-16 shows that there is a steep increase in the requirement and is asymptotic to 100%. Every prime number will be <100% due

to being divisible by 1 and itself so there will always be 2 output voltages which won't require the technique.

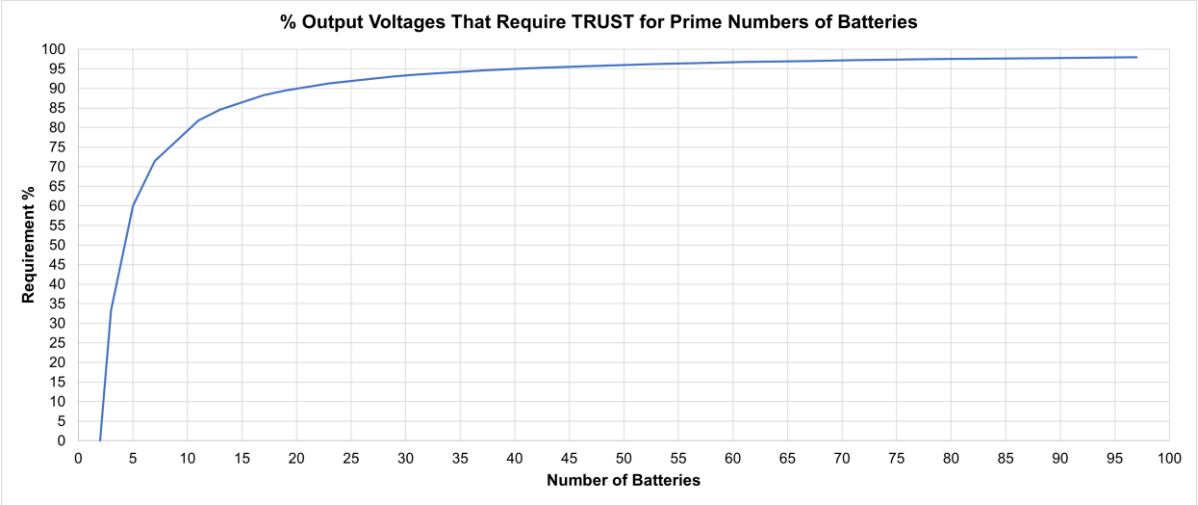

Figure 6-16: % of Output Voltages that Require TRUST, for Prime Numbers

If the number of batteries in the system (N) is a prime number (P), then the number of output voltages which require the shuffling technique (S_Y) is equal to 2 less than the prime number itself. Then its complement (S_N) is equal to 2 in every case which is simply the number of factors for a prime number.

$$If\ N = P$$

$$S_Y = P - 2 \qquad (6\text{-}14)$$

$$S_N = 2$$

Only odd prime numbers of batteries require shuffling because the first prime number, 2, can fully utilise both batteries for voltage outputs of 1V (both in parallel) or 2V (both in series).

Table 6-14: Shuffling Requirements for First 4 Odd Prime Numbers of Batteries

Number of Batteries	Output Voltage (V)	Shuffle Required?	Best Step Size	Minimum Number of Shuffles
3	2	Y	1, 2	2
5	2	Y	1, 2, 3, 4	4
5	3	Y	1, 2, 3, 4	4
5	4	Y	1, 2, 3, 4	4
7	2	Y	1, 2, 3, 4, 5, 6	6
7	3	Y	1, 2, 3, 4, 5, 6	6
7	4	Y	1, 2, 3, 4, 5, 6	6
7	5	Y	1, 2, 3, 4, 5, 6	6
7	6	Y	1, 2, 3, 4, 5, 6	6
11	2	Y	1, 2, 3, 4, 5, 6, 7, 8, 9, 10	10
11	3	Y	1, 2, 3, 4, 5, 6, 7, 8, 9, 10	10
11	4	Y	1, 2, 3, 4, 5, 6, 7, 8, 9, 10	10
11	5	Y	1, 2, 3, 4, 5, 6, 7, 8, 9, 10	10
11	6	Y	1, 2, 3, 4, 5, 6, 7, 8, 9, 10	10
11	7	Y	1, 2, 3, 4, 5, 6, 7, 8, 9, 10	10
11	8	Y	1, 2, 3, 4, 5, 6, 7, 8, 9, 10	10
11	9	Y	1, 2, 3, 4, 5, 6, 7, 8, 9, 10	10
11	10	Y	1, 2, 3, 4, 5, 6, 7, 8, 9, 10	10

For any prime number (P) of batteries (N), the minimum number of shuffles (S) required regardless of output voltage (except 1V and max voltage) is equal to 1 less than the prime number itself (N-1).

$$If\ N = P, then\ for\ all\ non - factors$$
$$S = N - 1 \qquad (6\text{-}15)$$

The worst cases are when the output voltage is a prime number, and it results in a prime number of unused batteries. For example, 19V from 720 batteries leaves 17 unused batteries if using 37 parallel groups of 19 series batteries in each (19x37=703). This results in the minimum number of shuffles being N-1 (719) regardless of the shuffle step size so there is no benefit to shuffling in step sizes larger than 1.

Conversely to this, any prime number output voltage which results in a highly divisible number of unused batteries (especially a factorial number) can be quite efficient. For example, 24 parallel groups of 29V from 720 batteries, 29x24=696 leaving 24 unused batteries. The minimum number of shuffles in this case is equal to the prime number itself, 29. Indeed, the output voltages of 47V, 59V, 71V, 79V, 89V, and 179V all have minimum number of shuffles equal to the prime number itself when the number of batteries in the system is 720 regardless of the shuffle step size. Likewise for a system with 120 batteries, the output voltages 11V, 19V, 23V, 29V and 59V all have minimum number of shuffles equal to the prime number itself regardless of step size.

It is therefore generally best to avoid prime numbers of batteries in the system and avoid output voltages which are prime numbers.

6.5 Unequal Resources

If designing a system from scratch, the designers can decide what the resources will be in advance, in which case identical resources is preferred as it is the easiest and

best composition. In many existing systems, however, the resources will not necessarily be identical, and this requires more careful consideration. When the resources are not all equal, the computational complexity increases exponentially as the size of the system grows.

Different resources can have different weightings associated with them such as different workers in a company having different levels of training or experience and there will therefore be variation in suitability for each individual job.

For existing systems that the shuffling technique is to be applied to, extensive analysis may be required to fully understand the system and determine the best approach. Modern AI would be attractive to be able to quickly deliver a solution. AI could also be used to monitor the system and make minor improvements to the operation of the shuffling technique dynamically as its understanding of usage over time develops. It could also make any major adjustments if the system changes considerably or suddenly. Planned changes to a system are easily handled, such as scheduled maintenance or training where some individual resources are temporarily removed from the system. Unplanned changes to a system are more difficult to deal with, such as when a resource fails or is accidentally removed from the system. AI would be able to adjust the group size and shuffle step size to maintain the ideal configuration.

There may, however, be some configurations of unequal resource systems which will not work with the shuffling technique. An example would be one which includes a combination of batteries and capacitors as charge storers. Supercapacitors have become more common in systems which are required upon to deliver huge surges as capacitors and supercapacitors can charge and discharge at extremely high speeds compared to battery technologies. Utilising batteries as main power storage devices to be used to deliver constant power over long periods of time and using

supercapacitors in parallel to deliver short bursts of large amounts of energy when required could be a tricky system to design a shuffling technique for. It would have to be a split system and shuffle each type of resource separately and combine them after each shuffle, again this would require dynamic computing to ensure optimum and fast reconfiguration.

6.6 Matrix Structure

Linear combinations of resources in either vertical or horizontal configurations can be electrically identical with the only difference effectively being the viewpoint of the observer. The final consideration, however, is entirely different and is where the resources are arranged in a matrix form such that diagonal combinations can also be utilised. This enables connections to be physically and electrically shorter as well as the connections themselves being made and broken quicker than in a linear topology. The main disadvantage with the matrix configuration, however, is the computational complexity compared to the linear versions; it effectively becomes a 3-dimensional problem compared to the linear version which is a 2-dimensional problem.

6.7 Conclusion

This chapter introduces the new concept of the shuffling technique, TRUST, where multiple resources can be combined in ways which enable each one to be loaded equally with the aim of extending the lifespan of systems by not overloading individual resources. Table 6-15 summarises the benefits of TRUST.

Table 6-15: Summary of Shuffling Technique Benefits

Benefit	Description
Increased system longevity	When resources are unequally loaded, some parts of the system are far more likely to fail than others due to extra stresses. Thus, when each resource is equally stressed, the overall life expectancy of the system increases
Resource agility	In the context of voltage sources such as batteries, the voltage agility is the key benefit, meaning that the system has a wider range of possible useful outputs
Reduced cooling requirements	When a system is more stable and equitable, it may lead to a decreased need for cooling such as in data centres, meaning there is an operational cost benefit
Increased power efficiency	In some applications such as using batteries as the resources, the equal loading should reduce the number of concentrated stressed points; this can lead to increased power efficiency as the resources are each working a little less hard when the demands are equally distributed
Lower operating costs	In most applications, whenever efficiency is increased there is a financial reward usually in terms of operating costs

The shuffling technique could enhance existing photovoltaic installations and maximum power point tracking (MPPT) systems by equally sharing the load between each panel and combining different panels in series and parallel to achieve the desired output characteristics.

This is also a consideration for so-called night-time photovoltaic cells which are a new area of research recently, albeit with efficiencies roughly one quarter of their conventional counterparts [76] but this is also an option for continued power generation through the night or in locations that experience extended periods of darkness.

TRUST can be applied to a plethora of situations where multiple resources are utilised. Resources do not have to be voltage sources such as batteries. Resources can mean many different things in different contexts. Table 6-16 describes some alternative applications.

Table 6-16: Alternative Applications for the Shuffling Technique

Alternative Application	**Description and Benefits**
Battery usage	Equal and unequal resource allocation for batteries is a major beneficiary of TRUST. There are many alternative applications of batteries which could all benefit, including: - Residential home storage for solar energy - Industrial storage for solar, wind turbines, or hydro power - Electric car battery cells - Off-grid storage for pop-up events - Backups for remote transmitter stations such as on the far sides of racing circuits. Usually wireless to minimise cable runs - UPS backup supplies for a variety of applications
Solar panel loading and distribution	Uniform distribution of load across all solar cells can increase the longevity of each cell and maintain maximum possible output for each panel regardless of the changing environment. Individual panels can become shaded at different times. Tracking the output of each individual panel could, over time, unveil some concerning patterns which might help to inform on any issues
Other renewables (wind, hydro, biomass)	Wind power and hydro power could also utilise the shuffling technique. There is unequal resource distribution across many sites throughout the UK, as well as variations in weather patterns. Each power generation site is expected to have different levels of output as well as different levels of demand. Weather is semi-predictable so some predictive techniques could be explored, using AI to dynamically adjust parameters to maximise output and distribution

National grid electricity distribution	Ageing infrastructure could benefit from the technique as power could effectively be shuffled around the country in anticipation of peaks, the grid would experience fewer problems relating to demand spikes, which could increase the lifetime of the equipment. This may require AI to generate the data required to predict the peaks that would be worth acting on
Data centre utilisation	By equally spreading the load across all resources in a data centre, the life expectancy of the critical systems can be increased
Contractor deployment	Assess nearest available qualified worker for more efficient resource deployment
Office hot desking	Optimise the space allocation in a dynamic office, particularly useful in the age of hybrid working
Logistics industry	Further increase algorithms for efficiency of delivery routes

Increasing efficiency is a hot research topic in most sectors of industry, maximising output whilst minimising input. Servicing the rapidly growing electric vehicle sector is becoming more widely researched as the demand for electricity and charging points increases significantly, placing extra stresses on already ageing and underfunded infrastructure.

Resources do not often fail simultaneously, usually an over-stressed individual component fails before others, leading to potential stresses on other members of the system and can shorten their life expectancy too. In extreme cases, the failure of a single resource can rapidly cause a cascade of failures in the other resources. For this reason, machine health has become a more popular research topic in the last couple of decades, as pre-emptive maintenance is better than reactive reparations; choosing when to have downtime in a system is an incredibly powerful tool to have at the disposal of the operator. Therefore, being able to equally load each resource using TRUST, gives system designers and operators more freedom.

Regardless of horizontal, vertical, or diagonal orientations of resources to be shuffled for equal loading. The technique also features a dynamic analysis of the optimum group size to determine the most efficient shuffling configuration.

The total resource utilisation shuffling technique (TRUST) is an innovative technique developed with the aim of increasing the efficiency of systems with multiple resources. With a unique configuration and a huge number of potential uses, increasing efficiency across a wide range of industries and applications could be made easier with TRUST.

The next chapter summarises and concludes the work, looks at opportunities for future related work and discusses the alternative applications for the shuffling technique in greater detail.

Chapter 7:
Conclusions and Future Work

7.1 Summary and Conclusions

Considering the increasing reliance on wireless communications across the world in todays' society partnered with the rising concerns for the health of the planet, the need for more efficient techniques to save power are clearer now than ever before.

This research aimed to improve the efficiency of existing OFDM signal amplifiers, which are ubiquitous in wireless communication infrastructure, by developing a power supply control circuit architecture. To achieve this, four contributions were made:

1. **Probabilistic Envelope Tracking (PET)**

   The introduction of PET as a new statistical waveform analysis to achieve optimum voltage switching thresholds required the structure of OFDM signals to be first deconstructed and analysed using common statistical analysis techniques. This provided insight into how to achieve greater efficiency. The achievable efficiency with the optimum thresholds is 63.82% with infinite thresholds and 63.4% with 100 thresholds. It was then proven that uniform thresholds can achieve 63.35% with 100 thresholds. The method is generalised and can be applied to waveforms other than OFDM.

2. **A New Method for the Construction of Efficient Modular Golomb Rulers (MGR)**

   A new method for determining perfect modular Golomb rulers (MGRs) was developed based on optimal Golomb rulers. These new structures were then leveraged to develop a system architecture for the PSU control technique.

3. **Merry-Go-Round Power Supply Control System Based on Modular Golomb Rulers**

   The merry-go-round PSU architecture was developed and informed by the new MGR construction method. The optimum voltage switching thresholds were given by the PET technique.

4. **Total Resource Utilisation Shuffling Technique (TRUST)**

   The shuffling technique, TRUST, can provide a robust and efficient solution to resource management. The presented study focuses on batteries as the resources with the aim of increasing the system life expectancy. The technique is generalised so could be applied to any system with multiple resources.

Although the objective was to improve the efficiency of OFDM amplifiers, the methods and techniques presented in this research can be generalised and applied to other modulation schemes and other waveforms, including audio.

Božanić and Sinha highlight the need for greener approaches to telecommunications with the existing 5G network infrastructure and as the advent of 6G fast approaches [77]. Six recommendations are proposed to enable greener technologies, two of which are addressed in this thesis. Firstly, the authors expand on the work by Abrol and Jha [78] to determine that efficient resource management is required. The work in this thesis addresses this with the introduction of the new shuffling technique, TRUST, which could be applied to the problem the authors have stressed. They also recommend energy efficient radio technologies as essential to any communication infrastructure moving forward. The work in this thesis on efficient OFDM amplifiers tackles this problem head on. Energy harvesting techniques are also discussed which would synergise nicely with the efficient OFDM amplifier power supply approach, as well as with the TRUST method.

Overall, the work presented in the thesis contributes to the growing body of research focused on developing more efficient and sustainable technologies. By improving the efficiency of wireless communication systems, it is possible to reduce their impact on the environment while still meeting the demands of a connected world.

7.2 Overview of the Thesis

Chapter 1 of the thesis introduces the research by providing an overview of its context and problem statement, which is the need for more efficient power-saving techniques in wireless communications. It outlines the research goals and objectives, which involve enhancing existing OFDM signal amplifiers by developing an innovative power supply control architecture. The chapter also discusses the research methodology and motivation for pursuing the research driven by the growing demand for wireless communication and environmental concerns. The original contributions of the research are highlighted which are the PET technique, the new MGR generation method, the Golomb PSU structure and TRUST. Finally, the thesis structure is outlined.

Chapter 2, the literature review, provides an extensive background for the research, examining previous work and identifying research gaps which this work has addressed. It sets the context, covering essential concepts, including an in-depth analysis of the structure, features, advantages, and disadvantages of OFDM. The chapter also provides an overview of various modulation techniques used in wireless communication systems. A discussion of alternative efficiency improvement methods for OFDM signal amplifiers is also presented, drawn from existing research. These methods include, DC tracking, the Doherty system, envelope tracking, the Chireix technique, envelope elimination and restoration, and bias modulation. Finally, the

chapter looks at the different ruler structures and sets the scene for the new method of generating MGRs developed in this work.

Chapter 3 proposes a novel technique to determine the optimum voltage switching thresholds for OFDM amplifiers, using MATLAB to perform the optimisations. The chapter begins by explaining the significance of simulating OFDM signals in MATLAB, to better understand the characteristics and behaviour in different scenarios. The chapter investigates the differences between various orders of PSK and QAM and draws conclusions about the PAPR distributions and their impact on the research work. Multiple parameters are varied in the simulations, including different data sizes, modulation types, modulation orders, power levels and SNR values to represent signal and channel quality.

Mathematical analysis of the generated signals and the development of a probability density function (PDF) is presented, resembling a Rayleigh distribution. This OFDM PDF formed the basis of the calculations to determine the optimum switching levels. The novel probabilistic envelope tracking (PET) technique is mathematically derived and validated with the use of MATLAB. The result is an achievable efficiency of up to 63.82% dependent on the desired number of thresholds. PET is scalable and applicable to any waveform with a known or calculable PDF.

Chapter 4 starts with a comparison between two different circuit topologies, linear flow (LF) and non-linear matrix (NLM), both of which have advantages and disadvantages which are discussed, settling on the LF topology. The chapter then derives a new method for the generation of modular Golomb rulers (MGRs) based on known optimal Golomb rulers. The method is then used to develop an efficient power supply architecture. A simple proof of concept using a binary topology is first investigated

before simulations of the MGR circuit are provided and analysed. The chapter explains the design process and justifications of different component choices.

Chapter 5 discusses experiments conducted with real-world amplifiers and presents the PAE results from 14 different amplifiers of various RF output powers, gains, and frequency bands. This provides context for this research and shows the need for efficient power supply control techniques. One amplifier, a 1W PA operating in the 2-2.5GHz band was then tested more thoroughly at various RF output powers, with different modulation schemes, and under several different bias conditions. The experiments were conducted to provide a reference for the proposed circuit design compared to real-world conditions, and to evaluate the performance benefits of said solution. The experimental setup is described in detail, including the equipment used and the test scenarios. The chapter concludes with a discussion of the implications of the results for the rest of the work in this thesis.

Chapter 6 introduces the shuffling technique, TRUST, equitable sharing among multiple resources, such as batteries. The chapter begins by outlining the motivation for the development of the technique and its potential real-world applicability. The technique addresses the problem of load imbalance, preventing premature failure and reduced system efficiency. The chapter provides a detailed explanation of the technique which involves periodic redistribution of the resources, either singularly or in groups to maintain balanced usage. The chapter concludes by highlighting some of the potential applications of TRUST. The benefits of increased system performance, life expectancy, and reliability mean that the technique can be an attractive proposition for many applications.

7.3 Suggestions for Future Work

There are numerous opportunities for future research to build upon the work presented in this thesis. The techniques and principles developed in this research have the potential to be adapted and applied to a variety of different fields and systems, offering opportunities for increased efficiency and optimisation. The proposed circuitry and algorithms can be used for applications beyond regulators and batteries.

7.3.1 Extensions to Current Work

In addition to extending the current work to other systems, future research can also focus on improving and optimising the proposed methods by combining with existing techniques. Research in alternative industries such as specifically tailored to renewable energy sources or electric vehicles could present a new challenge and yield a different performance enhancement.

1. **Real-World Testing**

   The testing described in chapter 5 was performed in laboratory conditions at an RF test bench instead of the modules being tested out in the field where environmental changes are dynamic. This allowed for repeatable results to be obtained with minimal errors and the data throughput was not a determining factor for success. This does mean, however, that the system is yet untested in a real-world environment such as in an outside broadcast transmit/receive chain.

2. **Higher System Orders**

   Moving to higher orders of the system could also offer opportunities for further enhancements at the risk of increasing size and complexity. Depending on the

architecture of the application, longer Golomb rulers may provide more interesting solutions.

3. **Retrofitting to Existing Amplifiers**

   The techniques presented in this work could be retrofitted to an existing amplifier on the market instead of developing a new amplifier.

4. **Alternative Waveforms and Amplifiers**

   The work in this thesis has focused on the application of the developed power supply control circuitry for OFDM signal amplifiers, there is scope to adapt the technique for use with other types of waveforms and amplifiers.

5. **Alternative Power Management Strategies**

   The proposed circuitry and algorithms could potentially be integrated into existing power management systems. This could involve the development of new control strategies which combine the proposed techniques with other power management algorithms to create more efficient and intelligent systems.

7.3.2 Future Related Work

Technology is constantly evolving, and new components and techniques become available over time. Therefore, while the presented work has made a significant contribution to improving the efficiency of OFDM signal amplifiers, there are several ways in which it could be further improved.

1. **Utilisation of New Semiconductor Technologies**

   Newer, more efficient semiconductor devices and technologies are a constant topic of research, these devices can offer incremental improvements in efficiency, which could further reduce the power consumption of wireless communication systems.

2. **Smaller Components**

   Utilising smaller components in the design is one way to improve the efficiency of the design and reduce the footprint of the circuitry. This would be especially attractive for portable devices.

3. **Component Integration**

   Integrated components can help to further reduce the footprint size of the system. By integrating multiple components into a single packaged device, the overall size and complexity of the system can be reduced. Albeit usually less cost-effective, the performance of integrated components can often be higher.

4. **Newer, Cheaper Components**

   Newer and cheaper devices with equivalent performance could also lead to a more attractive system.

7.3.3 GFDM

Generalised Frequency Division Multiplexing (GFDM) is a modulation technique that builds upon the widely used and well-known OFDM scheme. While both GFDM and OFDM use multiple subcarriers to transmit data, GFDM offers several advantages over OFDM and other similar techniques [79].

1. **Flexibility in Spectrum Allocation**

   GFDM is flexible in accommodating non-contiguous spectrum allocations. In scenarios where spectrum resources are limited or need to be allocated to multiple users with different bandwidth requirements, GFDM's flexible subcarrier allocation allows for the use of different bandwidths and subcarrier spacings. OFDM requires contiguous spectrum, limiting its ability to operate in fragmented spectrum environments.

2. **Enhanced Spectral Efficiency**

   GFDM enhances spectral efficiency by shaping subcarriers using a filter bank, reducing the need for guard bands [80]. This advantage proves valuable in bandwidth-constrained settings like mobile or wireless networks. Furthermore, GFDM can incorporate efficient waveforms such as Filter Bank Multi-Carrier (FBMC) to minimize out-of-band emissions, further boosting spectral efficiency.

3. **Improved Interference Resilience**

   GFDM outperforms OFDM and similar techniques in handling interference and multipath propagation. By using a filter bank and spreading the data across multiple subcarriers, GFDM can achieve greater frequency diversity, which can help to mitigate the effects of multipath propagation and increase system robustness [81].

4. **Lower Computational Complexity**

   GFDM can have a lower computational complexity in terms of subcarrier allocation, equalisation, and inter-symbol interference (ISI) mitigation techniques [82]. This is because GFDM uses a filter bank for subcarrier allocation and data transmission, instead of the complex Fourier transform used in OFDM. Moreover, the filter bank used in GFDM helps to reduce the ISI, which is one of the major drawbacks of OFDM.

In summary, GFDM offers several advantages over OFDM and other similar techniques, particularly in scenarios where spectrum resources are limited or shared. Due to its flexibility, improved spectral efficiency, and robustness in challenging propagation environments, GFDM is an attractive approach for current and future wireless communication systems. GFDM offers some unique advantages for specific applications such as in cognitive radio and in satellite communications. GFDM can

easily adapt to various channel conditions and requirements of different service providers, making it an ideal choice for cognitive radio applications. Cognitive radio is essentially a broad term for a dynamic spectrum reconfiguration process, often performed by software-define radio hardware [83]. GFDM also offers a higher tolerance to Doppler shifts, making it a good choice for satellite communications, where the high-speed movement of satellites can cause frequency offsets and receiver discrepancies.

7.3.4 TRUST Uses in Alternative Applications

The shuffling technique, TRUST, presented in chapter 6, has a wide range of potential alternative applications. It could be used to improve the efficiency and performance of various systems, including those related to energy management, office work, courier services, and contractor deployment.

1. **Office Hot Desking**

   With the rise of hybrid and remote working, traditional hot desking practices may no longer be effective. By applying TRUST, it may be possible to optimise the use of office space and resources to accommodate the changing needs of employees working in different locations at different times.

2. **Logistics Industry**

   Courier companies have long used algorithms to optimise their delivery routes, this harks back to the recurring ‘travelling salesman’ problem. The term was first coined by Robinson in 1949 [84] although mathematically it was first developed in the mid-1850’s by Hamilton [85] [86] [87] known as the Icosian Game, colloquially ‘Santa’s path’.

A solution first proposed by Dantzig in 1959 was specifically aimed at trucks to reduce their fuel consumption, thereby increasing their efficiency [88]. When applied to large logistics companies, the savings are often enormous. In the US and other countries where the roads are right-hand traffic, many courier companies employ software algorithms to use right-handed loops back to distribution centres to minimise left turns, analogous with left-hand traffic countries.

TRUST could supplement existing algorithms by further reducing awkward turns, waiting times, yielding times, and fuel wastage by adapting the technique to route planning and driver deployment.

3. **Contractor Deployment**

   The deployment of contractors, sub-contractors and repair callouts could benefit from TRUST by identifying the nearest available worker and minimising distances travelled and fuel wasted. Previous techniques have been proposed and proven such as the type-2 fuzzy logic-based system approach presented by Starkey et al. [89].

4. **Water/Electricity Supplies**

   Both domestic and commercial/industrial use could benefit from TRUST, specifically by utilising community and connected network efficiencies to reduce energy usage and emissions. By optimising the distribution of water and electricity, it may be possible to reduce the energy overheads involved in the networks.

5. **Energy Storage Systems**

   TRUST could be used to profile domestic energy usage and reallocate stored energy to neighbours if required, otherwise feed back into the grid.

6. **National Grid Infrastructure**

   Current national grid infrastructure is ageing and underfunded, and with the rapidly increasing electric and plug-in hybrid vehicle industry it is becoming increasingly stressed. TRUST could be employed with the aim of equalising load on the network, power generation and distribution across the nation to ultimately reduce overloading, brownouts, and blackouts. Predictive usage statistics could be used to transfer available power across the country before demand peaks.

7. **Data Centres**

   TRUST could be used to reduce the load on specific units and the amount of cooling required. A data centre has a large carbon footprint per square metre so any reduction would be beneficial to both the operators and the environment.

In conclusion, TRUST has a wide range of potential applications ranging from energy storage and distribution systems to the logistics industry and contractor deployment, as well as in wireless communications which was the focus of this work.

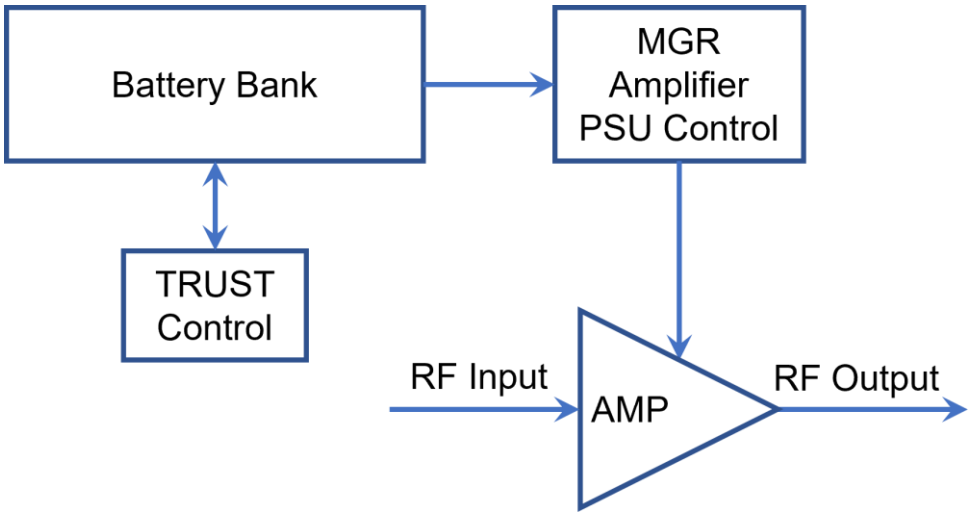

Figure 7-1: TRUST Power Storage and Delivery with MGR PSU Control using PET

All four original contributions in this work could be combined to produce the block diagram in figure 7-1. The power supply construction is informed by the waveform

analysis and uniform voltage switching threshold optimisations from the PET technique in chapter 3. The new method presented in chapter 4 of generating MGRs from optimal Golomb rulers is used to determine an efficient ruler composition. Then the technique would work with TRUST, from chapter 6, to arrange the battery bank appropriately to form the multi-level MGR PSU, also outlined in chapter 4. This layout would also work if the system were aimed at other input signals such as audio waveforms instead of modulated OFDM, the PET technique would be adjusted for the new waveform analysis.

The TRUST control algorithm can be applied to the power storage with feedback for potential diagnostic tools. The next step for TRUST, therefore, would be to configure a bank of batteries to produce the MGR structures explained in chapter 4. The 1,3,2,7 ruler could be configured from a bank of 13 batteries. Automatic control of the battery bank could utilise each cell equally, with intelligent feedback and control to recognise when individual batteries are being underused and prioritise them on the next shuffle dynamically. The result would be 13 batteries all equally utilised in a modular Golomb ruler structure to achieve any output voltage between 1-13V whilst maximising the endurance of each battery in the system.

The work in this thesis in parts is intended to be submitted to IEEE Transactions on Microwave Theory and Techniques or IEEE Transactions on Wireless Communications.

References

[1] X. Cheng, Y. Hu and L. Varga, “5G Network Deployment and the Associated Energy Consumption in the UK: A Complex Systems’ Exploration,” *Technological Forecasting and Social Change,* vol. 180, p. 24, 2022.

[2] A. S. Andrae and T. Edler, “On Global Electricity Usage of Communication Technology: Trends to 2030,” *Challenges,* vol. 6, no. 1, pp. 117-157, 2015.

[3] International Commission on Non-Ionizing Radiation Protection, “Guidelines for Limiting Exposure to Electromagnetic Fields (100KHz-300GHz),” *Health Physics,* vol. 118, no. 5, pp. 483-524, 2020.

[4] W. H. Bailey, R. Bodemann, J. Bushberg, C.-K. Chou, R. Cleveland, A. Faraone, K. R. Foster, K. E. Gettman, K. Graf and T. Harrington, “IEEE Standard for Safety Levels with Respect to Human Exposure to Electric, Magnetic, and Electromagnetic Fields, 0Hz to 300GHz,” *IEEE Access 7,* vol. 7, pp. 171346-171356, 2019.

[5] R. S. Tucker, “Energy Consumption in Telecommunications,” in *2012 Optical Interconnects Conference*, Santa Fe, 2012.

[6] L. Belkhir and A. Elmeligi, “Assessing ICT Global Emissions Footprint: Trends to 2040 and Recommendations,” *Journal of Cleaner Production,* vol. 177, pp. 448-463, 2018.

[7] L. Williams, B. K. Sovacool and T. J. Foxon, “The Energy Use Implications of 5G: Reviewing Whole Network Operational Energy, Embodied Energy, and Indirect Effects,” *Renewable and Sustainable Energy Reviews,* vol. 157, p. 18, 2022.

[8] C. Freitag, M. Berners-Lee, K. Widdicks, B. Knowles, G. S. Blair and A. Friday, “The Real Climate and Transformative Impact of ICT: A Critique of Estimates, Trends and Regulations,” *Patterns,* vol. 2, no. 9, p. 18, 2021.

[9] The World Bank, “Global Initiative to Reduce Gas Flaring: "Zero Routine Flaring by 2030",” The World Bank, 2015.

[10] International Energy Agency (IEA), “The Oil and Gas Industry in Energy Transitions,” IEA Publications, 2020.

[11] L. E. Barton, “Recent Developments of the Class B Audio-and Radio-Frequency Amplifiers,” *Proceedings of the Institute of Radio Engineers,* vol. 24, no. 7, pp. 985-1006, 1936.

[12] R. Caverly, F. Raab and J. Staudinger, “High-Efficiency Power Amplifiers,” *IEEE Microwave Magazine,* vol. 13, no. 7, pp. S22-S23, 2012.

[13] N. O. Sokal, “RF Power Amplifiers, Classes A Through S - How They Operate, and When to Use Each,” in *Professional Program Proceedings. Electronic Industries of New England*, 1997.

[14] B. Berglund, J. Johansson and T. Lejon, “High Efficiency Power Amplifiers,” *Ericsson Review,* vol. 83, no. 3, pp. 92-96, 2006.

[15] F. Raab, “Maximum Efficiency and Output of Class-F Power Amplifiers,” *IEEE Transactions on Microwave Theory and Techniques,* vol. 49, no. 6, pp. 1162-1166, 2001.

[16] N. O. Sokal, “Class E High-Efficiency Power Amplifiers, from HF to Microwave,” in *1998 IEEE MTT-S International Microwave Symposium Digest Cat No. 98CH36192*, 1998.

[17] M. Vasić, O. Garcia, J. A. Oliver, P. Alou, D. Diaz and J. A. Cobos, “Multilevel Power Supply for High-Efficiency RF Amplifiers,” *IEEE Transactions on Power Electronics,* vol. 25, no. 4, pp. 1078-1089, 2009.

[18] W. H. Doherty, “Amplifier”. United States Patent US2210028A, 6 August 1940.

[19] W. H. Doherty, “A New High Efficiency Power Amplifier for Modulated Waves,” *Proceedings of the Institute of Radio Engineers,* vol. 24, no. 9, pp. 1163-1182, 1936.

[20] F. H. Raab, “Efficiency of Doherty RF Power-Amplifier Systems,” *IEEE Transactions on Broadcasting,* Vols. BC-33, no. 3, pp. 77-83, 1987.

[21] W. H. Doherty, “High Frequency Amplifier”. United States Patent US2314132A, 16 March 1943.

[22] W. H. Doherty, “Translation of Microwaves”. United States Patent US2426185A, 26 August 1947.

[23] R. Giofrè, L. Piazzon, P. Colantonio and F. Giannini, “A Closed-Form Design Technique for Ultra-Wideband Doherty Power Amplifiers,” *IEEE Transactions on Microwave Theory and Techniques,* vol. 62, no. 12, pp. 3414-3424, 2014.

[24] L. Piazzon, R. Giofrè, P. Colantonio and F. Giannini, “A Wideband Doherty Architecture with 36% of Fractional Bandwidth,” *IEEE Microwave and Wireless Components Letters,* vol. 23, no. 11, pp. 626-628, 2013.

[25] G. Sun and R. H. Jansen, “Broadband Doherty Power Amplifier via Real Frequency Technique,” *IEEE Transactions on Microwave Theory and Techniques,* vol. 60, no. 1, pp. 99-111, 2011.

[26] J. M. Rubio, J. Fang, V. Camarchia, R. Quaglia, M. Pirola and G. Ghione, “3-3.6GHz Wideband GaN Doherty Power Amplifier Exploiting Output Compensation Stages,” *IEEE Transactions on Microwave Theory and Techniques,* vol. 60, no. 8, pp. 2543-2548, 2012.

[27] H. Chireix, “High Power Outphasing Modulation,” *Proceedings of the Institute of Radio Engineers,* vol. 23, no. 11, pp. 1370-1392, 1935.

[28] J. Staudinger, B. Gilsdorf, D. Newman, G. Norris, G. Sadowniczak, R. Sherman and T. Quach, “High Efficiency CDMA RF Power Amplifier Using Dynamic Envelope Tracking Technique,” in *IEEE MTT-S International Microwave Symposium Digest Cat No 00CH37017*, 2000.

[29] B. Sahu and G. A. Rincón-Mora, “A High-Efficiency Linear RF Power Amplifier with a Power-Tracking Dynamically Adaptive Buck-Boost Supply,” *IEEE Transactions on Microwave Theory and Techniques,* vol. 52, no. 1, pp. 112-120, 2004.

[30] Q. Zhu, *Envelope Amplifier for Broadband Base-station Envelope Tracking Power Amplifier,* San Diego: UC San Diego, 2011.

[31] G. Hanington, P.-F. Chen, P. Asbeck and L. Larson, “High-Efficiency Power Amplifier Using Dynamic Power-Supply Voltage for CDMA Applications,” *IEEE Transactions on Microwave Theory,* vol. 47, no. 8, pp. 1471-1476, 1999.

[32] Y. Komatsuzaki, S. Lanfranco, T. Kolmonen, O. Piirainen, J. K. Tanskanen, S. Sakata, R. Ma, S. Shinjo, K. Yamanaka and P. Asbeck, “A High-Efficiency 3.6-4.0GHz Envelop-Tracking Power Amplifier Using GaN Soft-Switching Buck-Converter,” in *IEEE/MTT-S International Microwave Symposium-IMS*, Philadelphia, 2018.

[33] M. Özen and C. Fager, “Symmetrical Doherty Amplifier with High Efficiency over Large Output Power Dynamic Range,” in *2014 IEEE MTT-S International Microwave Symposium*, Tampa, 2014.

[34] L. R. Kahn, “Single-Sideband Transmission by Envelope Elimination and Restoration,” *Proceedings of the Institute of Radio Engineers,* vol. 40, no. 7, pp. 803-806, 1952.

[35] R. W. Chang, “Synthesis of Band-Limited Orthogonal Signals for Multichannel Data Transmission,” *Bell System Technical Journal,* vol. 45, no. 10, pp. 1775-1796, 1966.

[36] N. LaSorte, J. W. Barnes and H. H. Refai, “The History of Orthogonal Frequency Division Multiplexing,” in *IEEE GLOBECOM 2008 IEEE Global Telecommunications Conference*, New Orleans, 2008.

[37] M.-J. Hao and W.-W. Pi, “PAPR Reduction in OFDM Signals by Self-Adjustment Gain Method,” *Electronics,* vol. 10, no. 14, p. 1672, 2021.

[38] M. C. P. Parades and M. J. F.-G. Garcia, “The Problem of Peak-to-Average Power Ratio in OFDM Systems,” 2015.

[39] M. H. Aghdam and A. A. Sharifi, “PAPR Reduction in OFDM Systems: An Efficient PTS Approach Based on Particle Swarm Optimisation,” *ICT Express,* vol. 5, no. 3, pp. 178-181, 2019.

[40] W. Shieh and I. Djordjevic, “Chapter 2 - OFDM Principles,” in *OFDM for Optical Communications*, Oxford, Academic Press, 2010, pp. 31-52.

[41] R. W. Bäuml, R. F. H. Fischer and J. B. Huber, “Reducing the Peak-to-Average Power Ratio of Multicarrier Modulation by Selected Mapping,” *Electronis Letters,* vol. 32, no. 22, pp. 2056-2057, 1996.

[42] P. D. Pamungkasari, I. Shubhi, F. H. Juwono, P. D. Mariyam and D. Gunawan, “Time Domain Cyclic Selective Mapping for PAPR Reduction in MIMO-OFDM Systems,” in *2018 IEEE International Conference on Innovative Research and Development (ICIRD)*, Thailand, 2018.

[43] M. A. Taher, M. J. Singh, M. B. Ismail, S. A. Samad and M. T. Islam, “Sliding the SLM-Technique to Reduce the Non-Linear Distortion in OFDM Systems,” *Elektronika ir Elektrotechnika,* vol. 19, no. 5, pp. 103-111, 2013.

[44] H. Ochiai and H. Imai, “On Clipping for Peak Power Reduction of OFDM Signals,” in *IEEE Conference and Exhibition on Global Telecommunications (GLOBECOM)*, San Francisco, 2000.

[45] K. Anoh, B. Adebisi, C. Tanriover and M. Hammoudeh, “A New Approach to Iterative Clipping and Filtering PAPR Reduction Scheme for OFDM Systems,” *IEEE Access,* vol. 6, pp. 17533-17544, 2017.

[46] R. Xu, M. Chen, C. Tian, X. Lu and C. Diao, “Statistical Distributions of OFDM Signals on Multi-path Fading Channels,” in *2011 International Conference on Wireless Communications and Signal Processing*, Nanjing, China, 2011.

[47] J. Ma, G. Jindal, M. Nair, T. A. Cappello, G. T. Watkins, K. Morris and M. Beach, “Highly Efficient 3-Bit Digital Power Amplifier for OFDM Waveform Application,” *IEEE Transactions on Microwave Theory and Techniques,* vol. 71, no. 1, pp. 35-47, 2022.

[48] W. Shi, S. He, X. Zhu, B. Song, Z. Zhu, G. Naah and M. Zhang, “Broadband Continuous-Mode Doherty Power Amplifiers with Noninfinity Peaking Impedance,” *IEEE Transactions on Microwave Theory and Techniques,* vol. 66, no. 2, pp. 1034-1046, 2018.

[49] Y. Cao and K. Chen, “Pseudo-Doherty Load-Modulated Balanced Amplifier with Wide Bandwidth and Extended Power Back-Off Range,” *IEEE Transactions on Microwave Theory and Techniques,* vol. 68, no. 7, pp. 3172-3183, 2020.

[50] R. C. Alperin and V. Drobot, “Golomb Rulers,” *Mathematics Magazine,* vol. 84, no. 1, pp. 48-55, 2011.

[51] W. C. Babcock, “Intermodulation Interference in Radio Systems Frequency of Occurence and Control by Channel Selection,” *The Bell System Technical Journal,* vol. 32, no. 1, pp. 63-73, 1953.

[52] H. Halberstam and R. R. Laxton, “Perfect Difference Sets,” *Glasgow Mathematical Journal,* vol. 6, no. 4, pp. 177-184, 1964.

[53] S. W. Golomb, “Shift-Register Sequences and Spread-Spectrum Communications,” in *IEEE Third International Symposium on Spread Spectrum Techniques & Applications*, Oulu, Finland, 1994.

[54] J. P. Robinson and A. J. Bernstein, “A Class of Binary Recurrent Codes with Limited Error Propagation,” *IEEE Transactions on Information Theory,* vol. 13, no. 1, pp. 106-113, 1967.

[55] F. Biraud, E. Blum and J. Ribes, “On Optimum Synthetic Linear Arrays with Application to Radioastronomy,” *IEEE Transactions on Antennas and Propagation,* vol. 22, no. 1, pp. 108-109, 1974.

[56] R. C. Alperin and V. Drobot, “Golomb Rulers,” *Mathematics Magazine,* vol. 84, no. 1, pp. 48-55, 2011.

[57] A. Gerling, L. Becke, S. Tonder, M. R. Hofmann, J. C. Balzer and C. Brenner, “Golomb Ruler Based Discrete Frequency Multimodal Continuous Wave THz Spectroscopy System,” in *2019 Second International Workshop on Mobile Terahertz Systems (IWMTS)*, Bad Neuenahr, Germany, 2019.

[58] G. S. Bloom and S. W. Golomb, “Applications of Numbered Undirected Graphs,” *Proceedings of the IEEE,* vol. 65, no. 4, pp. 562-570, 1977.

[59] F. Brglez, B. Bošković and J. Brest, “On Asymptotic Complexity of the Optimum Golomb Ruler Problem: From Established Stochastic Methods to Self-Avoiding Walks,” in *2017 IEEE Congress on Evolutionary Computation*, Donostia/San Sebastián, 2017.

[60] J. P. Robinson, “Optimum Golomb Rulers,” *IEEE Transactions on Computers,* vol. 100, no. 12, pp. 943-944, 1979.

[61] J. Singer, “A Theorem in Finite Projective Geometry and Some Applications to Number Theory,” *Transactions of the American Mathematical Society,* vol. 43, no. 3, pp. 377-385, 1938.

[62] T. P. Kirkman, “On the Perfect r-Partitions of r^2-r+1,” *Transactions of the Historic Society of Lancashire and Cheshire,* vol. 9, pp. 127-142, 1857.

[63] R. C. Bose and S. Chowla, “Theorems in the Additive Theory of Numbers,” *Comentarii Mathematici Helvetici,* vol. 37, pp. 141-147, 1962.

[64] I. Z. Rusza, “Solving a Linear Equation in a Set of Integers I,” *Acta Arithmetica,* vol. 65, no. 3, pp. 259-282, 1993.

[65] ETSI, EN, “300 744 V1.6.2 (2015-10),” *Digital Video Broadcasting (DVB). Framing Structure, Channel Coding and Modulation for Digital Terrestrial Television,* 2015.

[66] ETSI, “TS 138 521-1 V15.3.0 (2019-07),” ETSI, Valbonne, 2019.

[67] A. Zaidi, F. Athley, J. Medbo, U. Gustavsson, G. Durisi and X. Chen, 5G Physical Layer: Principles, Models and Technology Components, London: Academic Press, 2018.

[68] A. Al-Jzari and K. Iviva, “Cyclic prefix length determination for orthogonal frequency division multiplexing system over different wireless channel models based on the maximum excess delay spread,” *American Journal of Engineering and Applied Sciences,* vol. 8, no. 1, pp. 82-93, 2015.

[69] T. Yücek, R. M. Tannious and A. Hüseyin, “Doppler Spread Estimation for Wireless OFDM Systems,” in *IEEE/Sarnoff Symposium on Advances in Wired and Wireless Communication*, Princeton, New Jersey, 2005.

[70] W. Mixon (Unpublished, cited in) and M. Gardner, “Mathematical Games,” *Scientific American,* pp. 116-118, June 1972.

[71] K. Davaslioglu and E. Ayanoglu, “Quantifying Potential Energy Efficiency Gain in Green Cellular Wireless Networks,” *IEEE Communications Surveys & Tutorials,* vol. 16, no. 4, pp. 2065-2091, 2014.

[72] G. Leighton and M. Evans, *3.25GHz Amplifier Tx/Rx Channel Testing,* Colchester: ABER Electronics Ltd., 2020.

[73] M. Evans and G. Leighton, *ABER S-Band Downconverter,* Colchester: ABER Electronics Ltd., 2021.

[74] J. W. Rosenthal, “Card Shuffling,” *Mathematics Magazine,* vol. 54, no. 2, pp. 64-67, 1981.

[75] D. Aldous and P. Diaconis, “Shuffling Cards and Stopping Times,” *The American Mathematical Monthly,* vol. 93, no. 5, pp. 333-348, 1986.

[76] T. Deppe and J. N. Munday, “Nighttime Photovoltaic Cells: Electrical Power Generation by Optically Coupling with Deep Space,” *ACS Photonics,* vol. 7, no. 1, pp. 1-9, 2019.

[77] M. Božanić and S. Sinha, “6G: The Green Network,” in *Mobile Communication Networks: 5G and a Vision of 6G*, Springer, 2021, pp. 189-220.

[78] A. Abrol and R. K. Jha, “Power Optimization in 5G Networks: A Step Towards GrEEn Communication,” *IEEE Access,* vol. 4, pp. 1355-1374, 2016.

[79] N. Michailow, M. Matthé, I. S. Gaspar, A. N. Caldevilla, L. L. Mendes, A. Festag and G. Fettweis, “Generalized Frequency Division Multiplexing for 5th Generation Cellular Networks,” *IEEE Transactions on Communications,* vol. 62, no. 9, pp. 3045-3061, 2014.

[80] M. Towliat, S. M. J. A. Tabatabaee and M. Rajabzadeh, “A Simple ML Detection for Coded Generalized Frequency Division Multiplexing in MIMO Channels,” *IEEE Transactions on Signal Processing,* vol. 67, no. 3, pp. 798-807, 2018.

[81] S. Han, Y. Sung and Y. H. Lee, “Filter Design for Generalized Frequency-Division Multiplexing,” *IEEE Transactions on Signal Processing,* vol. 65, no. 7, pp. 1644-1659, 2016.

[82] A. Farhang, N. Marchetti and L. E. Doyle, “Low-Complexity Modem Design for GFDM,” *IEEE Transactions on Signal Processing,* vol. 64, no. 6, pp. 1507-1518, 2015.

[83] B. Wang and R. K. Liu, “Advances in Cognitive Radio Networks: A Survey,” *IEEE Journal of Selected Topics in Signal Processing,* vol. 5, no. 1, pp. 5-23, 2010.

[84] J. Robinson, “On the Hamiltonian Game (a Traveling Salesman Problem),” 1949.

[85] W. R. Hamilton, “Memorandum respecting a new system of roots of unity,” *Philosophical Magazine,* vol. 12, no. 4, p. 446, 1856.

[86] W. R. Hamilton, “XLIII. On the calculation of the numerical values of a certain class of multiple and definite integrals,” *The London, Edinburgh, and Dublin Philosophical Magazine and Journal of Science,* vol. 14, no. 94, pp. 375-382, 1857.

[87] W. R. Hamilton, “Account of the Icosian Calculus,” in *Proceedings of the Royal Irish Academy*, Dublin, 1858.

[88] G. B. Dantzig and J. H. Ramser, “The Truck Dispatching Problem,” *Management Science,* vol. 6, no. 1, pp. 80-91, 1959.

[89] A. Starkey, H. Hagras, S. Shakya and G. Owusu, “A multi-objective genetic type-2 fuzzy logic based system for mobile field workforce area optimization,” *Information Sciences,* vol. 329, pp. 390-411, 2016.

Appendix A:
OFDM Signal Generation, Modulation, Transmission, Demodulation, PAPR Histograms

```
%=========================================================================
% Parameters
%=========================================================================
m = 4;                      % Number of symbols in QAM
n = 512;                    % Number of subcarriers
cp = 92;                    % Length of cyclic prefix
snr_dB = 15;                % SNR in dB
num_trials = 100000;        % Number of trials for PAPR calculation

%=========================================================================
% Generate OFDM Signal and QAM Modulate the Symbols
%=========================================================================
% Generate OFDM signal
pseudo_data = randi([0 m-1], n, num_trials); % Random data symbols in [0, M-1]

% Perform QAM modulation
ofdm_signal = qammod(pseudo_data, m);

% Perform IFFT
ofdm_signal = ifft(ofdm_signal);

% Add cyclic prefix
ofdm_signal = [ofdm_signal(:, end-cp+1:end) ofdm_signal];

%=========================================================================
% AWGN Channel
%=========================================================================
% Pass through AWGN channel
snr = 10^(snr_dB/10);       % Convert SNR from dB to linear scale
EbNo = snr/log2(m);         % Convert SNR to Eb/No
ofdm_signal_noisy = awgn(ofdm_signal, EbNo, 'measured');

%=========================================================================
% PAPR Calculation and Kernel Density Estimation (KDE) for Tx Data
%=========================================================================
% Calculate PAPR of transmitted signal
papr_tx = max(abs(ofdm_signal).^2,[],1)./mean(abs(ofdm_signal).^2,1);

% Plot PAPR histogram of Tx data
figure
histogram(papr_tx,'Normalization','pdf')
hold on
```

```
% Compute and plot KDE of Tx PAPR data
[fi,xi] = ksdensity(papr_tx);
plot(xi, fi, 'LineWidth', 2);
hold off

xlabel('Peak-to-Average Power Ratio (dB)')
ylabel('Normalised Probability Density')
title('Normalised PDF of OFDM PAPR for Tx')
legend('Histogram', 'KDE')

%=========================================================================
% Signal Demodulation
%=========================================================================
% Remove cyclic prefix
ofdm_signal_noisy = ofdm_signal_noisy(:, cp+1:end);

% Perform FFT on signal
ofdm_signal_noisy = fft(ofdm_signal_noisy);

% Perform demodulation
demod_data = qamdemod(ofdm_signal_noisy, m);

%=========================================================================
% Calculate BER of Rx Signal
%=========================================================================
% Calculate BER
[num_errors, ber] = biterr(data, demod_data);
fprintf('Bit Error Rate: %e\n', ber);
```

Appendix B:
Modulation Constellation Diagrams, EVM, SNR Plots

```
%==========================================================================
% OFDM Signal Generation, Modulation, Transmission, Demodulation
%==========================================================================
% .
% MAIN CODE FOR OFDM SIGNAL GENERATION, MODULATION, TRANSMISSION ACROSS
% AWGN CHANNEL, DEMODULATION
% .
%==========================================================================
% Extra Parameters
%==========================================================================
snr_range = 0:0.01:30;                % SNR range
snr_values = [5, 10, 15, 20, 25, 30]; % SNR values for BPSK-64QAM
%snr_values = [12.5, 16, 19.5, 23, 26.5, 30]; % SNR values for 256QAM
%snr_values = [17.5, 20, 22.5, 25, 27.5, 30]; % SNR values for 1024QAM
ber = zeros(1,length(snr_range));     % Preallocate BER vector
t = 1/15e3;                           % Symbol duration in seconds
m_values = [2, 4, 16, 64, 256];       % Set of different modulation orders

%==========================================================================
% Plot Constellation Diagrams of Tx and Rx Modulated Signals
%==========================================================================
% Constellation diagram before transmission
scatterplot(ofdm_signal);
title(sprintf('%dQAM Tx Constellation: 5-30dB SNR, 512-2048 Subcarriers', m));

% Constellation diagram after transmission
scatterplot(ofdm_signal_noisy);
title(sprintf('Rx Constellation: %dQAM OFDM, %ddB SNR, %d Subcarriers', m, snr_dB,
n));

%==========================================================================
% Iterate through several SNR values and plot on the same graph in subplots
%==========================================================================
% .
% MAIN CODE TO ITERATE THROUGH SERVERAL SNR VALUES AND SUBPLOT EACH GRAPH
% .
%==========================================================================
% Nested For Loops for Range of SNR Values for Different Modulation Orders
%==========================================================================
% Modulation order loop
figure
hold on;
for i = 1:length(m_values)
    m_range = m_values(i);
```

```
    % SNR range loop
    for j = 1:length(snr_range)

        % Number of trials loop
        for k = 1:num_trials
            % Generate random data symbols
            data = randi([0 m_range-1], n, 1);

            % Perform QAM modulation
            ofdm_signal_no_cp = qammod(data, m_range);

            % Add cyclic prefix
            ofdm_signal = [ofdm_signal_no_cp(end-cp+1:end); ofdm_signal_no_cp];

            % Perform IFFT
            ofdm_signal = ifft(ofdm_signal);

            % Pass through AWGN channel
            snr = 10^(snr_range(j)/10);     % Convert SNR from dB to linear scale
            EbNo = snr/log2(m_range);       % Convert SNR to Eb/No
            ofdm_signal_noisy = awgn(ofdm_signal, EbNo, 'measured');

            % Perform FFT
            rx_ofdm_signal = fft(ofdm_signal_noisy);

            % Remove cyclic prefix
            rx_ofdm_signal = rx_ofdm_signal(cp+1:end);

            % Demodulate the signal
            rx_data = qamdemod(rx_ofdm_signal, m_range);

            % Count the number of errors
            ber(j) = ber(j) + sum(data ~= rx_data);
        end

        % Calculate BER for the current SNR value
        ber(j) = ber(j)/(n*num_trials);
    end

    % Plot Average BER vs SNR
    plot(snr_range, ber, 'lineWidth', 1.5);
end

hold off;
xlabel('SNR (dB)');         % Label x-axis
ylabel('BER');              % Label y-axis
title('BER versus SNR for Various Modulation Orders')
legend('BPSK', 'QPSK', '4QAM', '16QAM', '64QAM', '256QAM');
set(gca, 'YScale', 'log')   % Set y-axis scale to logarithmic
ylim([5e-5 1e1])            % Set y-axis limits
```

Appendix C:
256QAM, 1024QAM Rx Constellation Diagrams

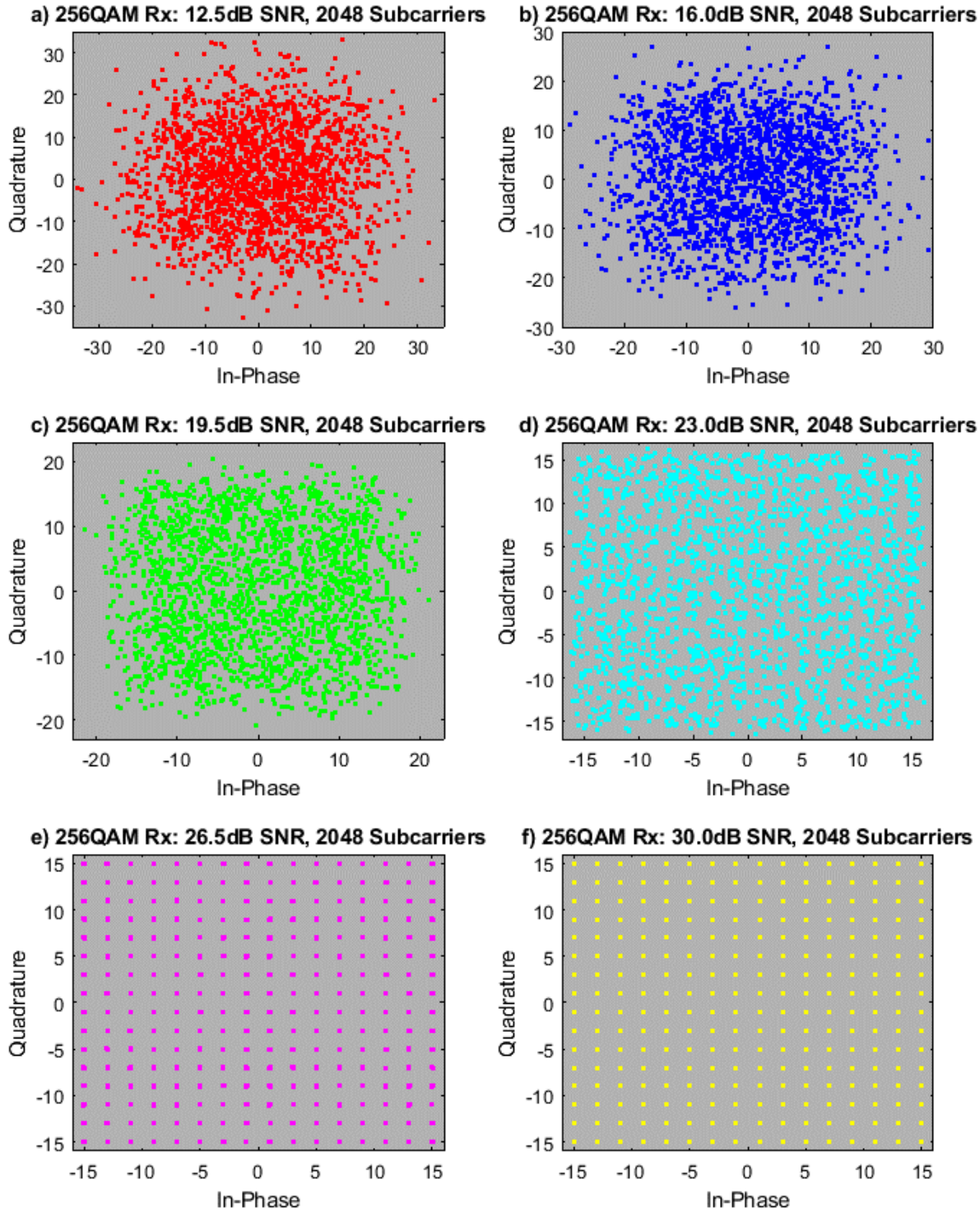

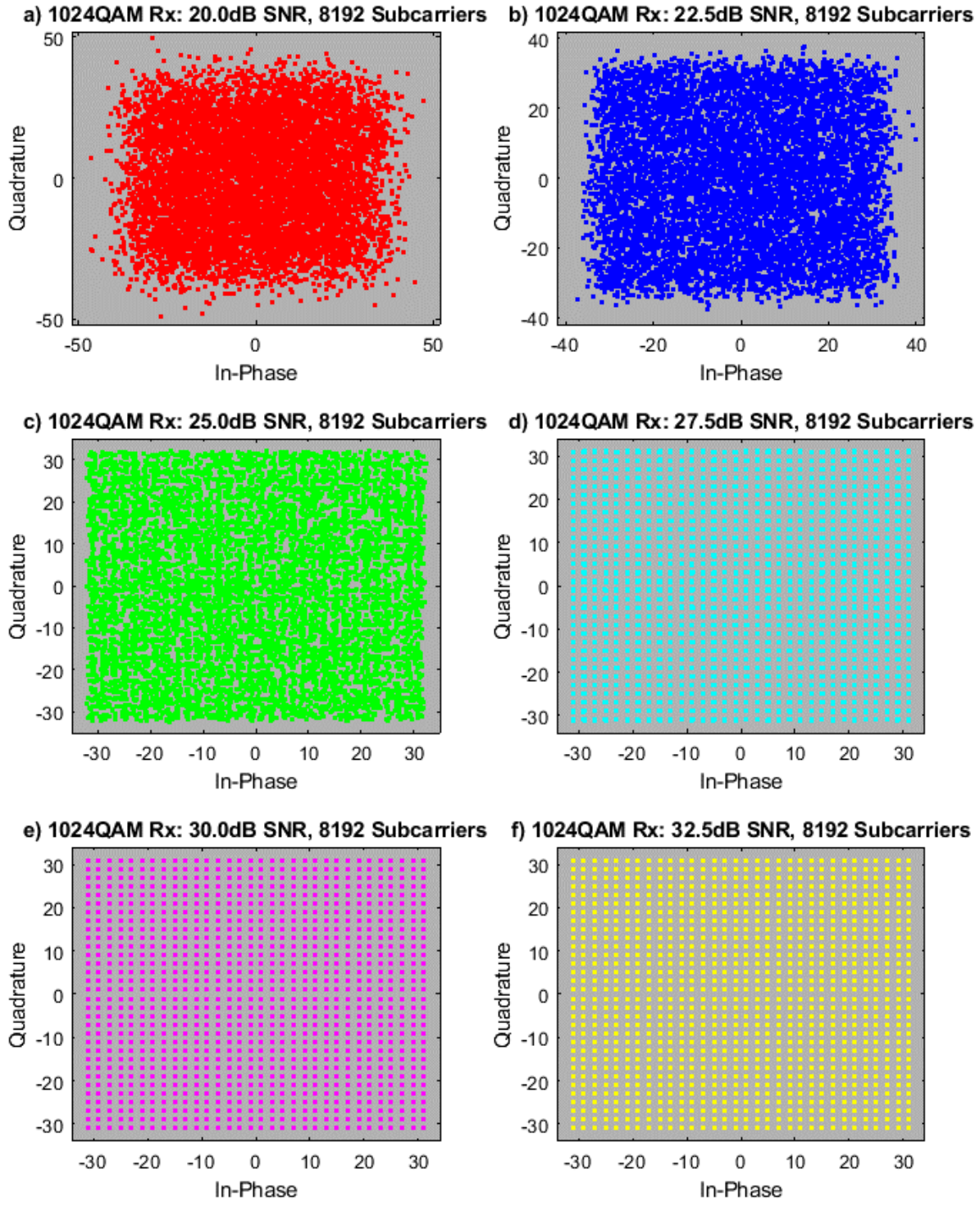
a) 1024QAM Rx: 20.0dB SNR, 8192 Subcarriers
b) 1024QAM Rx: 22.5dB SNR, 8192 Subcarriers
c) 1024QAM Rx: 25.0dB SNR, 8192 Subcarriers
d) 1024QAM Rx: 27.5dB SNR, 8192 Subcarriers
e) 1024QAM Rx: 30.0dB SNR, 8192 Subcarriers
f) 1024QAM Rx: 32.5dB SNR, 8192 Subcarriers
Quadrature
In-Phase

Appendix D:
Optimal Switching Thresholds for PET

```
% Choose number of variables to evaluate
m = 31;

% Initialise a cell array to store minimum values for different n
all_minimum_values = cell(1, m);

for n = 1:m
    % Define the objective function
    objective_function = @(a) a(1) * (1 - exp(-6 * a(1)^2));

    for i = 2:n
        objective_function = @(a) objective_function(a) + a(i) * (exp(-6 * a(i-
1)^2) - exp(-6 * a(i)^2));
    end
    objective_function = @(a) objective_function(a) + exp(-6 * a(n)^2);

    % Initialise the cell array to store initial guesses
    initial_guess = cell(1, n);

    % Call fminsearch to find the minimum
    options = optimset('Display', 'off');  % Turn off optimisation progress
display
    minimum = fminsearch(objective_function, initial_guess{end}, options);

    % Store the minimum values for this n
    all_minimum_values{n} = minimum;
end

% Create headers for all values of n
headers = cell(1, m);
for n = 1:m
    headers{n} = sprintf('Value%d', n);
end

% Pad cell arrays with NaN values for cases where n is less than 20
for n = 1:m
    if numel(all_minimum_values{n}) < m
        all_minimum_values{n}(end+1:m) = NaN;
    end
end

% Add a column with objective function values to the minimum_matrix
minimum_matrix = cell2mat(all_minimum_values');
minimum_matrix = [objective_function_values' minimum_matrix];

% Create headers with 'Objective' and 'ValueX' for all values of n
headers = cell(1, m + 1);
```

```
headers{1} = 'Objective';
for n = 1:m
    headers{n + 1} = sprintf('Value%d', n);
end

% Create a table with headers and minimum values
data = array2table(minimum_matrix, 'VariableNames', headers);

% Save the table to a CSV file
writetable(data, 'minimum_values.csv');

% Define the start and end points
start_value = 0;
end_value = 1;

% Specify the number of values you want
number_of_values = 101;

% Use linspace to generate the values
values = linspace(start_value, end_value, number_of_values);

% Display the result
disp(values);
```

Appendix E:
Uniform Switching Thresholds (1,2,3,6) for PET

```
v = 6;    % Choose number of variables to evaluate
if v == 1
    % 1 Variable
    a(1) = 0.4;
    y1 = (a(1)).*(1-exp(-6*(a(1)^2))) + exp(-(6*(a(1)^2)));
    disp(y1);    % Display the result
elseif v == 2
    % 2 Variables
    a(1) = 0.25;
    a(2) = 0.5;
    y2 = (a(1)).*(1-exp(-(6*a(1)^2))) + (a(2)).*(exp(-(6*a(1)^2))-exp(-
(6*a(2)^2))) + exp(-(6*a(2)^2));
    disp(y2);    % Display the result
elseif v == 3
    % 3 Variables
    a(1) = 0.2;
    a(2) = 0.45;
    a(3) = 0.7;
    y3 = (a(1)).*(1-exp(-(6*a(1)^2))) + (a(2)).*(exp(-(6*a(1)^2))-exp(-
(6*a(2)^2))) + (a(3)).*(exp(-(6*a(2)^2))-exp(-(6*a(3)^2))) + exp(-(6*a(3)^2));
    disp(y3);    % Display the result
elseif v == 6
    % 6 Variables
    a(1) = 0.14;
    a(2) = 0.28;
    a(3) = 0.42;
    a(4) = 0.56;
    a(5) = 0.7;
    a(6) = 0.84;
    y6 = (a(1)).*(1-exp(-(6*a(1)^2))) + (a(2)).*(exp(-(6*a(1)^2))-exp(-
(6*a(2)^2))) + (a(3)).*(exp(-(6*a(2)^2))-exp(-(6*a(3)^2))) + (a(4)).*(exp(-
(6*a(3)^2))-exp(-(6*a(4)^2))) + (a(5)).*(exp(-(6*a(4)^2))-exp(-(6*a(5)^2))) +
(a(6)).*(exp(-(6*a(5)^2))-exp(-(6*a(6)^2))) + exp(-(6*a(6)^2));
    disp(y6);    % Display the result
else
end
% .
% .
% MAIN CODE FOR UNIFORM THRESHOLD CALCULATION AND OUTPUT
% .
% .
```

Appendix F:
3-Regulator Binary Circuit Test Results

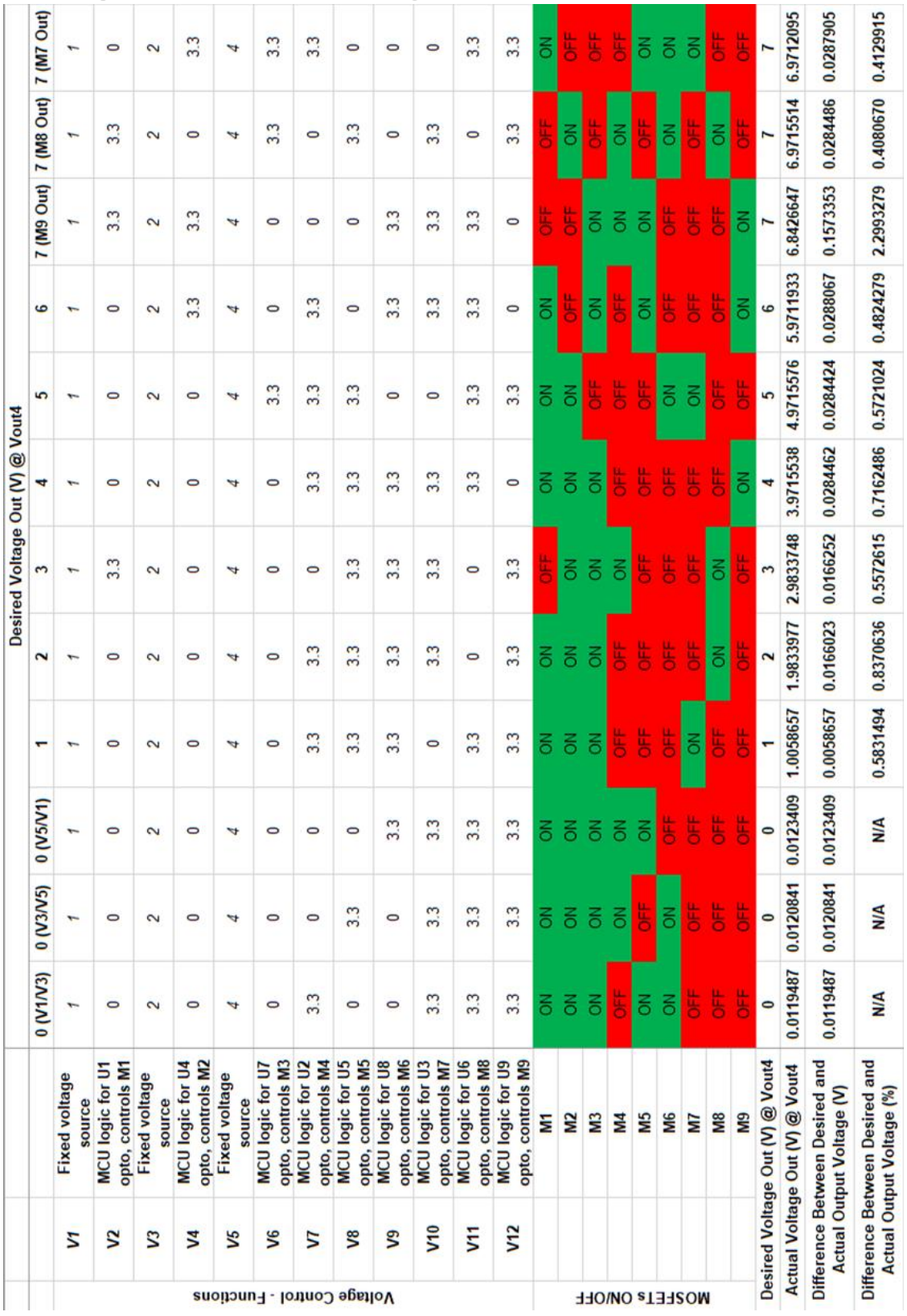

		Desired Voltage Out (V) @ Vout4										
		0 (V1/V3)	0 (V3/V5)	0 (V5/V1)	1	2	3	4	5	6	7 (M9 Out)	7 (M8 Out)	7 (M7 Out)
Voltage Control - Functions	V1 Fixed voltage source	1	1	1	1	1	1	1	1	1	1	1	1
	V2 MCU logic for U1 opto, controls M1	0	0	0	0	0	3.3	0	0	0	3.3	3.3	0
	V3 Fixed voltage source	2	2	2	2	2	2	2	2	2	2	2	2
	V4 MCU logic for U4 opto, controls M2	0	0	0	0	0	0	0	0	3.3	3.3	0	3.3
	V5 Fixed voltage source	4	4	4	4	4	4	4	4	4	4	4	4
	V6 MCU logic for U7 opto, controls M3	0	0	0	0	0	0	0	3.3	0	0	3.3	3.3
	V7 MCU logic for U2 opto, controls M4	3.3	0	0	3.3	3.3	0	3.3	3.3	3.3	0	0	3.3
	V8 MCU logic for U5 opto, controls M5	0	3.3	0	3.3	3.3	3.3	3.3	3.3	0	0	3.3	0
	V9 MCU logic for U8 opto, controls M6	0	0	3.3	3.3	3.3	3.3	3.3	0	3.3	3.3	0	0
	V10 MCU logic for U3 opto, controls M7	3.3	3.3	3.3	0	3.3	3.3	3.3	0	3.3	3.3	3.3	0
	V11 MCU logic for U6 opto, controls M8	3.3	3.3	3.3	3.3	0	0	3.3	3.3	3.3	3.3	0	3.3
	V12 MCU logic for U9 opto, controls M9	3.3	3.3	3.3	3.3	3.3	3.3	0	3.3	0	0	3.3	3.3
MOSFETs ON/OFF	M1	ON	ON	ON	ON	ON	OFF	ON	ON	ON	OFF	OFF	ON
	M2	ON	ON	ON	ON	ON	ON	ON	ON	OFF	OFF	ON	OFF
	M3	ON	ON	ON	ON	ON	ON	ON	OFF	ON	ON	OFF	OFF
	M4	OFF	ON	ON	OFF	OFF	ON	OFF	OFF	OFF	ON	ON	OFF
	M5	ON	OFF	ON	OFF	OFF	OFF	OFF	OFF	ON	ON	OFF	ON
	M6	ON	ON	OFF	OFF	OFF	OFF	OFF	ON	OFF	OFF	ON	ON
	M7	OFF	OFF	OFF	ON	OFF	OFF	OFF	ON	OFF	OFF	OFF	ON
	M8	OFF	OFF	OFF	OFF	ON	ON	OFF	OFF	OFF	OFF	ON	OFF
	M9	OFF	OFF	OFF	OFF	OFF	OFF	ON	OFF	ON	ON	OFF	OFF
Desired Voltage Out (V) @ Vout4		0	0	0	1	2	3	4	5	6	7	7	7
Actual Voltage Out (V) @ Vout4		0.0119487	0.0120841	0.0123409	1.0058657	1.9833977	2.9833748	3.9715538	4.9715576	5.9711933	6.8426647	6.9715514	6.9712095
Difference Between Desired and Actual Output Voltage (V)		0.0119487	0.0120841	0.0123409	0.0058657	0.0166023	0.0166252	0.0284462	0.0284424	0.0288067	0.1573353	0.0284486	0.0287905
Difference Between Desired and Actual Output Voltage (%)		N/A	N/A	N/A	0.5831494	0.8370636	0.5572615	0.7162486	0.5721024	0.4824279	2.2993279	0.4080670	0.4129915

Appendix G:
Generation and Validation of MGRs

```
%=========================================================================
% Linear Ruler
%=========================================================================
% Ask the user for the ruler order
ruler_order = input('Enter the Ruler Order: ');

% Initialize variables
marks = zeros(1, ruler_order - 1);
pos = 1;

%=========================================================================
% Request all ruler marks up to the ruler order
%=========================================================================
% Loop through and ask for the magnitude of each mark
for i = 1:ruler_order
    marks(pos) = input(sprintf('Enter the Position of Mark #%d: ', i));
    pos = pos + 1;
end

% Display the ruler marks
disp('Linear Ruler Marks:')
disp(marks)

%=========================================================================
% Calculate the number of possible differences with a linear ruler
%=========================================================================
diffs = zeros(1, ruler_order - 1);
for j = 1:ruler_order - 1
    diffs(j) = ruler_order - j;
end
num_diffs = sum(diffs);
% Display the number of differences
disp('The Number of Differences Between Pairs of Marks is:')
disp(num_diffs)

%=========================================================================
% Calculate the differences between pairs of marks on a linear ruler
%=========================================================================
all_diffs = zeros(ruler_order - 1, ruler_order - 1);
for i = 1:numel(diffs)
    for j = 1:diffs(i)
        all_diffs(i,j) = marks(ruler_order + 1 - i) - marks(j);
    end
end

% Display the differences between each pair of marks
disp('Matrix of Differences Between Each Pair of Marks:')
```

```
disp(all_diffs)

% Reshape the matrix into a single row
all_diffs_row = reshape(all_diffs,1,[]);

% Remove all zeros from the array, cannot have a zero distance
sorted_diffs = nonzeros(sort(all_diffs_row));
disp('Sorted Differences:')
disp(sorted_diffs')

%=========================================================================
% Modular/Circular Ruler
%=========================================================================
%=========================================================================
% Translate the linear ruler into a modular/circular ruler
% Make the first and last marks the same (0 and length)
%=========================================================================
circ_ruler_order = ruler_order - 1;

circ_marks = reshape(nonzeros(marks),1,[]);
disp('Circular Ruler Marks:')
disp(circ_marks)
% .
% .
% CODE FOR CALCULATING NUMBER OF POSSIBLE DIFFERENCES, CALCULATE THE DIFFERENCES
AND DISPLAY THEM
% .
% .
%=========================================================================
% Display all measurable distances in ascending order for a circular ruler
%=========================================================================
all_circ_diffs = cat(1, sorted_diffs, sorted_extra_circ_diffs);

sorted_all_circ_diffs = sort(all_circ_diffs);
disp('Sorted All Circular Differences:')
disp(sorted_all_circ_diffs')
% .
% .
% CODE FOR CALCULATING AND DISPLAYING REPEATED AND MISSING DIFFERENCES
% .
% .
```

Appendix H:
4-Regulator MGR Circuit Test Results

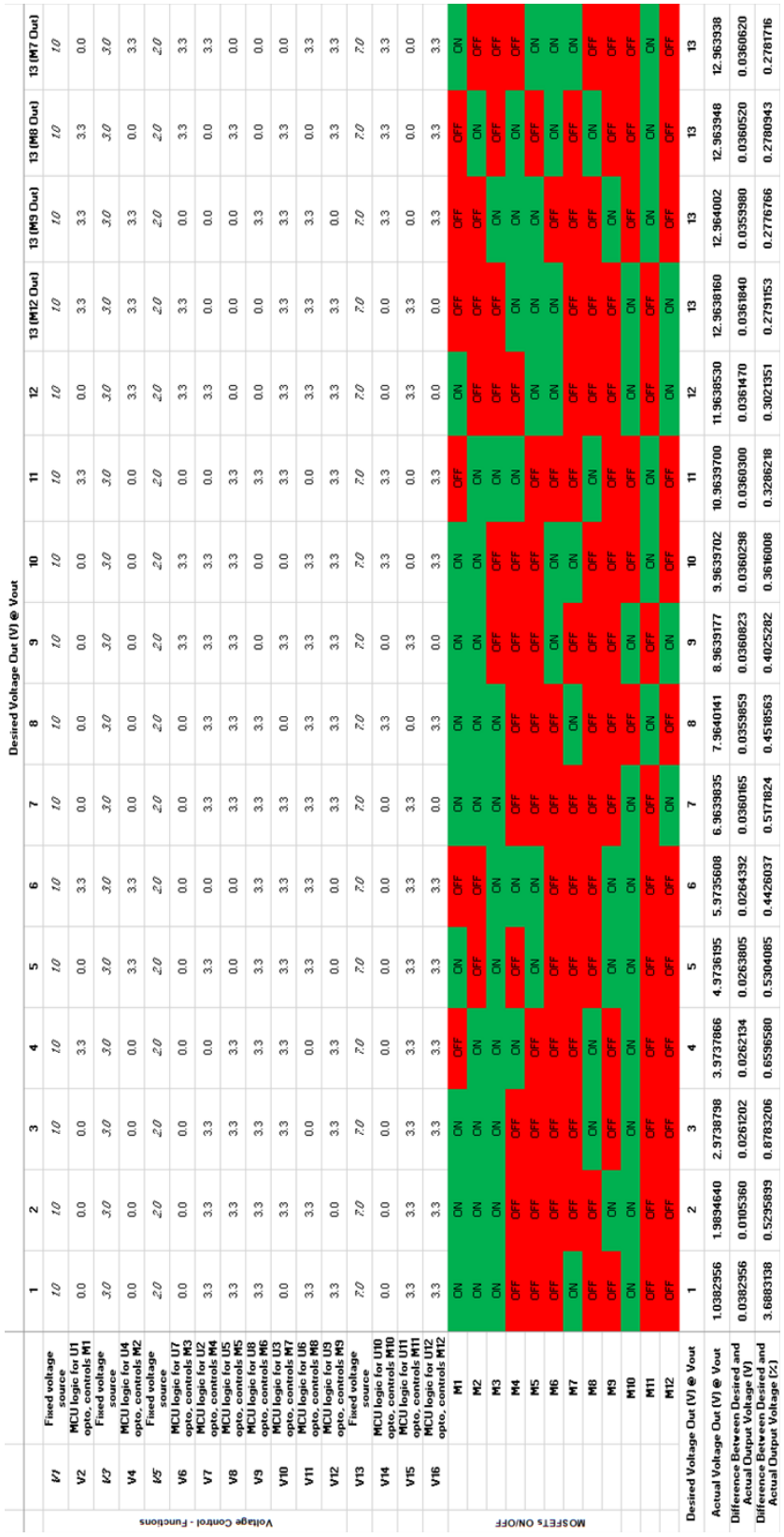

			Desired Voltage Out (V) @ Vout																
			1	2	3	4	5	6	7	8	9	10	11	12	13 (M12 Out)	13 (M9 Out)	13 (M8 Out)	13 (M7 Out)
Voltage Control - Functions	V1	Fixed voltage source	1.0	1.0	1.0	1.0	1.0	1.0	1.0	1.0	1.0	1.0	1.0	1.0	1.0	1.0	1.0	1.0
	V2	MCU logic for U1 opto, controls M1	0.0	0.0	0.0	3.3	0.0	3.3	0.0	0.0	0.0	0.0	3.3	0.0	3.3	3.3	3.3	0.0
	V3	Fixed voltage source	3.0	3.0	3.0	3.0	3.0	3.0	3.0	3.0	3.0	3.0	3.0	3.0	3.0	3.0	3.0	3.0
	V4	MCU logic for U4 opto, controls M2	0.0	0.0	0.0	0.0	3.3	3.3	0.0	0.0	0.0	0.0	0.0	3.3	3.3	3.3	0.0	3.3
	V5	Fixed voltage source	2.0	2.0	2.0	2.0	2.0	2.0	2.0	2.0	2.0	2.0	2.0	2.0	2.0	2.0	2.0	2.0
	V6	MCU logic for U7 opto, controls M3	0.0	0.0	0.0	0.0	0.0	0.0	0.0	0.0	3.3	3.3	0.0	3.3	3.3	0.0	3.3	3.3
	V7	MCU logic for U2 opto, controls M4	3.3	3.3	3.3	0.0	3.3	0.0	3.3	3.3	3.3	3.3	0.0	3.3	3.3	3.3	0.0	3.3
	V8	MCU logic for U5 opto, controls M5	3.3	3.3	3.3	3.3	0.0	0.0	3.3	3.3	3.3	3.3	3.3	0.0	0.0	0.0	3.3	0.0
	V9	MCU logic for U8 opto, controls M6	3.3	3.3	3.3	3.3	3.3	3.3	3.3	3.3	0.0	0.0	3.3	0.0	0.0	3.3	0.0	0.0
	V10	MCU logic for U3 opto, controls M7	0.0	3.3	3.3	3.3	3.3	3.3	3.3	3.3	3.3	0.0	3.3	3.3	3.3	3.3	3.3	0.0
	V11	MCU logic for U6 opto, controls M8	3.3	3.3	0.0	0.0	3.3	3.3	3.3	3.3	3.3	3.3	0.0	3.3	3.3	3.3	0.0	3.3
	V12	MCU logic for U9 opto, controls M9	3.3	0.0	3.3	3.3	0.0	0.0	3.3	3.3	3.3	3.3	3.3	3.3	3.3	0.0	3.3	3.3
	V13	Fixed voltage source	7.0	7.0	7.0	7.0	7.0	7.0	7.0	7.0	7.0	7.0	7.0	7.0	7.0	7.0	7.0	7.0
	V14	MCU logic for U10 opto, controls M10	0.0	0.0	0.0	0.0	0.0	0.0	0.0	3.3	0.0	3.3	3.3	0.0	0.0	3.3	3.3	3.3
	V15	MCU logic for U11 opto, controls M11	3.3	3.3	3.3	3.3	3.3	3.3	3.3	0.0	3.3	0.0	0.0	3.3	3.3	0.0	0.0	0.0
	V16	MCU logic for U12 opto, controls M12	3.3	3.3	3.3	3.3	3.3	3.3	0.0	3.3	0.0	3.3	3.3	0.0	0.0	3.3	3.3	3.3
MOSFETs ON/OFF		M1	ON	ON	ON	OFF	ON	OFF	ON	ON	ON	ON	OFF	ON	OFF	OFF	OFF	ON
		M2	ON	ON	ON	ON	OFF	OFF	ON	ON	ON	ON	ON	OFF	OFF	OFF	ON	OFF
		M3	ON	ON	ON	ON	ON	ON	ON	ON	OFF	OFF	ON	OFF	OFF	ON	OFF	OFF
		M4	OFF	OFF	OFF	ON	OFF	ON	OFF	OFF	OFF	OFF	ON	OFF	ON	ON	ON	OFF
		M5	OFF	OFF	OFF	OFF	ON	ON	OFF	OFF	OFF	OFF	OFF	ON	ON	ON	OFF	ON
		M6	OFF	OFF	OFF	OFF	OFF	OFF	OFF	OFF	ON	ON	OFF	ON	ON	OFF	ON	ON
		M7	ON	OFF	OFF	OFF	OFF	OFF	OFF	ON	OFF	ON	OFF	OFF	OFF	OFF	OFF	ON
		M8	OFF	OFF	ON	ON	OFF	OFF	OFF	OFF	OFF	OFF	ON	OFF	OFF	OFF	ON	OFF
		M9	OFF	ON	OFF	OFF	ON	ON	OFF	OFF	OFF	OFF	OFF	OFF	OFF	ON	OFF	OFF
		M10	ON	ON	ON	ON	ON	ON	ON	OFF	ON	OFF	OFF	ON	ON	OFF	OFF	OFF
		M11	OFF	OFF	OFF	OFF	OFF	OFF	OFF	ON	OFF	ON	ON	OFF	OFF	ON	ON	ON
		M12	OFF	OFF	OFF	OFF	OFF	OFF	ON	OFF	ON	OFF	OFF	ON	ON	OFF	OFF	OFF
	Desired Voltage Out (V) @ Vout		1	2	3	4	5	6	7	8	9	10	11	12	13	13	13	13
	Actual Voltage Out (V) @ Vout		1.0382956	1.9894640	2.9738798	3.9737866	4.9736195	5.9735608	6.9639835	7.9640941	8.9639177	9.9639702	10.9639700	11.9638530	12.9638160	12.964002	12.963948	12.963938
	Difference Between Desired and Actual Output Voltage (V)		0.0382956	0.0105360	0.0261202	0.0262134	0.0263805	0.0264392	0.0360165	0.0359859	0.0360823	0.0360298	0.0360300	0.0361470	0.0361840	0.0359980	0.0360520	0.0360620
	Difference Between Desired and Actual Output Voltage (%)		3.6883138	0.5295839	0.8783206	0.6596580	0.5304085	0.4426037	0.5171824	0.4518563	0.4025282	0.3616008	0.3286218	0.3021351	0.2791153	0.2776766	0.2780943	0.2781716

Appendix I:
TRUST Simulation and Validation

```
% Cycle through different numbers of batteries
for numBatteries = 1:50

    % Cycle through different output voltages (1 to numBatteries)
    for outputVoltage = 1:numBatteries
        % Initialise variables for series and parallel configuration
        seriesRemainder = mod(numBatteries, outputVoltage);
        seriesWhole = floor(numBatteries / outputVoltage);
        numSeries = outputVoltage;
        numParallel = 0;

        if seriesWhole > 1
            numParallel = seriesWhole;
            batteryBlock = numParallel * numSeries;
        elseif seriesWhole == 1
            numParallel = 1;
            batteryBlock = numParallel * numSeries;
        else
            batteryBlock = numBatteries;
        end
        fprintf('Number of Batteries in Series = %d\n', numSeries);
        fprintf('Number of Parallel Groups = %d\n', numParallel);
        fprintf('Batteries in Use at Any One Time: %d\n', batteryBlock);
        fprintf('Number of Unused Batteries: %d\n', seriesRemainder);
% Check if shuffling is required
        if seriesRemainder > 0
            %fprintf('Shuffling Technique Required\n');
            shuffleRequired = "Y";
% .
% MAIN CODE FOR SHUFFLING TECHNIQUE
% .
            % Determine the positions of the lowest non-zero numbers in
shuffleCounts
            bestStepSizes = find(shuffleCounts > 0 & shuffleCounts ==
min(shuffleCounts(shuffleCounts > 0)));

            % Display the positions
            fprintf('\nBest Step Sizes to Achieve Equal Utilisation: %s\n',
mat2str(bestStepSizes));

            % Record min # of shuffles for each output voltage and battery
combination
            minShuffleCount = min(shuffleCounts(shuffleCounts > 0));
% Write the data to a CSV file
```

Appendix J:
TRUST Output Data (1-15 Batteries)

# Batteries	Output Voltage (V)	# Series	# Parallel Groups	Battery Block	Unused Batteries	Shuffle Required?	Best Step Sizes	Minimum # of Shuffles
1	1	1	1	1	0	N	[]	0
2	1	1	2	2	0	N	[]	0
2	2	2	1	2	0	N	[]	0
3	1	1	3	3	0	N	[]	0
3	2	2	1	2	1	Y	[1 2]	2
3	3	3	1	3	0	N	[]	0
4	1	1	4	4	0	N	[]	0
4	2	2	2	4	0	N	[]	0
4	3	3	1	3	1	Y	[1 3]	3
4	4	4	1	4	0	N	[]	0
5	1	1	5	5	0	N	[]	0
5	2	2	2	4	1	Y	[1 2 3 4]	4
5	3	3	1	3	2	Y	[1 2 3 4]	4
5	4	4	1	4	1	Y	[1 2 3 4]	4
5	5	5	1	5	0	N	[]	0
6	1	1	6	6	0	N	[]	0
6	2	2	3	6	0	N	[]	0
6	3	3	2	6	0	N	[]	0
6	4	4	1	4	2	Y	[2 4]	2
6	5	5	1	5	1	Y	[1 5]	5
6	6	6	1	6	0	N	[]	0
7	1	1	7	7	0	N	[]	0
7	2	2	3	6	1	Y	[1 2 3 4 5 6]	6
7	3	3	2	6	1	Y	[1 2 3 4 5 6]	6
7	4	4	1	4	3	Y	[1 2 3 4 5 6]	6
7	5	5	1	5	2	Y	[1 2 3 4 5 6]	6
7	6	6	1	6	1	Y	[1 2 3 4 5 6]	6
7	7	7	1	7	0	N	[]	0
8	1	1	8	8	0	N	[]	0
8	2	2	4	8	0	N	[]	0
8	3	3	2	6	2	Y	[2 6]	3
8	4	4	2	8	0	N	[]	0
8	5	5	1	5	3	Y	[1 3 5 7]	7
8	6	6	1	6	2	Y	[2 6]	3
8	7	7	1	7	1	Y	[1 3 5 7]	7
8	8	8	1	8	0	N	[]	0

9	1	1	9	9	0	N	[]	0
9	2	2	4	8	1	Y	[1 2 4 5 7 8]	8
9	3	3	3	9	0	N	[]	0
9	4	4	2	8	1	Y	[1 2 4 5 7 8]	8
9	5	5	1	5	4	Y	[1 2 4 5 7 8]	8
9	6	6	1	6	3	Y	[3 6]	2
9	7	7	1	7	2	Y	[1 2 4 5 7 8]	8
9	8	8	1	8	1	Y	[1 2 4 5 7 8]	8
9	9	9	1	9	0	N	[]	0
10	1	1	10	10	0	N	[]	0
10	2	2	5	10	0	N	[]	0
10	3	3	3	9	1	Y	[1 3 7 9]	9
10	4	4	2	8	2	Y	[2 4 6 8]	4
10	5	5	2	10	0	N	[]	0
10	6	6	1	6	4	Y	[2 4 6 8]	4
10	7	7	1	7	3	Y	[1 3 7 9]	9
10	8	8	1	8	2	Y	[2 4 6 8]	4
10	9	9	1	9	1	Y	[1 3 7 9]	9
10	10	10	1	10	0	N	[]	0
11	1	1	11	11	0	N	[]	0
11	2	2	5	10	1	Y	[1 2 3 4 5 6 7 8 9 10]	10
11	3	3	3	9	2	Y	[1 2 3 4 5 6 7 8 9 10]	10
11	4	4	2	8	3	Y	[1 2 3 4 5 6 7 8 9 10]	10
11	5	5	2	10	1	Y	[1 2 3 4 5 6 7 8 9 10]	10
11	6	6	1	6	5	Y	[1 2 3 4 5 6 7 8 9 10]	10
11	7	7	1	7	4	Y	[1 2 3 4 5 6 7 8 9 10]	10
11	8	8	1	8	3	Y	[1 2 3 4 5 6 7 8 9 10]	10
11	9	9	1	9	2	Y	[1 2 3 4 5 6 7 8 9 10]	10
11	10	10	1	10	1	Y	[1 2 3 4 5 6 7 8 9 10]	10
11	11	11	1	11	0	N	[]	0
12	1	1	12	12	0	N	[]	0
12	2	2	6	12	0	N	[]	0
12	3	3	4	12	0	N	[]	0
12	4	4	3	12	0	N	[]	0
12	5	5	2	10	2	Y	[2 10]	5
12	6	6	2	12	0	N	[]	0
12	7	7	1	7	5	Y	[1 5 7 11]	11
12	8	8	1	8	4	Y	[4 8]	2
12	9	9	1	9	3	Y	[3 9]	3
12	10	10	1	10	2	Y	[2 10]	5
12	11	11	1	11	1	Y	[1 5 7 11]	11
12	12	12	1	12	0	N	[]	0
13	1	1	13	13	0	N	[]	0
13	2	2	6	12	1	Y	[1 2 3 4 5 6 7 8 9 10 11 12]	12

13	3	3	4	12	1	Y	[1 2 3 4 5 6 7 8 9 10 11 12]	12
13	4	4	3	12	1	Y	[1 2 3 4 5 6 7 8 9 10 11 12]	12
13	5	5	2	10	3	Y	[1 2 3 4 5 6 7 8 9 10 11 12]	12
13	6	6	2	12	1	Y	[1 2 3 4 5 6 7 8 9 10 11 12]	12
13	7	7	1	7	6	Y	[1 2 3 4 5 6 7 8 9 10 11 12]	12
13	8	8	1	8	5	Y	[1 2 3 4 5 6 7 8 9 10 11 12]	12
13	9	9	1	9	4	Y	[1 2 3 4 5 6 7 8 9 10 11 12]	12
13	10	10	1	10	3	Y	[1 2 3 4 5 6 7 8 9 10 11 12]	12
13	11	11	1	11	2	Y	[1 2 3 4 5 6 7 8 9 10 11 12]	12
13	12	12	1	12	1	Y	[1 2 3 4 5 6 7 8 9 10 11 12]	12
13	13	13	1	13	0	N	[]	0
14	1	1	14	14	0	N	[]	0
14	2	2	7	14	0	N	[]	0
14	3	3	4	12	2	Y	[2 4 6 8 10 12]	6
14	4	4	3	12	2	Y	[2 4 6 8 10 12]	6
14	5	5	2	10	4	Y	[2 4 6 8 10 12]	6
14	6	6	2	12	2	Y	[2 4 6 8 10 12]	6
14	7	7	2	14	0	N	[]	0
14	8	8	1	8	6	Y	[2 4 6 8 10 12]	6
14	9	9	1	9	5	Y	[1 3 5 9 11 13]	13
14	10	10	1	10	4	Y	[2 4 6 8 10 12]	6
14	11	11	1	11	3	Y	[1 3 5 9 11 13]	13
14	12	12	1	12	2	Y	[2 4 6 8 10 12]	6
14	13	13	1	13	1	Y	[1 3 5 9 11 13]	13
14	14	14	1	14	0	N	[]	0
15	1	1	15	15	0	N	[]	0
15	2	2	7	14	1	Y	[1 2 4 7 8 11 13 14]	14
15	3	3	5	15	0	N	[]	0
15	4	4	3	12	3	Y	[3 6 9 12]	4
15	5	5	3	15	0	N	[]	0
15	6	6	2	12	3	Y	[3 6 9 12]	4
15	7	7	2	14	1	Y	[1 2 4 7 8 11 13 14]	14
15	8	8	1	8	7	Y	[1 2 4 7 8 11 13 14]	14
15	9	9	1	9	6	Y	[3 6 9 12]	4
15	10	10	1	10	5	Y	[5 10]	2
15	11	11	1	11	4	Y	[1 2 4 7 8 11 13 14]	14
15	12	12	1	12	3	Y	[3 6 9 12]	4
15	13	13	1	13	2	Y	[1 2 4 7 8 11 13 14]	14
15	14	14	1	14	1	Y	[1 2 4 7 8 11 13 14]	14
15	15	15	1	15	0	N	[]	0